PHOTOFERMENTATIVE HYDROGEN PRODUCTION USING DARK FERMENTATION EFFLUENT OF SUGAR BEET THICK JUICE BY RHODOBACTER CAPSULATUS

A THESIS SUBMITTED TO
THE GRADUATE SCHOOL OF NATURAL AND APPLIED SCIENCES
OF
MIDDLE EAST TECHNICAL UNIVERSITY

BY

ENDAM ÖZKAN

IN PARTIAL FULFILLMENT OF THE REQUIREMENTS
FOR
THE DEGREE OF MASTER OF SCIENCE
IN
BIOTECHNOLOGY

SEPTEMBER 2011

Approval of the thesis:

PHOTOFERMENTATIVE HYDROGEN PRODUCTION USING DARK FERMENTATION EFFLUENT OF SUGAR BEET THICK JUICE BY RHODOBACTER CAPSULATUS

submitted by **ENDAM ÖZKAN** in partial fulfillment of the requirements for the degree of **Master of Science in Biotechnology Department, Middle East Technical University** by,

Prof. Dr. Canan Özgen _____
Dean, Graduate School of **Natural and Applied Sciences**

Prof. Dr. İnci Eroğlu _____
Head of Department, **Biotechnology**

Prof. Dr. Ufuk Gündüz _____
Supervisor, **Biological Sciences Dept., METU**

Assist. Prof. Dr. Başar Uyar _____
Co-Supervisor, **Chemical Engineering Dept., Kocaeli Univ.**

Examining Committee Members:

Prof. Dr. İnci Eroğlu _____
Chemical Engineering Dept., METU

Prof. Dr. Ufuk Gündüz _____
Biological Sciences Dept., METU

Assist. Prof. Dr. Başar Uyar _____
Chemical Engineering Dept., Kocaeli Univ.

Assist. Prof. Dr. Can Özen _____
Biotechnology Dept., METU

Dr. Tuba Hande ERGÜDER _____
Environmental Engineering Dept., METU

Date: 15.09.2011

I hereby declare that all information in this document has been obtained and presented in accordance with academic rules and ethical conduct. I also declare that, as required by these rules and conduct, I have fully cited and referenced all material and results that are not original to this work.

Name, Last Name: ENDAM ÖZKAN

Signature :

ABSTRACT

PHOTOFERMENTATIVE HYDROGEN PRODUCTION USING DARK FERMENTATION EFFLUENT OF SUGAR BEET THICK JUICE BY RHODOBACTER CAPSULATUS

Özkan, Endam

M.Sc., Department of Biotechnology

Supervisor : Prof. Dr. Ufuk Gündüz

Co-Supervisor : Assist. Prof. Dr. Başar Uyar

September 2011, 187 pages

Biological hydrogen production through integration of dark and photo-fermentation by using biomass is a promising alternative for energy supply problems. The main purpose of this study was to investigate photobiological H_2 production by the purple non-sulfur (PNS) bacteria *Rb. capsulatus* on dark fermentation effluent of sugar beet thick juice (DFESBTJ). Presence of NH_4^+ in effluents is an important parameter since NH_4^+ inhibit the nitrogenase enzyme activity. Therefore, the influence of different NH_4^+ concentrations in the DFESBTJ by removing using natural zeolite clinoptilolite on photofermentative H_2 production were studied using *Rb. capsulatus* DSM1710 and *Rb. capsulatus* YO3 (hup^-). Also, the effect of EtOH concentrations (between 6.25 and 200 mM) in the defined medium on H_2 production were studied using both bacterial strains since EtOH is a possible by-product of dark fermentation process. The experiments were carried out in small scale bottle photobioreactors (PBRs) and outdoor panel PBR (4 L). H_2 productivity of 1.12 mmol/L_c/h was attained over 15 days of operation for panel PBR. The results showed that the zeolite was effective in removing NH_4^+ from the DFESBTJ as its concentration decreased by 95% after treatment. In both bacterial strains, an increase in the maximum productivities and molar H_2 yields was observed with the decrease in NH_4^+

concentrations. There was no significant effect of EtOH on H_2 production except the inhibition at 200 mM. The main conclusions were that both bacterial strains could effectively utilize the DFESBTJ for growth and H_2 production, therefore facilitating the integration of the dark and photo-fermentation for sustainable biohydrogen production.

Keywords: *Rb. capsulatus*, photofermentation, sugar beet thick juice, panel photobioreactor, ethanol

ÖZ

RHODOBACTER CAPSULATUS İLE ŞEKER PANCARI KARANLIK FERMENTASYON ATIĞI KOYU ŞERBET KULLANILARAK FOTOFERMENTATİF HİDROJEN ÜRETİMİ

Özkan, Endam
Yüksek Lisans, Biyoteknoloji Bölümü
Tez Yöneticisi : Prof. Dr. Ufuk Gündüz
Ortak Tez Yöneticisi : Yrd. Doç. Dr. Başar Uyar

Eylül 2011, 187 sayfa

Karanlık ve foto-fermentasyonu birleştirerek biyokütleden biyolojik hidrojen üretimi enerji sağlama problemleri için umut vadeden alternatif bir yöntemdir. Bu çalışmanın ana amacı şeker pancarı koyu şerbetinin karanlık fermentasyon atığı kullanılarak mor kükürtsüz bir bakteri olan *Rb. capsulatus* tarafından fotobiyolojik H_2 üretiminin araştırılmasıdır. Atıklar içerisinde NH_4^+ bulunması, nitrojenaz enziminin aktvitesini inhibe etmesinden dolayı önemli bir parametredir. Bundan dolayı, atık içerisindeki değişik konsantrasyonlardaki NH_4^+'ün doğal zeolite klinoptilolit kullanılarak uzaklaştırılmasıyla *Rb. capsulatus* DSM1710 ve *Rb. capsulatus* YO3 (hup^-) bakterilerinin fotofermentatif H_2 üretimi üzerine etkisi araştırılmıştır. Ayrıca EtOH'ın karanlık fermentasyonun olası bir yan ürünü olmasından dolayı, tanımlanmış besiyeri içerisindeki EtOH konsantrasyonlarının (6.25 ve 200 mM arası) H_2 üretimi üzerine etkisi her iki bakteri suşu için araştırılmıştır. Deneyler, küçük ölçekli şişe fotobiyoreaktör ve açık hava panel tipi fotobiyoreaktör (4 L) içerisinde yürütülmüştür. 15 gün süren operasyon süresi içerisinde panel fotobiyoreaktörden 1.12 mmol/L_c/h H_2 üretim hızı elde edilmiştir. Sonuçlar zeolitin karanlık fermentasyon atığından NH_4^+ uzaklaştırma işleminde, NH_4^+'ün uygulama

sonrasında %95 azalmasıyla etkili olduğunu göstermiştir. Her iki bakteri suşunda, NH_4^+ konsantrasyonun azalmasıyla maksimum üretim hızında ve molar H_2 veriminde artış gözlenmiştir. 6.25 ve 100 mM EtOH konsantrasyonu arasında EtOH'ün H_2 üretimine belirgin bir etkisi bulunamamıştır; fakat, 200 mM EtOH konsantrasyonunda inhibisyon gözlenmiştir. Elde edilen sonuçlara göre iki bakteri suşu karanlık fermentasyon atığını büyüme ve H_2 üretimi için etkili bir şekilde tüketebilmiştir ve bu şekilde sürdürülebilir biyohidrojen üretimi için karanlık ve foto-fermentasyonun birleştirilmesine olanak sağlayabileceği sonucuna varılmıştır.

Anahtar Kelimeler: *Rb. capsulatus*, fotofermentasyon, şeker pancarı koyu şerbeti, panel fotobiyoreaktör, etanol

To My Family

ACKNOWLEDGMENTS

I would like to express my deep appreciation to my supervisor Prof. Dr. Ufuk Gündüz and co-supervisor Assist. Prof. Dr. Başar Uyar for their guidance, advice and supervision throughout the course of this study. I would also like to thank Prof. Dr. İnci Eroğlu and Prof. Dr. Meral Yücel for their constructive critisims, helpful support and inspiration during the study. I would like to thank Dr. Ebru Özgür for her prudent observations and heplful comments.

I appreciatively acknowledge the technical asisstance of Kerime Güney for the elemental analysis and Gülten Orakçı for her deep HPLC and GC knowledge during my study. Also, I want to thank Şerife Topçu for her grate accompanying during long hours of laboratory work.

I especially wish to gratefully thank to my lab mates, Nilüfer Afşar, Pelin Sevinç, Dominic Deo Androga, Muazzez Gürgan Doğan and S.Gökçe Avcıoğlu for their understanding, support, friendship and continual encouragement that could never be forgotten throughout this whole process. I acknowledge my lab-mates Begüm Peksel, Emrah Sağır, Efe Boran, Kamal ElKahlout, Gülşah Pekgöz, Burcu Özsoy, Görkem Baysal and the members of lab 206 for their support and friendship.

Lastly, I cordially would like to send thanks to my parents, my sisters, my aunt and my niece for believing in me when times were diffucult and for being there to share hapiness when times were good.

This study was supported by 6th frame European Union Project —"Hyvolution", and BAP project with number of BAP-07-02-2010-00-01.

TABLE OF CONTENTS

LIST OF TABLES

TABLES

LIST OF FIGURES

FIGURES

LIST OF SYMBOLS AND ABBREVIATIONS

A:	Irradiated area (m^2)
Acetyl-CoA:	Acetyl Coenzyme A
ATP:	Adenosine tri-Phosphate
Bchl *a*:	Bacteriochlorophyll *a*
COD:	Chemical oxygen demand
DFE:	Dark fermentation effluent
DFESBTJ:	Dark Fermentation Effluent of Sugar Beet Thick Juice
EtOH:	Ethanol
Fd:	Ferredoxin
FID:	Flame ionization detector
GC:	Gas Chromatography
gdw:	Gram dry weight of bacteria
H_2:	Hydrogen gas
hup^-:	Uptake hydrogenase deficient (mutant)
HPLC:	High Performance Liquid Chromatography
k_0	Rate constant for a zero order reaction, mM/h
k_1	Rate constant for a first order reaction, 1/h
k_2	Rate constant for a second order reaction, 1/mM-h
mmol	Millimole
n	Order of the reaction
NAD	Nicotinamide adenine dinucleotide
OD	Optical Density
PBR:	Photobioreactor
PHB:	Polyhydroxybutyrate
PNS:	Purple Non-Sulfur
Rb. capsulatus	*Rhodobacter capsulatus*
$R_{e/a}$	Molar ratio of ethanol to acetic acid

TC:	Total carbon
TCA:	Citric acid cycle
TN:	Total nitrogen
V_{PBR}:	volume of photobioreactor
Greek Letters:	
η:	Light conversion efficiency (%)
μ_{max}:	Specific growth rate constant obtained by exponential model, (1/h)

CHAPTER 1

INTRODUCTION

A major part of transport and energy systems today rely on fossil energy carriers. The global energy demand is forecasted to increase by more than 50% until 2030 with the increasing world population; especially in the developing and industrializing nations in Asia and also South America. The rise in energy demand leads to usage of more fossil energy sources (crude oil and natural gas). The fossil energy sources are limited and release pollutants that are known to cause global warming. Therefore, the challenge of controlling green house gas emissions and searching for alternative energy sources exists (Ball et al., 2009). Hydrogen is considered an alternative energy carrier as it is a ‘‘clean’’ and efficient fuel. On combustion it produces only water and energy and it has the highest energy to mass ratio of any known fuel; 1 kg of hydrogen carries the same amount of energy as 2.7 kg of natural gas or 3 kg of gasoline (Das and Veziroğlu, 2001).

1.1 Hydrogen Production Methods

Today, about 50 million tones of hydrogen is produced yearly worldwide (representing less than 2% of the world’s primary energy demand) (Olah et al., 2009). Most of the hydrogen produced is mainly used as a feedstock for production of ammonia, refined petroleum products and a wide variety of chemicals in the chemical and petrochemical industry. It is also used in metallurgical, electronical and pharmaceutical industries (Olah et al., 2009).

Hydrogen production can be mainly divided into two groups:

- Hydrogen production using fuel processing technologies
- Hydrogen from alternative resources such as biomass and water

Currently, sources of worldwide hydrogen production are water electrolysis (4%), coal (18%), liquid hydrocarbons (30%) and natural gas (48%). Consequently, most of the hydrogen is produced from fossil fuels (96%) (Olah et al., 2009). Steam reforming from natural gas caters for 48% of the hydrogen produced from the fossil fuels. In this process, hydrocarbon (natural gas) and a steam line is passed over a catalyst at high temperatures to form hydrogen and carbonmonoxide (Holladay et al., 2009). Hydrogen is also produced by the gasification of coal. The coal is reacted with oxygen and steam (water vapor) under high temperature and pressure to produce hydrogen and carbonmonoxide.

Electrolysis is another hydrogen production method. During this process, water is split into hydrogen and oxygen using electricity. The process can either be thermochemical water dissociation (if heat is supplied) or photoelectrolytic (if sunlight is used) (Holladay et al., 2009). About 4% of hydrogen is produced via electrolysis (Olah et al., 2009). A major advantage of hydrogen production via electrolysis is that it can be generated more efficiently in less time with the using energy sources like sunlight or nuclear energy. However, hydrogen and oxygen from water can be generated without using electricity through a thermochemical process called the sulfur-iodine cycle. This process is presently one of the most studied alternative hydrogen production processes (Olah et al., 2009). Although using thermochemical reactions or nuclear power plants for electrolysis do not emit CO_2 or other pollutants to the atmosphere, none of these processes have been demonstrated at production levels. In addition, especially for the nuclear power plants, several safety issues like disposal of reactive waste remain to be solved. In Figure 1.1, different routes for the production of hydrogen are illustrated. In order to have a sustainable hydrogen economy, renewable sources shown in Figure 1.1 should be taken into account for the future energy supply system in the world.

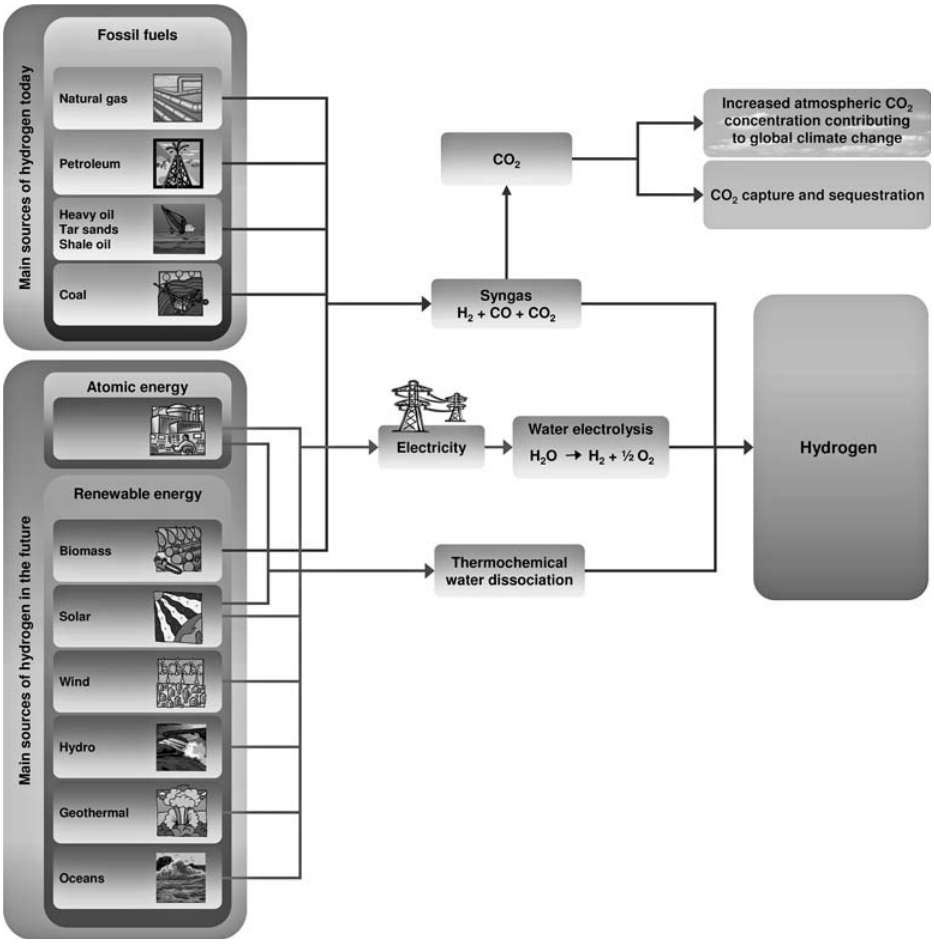

Figure 1.1 Different routes for the production of hydrogen (Olah et al., 2009)

Hydrogen production from biomass can be achieved by pyrolysis or gasification and by biological systems. Biological hydrogen production relies on renewable resources such as water, biomass and sunlight. In addition, it can be carried out at ambient temperature and pressure, is less energy intensive and cleaner in comparison to conventional hydrogen production methods such as steam reforming, coal gasification and electrolysis (Manish and Banarjee, 2008).

1.2 Biological Hydrogen Production

Biological hydrogen production can be divided into five main categories; biophotolysis of water using algae and cyanobacteria, fermentative hydrogen production from organic compounds, photodecomposition of organic compounds by photosynthetic bacteria, integrated systems using photosynthetic and fermentative bacteria, and microbial fuel cells (MFCs). In Table 1.1, various types of bacteria related to hydrogen production are shown.

Table 1.1 Classification of hydrogen producing bacteria (Basak and Das, 2007)

Available energy form	Enzyme for H_2 generation	Class of bacteria	Sub-class of bacteria	Genus of bacteria	Electron donor
Photosynthesis	Hydrogenase	Green algae	–	*Chlamydomonas*	Water
				Chlorella	Water
		Cyano-bacteria	Heterocyst	*Anabaena*	Water
			Non-heterocyst	*Oscillataria*	Water
	Nitrogenase	Photo-synthetic bacteria	**Purple-non-sulfur (PNS) bacteria**	*Rhodobacter*	Organic acids
				Rhodopseudomonas	Organic acids
			(Facultative anaerobe)	*Rhodospirillum*	Organic acids
			Purple sulfur bacteria	*Chromatium*	Sulfates
				Thiocapsa	Sulfates
Non-photosynthesis	Hydrogenase	Obligate anaerobe	–	*Clostridium*	Sugars
		Facultative anaerobe	–	*Methanobacterium*	Sugars
			–	*Escherichia*	Sugars
			–	*Enterobacter*	Sugars
	Nitrogenase	Nitrogen fixing bacteria	Facultative aerobes	*Azotobacter*	Sugars
				Clostridium	Sugars
			Facultative anaerobes	*Klebsiella*	Sugars

1.2.1 Biophotolysis

Biophotolysis is the production of hydrogen from water using energy from absorbed light by microorganisms. This process can be either direct (green algae) or indirect (cyanobacteria).

- **Direct biophotolysis:** Light energy is entraped by photosynthetic apparatus and by using the gathered energy water is split by the following general reaction:

$$2H_2O \xrightarrow{\text{light energy}} 2H_2+O_2 \qquad (1.1)$$

Photosystem II and photosystem I for capturing light energy are included in green algae to exhibit oxygenic photosynthesis like higher plants (Dasgupta et al., 2010). In this process, in order to reduce H^+ to H_2, electrons are moved to hydrogenase or nitrogenase via ferredoxin (Fd). The main advantage of this process is the capability of producing hydrogen directly from water and having a carbon free energy cycle. However, the generated oxygen during the splitting of water inhibits both nitrogenase and hydrogenase enzymes. In addition, the separation of H_2 and O_2 makes this approach costly and economically challenging (Melis, 2002).

- **Indirect biophotolysis:** This process mostly observed in cyanobacteria and the stored carbohydrate is oxidized to produce hydrogen by the following reaction:

$$12H_2O+6CO_2 \xrightarrow{\text{light energy}} C_6H_{12}O_6+6O_2 \quad (1.2)$$

$$C_6H_{12}O_6+12H_2O \xrightarrow{\text{light energy}} 12H_2+6CO_2 \quad (1.3)$$

As it can be seen in reactions (1.2) and (1.3) H_2 evolution is separated from O_2 evolution and this prevents the inhibition of hydrogen producing enzymes because of O_2 sensitivity. For this reason, this process is attractive; however, the low photochemical efficiency and presence of uptake hydrogenase enzyme constitute the major disadvantages of this process (Dasgupta et al., 2010).

1.2.2 Dark Fermentation

In dark fermentation, carbohydrate-rich substrates are decomposed into organic acids and alcohols by anaerobic bacteria, liberating H_2 and CO_2 in the process. Most of the microbial anaerobic hydrogen production is forced by the anaerobic metabolism of pyruvate, produced during the catabolism of various substrates. The breakdown of pyruvate is driven by one of two enzymes (Hallenbeck and Benemann, 2002):

1. *Pyruvate: formate lyase* (PFL)

$$\text{Pyruvate} + \text{CoA} \xrightarrow[\text{PFL}]{} \text{acetyl-CoA} + \text{formate} \qquad (1.4)$$

2. *Pyruvate: ferredoxin oxido reductase* (PFOR)

$$\text{Pyruvate} + \text{CoA} + 2\text{Fd (ox)} \xrightarrow[\text{PFOR}]{} \text{acetyl-CoA} + CO_2 + 2\text{Fd (red)} \qquad (1.5)$$

During pyruvate oxidation ferredoxin is reduced. The reduced ferredoxin transfers the electrons to hydrogenase enzyme which catalyzes the production reaction of molecular hydrogen.

There are several advantages of dark fermentation. The carbohydrate-rich substrates can be provided by various wastewater streams (starch or cellulose containing solid wastes) which enables the dual functions of treatment (disposing the waste stream) and energy production (H_2 production). Fermentors commonly are inoculated with a mixture of undetermined microorganisms which means that dark fermentation is mixed-culture friendly. Chosen strains are specified upon the feedstock delivered to the bioreactor and the reactor conditions (Brentner et al., 2010).

However, the major drawback of dark fermentation is the relatively lower yields of H_2 production. When the hydrogen production yield increases the reaction becomes thermodynamically unfavorable (because of the increase in H_2 partial pressure) (Nath and Das, 2004). In addition, many by-products that would affect a consequent photofermentation can be formed during dark fermentation. Besides by-products, an intensive biogas separation to retrieve hydrogen would be needed during the process. In fermentation, complete oxidation of 1 mole of glucose yields 12 moles of hydrogen. However, complete oxidation of glucose into hydrogen and carbon dioxide is not possible due to thermodynamically reasons. This topic will be debated in integrated systems section.

1.2.3 Photofermentation

Purple and some green photosynthetic bacteria related to gram-negative prokaryotes, heliobacteria related to the section of gram-positive Clostridia, are active diazotrophs which can produce nitrogenase for N_2 fixation under anaerobic nitrogen-limiting conditions resulting hydrogen production (Madigan et al., 1984).

Photosynthetic bacteria can utilize sunlight as a source of energy and decompose volatile fatty acids (i.e. acetate, lactate and glutamate) into biomass with H_2 and CO_2 via anoxygenic photosynthesis that has been known for nearly sixty years (Gest and Kamen, 1949).

Purple/green sulfur and purple non-sulfur (PNS) bacteria perform anoxygenic photosynthesis and produce hydrogen by using the sulphide compounds and organic acids as electron donors, respectively. Unlike the purple and green sulfur bacteria, PNS bacteria do not produce H_2S and off-gas contains typically >90% H_2 (Redwood et al., 2009).

In bacterial photofermentation and hydrogen production, species like *Rhodospirillum rubrum*, *Rhodopseudomonas palustris*, *Rhodobacter sphaeroides*, and *Rhodobacter capsulatus* have been broadly studied for genetic and physiological aspects (Eroglu and Melis, 2011).

Although purple non-sulfur bacteria contain hydrogenase, hydrogen is normally produced by nitrogenase when extra energy from sunlight in ATP form, nitrogen-limitation and electrons from organic acids transported via ferredoxin are available (Sasikala et al., 1993). The reaction photofermentative hydrogen production is shown below (Reaction 1.6).

$$CH_3COOH+2H_2O \xrightarrow{\text{light energy}} 4H_2+2CO_2 \qquad (1.6)$$

Hydrogen production by PNS bacteria are shown as the most promising microbial way in literature due to following abilities (Das and Veziroglu et al., 2001):

- High substrate conversion efficiencies,
- Lack of O2 evolving activity, which removes the oxygen sensitivity issue that affects biological systems,
- Ability to use both the visible (400-700 nm) and near infrared (700-950 nm) areas of light spectrum
- Ability to utilize wide range of organic substrates that supports association with wastewater treatment.

1.2.4 Integrated Systems

In dark fermentation, organic compounds cannot be degraded completely due to thermodynamic limitations and the end products include hydrogen, carbondioxide and lower molecular weight organic acids (Claassen and Vrije, 2006).The ΔG_o of reaction 1.7 is +3.2 kJ/mole, which is not feasible thermodynamically (Manish and Banerjee, 2008).

$$C_6H_{12}O_6 + 6H_2O \rightarrow 12\ H_2 + 6CO_2 \qquad \Delta G_o = +3.2\ kJ \qquad (1.7)$$

As it can be seen in reaction 1.8 (Manish and Banerjee, 2008), the effluent from dark fermentation is particularly rich in organic acids such as acetate (Reaction 1.8).

$$C_6H_{12}O_6 + 2H_2O \rightarrow 4H_2 + 2CO_2 + 2CH_3COOH \qquad \Delta G_o = -206\ kJ \qquad (1.8)$$

Continually, in order to achieve a complete decomposition of these substrates, integration with further processes such as methanogenic anaerobic digestion technology, bioelectrochemical systems (i.e. microbial fuel cells) and photofermentation can be employed (Guwy et al., 2011).

In addition, Melis and Melnicki (2006) proposed three component integration that includes dark fermentation, oxygenic and anoxygenic fermentation. Either consequent dark-photofermentation or simultaneous dark-photofermentation is conducted in various studies (Laurinavichene et al., 2010, Fang et al., 2006). Nearly stoichiometric conversion of organic acids to hydrogen can be achieved through photofermentation in reaction 1.6. Therefore, a sequential dark and photofermentation of organic compounds can be a promising way to increase the overall hydrogen yield by using renewable sources. The latter can produce hydrogen using sunlight while the former produces substrate for photofermentation.

HYVOLUTION (acronym for "Non-thermal production of pure hydrogen from biomass"), was a European Union 6^{th} framework integrated project that aimed to develop such a sequential two-stage bioprocess for the cost-effective production of pure hydrogen at small scale from locally obtained biomass feedstock. In the first stage biomass is fermented to acetate, carbon dioxide, and hydrogen by thermophilic dark fermentation, while in the second step, acetate is converted to hydrogen and carbon dioxide, thereby reaching the theoretical maximum hydrogen production of 12 mol/mol glucose (Claassen and Vrije, 2006).

Laurinavichene et al. (2010) studied on integrated system of dark and photofermentation using mixed culture and *Rb. capsulatus*, respectively. The carbon source of this study was potato starch and they received 5.6 mol mol^{-1} glucose equivalents for the two-stage integrated process. In another study on integration of dark and photofermentation were demonstrated by Özgür et al. (2010a) in which sugar beet molasses was decomposed by *Caldicellulusiruptor saccharolyticus* in dark fermentation and followed by photofermentation by *Rb. capsulatus.* They reported the overall yield of the two-stage hydrogen production as 13.7 mol H_2/mol sucrose. Similar study was reported by Özgür et al. (2010b), they found 3.58 mol H_2/mol glucose, 3.91 mol H_2/mol glucose of overall hydrogen yield for two-stage fermentation of glucose, and potato steam peel, respectively. Up to present, mostly batch scale two phase dark-light fermentation has been demonstrated by many researchers. However, data from larger scale experiments are required to show the feasibility of two-stage hydrogen production (Guwy et al., 2011).

1.2.5 Microbial Fuel Cells

Microbial fuel cells (MFC) represent an innovative alternative for consequent decomposition of organic materials after dark fermentation. In a MFC, bacteria are used as the catalysts to oxidize organic substrate in anode chamber. As a result of this oxidation protons are formed and these protons move towards cathode (producing current) where the electrons reduce oxygen to water (Ditzig et al., 2007, Rozendal et al., 2006). Both anode and cathode connected by a proton exchange membrane. Due to inadequate potential that were generated from a substrate such as acetate, a small input of electrical energy is required to drive hydrogen evolution at the cathode.

However, MFC's hydrogen production rates and efficiencies were quite low for biotechnological generation of fuels even it suggests a smart offer by means of thermodynamic principles (Hallenbeck, 2009).

1.3 Physiology of *Rhodobacter capsulatus* and other PNS bacteria

PNS bacteria are prokaryotic microorganisms capable of performing photosynthesis with the participation of chlorophyll pigments and without releasing oxygen. PNS bacteria have relatively simple phototransduction machinery, with a single photosystem (lack of photosystem II). They are found in various areas in nature, particularly freshwater, marine habitats and soil (Garrity et al., 2005). Water-soluble vitamins (one or more) are required for phototropic growth of PNS bacteria. In addition, PNS bacteria demands pH of 6-9 and temperature of 25-35 ºC (Sasikala et al., 1993). When grown anaerobically, the PNS bacteria show a yellowish brown to greenish and deep brown color under illumination but turn red in the presence of oxygen; carotenoids are transformed to corresponding ketocarotenoids that cause the red color change (Pellerin and Gest, 1983).

PNS bacteria have ability to grow in different modes of growth such as aerobic/anaerobic respiration, fermentation, photoautotrophy and photoheterotrophy

depending on available conditions and they can switch their mode of growth from one mode to another. PNS bacteria generally prefer to grow in photoheterotrophic mode and this mode of growth is the only mode resulting hydrogen production (Koku et al., 2002).

Rhodobacter capsulatus is a gram negative PNS bacterium and belongs to Proteobacteria group. In Table 1.2 the taxonomy of *Rb. capsulatus* can be seen.

Table 1.2 The taxonomy of *Rb. capsulatus* (Sevinç, 2010)

Super Kingdom	*Prokaryota*
Kingdom	*Monera*
Sub Kingdom	*Eubacteria*
Phylum	*Gracilicutes*
Class	*Photosynthetic eubacteria*
Order	*Rhodospirillates*
Family	*Rhodospirillaceae*
Genus	*Rhodobacter*
Species	*capsulatus*

1.3.1 Hydrogen Production Mechanism

As explained previously in section 1.3, PNS bacteria can only produce hydrogen in photoheterotrophic mode of growth. In order to induce PNS bacteria for hydrogen production, the following items should be gathered all together.

- Anaerobic atmosphere
- Availability of carbon source such as volatile fatty acids
- Availability of light source such as sunlight or artificial illumination
- Nitrogen limitation (i.e. a high C/N ratio compels bacteria to “dump” the excess energy)

After establishing all the items explained above, the photofermentative hydrogen production can be catalyzed by enzymes of PNS bacteria. In addition to enzymes that are major components of hydrogen production metabolism, the carbon flow and

photosynthetic membrane apparatus are also involved during the process of hydrogen production (Koku et al., 2002). In Figure 1.2, the overall view of carbon flow of PNS bacteria can be seen.

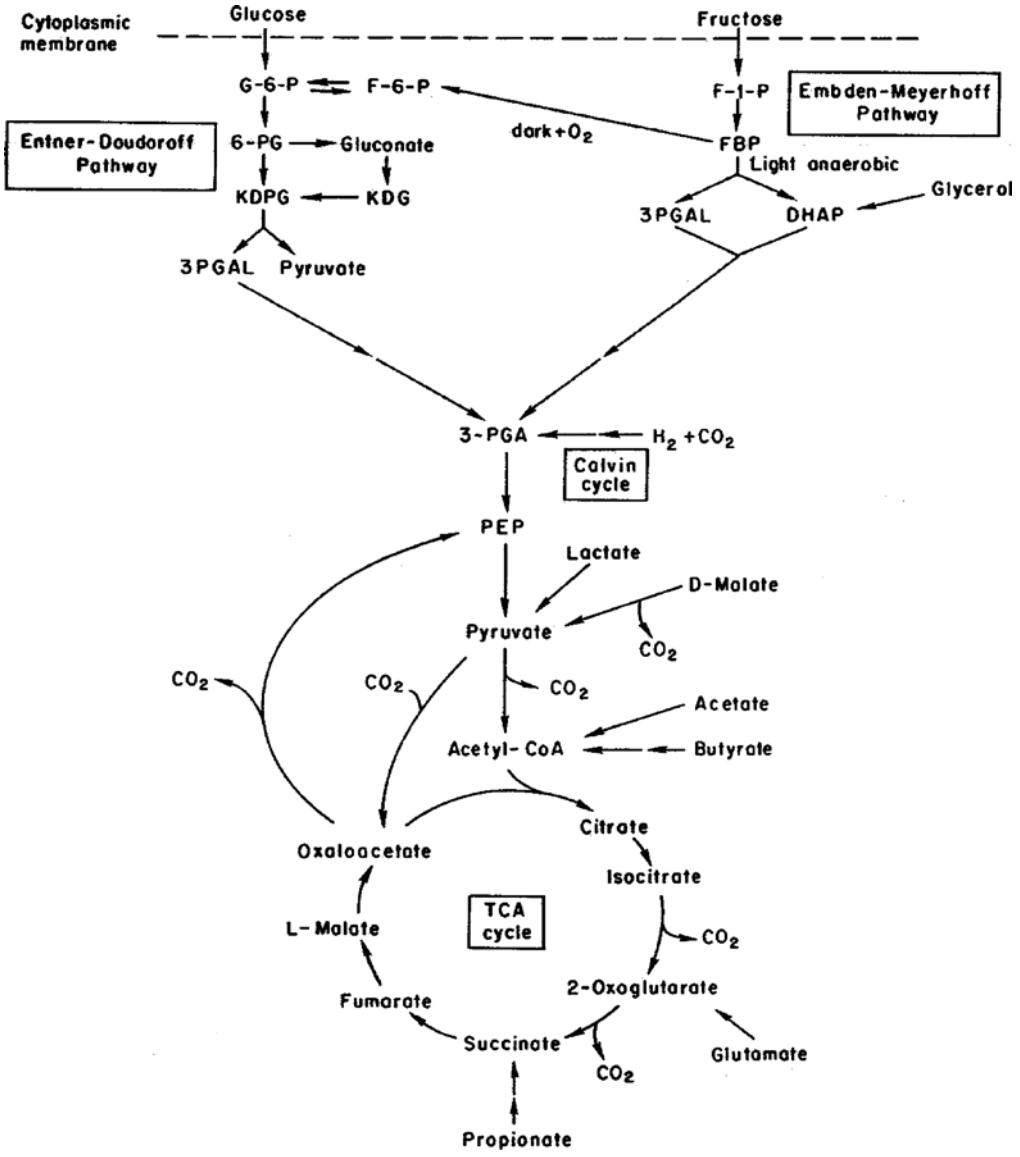

Figure 1.2 The overall scheme of the carbon metabolism in PNS bacteria (Koku et al., 2002)

PNS bacteria can use a wide range of organic electron donors including organic acids, alcohols, and carbohydrates. However, most efficient electron donors for nitrogenase-dependent hydrogen production are organic acids (Sasikala et al., 1993). The theoretical conversion reactions of these carbon sources are given in Reactions 1.9, 1.10, 1.11 and 1.12.

Acetate: $C_2H_4O_2 + 2H_2O \rightarrow 2CO_2 + 4H_2$ (1.9)

Lactate: $C_3H_6O_3 + 3H_2O \rightarrow 3CO_2 + 6H_2$ (1.10)

Glucose: $C_6H_{12}O_6 + 6H_2O \rightarrow 6CO_2 + 12H_2$ (1.11)

Ethanol: $C_2H_6O + 3H_2O \rightarrow 2CO_2 + 6H_2$ (1.12)

The assimilation of acetate has a special pathway called “citramalate cycle” in *Rb. capsulatus* (Kars and Gündüz, 2010).

Organic compounds are oxidized in TCA (Tricarboxylic acid or Citric acid) cycle where CO_2, protons and electrons are gained for further process in hydrogen production metabolism (Figure 1.2). The ions of TCA cycle are transferred by electron carriers NAD (nicotinamide adenine dinucleotide) and Fd (ferredoxin) through the nitrogenase enzyme. Meanwhile, ATP is produced by generation of a proton gradient formed during electron flow through the photosynthethic membrane apparatus (bacteriochlorophyll in the reaction center) forced by captured light energy. Nitrogenase enzyme incorporates all the protons, electrons and ATPs that are channeled towards it and produces molecular hydrogen by reducing protons (Koku et al., 2002). In Figure 1.3, the overall scheme of hydrogen production by PNS bacteria is shown.

It was reported by Fujii et al. (1987) that alcohols is a suitable electron donors than organic acids by means of their chemical structure; however, information on hydrogen evolution by using alcohols are limited. Imhoff et al. (2005) indicated that

Rhodospirillum rubrum and some strains of *Rhodopseudomonas palustris* can utilize ethanol as carbon source. In another study, Garrity et al. (2005) presented that *Rhodobacter sphaeroides* can utilize ethanol while *Rhodobacter capsulatus* can not use ethanol as photosynthetic electron donor. However, *Rhodobacter capsulatus* can utilize propanol, some strains can also utilize mannitol, sorbitol as photosynthetic electron donor (Garrity et al. 2005). These findings were also supported by Weaver et al. (1975), they screened thirty-three strains of *Rhodobacter capsulatus* by using different carbon sources including 51 mM EtOH (calculated based on the data in paper) in the media and showed that bacteria can not consume ethanol. Foster (1944), explained that an external supply of CO_2 (i.e. $NaHCO_3$), source is needed while using alcohols for biohydrogen production. The reason of this is explained as alcohols are more reduced than the cell material so CO_2 should be in the system to be the final electron acceptor during the dehydrogenation of alcohols and this reaction results in a net uptake of CO_2 (Foster, 1944). The need of external final electron acceptor while using alcohols as carbon sources was also supported by findings of Quayle and Pfennig (1975) and they used formate and ethanol together. Fujii et al. (1987) indicated that no bicarbonate was required for the hydrogen evolution of *Rhodopseudomonas* sp. No. 7 from media containing ethanol (21.7 mM) and malate (7.4 mM) as electron donors and yielded 48% conversion. Also, cells grown in a media containing glutamic acid as nitrogen source could produce hydrogen regardless presence of bicarbonate, but it was opposite when ammonium chloride was used as nitrogen source (Fujii et al., 1987). In addition, it was showed that hydrogen production was increased by up to 0.1% ethanol (21.7 mM) but above 0.2% (43.4 mM) was inhibited and stopped at about 0.6% (130.2 mM) (Fujii et al., 1987). In this context, the concentration of the ethanol inside the medium and the presence of other nutrients may come up to be important for photofermentative hydrogen production. The molarity ratio of ethanol to organic acid in the hydrogen production media or dark fermentation effluent ($R_{ethanol/abundant\ organic\ acid}$) may have an important role for an efficient photofermentative hydrogen production. Moreover, in the perspective of using dark fermentation effluents, $R_{e/a}$ may give the prospective hydrogen yield during the photofermentation.

Although Weaver et al. (1975) presented that *Rb. capsulatus* B10 can not grow on ethanol, methanol, or glycerol, Pantazopoulous and Madigan (2000) used primary alcohols and di-alcohols as growth substrates to show versality of *Rb. capsulatus* B10 in order to screen the growth characteristics of this microorganism. They indicated *Rb. capsulatus* B10 can grow phototrophic but not chemotrophic only on ethanol and the optimum and maximum ethanol concentration in media found to be 0.2% (v/v) and 4% (v/v), respectively. In addition, they observed longer generation time when ethanol was used as growth substrate compared to other alcohols which have carbons between 3 and 9. Laurinavichene et al. (2008) indicated ethanol and methanol inhibited the growth of *Rb. capsulatus* B10 by 50% at ~0.65 M and showed 50% inhibition of hydrogen production at ~1.3-1.8 M while butanol hampered both growth and hydrogen production at only ~0.05 M.

In order to metabolize alcohols, the first enzyme that comes to one's mind is alcohol dehydrogenase enzyme due to being the first enzyme of the alcohol degradation process by cells as indicated also by Pantazopoulous and Madigan (2000). Yamanaka and Minoshima (1984) have found two dye-linked alcohol dehydrogenases in *Rhodopseudomonas acidophila* 10050 grown anaerobically on methanol and in *Rhodopseudomonas acidophila* M402 grown aerobically on vanillyl alcohol. Also, it was presented that *Rhodopseudomonas* sp. No. 7 (Fujii et al., 1987) and *Rhodospirillum rubrum* (Fujii et al., 1983) possess NAD-linked alcohol dehydrogenase. Fujii et al. (1998) suggested that ethanol metabolized through Calvin-Benson cycle due to the fact that photoanaerobic growth requires an external CO_2 as bicarbonate and high activity of phosphoenolpyruvate carboxylase (PEPC) and phosphoenolpyruvate carboxykinase (PEPK) in *Rhodopseudomonas* sp. No. 7 when ethanol-bicarbonate medium was used. And these enzymes link Embden Meyerhof Parnas and Calvin Benson cycle side and the TCA cycle-glyoxylic acid cycle side in PNS bacteria (Fujii et al., 1998). Haselkorn et al. (2001) reported that *Rb. capsulatus* involves periplasmic ethanol deyhydrogenase and acetaldehyde dehydrogenase in its genome which resemble *P. aeruginosa*'s open reading frames. However, all the genes that are related to ethanol degradation pathway are clustered in *P. aeruginosa*, while in *Rhodobacter* genome they are distributed. In this context,

ethanol seems to enter the carbon cycle from Acetyl-CoA (synthesized from acetate by Acetyl-coenzyme A synthase), after converted to acetate by acetaldehyde dehydrogenase. And then acetate can be metabolized through citramalate cycle furtherly in *Rb. capsulatus* (Meister et al., 2005).

Maeda et al. (1999) demonstrated that nitrogenase enzyme was completely repressed at an ethanol concentration of 1 mM in nitrogen-deprived cultures of *Rhodovulum sulfidophilum*. Nepple and Bachofen (1997) reported that *Rb. sphaeroides* 4% ethanol in the media caused modification in the protein pattern of bacteria and specific or general stress responses were detected. In addition, it was reported that alcohols may influence the lipid composition of the cell membrane which may cause changes in the activity of a membrane fixed enzyme, nitrogenase, or the permeability of the cell membrane for substrates and hydrogen (Fujii et al., 1987). Sharp et al. (1998) studied on electron transfer chains of *Rb.capsulatus* which includes ubiquinone: cytochrome (cyt) *c* oxidoreductases (bc_1 complexes). They found that bc_1 complex were not affected by ethanol (even at 900 mM EtOH) resulting no effect on the redox state in the structure. The *bc*1 complex is associated with both light-driven electron transfer and dark respiration in facultative phototrophic bacteria, but is necessary only for photosynthetic growth (Liebl et al., 1997).

Besides nitrogenase enzyme, hydrogenase enzyme participates in hydrogen metabolism. Since hydrogenase enzyme acts as an uptake enzyme that utilizes the produced hydrogen, the final produced hydrogen is the quantity produced by nitrogenase minus the amount consumed by uptake hydrogenase (Vignais et al., 1985).

During the hydrogen production by-products such as Poly-β-hydroxyl butyric acid (PHB) and carotenoids can be synthetized. The general view of H_2 related pathways in PNS bacteria is shown in Figure 1.3.

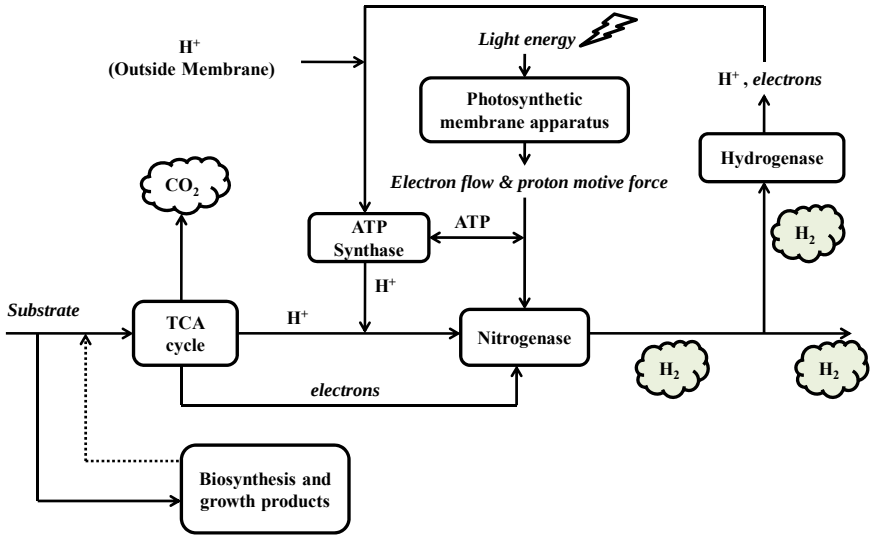

Figure 1.3 The overall scheme of hydrogen production by PNS bacteria, adapted from Koku et al. (2002)

1.3.2 Enzyme System Components

Hydrogenase and nitrogenase mediate the hydrogen production metabolism of PNS bacteria. The comparison of hydrogenase and nitrogenase can be seen in Table 1.3.

Table 1.3 Comparison of nitrogenase and hydrogenase enzymes, adapted from Basak and Das (2007)

Characteristics	Hydrogenase	Nitrogenase
H_2 production	Yes	Yes
H_2 uptake	Yes	No
Reaction Energy dependent	No	Yes
Oxygen sensitivity	Yes	Yes
Catalytic rate	High	Low
Present in prokaryotes	Yes	Yes
Present in eukaryotes	Yes	No

1.3.2.1 Hydrogenases

Hydrogenase enzymes are found in microalgae, cyanobacteria, and anoxygenic photosynthesis and fermentative bacteria. These enzymes can perform either "uptake" or "evolution" act of the individual hydrogen metabolism. [NiFe]-hydrogenases (in bacteria and cyanobacteria) and [FeFe]-hydrogenases (in obligate anaerobic fermentative bacteria and green microalgae) are the most familiar hydrogenase enzymes in literature. Nitrogen-fixing bacteria possess [NiFe]-hydrogenases that can consume the by-product of nitrogenase (molecular hydrogen) (Eroglu and Melis, 2011).

Hydrogenase enzyme is a membrane-bound H_2-uptake hydrogenase (shown in Figure 1.6) and can catalyze the reversible Reaction 1.13:

$$2H^+ + 2e^- \longleftrightarrow H_2 \qquad (1.13)$$

Due to the consumption of hydrogen by hydrogenase decreasing the hydrogen production yield, genetic studies related to deletion of hydrogen enzyme performed by researchers. One of the studies about this approach is the deletion hydrogenase enzyme of *Rb. capsulatus* MT1131 through interposing mutagenesis which developed a hup^- mutant strain (YO3). It is reported that hydrogen production rate and substrate conversion efficiency of mutant were higher than those with wild type *Rb. capsulatus* MT1131 strain (Öztürk et al., 2006).

1.3.2.2 Nitrogenases

Although nitrogenase was primarily designed for nitrogen fixation in PNS bacteria, the hydrogen is produced by nitrogenase enzyme in PNS bacteria as a by-product (Reaction 1.14). In this context, the specific conditions which were explained in section 1.3.1 should be set for efficient hydrogen production.

$$N_2 + 8H^+ + 8e^- + 16ATP \rightarrow 2NH_3 + H_2 + 16ADP + 16P_i \quad (1.14)$$

There are two main parts of nitrogenase (Eroglu and Melis 2011):

- **The reductase subunit:** It is a Fe-S protein encoded by the *nif*H gene and it transfers electrons that were gathered from electron donor to dinitrogenase complex.
- **The dinitrogenase complex:** It is a Mo-Fe-S protein encoded by the *nif*D and *nif*K genes. Its duty is to reduce the N_2 bonds resulting 2 moles of NH_3.

Separately, each of these two proteins has no activity; the two together form the active nitrogen complex.

Nitrogenases can be ordered with respect to their metal cofactor in the catalytic site. Depending on the cofactor, nitrogenases have different stoichiometries of ammonia and hydrogen generation (Reaction 1.15, 1.16, 1.17) (Eroglu and Melis 2011).

Molybdenum-nitrogenase: $N_2 + 8H^+ + 8e^- \rightarrow 2NH_3 + H_2 \quad (1.15)$

Iron-nitrogenase: $N_2 + 21H^+ + 21e^- \rightarrow 2NH_3 + 7.5H_2 \quad (1.16)$

Vanadium-nitrogenase: $N_2 + 12H^+ + 12e^- \rightarrow 2NH_3 + 3H_2 \quad (1.17)$

During the decomposition of organic compounds surplus of electrons are formed by PNS bacteria and these excess electrons have to be sent from the system to provide growth and metabolic activity. Thus, under nitrogen limitation, the activity of nitrogenase through the reaction (1.18) comes up as a metabolic need to resume redox balance (Keskin et al., 2011). In other words, in the absence of N_2, nitrogenase behaves like ATP dependent hydrogenase and all the electrons are utilized for hydrogen production (Kars and Gündüz, 2010).

$$2H^+ + 2e^- + 4ATP \rightarrow H_2 + 4ADP + 4P_i \quad (1.18)$$

In contrast, when N_2 is available in the media, the need that occurs as a result of assimilation of organic compounds compensated by CO_2 fixation by RuBisCo and the released CO_2 during the growth is retaken through Calvin cycle (Keskin et al., 2011).

Nitrogenase is an iron-sulfur molybdenum enzyme and it is so sensitive to oxygen. In addition, active enzyme demands molybdenum and iron (Masepohl and Hallenbeck, 2010). Akköse et al. (2009) reported that hydrogen production of *Rb. sphaeroides* O.U.001 under anaerobic conditions was 3 times as higher than under aerobic conditions. In addition, regarding to the mechanism of nitrogenase that is mentioned earlier, high ammonium concentrations also repress nitrogenase activity (Akköse et al., 2009).

1.4 By-products

PNS bacteria offer possible application areas other than hydrogen production. Due to the rich content of PNS bacteria's biomass, the biomass can be recycled as fertilizer, supplementary animal food etc (Pekgöz, 2010).

PHB is the most common polyhydroxyalkanoic acid (PHA) produced by the PNS bacteria. PHB (Poly-β-hydroxy butyric acid) is a widespread intracellular storage compound which is produced during unfavorable growth conditions, especially under stress. Accumulation of PHB is induced by high C/N ratio conditions as a consequence of limited growth by lack of nitrogen and sulfur source (Hustede et al., 1993). They have also observed that PHB production tends to increase when the carbon source is acetate. *Rb. capsulatus* has a different acetate assimilation pathway (citramalate cycle) as noted before in section 1.3.1. This pathway is apart from CO_2 fixation and PHB biosynthesis; therefore, it might indicate that *Rb. capsulatus* has a better ability to produce hydrogen on acetate which is the product of dark fermentation (Kars and Gündüz, 2010).

PHB biosynthesis competes with hydrogen production since it is another pathway for maintaining the redox balance in the cell owing to the organic compound assimilation. To overcome this competition, Kim et al. (2006) examined on wild type and phb$^-$ mutant strains of *Rb. sphaeroides* KD131 and demonstrated that maximum hydrogen production with the mutant strain was 1.3 fold higher than the wild type.

1.5 Feedstocks for Biological Hydrogen Production

Biomass materials which are used for biological hydrogen production can be waste or by-products of other biological processes (i.e. agricultural residue, wood trimmings) and those that are grown particularly for energy production (energy crops). There are several important features that are searched for biomass materials; availability, cost, carbohydrate content, and biodegradability. Pure carbohydrate sources such as glucose and sucrose are suitable substrates for hydrogen production but they are not applicable owing to their costs (Kapdan and Kargı, 2006). Therefore, wastes offer a good opportunity for energy production. Available feedstocks for photofermentation can be classified as organic acid, simple sugar and complex carbohydrate containing wastes according to their carbon content. Waste streams of brewing, dairy, sugar, olive oil industries, and also cassava, corncobs, potato steam peels, and wheat ground solution constitute famous waste sources recently (Keskin et al., 2011). Using abundant organic residue effluents from these various industries especially sugar beet processing may reduce cost and environmental impact. From this point of view, sucrose containing biomass (i.e. sugar beet, sugar cane, sweet sorghum) and by-products from these biomass processing industries could be suitable sources for hydrogen production due to their content of fermentable sugars which have the simplicity of direct usage for fermentation (Urbaniec et al., 2009). Thick juice is the concentrated form of sugar beet juice after evaporation with a total soluble solids content of about 69 ^{o}Bx (Justé et al., 2008). Therefore, it reveals a good choice of biomass source for dark fermentation, not only for its fermentable sugar content but also for its abundance.

These biomass sources can be used through either one-step photofermentation or separately two-step dark-photofermentation. Studies on two step biohydrogen

production using different feedstocks have been reported for molasses (Özgür et al., 2010a), potato steam peels (Özgür et al., 2010b), miscanthus hydrolysate (Uyar et al., 2009b), ground wheat solution (Argun et al. 2009), and cassava starch (Su et al. 2009). Most of these studies were carried out in small scale, indoor and batch experiments.

The variety of produced by-products during the dark fermentation may depend on the the nature of plant biomass. In this context, the NH_4^+ concentration, pH, C/N ratio are important on account of photofermentation needs as mentioned previously. In addition, concentration of carbon source, type, and clarity of the dark fermentation effluent, absence of major cofactors of nitrogenase enzyme (Mo and Fe) or presence of inhibitory factors (i.e. high concentrations of ethanol, heavy metals, phenolics or other aromatic hydrocarbons) may lead to an adjustment such as addition of Fe and Mo and dilution of the effluent. In addition, before photofermentation, wastewater may need to be sterilized to prevent growth of indigenous fermentative bacteria, which remained after dark fermentation of the biomass (Keskin et al., 2011).

In brief, in order to combine thermophilic fermentation and photofermentation, it is mandatory to show the suitability of dark fermentation effluents and to proceed the necessary treatments for the photofermentative hydrogen production.

1.6 Photobioreactors

A bioreactor is the equipment which enables the microbial growth. In case of a photobioreactor design and operation, additional factors, which are how to use proper light sources (intensity and wavelength), how to improve light conversion efficiency, and how to resume suitable cell concentration during continuing process should be considered (Chen et al., 2011).

The physical factors influencing the performance of a photobioreactor can be listed as (Dasgupta et al., 2010):

- Light penetration
- High area to volume ratio (A/V ratio)
- Temperature control
- Transparency and durability of the material construction
- Gas exchange
- Agitation system

Among these physical parameters, materials of construction have a major effect on construction and sustainability costs. Construction material should have high transparency and resistance to produced chemicals, and it should be flexible, non-toxic, cheap and durable (Dasgupta et al., 2010). Many types of construction materials can be used for photofermentive hydrogen production operations; including photobioreactors made of acrylic sheet (Modigel et al., 1998), stainless steel frame and polycarbonate panels (Hoekama et al., 2002), glass bottles (Eroglu et al., 2004) and low density polyethylene (LDPE) (Boran, 2011). Polyethylene (PE) and polypropylene (PP), polycarbonate (PC), polyvinyl chloride (PVC) tubes can lose their transparency due to being exposed to sunlight. However, polymethyl methyl acrylate (PMMA) and teflon could retain their transparency in outdoor conditions (Tredici, 1999).

Temperature control of the photobioreactors plays a significant role during the outdoor operations to prevent the death of bacteria. Several methods can be used to control the temperature in outdoor PBRs such as immersion of the reactor in a cooling water, water spraying, and shading (Tredici, 1999). Dasgupta et al. (2010) reported that water spraying only during overheating and collecting the used water for another time is the most economical cooling method. Another cooling method was reported by Avcıoglu et al. (2011), they used chilled water circulating through cooling coils placed inside the PBRs. Photobacterial growth and the hydrogen productivity of photosynthetic bacteria in an outdoor reactor system are strongly

affected by fluctuations in temperature and light intensity due to day/night cycles and due to seasonal, geographic, and climatic conditions (Özgür et al., 2010c, Androga et al., 2011a). In addition to temperature, solar radiation is a major physical variable in outdoor conditions. A PBR should have high A/V ratio in order to dilute the light and distribute it as much as possible. This improves the biological process and decreases the duration of light exposing of cells (Akkerman et al., 2002). Thus, light utilization in PBRs is an important parameter to have high yields of hydrogen. Androga et al. (2011a) demonstrated the effect of low temperature/low light intensity and high temperature/high light intensity in winter and summer seasons, by using flate-panel PBRs. They showed that the yield factor found in summer was 4.1 times higher than the one acquired in winter.

Photobioreactors can be classified by according to their design or mode of operation. Various photobioreactor types are given in Figure 1.4.

- **In design terms:** (1) Flat or tubular (2) horizontal, inclined, vertical or spiral (3) manifold or serpentine (Tredici, 1999)

- **In operational terms:** (1) batch (2) fed-batch (3) continuous (Dasgupta et al., 2010)

Flat and tubular PBRs are usually most preferred types of PBRs (Akkerman et al., 2002).

- **Flat panel PBRs:** It consists of rectangular transparent box with a depth of only 1-5 cm and the height and width can be varied to some extent (Akkerman et al., 2002). It has a large illumination surface area which enhances the cultivation of photosynthetic bacteria and also it is cheap and easy to clean up. However, their scale-up and temperature control are difficult and also biofilm formation on the surface of the PBR can be observed (Chen et al., 2011).

- **Tubular PBRs:** It consists of long transparent tubes (diameters 3 to 6 cm) and lengths ranging from 10 to 100 m. The culture liquid is pumped inside the tubes. The position of tubes can be positioned according to the design. The length of the tubes is limited due to accumulation of gas. Scale-up is easy to do for tubular PBRs, a number of tubes via manifolds can be connected (Akkerman et al., 2002).

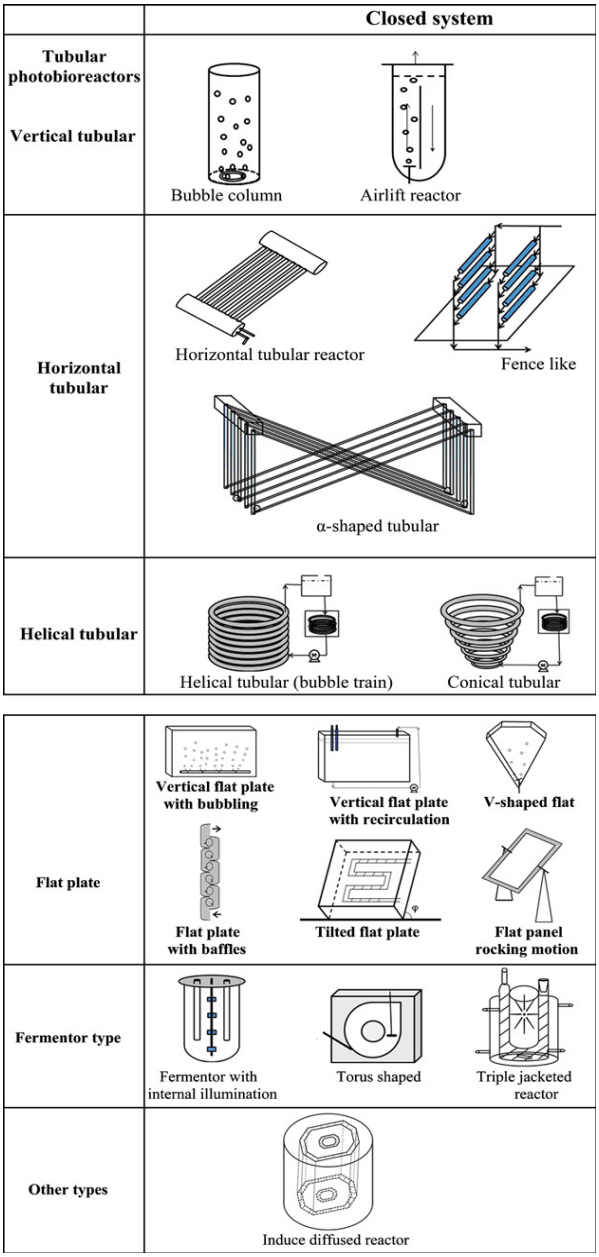

Figure 1.4 Schematic representation of the different photobioreactor for biomass and hydrogen production (Dasgupta et al., 2010)

In batch process, hydrogen production stops when the cells attain stationary phase. There are many batch-indoor conducted studies in literature and they leaded the outdoor studies (Argun and Kargı, 2011). On the other hand, continuous culture studies are in limited number. Hoekama et al. (2006) presented continuous hydrogen production in a pneumatic flat panel PBR and they indicated that during continuous hydrogen production the concentration of NH_4^+ less than 2 mM and total volatile fatty acids lower than 2500 mg L^{-1} should be provided.

Apart from the batch and continuous mode of operations, fed-batch mode offers several advantages. The feed flow and composition can be regulated, which enables to adjust metabolic rates. Boran et al. (2011) reported fed-batch operation of 80 L tubular photobioreactor by using defined medium (40 mM acetate / 2 mM glutamate) with over all yield of 0.6 mol H_2/mol acetic acid in outdoor conditions for 30 days. Gebicki et al. (2010) worked with fed-batch operated flate-panel PBR by using acetate/lactate medium and they received productivity of 1.09 mmolH_2/L_c/h for 25 days. The first outdoor, panel, fed-batch experiment was conducted by Kim et al. (1987) and they reported the hydrogen productivity of 2.19 mmolH_2/L_c/h by using lactate medium for 47 days.

1.7 Clinoptilolite Zeolite

Effluents that have high ammonia concentrations are doubtful for use in photofermentation owing to inhibition of nitrogenase synthesis or activity (Keskin et al., 2011). In order to prevent the inhibitory effect of ammonium ions, removal of these ions from the effluents is necessary.

The natural zeolite clinoptilolite allows the removal of ammonium ion in dark fermentation effluents via ion-exchange method. Actually, natural zeolites have been used in water and wastewater treatment applications (the removal of toxic and noxious cations) due to their capability to endure ion-exchange and adsorption (Bahaallddin, 2010). Other applications of natural zeolites can be listed as animal feeding, horticulture, odor control, desiccant, fungicide and pesticide carrier, water

filtration, gas adsorbent, catalysis, aquaculture, medicinal and pharmaceutical applications (Renzo and Fajula, 2005).

Clinoptilolite zeolite has been mined in USA, Australia, Russia, Slovenia, Cuba, Indonesia , South Africa, Greece, Bulgaria, New Zealand, Turkey, China, Mexico, Hungary, Jordan and Outer Mongolia (Dyer, 2005). Western Anatolia region, especially Manisa-Gördes and Balıkesir-Bigadiç have the most reserves in Turkey (Bahaallddin, 2010). Therefore, natural zeolites, exist abundantly and their low-cost, simplicity of application and regenerative properties make them attractive (Androga et al., 2011b). Zeolites are natural minerals, which can be defined chemically as aluminum silicates (Abd El-Hady et al., 2001). Clinoptilolite, the natural zeolite, mineral has the most wide range of distribution in nature and this type of zeolites are broadly rich in K^+ and Na^+ exchangeable ions (Bahaallddin, 2010). The structure of clinoptilolite zeolite is $(Na, K)_6(Ca, Sr, Ba, Mg)_3[Al_6Si_{30}O_{72}].\sim 20H_2O$ and it was discovered in 1923 (Colella, 2005). The alumina tetrahedral channels containing exchangeable cations such as K^+, Na^+, Mg^{2+}, Ca^{2+} and microporous configuration of silica constitutes the clinoptilolite structure. As it is seen in its chemical formula, Si/Al of clinoptilolite is above 4 and it belongs to heulandite class of zeolites (Androga et al., 2011b). Si/Al ratio can vary within the same zeolite type family and it influences the cation selectivity of the zeolite during the cation exchange procedure; however, generally it is reported that zeolites with high silicon content tends to prefer cations with low charge density (i.e. NH_4^+) (Colella, 2005). Since clinoptilolite zeolite Si/Al ratio is high, it can be interpreted that clinoptilolite zeolite has a high affinity to NH_4^+. The selectivity of clinoptilolite zeolite is $NH_4^+ > Pb^{2+} > Na^+ > Cd^{2+} > Cu^{2+} \approx Zn^{2+}$ (Leung et al., 2007). During the cation exchange by zeolites, besides the zeolite type that is used in removal of specific compound, the temperature, the concentration of the cation species in effluent, pH, and the solvent can affect the process (Bahaallddin, 2010). To improve the zeolite's ion-exchange performance, conditioning of zeolite can be applied. At the end of this conditioning process, zeolite becomes homoionic by increasing the content of a single cation (i.e. Na^+). The most used chemical for pretreatment of zeolite is NaCl (Bahaallddin, 2010).

In a recent study, 80% of NH_4^+ ions in dark fermentation effluent of molasses were removed with Na-form clinoptilolite zeolite (Androga et al., 2011b). In an another study, Nguyen and Tanner (1998) reported that 87-98% of NH_4^+ ions were removed from wastewaters by using natural zeolite in batch mode.

1.8 Objective of this Study

The main objective of this thesis study was to investigate the hydrogen production using dark fermentation effluent of sugar beet thick juice (DFESGTJ) by *Rb. capsulatus*. First, the photofermentability of the effluent was analyzed using *Rb. capsulatus* YO3 in a panel PBR (4 L) operating in fed-batch mode in outdoor conditions. Throughout the study, biomass, pH, hydrogen production, air and PBR temperatures, organic acid concentration, PHB concentration, bacteriochlorophyll *a* concentration were followed and analyzed. Secondly, exploring the effect of ammonium removal by natural zeolite on DFESGTJ and following small scale (150 mL bottle PBRs) hydrogen production experiments by *Rb. capsulatus* DSM1710 and *Rb. capsulatus* YO3 (hup^-) were aimed since ammonium inhibits nitrogenase enzyme activity. Lastly, studying the effect of ethanol on the hydrogen production by *Rb. capsulatus* DSM1710 and *Rb. capsulatus* YO3 (hup^-) was also targeted as it is present in dark fermentation effluents and its interference with hydrogen production was not researched previously. For these small scale indoor experiments, pH, biomass, hydrogen production, ethanol concentration (just for the ethanol experiment), PHB concentration and organic acid concentration parameters were recorded in order to interpret the merit of hydrogen production.

CHAPTER 2

MATERIALS AND METHODS

2.1 The Organisms

The organisms used in this study were *Rhodobacter capsulatus* DSM 1710 strain and *Rhodobacter capsulatus* YO3 (hup^-). *Rhodobacter capsulatus* wild type (DSM 1710) strain was obtained from DSMZ (Deutsche Sammlung von Mikroorganismen und Zellkulturen GmbH, DSM, Braunsweig Germany). *Rhodobacter capsulatus* YO3 (hup^-) (mutant strain lack of uptake hydrogenase enzyme) was genetically modified strain from *Rhodobacter capsulatus* MT1131 (Öztürk et al., 2006).

2.2 Culture Media

2.2.1 Growth Media and Conditions

Modified form of the minimal medium of the Biebl and Pfennig (1981) was used for bacterial culture growth. Acetate (20 mM) and glutamate (10 mM) were used as carbon and nitrogen sources, respectively. All the components of medium were dissolved in distilled water and pH was adjusted to 6.3-6.4 by using NaOH and the media was autoclaved (Nüve). Previously sterilized vitamin solution, trace elements, and iron-citrate were added after autoclaving. The contents of medium, trace elements, iron-citrate, and vitamin solutions are given in Appendix A.

10% (v/v) inoculum were done into bottles containing growth media, and bottles were flushed with Argon to form anaerobic atmosphere. Then, bottles were placed in

an incubator with temperature control (Nüve, ES250) and illuminated with 75-100 W tungsten lamps. Light intensity on the bottles were adjusted to 2000-2500 lx. Bacterial culture were grown untill they reached approximately 1 g/L cell density.

2.2.2 Hydrogen Production Media

2.2.2.1 Artificial Media

The defined (artificial) medium of Biebl and Phennig (1981) containing 30 mM acetate and 2 mM glutamate was used as hydrogen production medium. Same procedure was applied to the preparation of defined hydrogen production medium as described in Section 2.2.1.

2.2.2.2 Dark Fermentation Effluent of Sugar Beet Thick Juice

Dark fermentation effluent of sugar beet thick juice (DFESBTJ) was acquired from PROFACTOR, Austria. It was obtained by fermentation of sugar beet thick juice by extreme thermophile *Caldicellulosiruptor saccharolyticus*. Three different DFESBTJ obtained from PROFACTOR. For the panel photobioreactor (PBR) experiment, DFESBTJ1 was used and for the small scale bottle experiments, DFESBTJ2 and DFESBTJ3 were used.

Several adjustments to the DFESBTJ were considered before feeding into the photofermentation. The adjustments applied were centrifugation, dilution, buffer addition, Fe (Fe(III)-citrate, 0.1 mM) and Mo ($Na_2MoO_4.2H_2O$, 0.16 μM) supplementation, pH adjustment and sterilization. The DFESBTJ was centrifuged prior to use in order to obtain a liquid which is visually clear and free from colloidal particles such as biomass from the dark fermentation process.

As can be seen in Table 2.1, the iron and molybdenum contents of DFESBTJ were below the detection limits of the instruments used for analysis. Therefore, in order to enhance the hydrogen production, Fe and Mo were added to the DFESBTJ. In order to keep pH stable at the desired level (6.0–8.0), 22 mM of KH_2PO_4 was added into

the centrifuged and diluted media as buffer and the initial pH was adjusted to 6.5 by addition of NaOH or HCl. The final DFESBTJ was sterilized by heat at 121°C for 15 min in order to kill other organisms that can interfere with the desired bioprocess.

Table 2.1 The composition of DFESBTJ used in experiments

Component	DFESBTJ1	DFESBTJ2	DFESBTJ3
Acetate (mM)	125	40	92
Lactate (mM)	0	16	10
Ethanol	NA	18.8	59
Molar ratio of Ethanol/Acetate	NA	0.470	0.641
NH_4^+ (mM)	7.7	9	23.6
TOC (mM)	168	80	78
TN (mM)	10	8.5	34.4
Molar C/N ratio	16.8	9.41	2.26
COD (mg/L)	12080	7360	18520
Mo (µM)	0	0	0
Fe (mM)	0	0.011	0.025
Ca (mM)	0.106	0.181	0.151
Zn (µM)	2	4.32	8.53
Mg (mM)	4.81	0.142	0.151
Na (mM)	206	59.1	165
Mn (µM)	0.901	NA	NA
Co (µM)	NA	0.0	1.51
Mn (µM)	NA	0.442	4.05
Cu (mM)	NA	0	0
Ni (µM)	NA	1.65	1.11

NA: not available

2.3 Experimental Set up and Procedure

2.3.1 Panel Photobiorector Experiment

The DFESBTJ which contained 125 mM of acetate was diluted three times with distilled water and the acetate concentration was decreased to 42 mM. Then, it was supplemented with iron (Fe(III)-citrate, 0.1 mM) and molybdenum ($Na_2MoO_4.2H_2O$, 0.16 µM) which are two essential co-factors of nitrogenase. One run of *Rhodobacter capsulatus* YO3 (hup^-) was carried out in this experiment.

Experiment was carried out in 4 L panel photobioreactor (PBR) (Height: 45 cm, Length: 45 cm, Width: 2 cm) made of transparent acrylic sheets (Figure 2.1). The reactor was sterilized chemically by using H_2O_2 (3% v/v) before the run. At the start up, 25% v/v inoculation was made into the bioreactors. Anaerobic atmosphere was created by using argon gas. The experiment was carried out in September 2009, in Ankara (Turkey). During day time, the temperature of the PBR was controlled with chilled water circulating through PVC cooling coils placed inside the PBR. The evolved gas was collected in a water filled graduated glass cylinder connected to the PBR (Figure 2.2). The PBR was first operated in batch mode until bacterial growth reached to the stationary phase (cell density≥0.7 gdw/L_c), then in fed-batch mode with a daily feeding of 10% by the volume of the bioreactor until the end of the run. Throughout the fed-batch part, liquid samples were taken for the analyses before feeding. The detailed total global solar radiation data were also taken from the National Meteorology Institute of Turkey.

Figure 2.1 Picture of outdoor panel PBR (4L) with internal cooling coil run by *Rb. capsulatus* YO3 (hup^-) on DFESBTJ

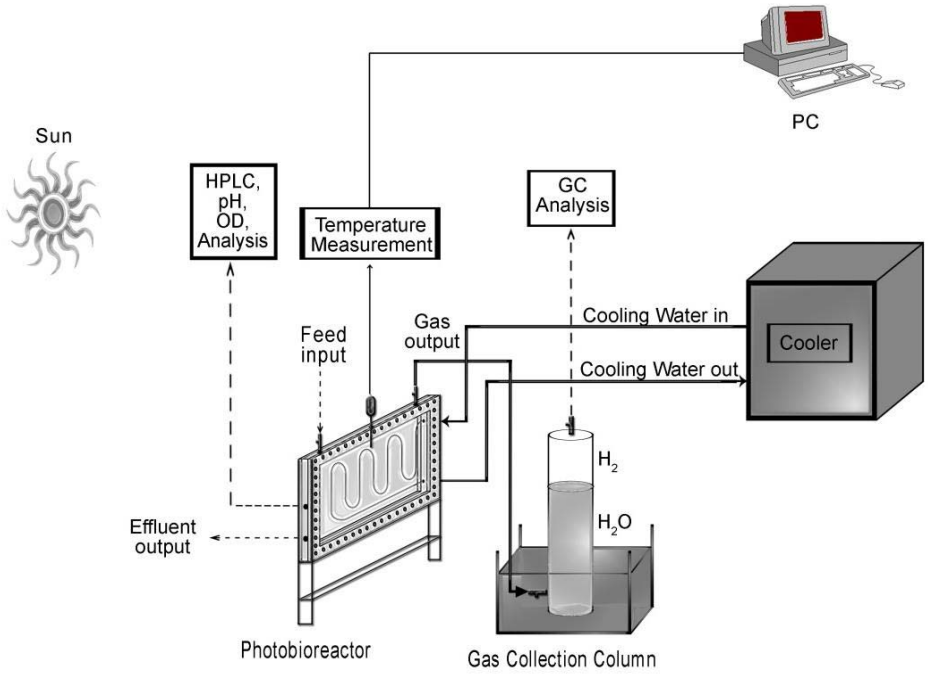

Figure 2.2 Experimental set up of the PBR with internal cooling coil (Avcıoğlu, 2010)

2.3.2 Bottle Photobioreactor Experiments

Small-scale experiments were carried out in 150 ml glass bottle PBRs in batch mode. 10% (v/v) bacterial cultures were added into hydrogen production media and the bottles were sealed with sterilized rubber tap. Anaerobic conditions were provided by purging the bottles with Argon. 2000-2500 lux light intensity was supplied using 75-100 W tungsten lamps (measured by luxmeter, Lutron LX-105 Light Meter). The conversion factor was determined as 1 W/m^2= 17.5 lux (Uyar, 2008) for indoor experiments. The evolved gas was collected in a water filled graduated glass cylinder connected to the PBR and determined volumetrically. The experimental setup of hydrogen production is shown in Figure 2.3.

Figure 2.3 The experimental setup of hydrogen production

DFESBTJ2 and DFE of DFESBTJ3 have a concentration of 40 and 90 mM acetate, respectively (Table 2.1). These DFESBTJ samples were diluted to reach 30 mM acetate with KH_2PO_4 (22 mM) buffer supplemented with Mo (0.16 μM) and Fe (0.1 mM) as described in section 2.2.2.2.

After inoculation of bacterial culture into hydrogen production media (30/2 Acetate/Glutamate), filter-sterilized (20 μm pore size) ethanol were added to the culture, and sealed with sterilized rubber tap. Ethanol concentrations in hydrogen production media are shown in Table 2.2.

Table 2.2 Ethanol concentration used in the defined medium

Ethanol (mM)	6.25	12.5	25	37.5	50	100	200
$R_{ethanol/acetic\ acid}$ (mM/mM)	0.2	0.4	0.8	1.2	1.6	3.3	6.6

In order to obtain anaerobic conditions, the bottles were sparged by argon gas for about 3 minutes. Samples (2.5 mL) were taken daily from the PBR using a sterile syringe and analyzed. The culture was flushed with argon gas for 10 seconds, in order to prevent the negative pressure in the PBR after sampling. All of the tests were repeated in duplicate.

2.3.3 Ammonium Ion Removal

2.3.3.1 Preatreatment of Clinoptilolite Zeolite

Clinoptilolite samples obtained from Gördes-Manisa, Turkey, were used in ammonium ion removal (Picture can be seen in Appendix G). In order to improve the zeolite's effective exchange capacity, the natural zeolite was pretreated with brine solution and the exchangeable cations in the zeolite (K^+, Mg^{2+}, Ca^{2+}) were replaced with more easily removable ones such as Na^+ ions (Inglezakis et al., 2001). 50 g of clinoptilolite samples with particle size of 0.42 mm to 0.853 mm were batch treated using 500 ml of 1M NaCl brine solution (Bayraktaroğlu, 2006). Mixtures were stirred using a wrist-action shaker (Fisher-Kendall mixer) at ambient temperature for 13 days and solution was renewed with freshly prepared 1 M NaCl at 24 hour intervals (Figure 2.4).

When the cation concentration (K^+, Ca^{2+} and Mg^{2+}) in the effluent exchange solution reached saturation, the pretreatment procedure was stopped. The mixture was then decanted and the zeolite was washed using deionized water to get rid of NaCl traces. The presence of sodium ion was checked using 1 N $AgNO_3$ solution while washing the zeolite. The clinoptilolite was dried in an oven set at 105°C for 24 hours in order to evaporate water (Karadağ et al., 2006).

Figure 2.4 Clinoptilolite pretreatment setup

2.3.3.2 Ammonium ion reduction in the DFE of sugar beet thick juice

Two samples of DFESBTJ containing 9 mM and 23.6 mM ammonium were batch treated using Na-form clinoptilolite zeolite. The chemical compositions of the DFESBTJ samples are given in Table 2.1 (2 and 3). In order to remove ammonium, for 9 mM DFESBTJ, 2, 4, 6,8, 10 g of; for 23.6 mM DFESBTJ 5, 10, 15, 20 g of clinoptilolite zeolite was added to every sample (200 ml) in an Erlenmeyer flask and the solution was mixed in a water bath shaker (Clifton NE25) set at 25°C at 70 rpm agitation (Figure 2.5). During the treatment procedure, the ammonium ion concentration, pH and color of the DFESBTJ samples were measured and recorded at certain intervals.

Figure 2.5 Ammonium ion reduction setup

2.4 Analyses

2.4.1 pH Measurements

pH measurements were done with a pH meter (Mettler Toledo 3311) which was calibrated with standard solutions of 4.0, 7.0 and 9.21 in advance.

2.4.2 Cell Concentration Analysis

Bacterial growth in the culture was monitored by measuring optical density at 660 nm in a spectrophotometer (Shimadzu UV-1201). Distilled water was used as blank. Dry cell weights were calculated from the calibration curve given in Appendix B.

2.4.3 Organic Acid Analysis

Daily taken samples from PBRs were centrifuged for 10 minutes at 13600 rpm to precipitate the bacteria and obtain the supernatants. Supernatants stored at -20 ^{o}C for organic acid analysis. In order to remove impurities that may exist in the solution, samples were filtered via 0.45 μm nylon filters before the HPLC analysis.

The filtered samples of small scale batch experiments were analyzed by an Alltech IOA-1000 (300mm ×7.8 mm) HPLC column. In the analysis, 0.085 M H_2SO_4 was used as the mobile phase and the oven (Schimadzu CTO-10AS VP) temperature was kept constant at 66 °C. A low gradient pump (Schimadzu LC-20AT) with a degasser unit (Shimadzu DGU-20A) were used to maintain the mobile phase flow rate at 0.4 mL/min. An auto-sampler (Shimadzu SIL-20AC) injected 10 μL sample and a UV/VIS detector (Shimadzu SPD-20A) with absorbance set at 210 nm, was used to determine the component separation.

Lactic, formic, acetic, propionic and butyric acid concentrations were determined according to the calibration curves of pure organic acid standards. A HPLC chromatogram and calibration curve are given as example in Appendix D.

2.4.4 Gas Composition Analysis

Evolved gas was sampled by a micro syringe (Hamilton, 500μL) and injected (100μL) to a gas chromatograph (Agilent technologies 6890N) equipped with thermal conductivity detector and a Supelco carboxen 1010 column. The oven, injector and detector temperatures were 140, 160 and 170 °C, respectively. Argon was used as carrier gas at a flow rate of 25 ml/min. A typical gas analysis chromatogram is given in Appendix C. Agilent Chemstation v: B.01.01 software was available for analyses and the results were given in percentage.

2.4.5 Ethanol Analysis

Samples were filtered through a 0.45 μm nylon filter. Filtered samples were injected (1μL) to gas chromatograph (Agilent technologies 6890N) equipped with FID detector and a HP-FFAP column (30 m x 320 μm x 0.25 μm). The oven temperature was initially at 90 °C for two minutes and had a ramp with 20 °C/min until 140 °C (The oven temperature was kept at 140 °C for 3 min). The inlet heater temperature was 180 °C at 7.26 psi. The split ratio was 10:1 and split flow was 13.7 mL/min. Argon gas was used as the mobile phase (1 mL/min) and for the FID detector; hydrogen (35 mL/min) and air (350 mL/min) were used. A sample GC chromatogram and a calibration curve for ethanol are given in Appendix C. Internal standard was used in order to prevent instrument drift in retention time and mismeasurements that may happen due to the evaporization of ethanol. Therefore, concentrated n-butanol (1000 mM) was added to every 1000 μl sample to reach 20 mM n-butanol in the final.

2.4.6 Total Carbon (TC), Total Nitrogen (TN), Chemical Oxygen Demand (COD), Ammonium Ion and Color Analysis

Total carbon (Direct Method, 10129), total nitrogen (Persulfate Digestion Method, 10071), chemical oxygen demand (Reactor Digestion Method, 8000) and ammonium ion (Salicylate Method, 10031) analysis were done spectrophotometrically using

Hach-Lange TOC, TN, COD and NH_4-N kit (DR/2400, Hach-Lange Spectrophotometer). For the thermal reactions depending on the method, a COD reactor (WTW 3200) was used. In order to adjust the total carbon, total nitrogen, chemical oxygen demand and ammonia ion level of the sample is within the range of the method, samples diluted according to their content. Then the proceedings of each method are implemented to samples and deionized water (blank).

The color of the DFESBTJ was also determined using a DR/2400 Hach-Lange spectrophotometer at 455 nm (Program No:120). The stored programme is calibrated according to the standards of American Public Health Association (APHA). 1 color unit equals to 1 mg/L platinum as chloroplatinate ion (PtCo units). Deionized water was used as a blank solution. Samples were measured directly without using any reagent.

2.4.7 Elemental Analysis

The elemental analyses (Mn, Na, Ni, Co, Zn, Cu, Ca, Cl, Mg) were carried by using an atomic absorption spectrophotometer (Philips, PU9200X) in Department of Chemical Engineering, METU. Potassium analysis were also done at Chemical Engineering Department, METU using Jenway Flame Photometer

2.4.8 Determination of PHB (Poly-β-hydroxybutyrate)

For the 4 L panel PBR 200 mL sample and for the batch small scale reactors the final volume at the end of the experiment were used for poly-β-hydroxybutyrate (PHB) measurement. Samples were centrifuged (Sigma 3K30 High Speed Refrigerated Centrifuge) at 12000 rpm for 20 minutes at 4 °C. And then the pellet that consist PHB were stored at deep freeze (- 20 °C). Lyophilization were applied to all the samples to remove water content (Christ Alpha 1-4 LD plus). The net weights of the lyophilized samples were determined by substracting the weight of eppendorf tubes. Then, they were transfered into screw capped test tubes in order to do the acid methanolysis reaction; methanol/sulfuric acid (Merck) solution containing 15 % (v/v)

of concentrated sulfuric acid. 2 mL of prepared methanol-sulfuric acid solution and 2 mL of chloroform (Merck) were added on to lyophilized samples. After homogenizing with the help of vortex, the samples were incubated at 100 °C for 3.5 hour. At every hour the samples were mixed by vortex (Heidolph Rax Top, D91126). At the end of the incubation period, samples were let to cool to room temperature and 1 mL of distilled water was added to each sample. Two phases became visible after the samples were mixed by vortex. Bottom (organic phase) phase was taken after discarding the upper (water) phase. And then, organic phase was filtered by 0.45μm nylon filters (Micropore) before the injection (1 μL) to the gas chromatograph (Agilent Technologies 6890 N).

For calibration curve, standard PHB (Sigma) solutions (2.5 to 10 mg/L) were prepared with same method as described above. The resulting samples were analyzed by gas chromatograph and calibration curve was constructed with using Agilent Chemstation v: B.01.01 software (Appendix C). The gas chromatography instrument operating parameters were as follows: HP-FFAP column (30 m x 0.320 mm x 0.25 μm) connected to FID detector was used at constant pressure (6.67 psi) with the carrier gas (Argon) flow at 1 mL/min. The oven temperature was initially at 70°C for a minute and had a ramp with 8 °C/min until maximum temperature of 160 °C (1 min hold at 160 °C). Total run time was 13.25 minute. Back inlet temperature was 230 °C and the split ratio was 20:1. The detector temperature was 250 °C.

2.4.9 Determination of Bacteriochlorophyll *a*

For determination of bacteriochlorophyll *a* concentration in the biomass, 1 ml culture sample was used. After centrifuging the sample at 13400 rpm for 10 minutes pellet was harvested by discarding the supernatant. For the extraction of the bacteriochlorophyll *a*, 1 ml acetone-methanol mixture (7:2 v/v) was used (Cohen-Bazire 1957). And then mixture was centrufuged at 13400 rpm for 10 minutes in order to remove ~92% of the proteins (Biel A. J., 1986). Bacteriochlorophyll *a* concentration was measured spectrophotometrically at 770nm assuming the extinction coefficient is 75 $mM^{-1}.cm^{-1}$ (Clayton R. K., 1963). The molecular formula

of bacteriochlorophyll *a* is $C_{55}H_{74}N_4O_6Mg$ (Senge and Smith, 1995). Blank solution was acetone-methanol mixture. For the cellular bacteriochlorophyll *a* calculation, dry cell weight was also used. Sample of calculation bacteriochlorophyll *a* concentration is given in Appendix F.

CHAPTER 3

RESULTS AND DISCUSSION

In this chapter, the results of photofermentative hydrogen production studies using DFE of sugar beet thick juice (DFESBTJ) in outdoor fed-batch operated panel photobioreactor (PBR) is given first. The removal of NH_4^+ ions from DFESBTJ via ion-exchange using clinoptilolite are discussed and hydrogen production on this ammonium ion reduced DFESBTJ are reported next. Lastly, effects of different ethanol concentrations on hydrogen production, biomass, pH and organic acid changes on cultures of *Rb. capsulatus* DSM1710 and *Rb. capsulatus* YO3 (hup^-) are given.

3.1 Fed-batch Hydrogen Production on DFE of Sugar Beet Thick Juice

The DFESBTJ was used as substrate in 4 L fed-batch panel PBR with cultivated culture of *Rb. capsulatus* YO3 (hup^-). This reactor was operated in outdoor conditions for 15 days. No ammonium ion removal employed on to DFESBTJ1 because the amount of ammonium ion was reduced to 2.5 mM after 3 times dilution in order to adjust acetate concentration to ~40 mM. Asada et al. (2008) and Androga (2009) reported the highest hydrogen yield on 21-42 mM and 40 mM of acetate, respectively. Also, the ammonium was consumed during the batch operation of panel PBR and in the daily feed (data not shown); the concentration of NH_4^+ (10% of the panel PBR volume) will be diluted again in the panel PBR and reach only 0.25 mM NH_4^+. Initially, buffer selection studies were done, which aimed to look for another buffer alternative rather than KH_2PO_4 that is environmentally friendly. According to the results in Appendix E, KH_2PO_4 buffer was used in DFESBTJ experiments.

Since the fed-batch operation of 4 L panel PBR was carried in outdoor conditions, there are several parameters that affect the hydrogen production including the light intensity, wavelength, diurnal (day-night) cycle and temperature variation.

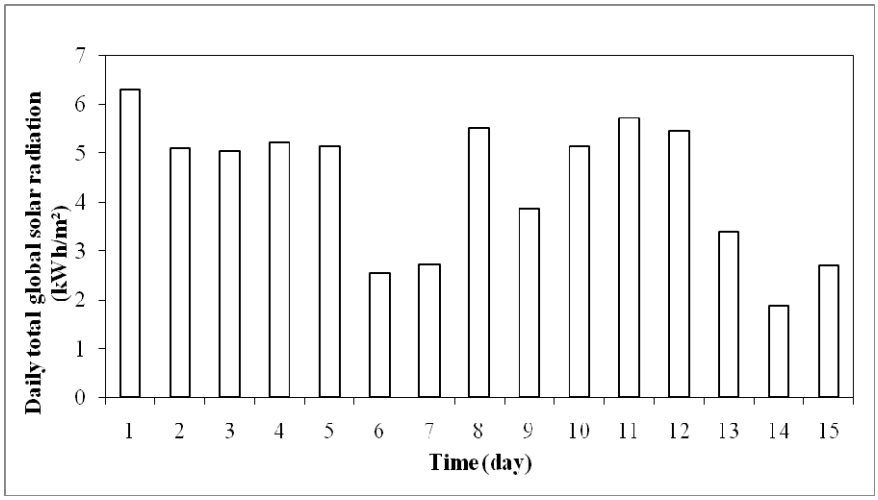

Figure 3.1 The daily global solar radiation data for Ankara. Day 1 corresponds to 7th of September, 2009

The daily global solar radiation data for the run is given in Figure 3.1. Throughout the run, the weather was mostly sunny and clear except for days 6, 7 and the last three days. The PNS bacteria require light energy for generation of ATP which is utilized by the nitrogenase enzyme for hydrogen production (Koku et al., 2002). Varying light intensities in outdoor conditions have been reported to greatly influence biomass concentration and hydrogen production (Avcioglu et al., 2011, Androga et al., 2011a, Boran et al. 2010, Gebicki et al., 2010). Temperature is another important parameter affecting outdoor hydrogen production studies. High PBR temperatures are inhibitory as they lead to the denaturing of the nitrogenase enzyme; cooling of the PBR is required to prevent death of the bacteria. Likewise, low temperatures are undesired as they lead to freezing of the bacterial cells. PNS bacteria are reported to grow optimally between 25-35 °C (Sasikala et al., 1993). In this study, the air and PBR temperatures were observed to fluctuate during the day; high air temperatures were experienced during the day and lower temperatures in the evening and night. These changes have drastic effects on hydrogen production and

yield as previously reported by (Özgür et al., 2010c, Androga et al., 2011a). In this study, chilled water was used to maintain the PBR temperature below 40°C during the day. At night, PBR temperature decreased to around 15 to 20 °C, due to the cold nights in Ankara. Significantly low reactor temperatures (8 to 10°C) were recorded on nights 3, 9 and 10. Highest daily temperature fluctuations due to the day/night cycles were recorded on days 11 and 12 (Figure 3.2).

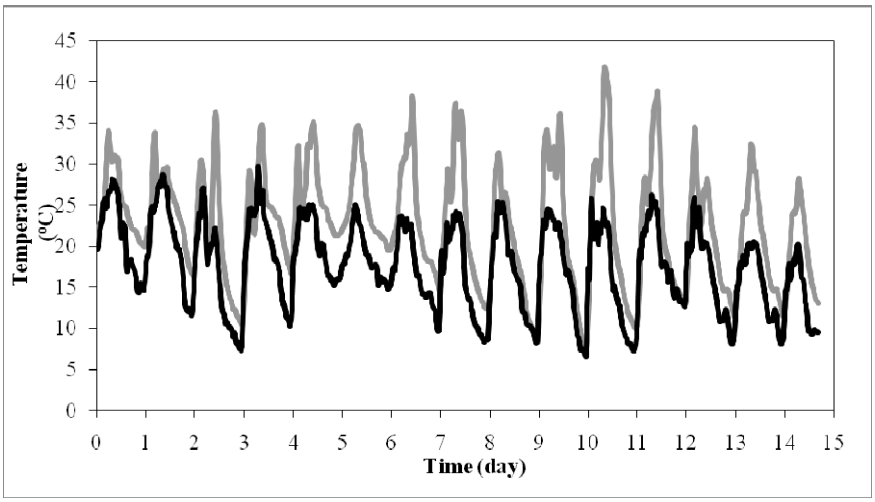

Figure 3.2 Air (—) and PBR (—) temperatures during the run. Day 1 corresponds to 7 September 2009

The patterns of biomass accumulation and cumulative hydrogen gas production are given in Figure 3.3. The PBR initial biomass concentration was 0.2 gdw/L_c which increased to an average concentration of 1 gdw/L_c by the end of 5th day. Feeding at a rate of 0.4 L/day was started on the 6th day when the bacterial growth reached the stationary phase. Because of the light/dark cycles and temperature fluctuations in outdoor conditions, the lag period of the growth lasted about 4 days, which was longer compared to those obtained in indoor studies reported previously (Eroglu et al., 2004, Eroglu et al., 2008). The biomass concentration remained stable between 0.9 to1.0 gdw/L_c during fed-batch operation. The specific growth rate at the exponential phase was found to be 0.021 h^{-1} which is comparable to those obtained in other studies operated in indoor with olive mill wastewater (Eroglu et al., 2004) and in outdoor with defined medium (Boran et al., 2010).

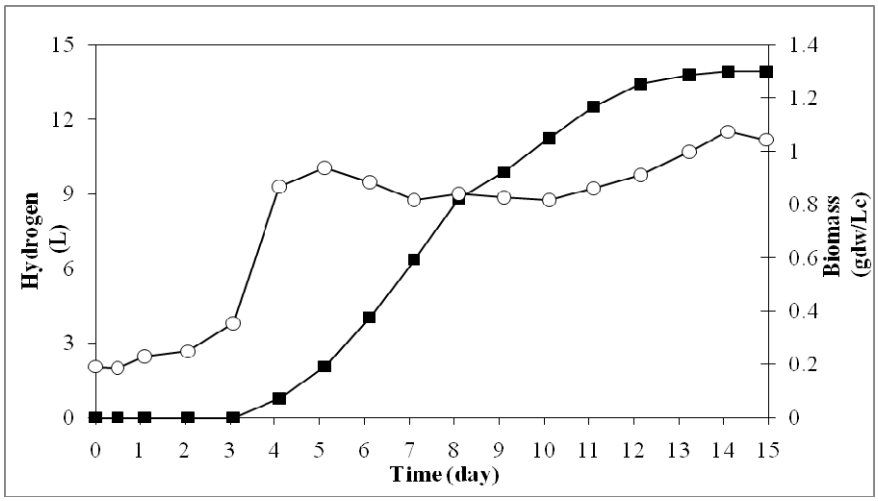

Figure 3.3 The biomass growth (○) and hydrogen production (■) of *Rb. capsulatus* YO3 (hup^-) on DFESBTJ

Hydrogen production started on the 4th day when the bacterial growth was in the exponential phase and continued for 9 days. Hydrogen productivity was at maximum in the 9th day (1.36 mmol/L_c/h), and gradually decreased until the end of the run. During the fed-batch operation period hydrogen productivity and molar yield of 1.12 mmol/L_c/h and 66% (of theoretical maximum over fed substrate), were attained, respectively. The decrease in hydrogen production observed during the 15 day operation could be caused by the low solar radiation during last three days of the operation (Figure 3.1). Another cause might be the high daily temperature fluctuations on days 11 and 12 (Figure 3.2). It was previously reported that hydrogen production was significantly reduced (50%) by temperature fluctuations and day/night cycles in batch cultures of *Rhodobacter capsulatus* (Özgür et al., 2010c). Produced gas was expected to contain mostly hydrogen, and a small amount of carbondioxide. However, in our case, produced gas was pure hydrogen and carbondioxide could not be detected. It should be noted that the CO_2 produced remains in the media as bicarbonate (HCO_3^-) and the bacteria are able to utilize it back as a C source, as reported previously (Uyar et al., 2009b). Other researchers reported hydrogen content of the produced gas to be between 95-99% in similar studies (Avcıoglu et al., 2010, Kars et al., 2008, Uyar et al., 2009b).

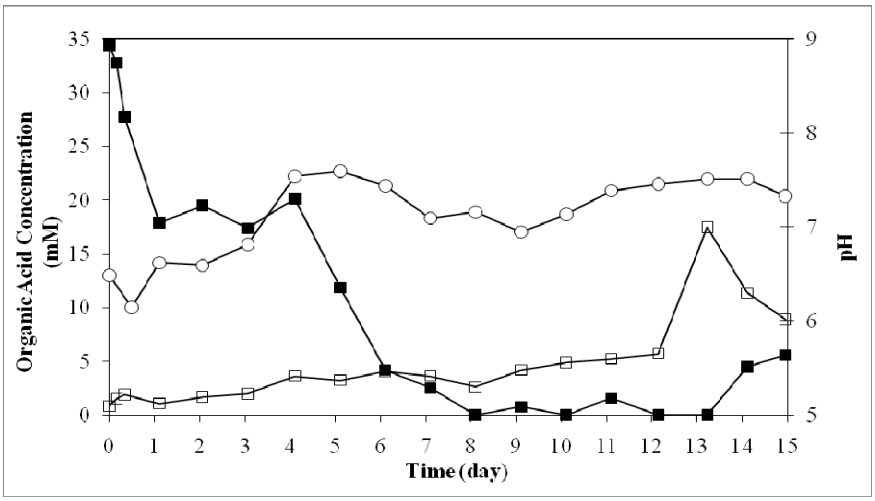

Figure 3.4 pH and organic acid composition of the culture media in the PBR during the operation. Samples were taken from the reactor before daily feeding. (○): pH, (■): Acetic acid, (□): Formic acid.

The pH ranged between 6.5-7.5, demonstrating that the amount of buffer added was sufficient to maintain the pH at the desired level for effective hydrogen production. Acetate, the main substrate in the DFESBTJ for photofermentation, was well utilized during continuous culturing. Previous studies have shown that *Rb. capsulatus* can utilize acetate for growth and hydrogen production (Özgür et al., 2010c, Androga et al., 2011a). Between the 8^{th} - 13^{th} days of the experiment, the daily fed acetate was completely consumed; however, lower hydrogen production rates were observed. The explanation could be that the bacteria consumed acetate for growth and maintenance purposes instead of hydrogen production in this period. Negligible amounts of butyric, lactic and propionic acid were detected throughout the process (data not shown). Formic acid concentration in the reactor slightly increased at the end of the run. The rise in the concentration of the formate might be related to the decline in total solar radiation (insufficient light intensity) during these days (Figure 3.1). Formate can be formed as a fermentation end product through pyruvate by the action of pyruvate formate lyase. Eroglu et al. (2008) observed formate formation during night in outdoor experiments when malate was the carbon source.

During the 15 days of fed-batch operation relatively low amounts of Poly-β-hydroxybutyrate (PHB) was produced in the system (Figure 3.5). On the other hand, Eroglu et al. (2008) reported higher amounts of PHB production in outdoor conditions compared to indoor studies by using *Rb. sphaeroides* O.U.001. The first sample was taken at the end of the set up of the experiment and the accumulated PHB is much more than the other days. This may explain the high amount of PHB in day 1, which may be attributed to the inoculation culture containing extra PHB and to the initial batch cultivation period which results in the accumulation of PHB.

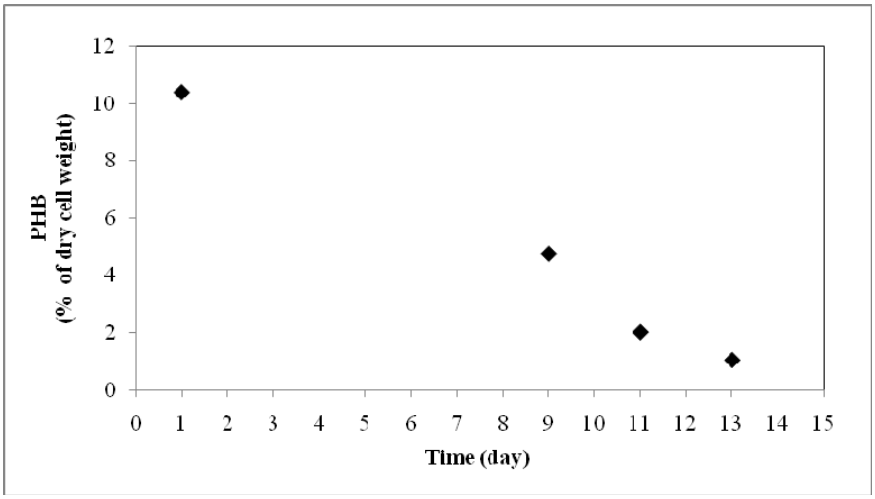

Figure 3.5 PHB production of the culture media in the PBR at 1st, 9th, 11th,and 13th days

Since the metabolism of PHB production is closely related to the hydrogen production mechanism, the low PHB content may also indicate that bacteria used up acetate only for biomass and hydrogen production throughout the system.

The major light absorbing pigments in purple bacteria are the bacteriochlorophylls (*a* and *b*) and the carotenoids (Zuber and Cogdell, 2004). Bacteriochlorophyll *a* (bchl *a*) concentration was measured in every 2 hours during 48 hours in order to show the relation between solar radiation and cellular bchl *a* content in outdoor conditions (Figure 3.6).

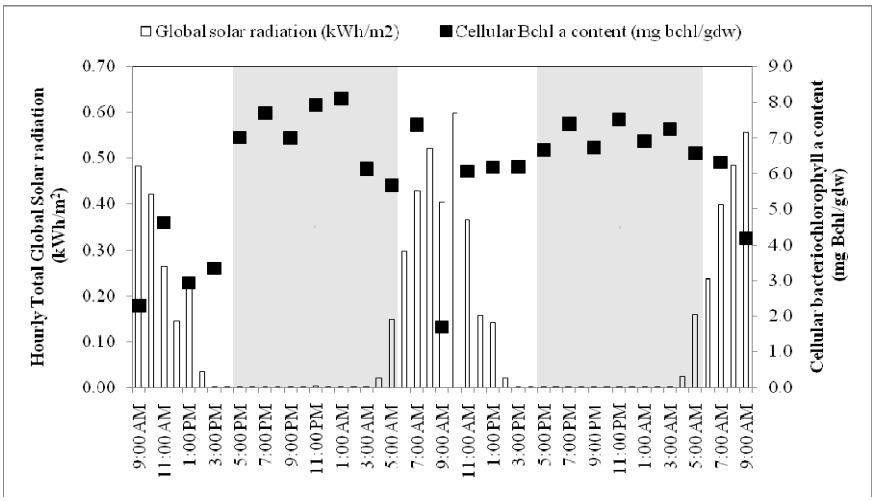

Figure 3.6 Effect of solar radiation on cellular bacteriochlorophyll a levels of *Rb.capsulatus* YO3 (hup$^-$) in DFESBTJ (The first 09:00 AM corresponds to the morning of 19.10.2009, and the last 09:00 AM corresponds to the morning of 21.10.2009, shaded areas represent night)

The PBR temperature range was 13-35 ^oC and 10-32 ^oC in the first and the second 24 hours period, respectively. The biomass concentration was almost stable at a concentration of 1 gdw/L_c during the whole 48 hours of observation. In the first 24 hours 0.32 L hydrogen and in the second 24 hours 0.74 L hydrogen were produced only during the day time when the solar radiation was sufficient for hydrogen production. Hydrogen production started especially approximately 2 hours later (at 08:00 AM) after sunrise (at 06:00 AM) and continued untill 02:00 PM. The reason of early cessation of hydrogen may be due to low solar radiation in the afternoons of experiment days (Figure 3.6). In addition, around 08:00 AM, the temperature of panel PBR was increasing from ~13^oC to ~25 ^oC with the increasing solar radiation (reached ~33 ^oC at noon) when the hydrogen production started. The variation of cellular bchl *a* with solar radiation in Figure 3.6 shows that cellular bchl *a* content decreases with the increasing solar radiation especially during the day time when solar radiation was at the top level. Although there was no solar radiation at night, cellular bchl *a* content started to increase aiming to enhance light caption capability. Tsygankov and Laurinavichene (1996) also stated that total bchl *a* content of *Rb. capsulatus* st. B10 increased when light limitation increased in a 1.25 L PBR.

Boran (2011) also observed an increase in produced bchl a when there was insufficient light intensity on tubular PBR in outdoor conditions. In a genetic level study, by radiolabelling with the bchl *a* biosynthetic precursor, when photosynthetically grown cells of *Rb. sphaeroides* were switched from high to low light growth conditions, it is reported that the cellular bchl *a* content increased (Hunter et al., 2005). The cellular bchl *a* content stayed almost stable 06:00 AM to 09:00 AM during the morning. However, when the solar radiation started to increase, cellular bchl *a* content decreased except the morning of second day because weather at 2nd day was more clouded than the other days. According to Figure 3.6, one might also conclude that bacteria can preserve its cellular bchl *a* content almost at a constant level during the night.

Hydrogen production yields and productivities reported in different studies using *Rb. capsulatus* YO3 (hup$^-$) in fed-batch PBRs were compared in Table 3.1. According to Table 3.1, molar yield and acetate conversion obtained in this study were comparable to those obtained on defined medium and on DFESBTJ in indoors. The molar hydrogen productivity obtained was much higher than those in other studies.

Table 3.1 The molar yield and acetate conversion (%) of *Rb.capsulatus* YO3 (hup$^-$) on various substrates in 4 L panel PBRs

Fed-Batch	Substrate	H_2 Productivity (mmol/L_c/h)	Molar Yield (%)	Acetate* Conversion (%)	References
Outdoor	DFESBTJ	1.12	77	92	This study
Outdoor	Defined medium	0.51	53	85-90	Androga et al., 2011a
Outdoor	Molasses DFE	0.67	78	NA	Avcıoglu et al., 2011
Indoor	DFESBTJ	0.89	48	87	Özgür et al., 2010d

***** Acetate conversion (%) was calculated by dividing the moles of acetate utilized by moles of acetate fed to the reactor

3.2 Batch Hydrogen Production on DFE of Sugar Beet Thick Juice

Ammonium ions in the dark fermentation effluent are undesired as they have an inhibitory effect on hydrogen production. Ammonium ions are reported to inhibit the PNS bacteria's nitrogenase enzyme expression and activity either directly via feedback inhibition or at the genetic level (Akköse et al., 2009, Pekgöz, 2010). The removal of ammonium ions from the DFESBTJ2 and DFESBTJ3 samples using natural clinoptilolite was investigated and reported in this study. Assessment of the treated and untreated DFESBTJ samples was done by means of hydrogen production capabilities.

3.2.1 Ammonium Ion Removal from DFE of Sugar Beet Thick Juice

In order to increase the absorption ability of zeolite, preparation of Na-form clinoptilolite zeolite was conducted in first. Component analyses of the solid clinoptilolite particle before and after treatment with brine solution showed that the sodium content of the zeolite was successfully increased by the batch treatment procedure. The Na_2O amount increased from 0.55% to 3.64% and 4.11% in the treatment Na-form-(1) and Na-form-(2), respectively (Table 3.2 A). The amount of the exchangeable cations (Fe^{3+}, K^+ and Mg^{2+}) decreased as they were replaced with Na^+ ions (Table 3.2 B and C). The results also showed that 10 days of treatment was sufficient to attain saturation, which corresponds to the findings of Bayraktaroğlu (2006) who also reported that 10 days was sufficient to obtain homoionic Na-form clinoptilolite.

Table 3.2 Component analysis of the clinoptilolite zeolite

(A)

Clinoptilolite	**0.42 to 0.853 mm particle size**		
Component (%)	**Original (%)**	**Na-form-(1) (%)**	**Na-form-(2) (%)**
SiO_2	35.2	33.6	33.6
Fe_2O_3	1.44	1.56	1.05
CaO	0.13	0	0
MgO	0.23	0.16	0.15
Al_2O_3	9.43	9.65	10.8
Na_2O	0.55	3.64	4.11
K_2O	1.39	0.52	0.65
Others	51.61	50.85	49.63

(B)

Before Treatment		**After Treatment of DFESGTJ2**				
Component (%)	**Na-form-(1) (%)**	**Zeolite (2 g) (%)**	**Zeolite (4 g) (%)**	**Zeolite (6 g) (%)**	**Zeolite (8 g) (%)**	**Zeolite (10 g) (%)**
SiO_2	33.6	28.98	32.46	30.73	34.53	32.62
Fe_2O_3	1.56	1.64	0.93	1.54	1.21	1.54
CaO	0	0	0	0	0	0
MgO	0.16	0.15	0.12	0.17	0.16	0.15
Al_2O_3	9.65	7.00	9.73	9.58	9.71	12.05
Na_2O	3.64	3.91	2.39	3.86	3.76	2.71
K_2O	0.52	0.67	0.92	0.74	0.64	1.20
Others	50.85	57.64	53.43	53.36	49.9	49.71

(C)

	Before Treatment	**After Treatment of DFESGTJ3**			
Component (%)	**Na-form-(2) (%)**	**Zeolite (5 g) (%)**	**Zeolite (10 g) (%)**	**Zeolite (15 g) (%)**	**Zeolite (20 g) (%)**
SiO_2	33.6	38.34	34.8	36.57	33.63
Fe_2O_3	1.05	1.18	1.64	1.49	1.49
CaO	0	0	0	0	0
MgO	0.15	0.14	0.13	0.14	0.14
Al_2O_3	10.8	11.74	10.41	8.78	9.68
Na_2O	4.11	3.57	3.31	2.95	4.50
K_2O	0.65	0.90	0.78	1.02	0.85
Others	49.63	44.10	48.91	49.03	49.68

Ammonium ions were effectively removed from the DFESBTJ using the clinoptilolite zeolite. In the treatment of the DFESBTJ2 sample that had initial 9 mM NH_4^+, the treatment procedure using 2, 4 and 6 g zeolite revealed that 30 minutes was sufficient to remove 74% of the NH_4^+; the zeolite samples became saturated and could not exchange further cations (Fe^{3+}, K^+ and Mg^{2+}) for NH_4^+ after 30 minutes of treatment. Higher ammonium ion removal was observed when the zeolite amount used for treatment was increased. The DFESBTJ2 treatment using 8 and 10 g zeolite showed that 95% NH_4^+ was removed and saturation attained after 45 minutes (Figure 3.7). In the treatment of the DFESBTJ3 that contained initial 23.6 mM NH_4^+, 80%, 85%, 93% and 95% of NH_4^+ ions were removed and saturation attained after 60, 90, 90 and 120 minutes in the 5, 10, 15 and 20 g zeolite containing batch treatment, respectively (Figure 3.8).

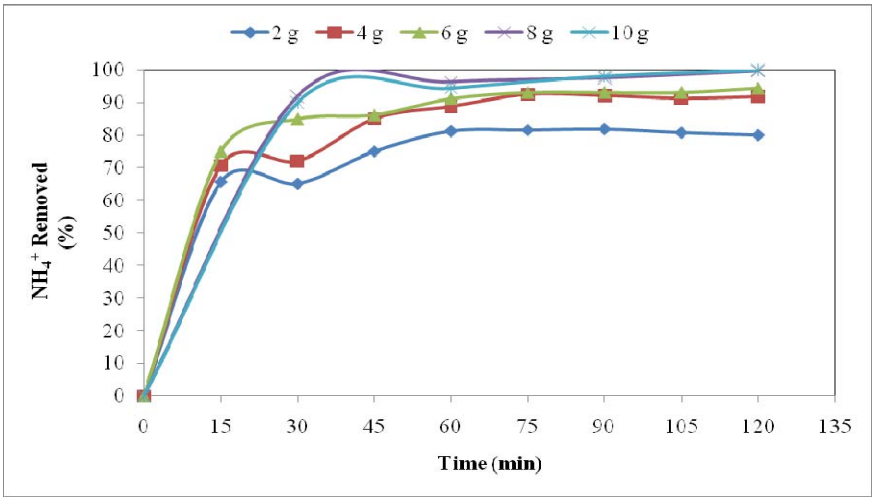

Figure 3.7 Ammonium ion removal from the DFESBTJ2 using different amounts of clinoptilolite zeolite

The batch treatment procedure had negligible effect on the pH of the DFESBTJ samples. The pH of DFESBTJ2 ranged between 5.98 to 6.13 during treatment while that of DFESBTJ3 varied between 6.03 and 6.14. The color of the DFESBTJ2 varied between 130 to 300 PtCo while that of DFESBTJ3 ranged between 510 to 740 PtCo during treatment.

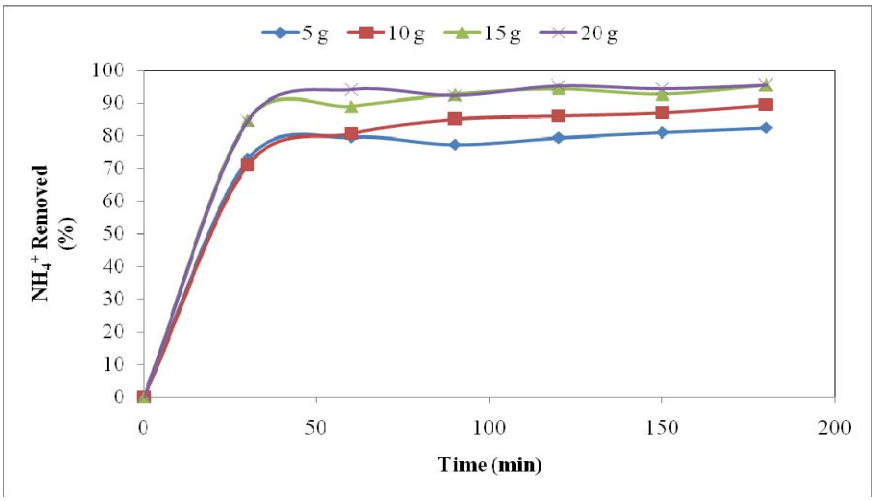

Figure 3.8 Ammonium ion removal from the DFESBTJ3 using different amounts of clinoptilolite zeolite

The concentrations of the exchangeable cations varied after treatment of the DFESBTJ with the zeolite samples; some cations were taken up from the solution (for example Fe^{3+} and K^+), others were released into the solution (for example Na^+) while others remained more or less the same (i.e. Mg^{2+}) (Table 3.2 B, C, Table 3.3 A, B). The uptake of Fe from the DFESBTJ is undesired as it is needed by the nitrogenase enzyme activity, thus important for bacterial growth and hydrogen production (Koku et al., 2002). Therefore, more studies are needed to optimize conditions that would prevent Fe uptake during ammonium ions removal using clinoptilolite.

Table 3.3 Elemental analysis results of the DFESBTJ samples before and after zeolite treatment

(A)

		Treated DFESBTJ2				
Elements	**Untreated DFESBTJ2**	**Zeolite (2 g)**	**Zeolite (4 g)**	**Zeolite (6 g)**	**Zeolite (8 g)**	**Zeolite (10 g)**
Ni (µM)	1.65	1.35	1.53	0.169	0.508	0.169
Cu (mM)	0	0	0	0	0	0
Mo (µM)	0	0.104	0.313	0	0	0
Fe (µM)	10.9	6.96	7.68	6.61	4.46	7.86
Zn (µM)	4.28	2.75	2.59	1.98	1.68	3.21
Ca (mM)	0.188	0.132	0.109	0.079	0.061	0.096
Mg (mM)	0.146	0.145	0.145	0.141	0.143	0.145
Mn (µM)	0.436	0.545	0.727	0.363	0.363	0.727
Co (µM)	0	0	0	0	0	0
Na (mM)	58.7	126	165	104	86.9	252

(B)

		Treated DFESBTJ3			
Elements (mg/L)	**Untreated DFESBTJ3**	**Zeolite (5 g)**	**Zeolite (10 g)**	**Zeolite (15 g)**	**Zeolite (20 g)**
Ni (µM)	1.02	2.03	2.88	0.677	1.69
Cu (mM)	0	0	0	0	0
Mo (µM)	0	0	0	0	0
Fe (µM)	25.4	17.1	16.3	12.7	12.8
Zn (µM)	8.56	6.88	6.57	5.65	5.51
Ca (mM)	0.151	0.171	0.161	0.133	0.124
Mg (mM)	0.151	0.153	0.106	0.148	0.150
Mn (µM)	4	3.27	3.27	2.91	2.54
Co (µM)	1.52	1.01	0.508	0	0
Na (mM)	165	274	270	235	196

The organic acid composition of the DFESGTJ samples remained more or less constant after treatment with clinoptilolite zeolite. TN decreased as ammonium ions were removed while COD and TOC remained almost same (Table 3.4).

Table 3.4 Organic acid, TN, COD and TOC analysis results of the DFESBTJ samples

Component	DFESBTJ2 Untreated	DFESBTJ2 Treated	DFESBTJ3 Untreated	DFESBTJ3 Treated
Ammonium (mM)	9	0.606	23.6	1.05
Acetic Acid (mM)	40	40	92	92
Lactic Acid (mM)	16	16	30	30
Formic Acid (mM)	0	0	0	0
Propionic Acid (mM)	0	0	0	0
TOC (mM)	80	78	78	78
TN (mM)	8.5	3.2	34.4	16.2
Molar TOC/TN ratio	9.41	24.3	2.26	4.83
COD	7360	6960	18520	14860

3.2.2 Hydrogen Production using Ammonium Ion Reduced Dark Fermentation Effluent of Sugar Beet Thick Juice

The NH_4^+ ion reduced DFESBTJ (2 and 3) samples were investigated for hydrogen production. The experiments were carried out in 150 mL PBRs using the setup and procedures explained in Section 2.3. The original (untreated) DFESBTJ that adjusted 30 mM acetate concentration via dilution with KH_2PO_4 buffer supplemented with Fe and Mo were used as the control PBRs. After dilution, DFESBTJ2 and DFESBTJ3 samples contained 6.7 mM and 7.7 mM NH_4^+, respectively.

In order to analyze the experimental data, maximum biomass, cumulative produced hydrogen, maximum productivity, molar yield, product yield factor, light conversion efficiency and produced PHB are tabulated in Tables 3.5 and 3.6 for *Rb.capsulatus* DSM1710 and *Rb.capsulatus* YO3 (hup^-), respectively. The calculations of these parameters are given in Appendix F.

As it is seen in Tables 3.5 and 3.6, the maximum biomass in the untreated DFESGTJ was higher than the treated DFESBTJ samples for both strains. This could be due to the high amount of ammonium ion in untreated DFESBTJ samples. Akköse et al. (2009) reported that increasing ammonium ion concentrations (1 to 10 mM NH_4^+) enhance the biomass development of *Rb. sphaeroides* O.U.001. Also, Pekgöz (2010) demonstrated biomass increased with the increasing NH_4^+ (1 to 8 mM NH_4^+).

Table 3.5 Photofermentative hydrogen production by *Rb.capsulatus* DSM1710 on untreated/treated DFESBTJ2 and DFESBTJ3

Type of DFESBTJ	Maximum Biomass (gdw/L_c)	Cumulative Produced H_2 (mmol)	Maximum Productivity (mmol $H_2/L_c/h$)	Molar H_2 Yield (% of theoretical maximum)	Product Yield Factor (mmol H_2/gdw)	Light Conversion Efficiency (%)	PHB Content (% of dry cell weight)
Untreated DFESBTJ2	1.13 ± 0.04	10.7 ± 0.6	1.02 ± 0.06	37.9 ± 2.1	71.1 ± 5.5	0.143 ± 0.008	4.70 ± 0.61
Treated DFESBTJ2	0.784 ± 0.052	18.1 ± 1.0	1.17 ± 0.01	64.0 ± 3.6	186 ± 18	0.242 ± 0.013	25.5 ± 7.9
Untreated DFESBTJ3	1.29 ± 0.01	4.06 ± 0.44	0.275 ± 0.019	15.3 ± 1.6	22.6 ± 2.5	0.054 ± 0.006	1.92 ± 0.65
Treated DFESBTJ3	0.922 ± 0.033	19.9 ± 0.3	1.05 ± 0.02	75.1 ± 1.1	173 ± 4	0.268 ± 0.003	13.5 ± 3.3

Table 3.6 Photofermentative hydrogen production by *Rb.capsulatus* YO3 (hup^-) on untreated/treated DFESBTJ2 and DFESBTJ3

Type of DFESBTJ	Maximum Biomass (gdw/L_c)	Cumulative Produced H_2 (mmol)	Maximum Productivity (mmol $H_2/L_c/h$)	Molar H_2 Yield (% of theoretical maximum)	Product Yield Factor (mmol H_2/gdw)	Light Conversion Efficiency (%)	PHB Content (% of dry cell weight)
Untreated DFESBTJ2	1.09 ± 0.00	16.5 ± 1.5	1.51 ± 0.02	55.9 ± 5.2	106 ± 9	0.220 ± 0.019	2.61 ± 0.07
Treated DFESBTJ2	0.800 ± 0.012	23.7 ± 1.4	1.62 ± 0.03	79.7 ± 5.0	221 ± 24	0.317 ± 0.019	10.8 ± 2.5
Untreated DFESBTJ3	1.50 ± 0.03	8.68 ± 0.45	0.823 ± 0.01	32.7 ± 1.7	40 ± 3	0.116 ± 0.007	0.446 ± 0.131
Treated DFESBTJ3	0.975 ± 0.003	22.9 ± 1.05	1.44 ± 0.00	86.4 ± 3.9	174 ± 6	0.308 ± 0.014	2.12 ± 1.11

The trend of biomass development for mutant and wild type strains are illustrated in Figures 3.9 and 3.10.

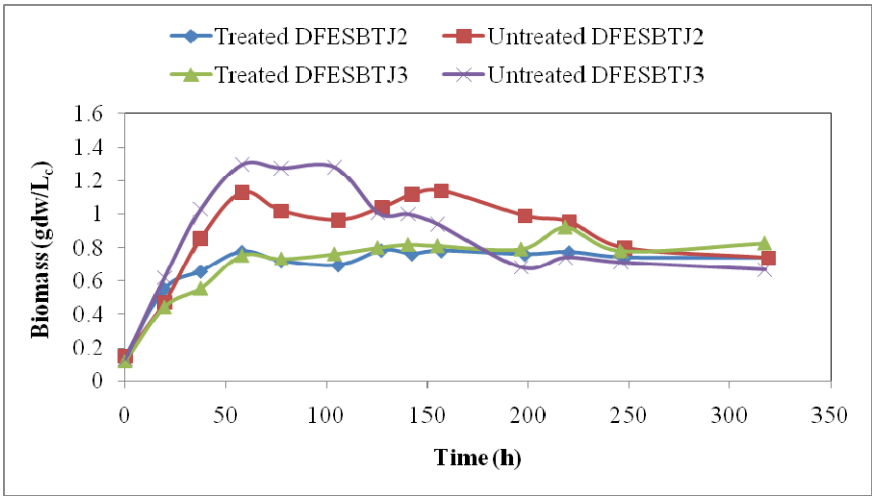

Figure 3.9 Cell growth of *Rb. capsulatus* DSM1710 for untreated/treated DFESBTJ2 and untreated/treated DFESBTJ3

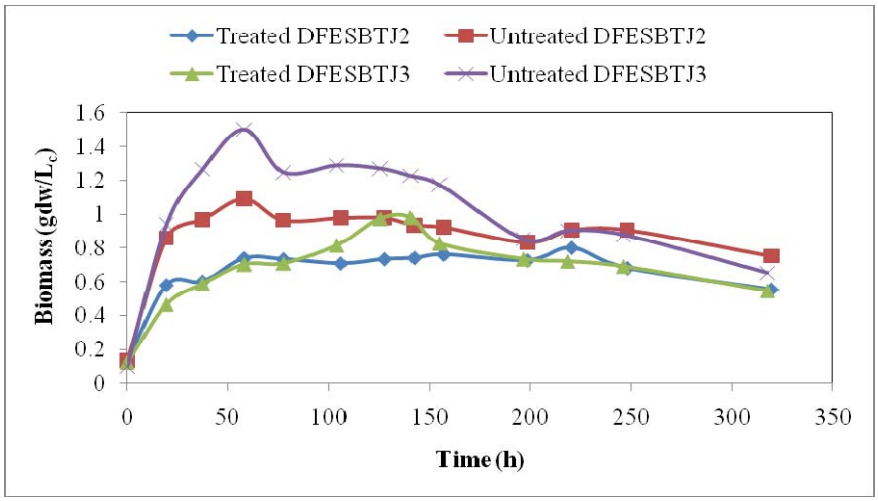

Figure 3.10 Cell growth of *Rb. capsulatus* YO3 (hup$^-$) for untreated/treated DFESBTJ2 and untreated/treated DFESBTJ3

The experimental data in Figure 3.9 and 3.10 are used for specific growth rate calculations (Appendix F). Depending on the ammonium ion content in both

untreated DFESBTJ (2 and 3) samples, *Rb.capsulatus* DSM1710 (0.046 and 0.050 h^{-1}) and *Rb. capsulatus* YO3 (hup^-) (0.053 and 0.069 h^{-1}) showed higher specific growth rates compared to treated DFESBTJ samples. The specific growth rates of *Rb.capsulatus* DSM1710 and *Rb. capsulatus* YO3 (hup^-) were ~0.040 h^{-1} on both treated DFESBTJ samples.

The obtained growth curves of *Rb. capsulatus* wild and mutant strains on treated/untreated DFESBTJ2 and DFESBTJ3 were fitted into the logistic growth model. Logistic growth model has been widely used to describe cell growth in mathematical form (Nath et al. 2008, Sevinç, 2010, Nath and Das, 2011). Androga (2009) demonstrated that growth curve of *Rb. capsulatus* DSM1710 fits into logistic growth model very well. The logistic model equation for a batch reactor can be expressed as:

$$dX/dt=k_cX(1-X/X_{max}) \quad (3.1)$$

where k_c is the specific growth rate (h^{-1}), X is the biomass concentration (gdw/L_c) and X_{max} is maxiumum biomass concentration (gdw/L_c). Integrating of this equation gives:

$$X=X_{max}/[1+\exp(-k_c.t)((X_{max}/X_o)-1)] \quad (3.2)$$

where X_o is the initial biomass concentration at the lag time (gdw/L_c).

The logistic growth equation does not include the substrate term and presents an approximation for the whole growth curve including lag, exponential and stationary phases (Nath and Das, 2011).

The cell growth of wild type and mutant strain which is illustrated in Figure 3.9 and 3.10, respectively, were fitted into logistic growth model by Curve Expert 1.4 software (Figure 3.11 and 3.12). The logistic model parameters of wild type and mutant strain are given in Tables 3.7 and 3.8, respectively. The fits for others are given in Appendix H.

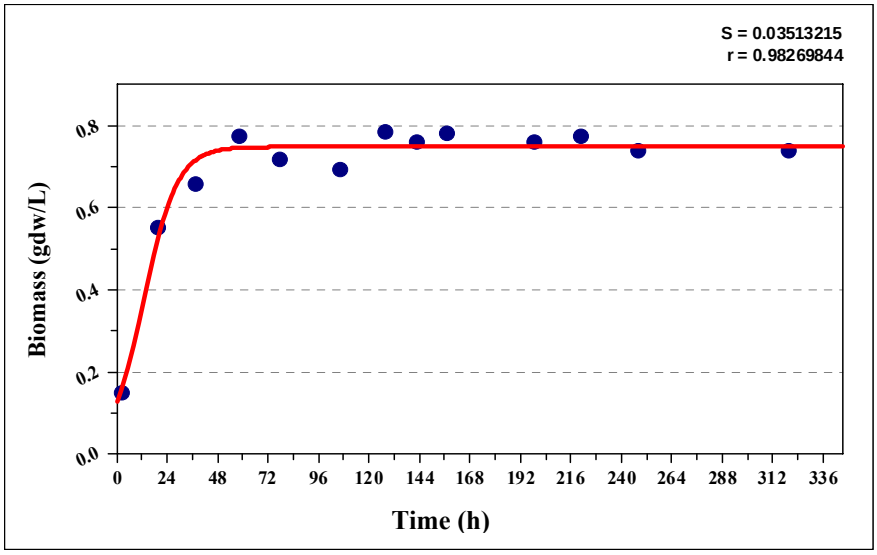

Figure 3.11 The logistic growth model on treated DFESBTJ2 for *Rb.capsulatus* DSM1710 (●: experimental data, ▬: order)

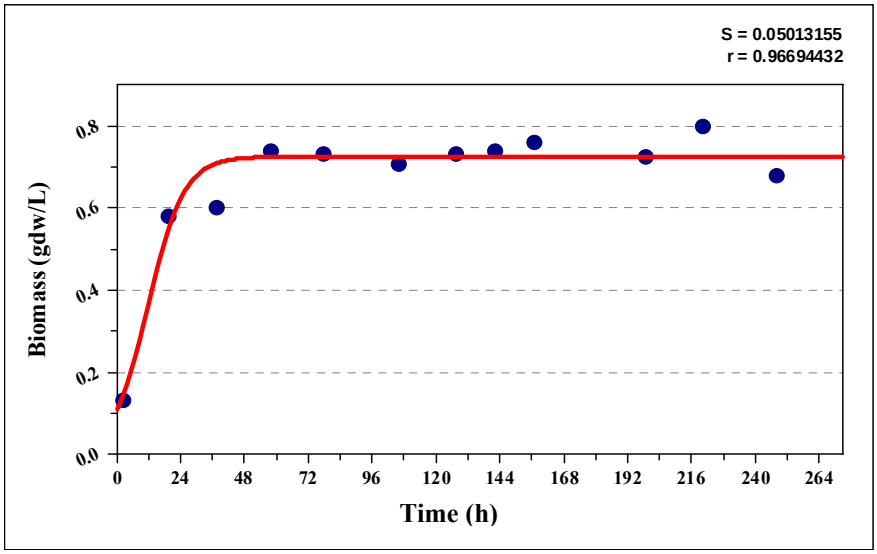

Figure 3.12 The logistic growth model on treated DFESBTJ2 for *Rb.capsulatus* YO3 (hup^-) (●: experimental data, ▬: order)

Table 3.7 Comparison of logistic model constants and experimental data for *Rb.capsulatus* DSM1710 on untreated/treated DFESBTJ (e: experimental, m: model)

	Treated DFESBTJ2	**Untreated DFESBTJ2**	**Treated DFESBTJ3**	**Untreated DFESBTJ3**
r	0.983	0.976	0.973	0.935
$X_{o,e}$	0.15	0.15	0.12	0.13
$X_{o,m}$	0.13	0.11	0.16	0.10
$X_{max,e}$	0.78	1.14	0.92	1.30
$X_{max,m}$	0.75	1.04	0.81	1.13
μ_{max}	0.039	0.046	0.040	0.050
k_c	0.125	0.102	0.064	0.133

Table 3.8 Comparison of logistic model constants and experimental data for *Rb.capsulatus* YO3 (hup^-) on untreated/treated DFESBTJ (e: experimental, m: model)

	Treated DFESBTJ2	**Untreated DFESBTJ2**	**Treated DFESBTJ3**	**Untreated DFESBTJ3**
r	0.967	0.968	0.953	0.975
$X_{o,e}$	0.13	0.14	0.12	0.10
$X_{o,m}$	0.11	0.09	0.22	0.07
$X_{max,e}$	0.80	1.09	0.98	1.50
$X_{max,m}$	0.73	0.95	0.90	1.28
μ_{max}	0.040	0.053	0.042	0.069
k_c	0.148	0.240	0.043	0.205

r: correlation coefficient (extent of fit)

$X_{o,e}$: Experimental initial bacterial concentration, (gdw/L_c)

$X_{o,m}$: Initial bacterial concentration obtained by logistic model, (gdw/L_c)

$X_{max,e}$: Experimental maximum bacterial concentration, (gdw/L_c)

$X_{max,m}$: Maximum bacterial concentration obtained by logistic model, (gdw/L_c)

μ_{max}: Specific growth rate constant obtained by exponential model, (h^{-1})

k_c: Specific growth rate constant obtained by logistic model, (h^{-1})

According to the Tables 3.7 and 3.8, experimental data fitted well to the model (r~1). Initial and maximum cell concentrations (X_o, X_{max}) of experimental and model are similar. Also maximum cell concentrations (X_{max}), specific growth rate (k_c or μ_{max}) increased in untreated DFESGTJ samples presumably due to the availability of ammonium ion.

In Figure 3.13 and 3.14, pH variations of the treated and untreated DFESBTJ samples during the run for both strains are illustrated. The pH variations in both cases (low and high ammonium) ranged between 6.5 and 7.8, which is in the range (pH 6-9) reported suitable for hydrogen production (Sasikala et al. 1993). This results showed that the buffer (22 mM KH_2PO_4) used in this study was sufficient to maintain the pH at the desired level. Özgür et al. (2010a, 2010b) also showed that KH_2PO_4 (20 mM KH_2PO_4) buffer was adequate to control pH during hydrogen production on molasses DFE by *Rb. capsulatus*. However, Androga et al. (2011b) observed a rapid increase in pH in control PBRs of molasses DFE containing high ammonium when Na_2CO_3 buffer was used in order to control the pH.

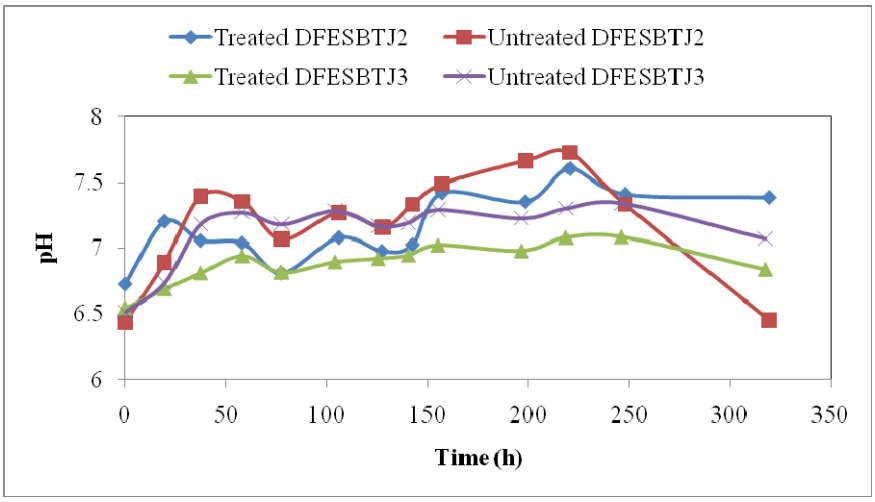

Figure 3.13 Variation of pH with time for *Rb.capsulatus* DSM1710 using untreated/treated DFESBTJ2 and untreated/treated DFESBTJ3

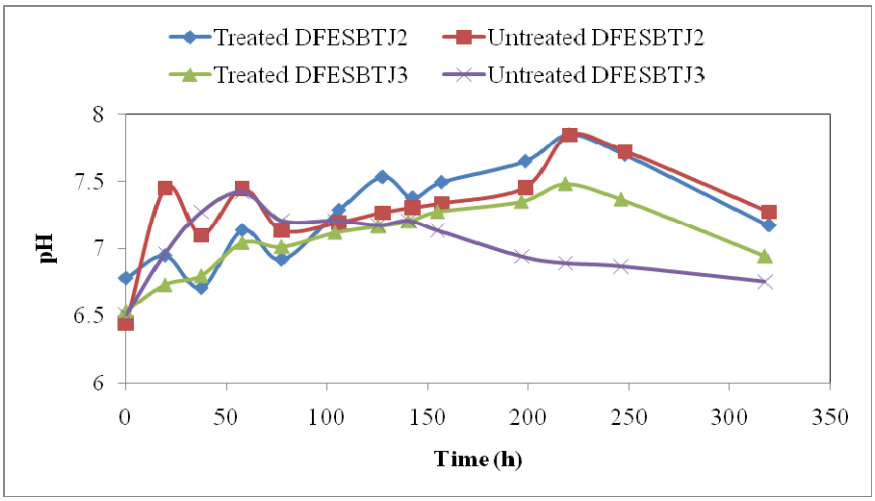

Figure 3.14 Variation of pH with time for *Rb.capsulatus* YO3 (hup$^-$) using untreated/treated DFESBTJ2 and untreated/treated DFESBTJ3

Higher hydrogen production was observed on the treated DFESBTJ samples than the untreated (control) DFESBTJ samples for both strains (Figure 3.15 and 3.16). The maximum cumulative hydrogen production of wild type strain was 18.1 and 19.9 mmol H_2 in treated DFESGTJ2 and DFESGTJ3, respectively (Table 3.5) while it was 23.7 and 22.9 mmol H_2 in treated DFESGTJ2 and DFESGTJ3, respectively (Table 3.6) for the mutant strain. Lower hydrogen production was observed in the untreated DFESGTJ samples, probably due to the higher NH_4^+ which provided N source for biomass. Infact it was observed higher biomass was obtained in the presence of high NH_4^+ in the media (Figure 3.9 and 3.10). Cessation of hydrogen production with increasing nitrogen source (sodium glutamate, 1, 2, 10 mM) was also reported by Eroglu et al. (1999). However, despite the high initial ammonium concentration in untreated DFESGTJ samples (6.7 and 7.7 mM), hydrogen production was observed in these samples for both strains. Özgür et al. (2010a) reported no hydrogen production in molasses DFE samples containing more than 2 mM NH_4^+. The differences between this study and theirs could be due to the nature of media used; thick juice DFE vs. molasses DFE.

Also, in this study, it was observed that the total hydrogen produced by *Rb.capsulatus* YO3 (hup$^-$) was higher than *Rb.capsulatus* DSM1710. This could be

attributed to the lack of uptake hydrogenase enzyme in the *Rb.capsulatus* YO3 (hup$^-$) which is reported to catalyze the production of electron and protons from hydrogen. Öztürk et al., 2006 reported a 20% increase in hydrogen production with the deletion of the upatake hydrogenase enzyme from *Rb.capsulatus* MT1131. The gas collected consisted of 90-95% hydrogen in all of the runs.

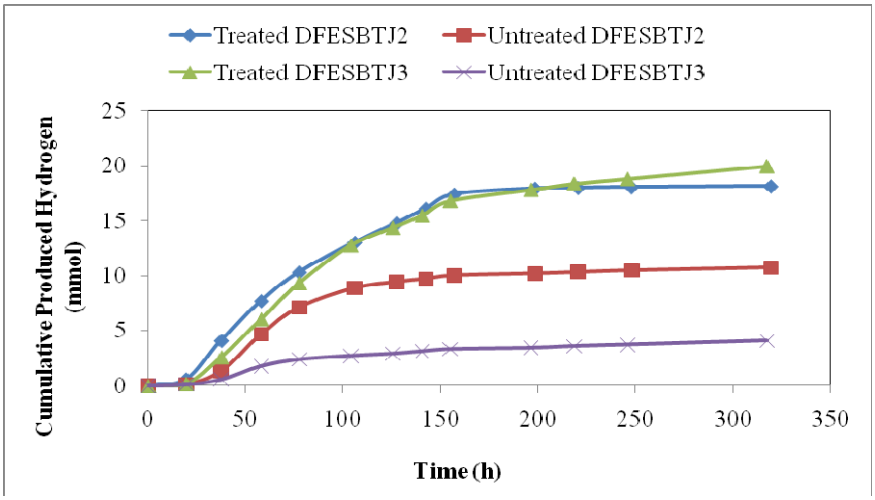

Figure 3.15 Cumulative Hydrogen Production for *Rb.capsulatus* DSM1710 using untreated/treated DFESBTJ2 and untreated/treated DFESBTJ3

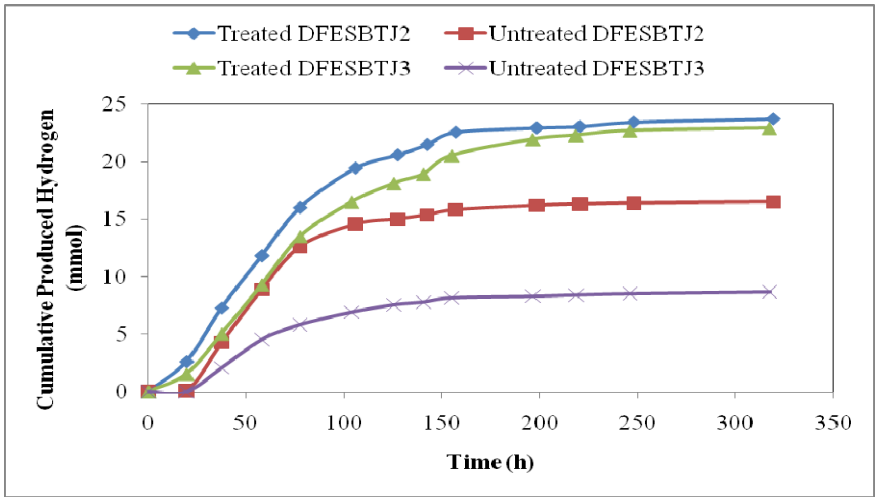

Figure 3.16 Cumulative Hydrogen Production for *Rb.capsulatus* YO3 (hup$^-$) using untreated/treated DFESBTJ2 and untreated/treated DFESBTJ3

In order to interpret the hydrogen production results of the experiments, "Modified Gompertz" equation were applied on to data which are shown in Figure 3.15 and 3.16 by using Curve Expert 1.4 software. Modified Gompertz equation has been widely used to express the development of hydrogen production (Mu et al., 2006, Mu et al., 2007, Nath et al., 2008, Wang and Wan, 2009, Sevinç, 2010). This model gives the best fitting for all steps of hydrogen production curve. The Modified Gompertz equation was described as:

$$H(t)=H_{max}\exp\left\{-\exp\left(\frac{R_{max}\, e}{H_{max}}(\lambda-t)+1\right)\right\} \qquad (3.3)$$

where, H(t) (mmol H_2/L_c) is the instantaneous hydrogen value, H_{max} (mmol H_2/L_c) is the maximum cumulative hydrogen value, R_{max} (mmol $H_2/L_c/h$) is the maximum hydrogen production rate, λ (h) the lag time and t process time (h).

The hydrogen production experimental data of *Rb.capsulatus* DSM1710 on treated DFESBTJ2 and *Rb.capsulatus* YO3 (hup^-) on treated DFESBTJ2 are fitted into the Modified Gompertz model (Figure 3.17, 3.18 and Appendix I). The Modified Gompertz model parameters of wild type and mutant strain are given in Tables 3.9 and 3.10, respectively.

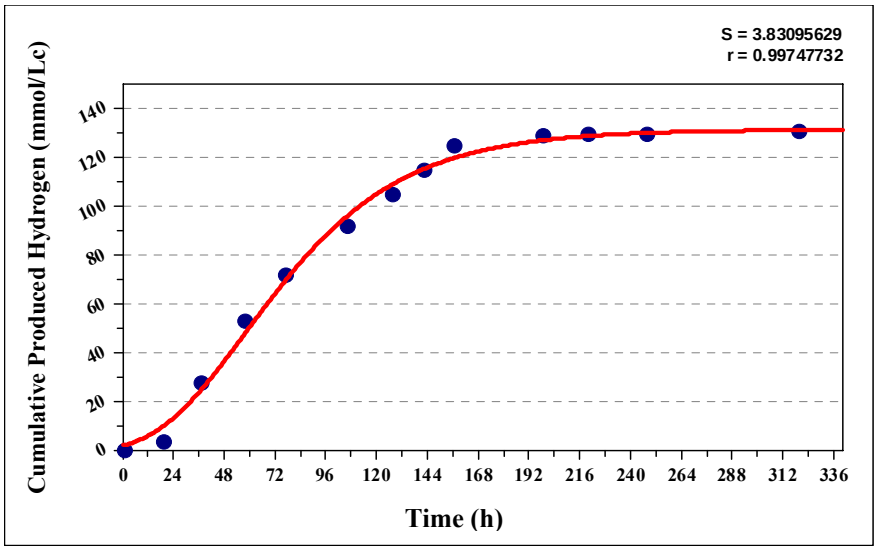

Figure 3.17 The Modified Gompertz Model on treated DFESBTJ2 *Rb.capsulatus* DSM1710 (●: experimental data, ▬: order)

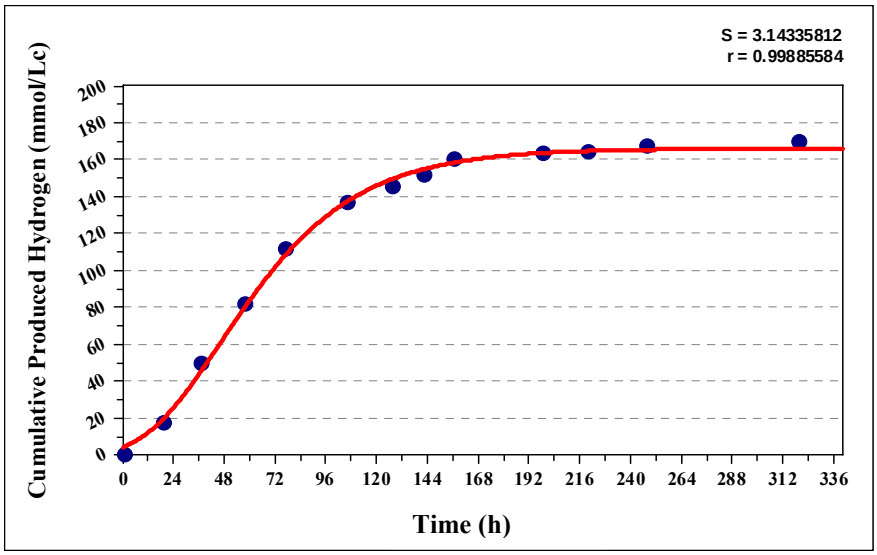

Figure 3.18 The Modified Gompertz Model on treated DFESBTJ2 *Rb.capsulatus* YO3 (hup$^-$) (●: experimental data, ▬: model fit)

Table 3.9 Comparison of the Modified Gompertz Model parameters with the experimental values acquired for *Rb.capsulatus* DSM1710 on untreated/treated DFESBTJ (e: experimental, m: model)

	Treated DFESBTJ2	**Untreated DFESBTJ2**	**Treated DFESBTJ3**	**Untreated DFESBTJ3**
r	0.998	0.998	0.998	0.987
$H_{max,e}$	131	77	146	30
$H_{max,m}$	132	74	140	27
$R_{max,e}$	1.18	1.02	1.06	0.275
$R_{max,m}$	1.17	1.02	1.12	0.230
λ_e	15	28	19	19
λ_m	16	28	14	14

Table 3.10 Comparison of the Modified Gompertz Model parameters with the experimental values acquired for *Rb.capsulatus* YO3 (hup^-) on untreated/treated DFESBTJ (e: experimental, m: model)

	Treated DFESBTJ2	**Untreated DFESBTJ2**	**Treated DFESBTJ3**	**Untreated DFESBTJ3**
r	0.999	0.998	0.998	0.996
$H_{max,e}$	170	118	166	62
$H_{max,m}$	166	114	163	60
$R_{max,e}$	1.62	1.51	1.45	0.705
$R_{max,m}$	1.7	1.72	1.38	0.730
λ_e	8	19	13	18
λ_m	10	22	13	19

r: extent of the fit

$H_{max,e}$: experimental maximum cumulative hydrogen (mmol H_2/L_c)

$H_{max,m}$: the maximum cumulative hydrogen obtained by the Modified Gompertz Model (mmol H_2/L_c)

$R_{max,e}$: experimental maximum hydrogen production rate (mmol $H_2/L_c/h$)

$R_{max,m}$: maximum hydrogen production rate obtained by the Modified Gompertz Model (mmol $H_2/L_c/h$)

λ_e : experimental lag time (h)

λ_m : lag time obtained by the Modified Gompertz Model (h)

e : constant (2.718282)

Tables 3.9 and 3.10 reveal that the experimental data fitted well to the model (r~1). Experimental/model maximum cumulative hydrogen values (H_{max}), experimental/model hydrogen production rates (R_{max}), experimental/model experimental lag time (λ) values are similar to each other. In addition, H_{max} values decreases in untreated DFESGTJ samples showing that high NH_4^+ concentration affected hydrogen production.

Shown in Table 3.5, are the maximum hydrogen productivities of the untreated and treated DFESGTJ. Higher maximum hydrogen productivities in the treated DFESGTJ were obtained compared to the untreated samples. The difference in productivities could be due to the presence of NH_4^+ in untreated effluent samples. It was demonstrated that nitrogenase can be inhibited rapidly by NH_4^+ via "switch-off" mechanism in *Rb.capsulatus* (Yakunin and Hallenbeck, 1998). Apart from this genetic level inhibition, nitrogenase can be inhibited simply by feedback inhibition as NH_4^+ is the end product of the hydrogen production reaction (Reaction 1.14).

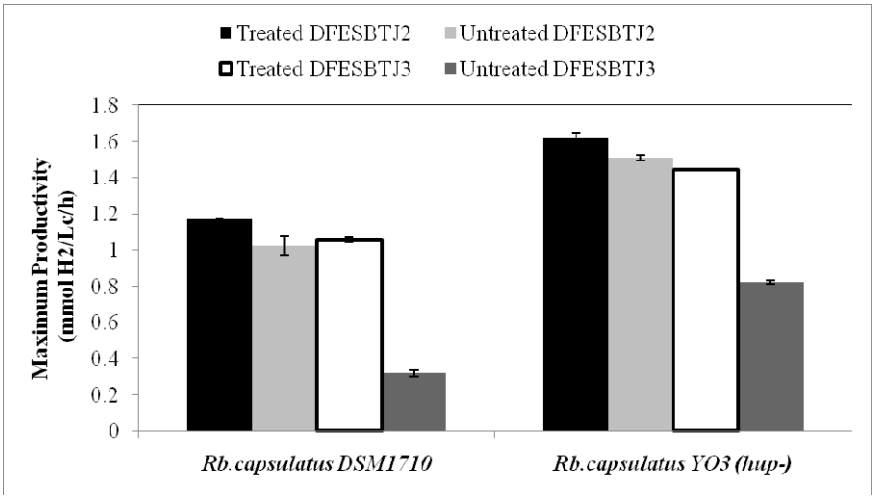

Figure 3.19 Comparison of the maximum productivities on untreated/treated DFESBTJ samples using *Rb.capsulatus* DSM1710 and *Rb.capsulatus* YO3 (hup^-)

When C/N ratio increased (Table 3.4), increase of the maximum hydrogen production and molar hydrogen yield for both bacteria strains was observed. For example, for *Rb.capsulatus* DSM1710 (Table 3.5) as the molar C/N ratio increased

from 9.41 to 24.3, the maximum hydrogen productivity and the molar yield increased from 1.02 to 1.17 and 37.9 to 64, respectively. For fed-batch operation of panel photobioreactors, Avcıoğlu (2010) and Androga et al. (2011a) reported the optimum C/N is to be 13 (molassed DFE) and 25 (defined medium), respectively. Also, Eroglu et al. (1999) indicated that C/N ratio is an important parameter for efficient hydrogen production.

Product yield factor was used in order to describe the amount of hydrogen (mmol) that was produced by 1 gram of bacteria. Low product yield factors were attained in the untreated DFESBTJ samples (Tables 3.5 and 3.6). This was an expected result due to the presence of higher biomass concentrations in untreated samples. Pekgöz (2010) also found that product yield factor decreases with the increasing biomass concentration owing to increasing NH_4^+ concentration.

In Tables 3.5 and 3.6, light conversion efficiencies were also proportional to the hydrogen production amounts because light intensity amount were constant. Due to the higher biomass of untreared DFESGTJ samples, light intensity penetration might be prevented by self shading especially in the deeper parts of the PBRs. Uyar et al. (2009a) also observed higher biomass accumulation when acetate was used as carbon source and they emphasized on decrease in the light intensity owing to high biomass.

PHB content was measured from the waste liquid at the end of the batch experiments in order to observe PHB production capabilities of both strains in DFESBTJ samples with respect to NH_4^+ concentration. The main carbon sources were acetate and lactate in DFESBTJ samples and especially acetate was reported to be a good substrate for PHB production by Hustede et al. (1993), Khatipov et al. (1998), Koku et al. (2002) and Kim et al. (2011). Higher amounts of PHB was obtained in the treated DFESBTJ than the untreated DFESBTJ samples (Tables 3.5 and 3.6). The maximum PHB (25.5%) was produced by *Rb.capsulatus* DSM1710 in treated DFESBTJ2 which had a C/N ratio of 24.3. This might be due to hydrogen production availability of treated DFESGTJ samples (high C/N ratio) since PHB is preferably produced under excess carbon and limited nitrogen sources (Hustede et al., 1993) and PHB production is a competitive process of hydrogen production (Kim et al.,

2006). Waligorska et al. (2009) also observed a direct correlation between increasing C/N ratio and PHB production.

The variation in the concentration of acetate and lactate were traced during the photofermentation on untreated/treated DFESGTJ samples. Acetate (30 mM) and lactate (~10 mM) that were initially present in DFESBTJ samples were consumed completely (Figure 3.20, 3.21, 3.22, 3.23). The organic acids were consumed sequentially with lactic acid being used first. Sevinç (2010) also reported that lactic acid was used first by *Rb. capsulatus* DSM1710 in acetate (40 mM) and lactate (7.5 mM) containing media. Lactic acid was consumed in first 58 hours in untreated effluents by both bacteria strains (Figures 3.20 and 3.21). However, the consumption of lactic acid took longer by wild type and mutant strain (155 and 78 hours, respectively) in treated effluents. In contrast, Eroglu et al. (1999) observed slow consumption of organic acid (malate) with the increasing nitrogen source (glutamate).

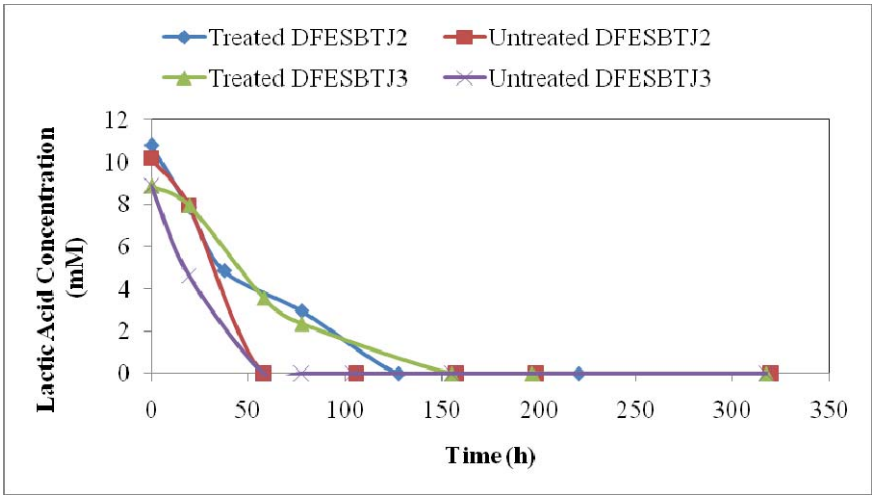

Figure 3.20 Lactic acid consumption for untreated/treated DFESBTJ2 and DFESBTJ3 using *Rb.capsulatus* DSM1710

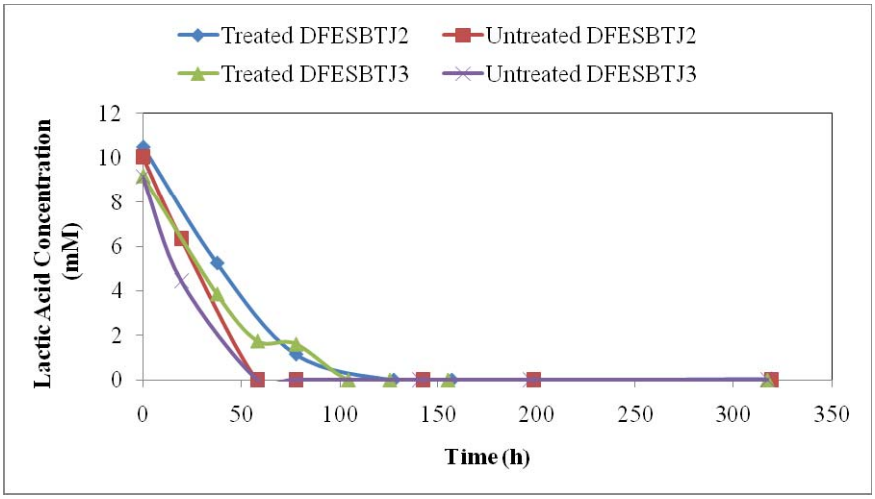

Figure 3.21 Lactic acid consumption for untreated/treated DFESBTJ2 and DFESBTJ3 using *Rb.capsulatus* YO3 (hup^-)

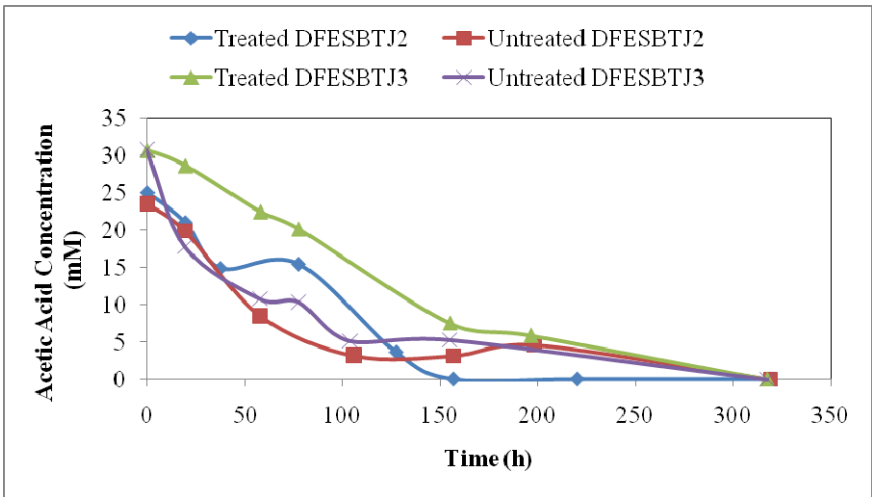

Figure 3.22 Acetic acid consumption for untreated/treated DFESBTJ2 and DFESBTJ3 using *Rb.capsulatus* DSM1710

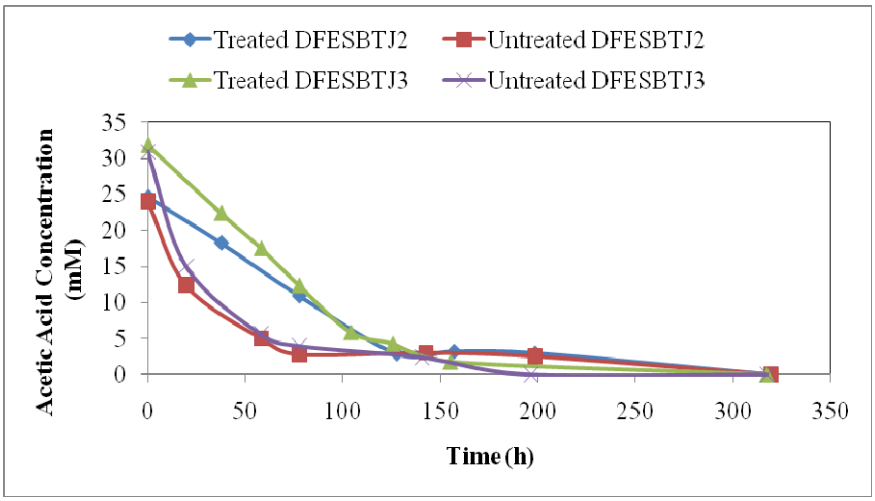

Figure 3.23 Acetic acid Consumption for untreated/treated DFESBTJ2 and DFESBTJ3 using *Rb.capsulatus* YO3 (hup^-)

There were negligible amounts of propionic acid and butyric acid in the PBRs (data not shown). However, there was a significant rise in formic acid concentration in all reactors (Figures 3.24 and 3.25). High concentration of formic acid (~up to 20 mM) was observed especially in treated effluents for both strains, which corresponded to lactic acid depletion time (58 h). Sevinç (2010) also observed formic acid production when lactic acid was present in the system. After this initial rise, fluctuations were observed in concentration of formic acid indicating that bacteria might have used and reproduced formic acid in all of the PBRs. Androga (2009) and Eroglu et al. (2008) also reported formation of formic acid in their studies on different carbon sources and formation of formic acid attributed to the low light intensity. However, in this study light intensity was constant; therefore, it can be speculated that both strains were probably induced by the components owing to the complex nature of DFESBTJ and had a change in their metabolism, which directed them to produce formic acid. Also, it should be noted that pyruvate formate lyase (PFL) which associates the conversion of pyruvate and CoA to acetyl-CoA and formate exist in *Rb.capsulatus* (Haselkorn et al., 2001). Therefore, before acetate consumption, lactate may be involved through pyruvate resulting formate production (Figure 1.2). In addition, PFL catalyzes a reversible reaction, one might think that acetate can also converted to formate by backward reaction.

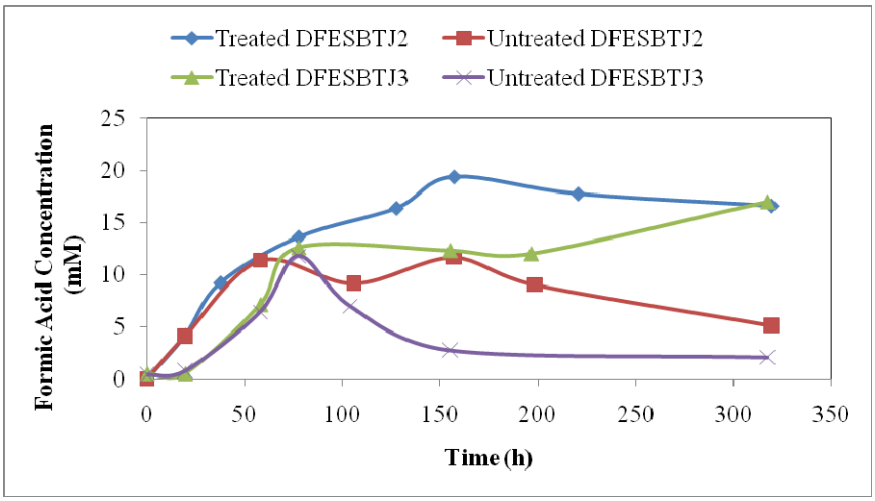

Figure 3.24 Formic acid Production for untreated/treated DFESBTJ2 and DFESBTJ3 using *Rb.capsulatus* DSM1710

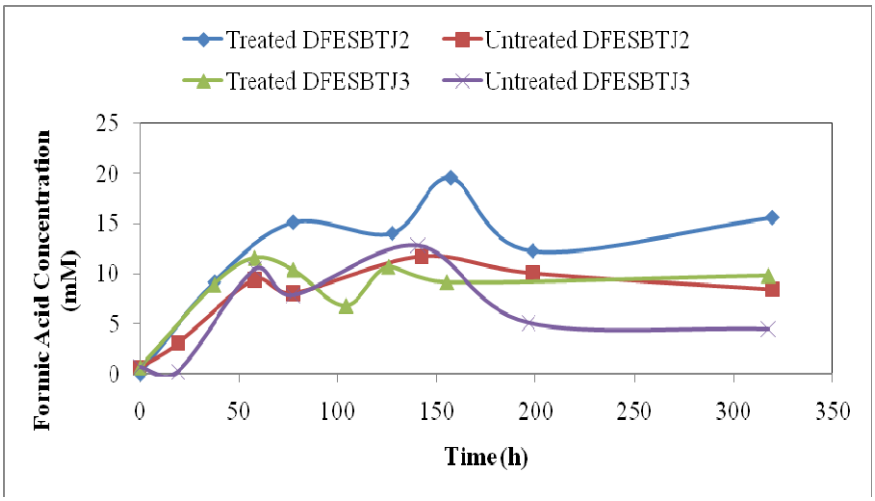

Figure 3.25 Formic acid Production for untreated/treated DFESBTJ2 and DFESBTJ3 using *Rb.capsulatus* YO3 (hup^-)

Integral method for analysis of data is a common way in interpretation of batch reactor data (Sevinç, 2010, Uyar et al., 2009a, Eroglu et al. 1999). Procedure of integral method for analysis of data is given in Appendix F.The rate constants (k) and the coefficient of determination values (R^2) of experimental data (Figure 3.22 and 3.23) are tabulated in Table 3.11 and 3.12 for *Rb.capsulatus* DSM1710 and *Rb.capsulatus* YO3 (hup^-), respectively. The curve for *Rb.capsulatus* DSM1710 on

treated DFESBTJ3 and for *Rb.capsulatus* YO3 (hup$^-$) on untreated DFESBTJ2 are given in Figure 3.26 and 3.27 as an example. The most fitted curves for other experiments are given in Appendix J.

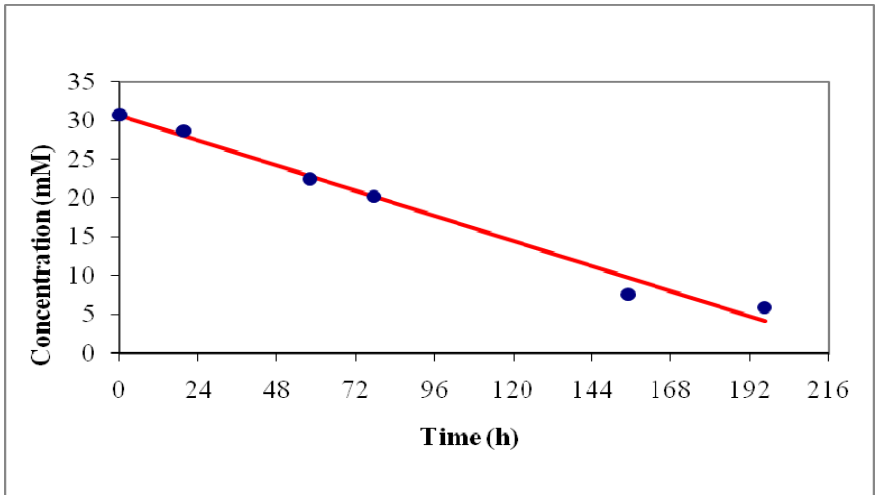

Figure 3.26 Zeroth order kinetics for acetic acid consumption for *Rb.capsulatus* DSM1710 on treated DFESBTJ3

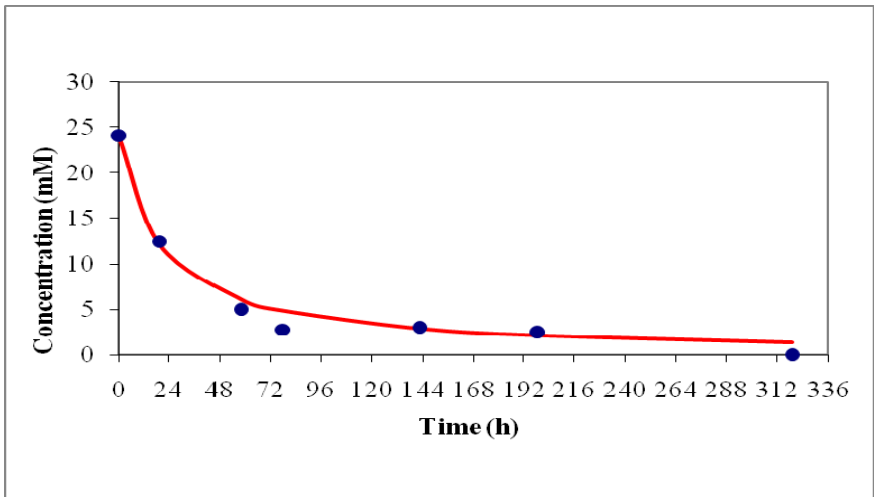

Figure 3.27 Second order kinetics for acetic acid consumption for *Rb.capsulatus* YO3 (hup$^-$) on untreated DFESBTJ2

Table 3.11 Extent of the fits and rate constants for acetic acid consumption for *Rb.capsulatus* DSM1710 on untreated/treated DFESBTJ

Type of DFESBTJ	Zeroth Order (n=0)		First Order (n=1)		Second Order (n=2)	
	k_o	R^2	k_1	R^2	k_2	R^2
Untreated DFESBTJ2	0.127	0.636	0.012	0.699	0.001	0.625
Treated DFESBTJ2	0.164	0.898	0.013	0.847	0.001	0.714
Untreated DFESBTJ3	0.215	0.533	0.014	0.830	0.001	0.872
Treated DFESBTJ3	0.136	0.984	0.008	0.959	0.001	0.890

Table 3.12 Extent of the fits and rate constants for acetic acid consumption for *Rb.capsulatus* YO3 (hup$^-$) on untreated/treated DFESBTJ

Type of DFESBTJ	Zeroth Order (n=0)		First Order (n=1)		Second Order (n=2)	
	k_o	R^2	k_1	R^2	k_2	R^2
Untreated DFESBTJ2	0.199	0.374	0.019	0.663	0.003	0.751
Treated DFESBTJ2	0.134	0.862	0.012	0.897	0.002	0.836
Untreated DFESBTJ3	0.267	0.414	0.021	0.842	0.003	0.994
Treated DFESBTJ3	0.220	0.950	0.016	0.934	0.002	0.635

In the batch experiments using *Rb.capsulatus* DSM1710, the untreated/treated samples obeyed varying acetic acid consumption orders (Table 3.11) while in the batch experiments using *Rb.capsulatus* YO3 (hup$^-$) it was observed that the untreated DFESBTJ (2 and 3) samples displayed second order kinetics for acetic acid consumption (Table 3.12). However, in the treated samples varying kinetic orders were obtained; the R^2 values were quite close to each other illustrating that probably the reaction order was complex.

The dark fermentation effluents used in these experiments were complex media that contained different concentrations of anions, cations and organic acids which could adversely affect the acetic acid consumption order. Uyar et al. (2009a) reported different tendencies of PNS bacteria that utilize organic acids. Sevinç (2010) found that *Rb.capsulatus* consumed acetic acid after utilizing lactic acid. Boran (2011) observed zero order kinetic for acetic acid consumption of *Rb.capsulatus* DSM1710 on dark fermentation effluent of thick juice during batch period of tubular reactor.

Hydrogen production yields and productivities reported in different studies using photo-fermentative bacteria in batch PBRs were compared in Table 3.13. According to Table 3.13, molar yield and acetate conversion obtained in this study were comparable to those obtained on other feedstocks.

Table 3.13 Comparison of various batch experiments using different feedstocks

Feedstock	Bacteria	V_{PBR} (mL)	Productivity (mmol $H_2/L_c/h$)	H_2 Yield	References
DFESBTJ[c]	*Rb. capsulatus* DSM1710	150	1.17	64%[a]	This study
DFESBTJ[c]	*Rb. capsulatus* YO3 (hup^-)	150	1.62	79.7%[a]	This study
Molasses DFE	*Rb. capsulatus* YO3 (hup^-)	55	1.37	58%[a]	Özgür et al., 2010a
Molasses DFE	*R. palustris* DSM127	55	1.16	46%[a]	Özgür et al., 2010a
Glucose DFE	*Rb. capsulatus* DSM1710	55	0.4	34%[a]	Özgür et al., 2010b
Glucose DFE	*Rb. capsulatus* YO3 (hup^-)	55	0.62	30%[a]	Afsar et al., 2011
Molasses DFE	*Rb. capsulatus* DSM1710	55	0.75	20%[a]	Özgür et al., 2010b
PSP hydrolysate DFE	*Rb. capsulatus* DSM1710	55	0.55	24%[a]	Özgür et al., 2010b
PSP hydrolysate DFE	*Rb. capsulatus* YO3 (hup^-)	55	0.50	23%[a]	Afsar et al., 2011
Cassava Starch DFE[d]	*R. palustris*	25	0.73[b]	131.9 mL H_2/g starch	Su et al., 2009
Miscanthus Hydrolysate DFE	*Rb. capsulatus* DSM155	105	0.85[b]	NA	Uyar et al., 2009b
Olive mill waste water	*Rb. sphaeroides* O.U.001	55	0.36[b]	NA	Eroglu et al., 2006
Corncob DFE[c]	*Rb. sphaeroides*	320	1.4[b]	51%	Yang et al., 2010

[a] Molar hydrogen yield % of theoretical maximum.

[b] Calculated based on the given value in the paper.

[c] Effluent contains ethanol.

[d] Effluent contains alcohol.

3.3 Batch Hydrogen Production on Ethanol Containing Medium

Many by-products are formed in dark fermentation. The direct usage of dark fermentation effluents can be done if the components of the medium and the products of the fermentation from the first reactor do not affect the viability of the purple bacteria (Laurinavichene et al., 2008). Ethanol may be produced in different amounts during dark fermentation of feedstocks depending on the fermentative bacteria. Therefore, for investigation of the effects of ethanol on hydrogen production by PNS bacteria, experiments were carried out in 150 mL PBRs using the setup and procedures explained in section 2.3. Control PBR contained 30/2 Acetate/Glutamate defined medium without ethanol.

In order to analyze the experimental data, maximum biomass, cumulative produced hydrogen, maximum productivity, molar hydrogen yield, product yield factor, light conversion efficiency and produced PHB at different concentrations of EtOH are tabulated in Tables 3.14 and 3.15 for *Rb.capsulatus* DSM1710 and *Rb.capsulatus* YO3 (hup^-), respectively. The calculations of these parameters are given in Appendix F.

Table 3.14 Effect of ethanol concentration on photofermentative hydrogen production by *Rb.capsulatus* DSM1710

Initial EtOH (mM)	$R_{c/a}$	Maximum Biomass (gdw/L_c)	Cumulative Produced H_2 (mmol)	Maximum Productivity (mmol H_2/L_c/h)	Molar H_2 Yield (% of theoretical maximum)	Product Yield Factor (mmol H_2/gdw)	Light Conversion Efficiency (%)	PHB Content (% of dry cell weight)
0	0	0.775 ± 0.007	9.53 ± 2.24	0.491 ± 0.009	53.9 ± 14.3	98.8 ± 33.8	0.161 ± 0.034	41.2 ± 4.2
6.25	0.2	0.857 ± 0.010	7.62 ± 0.54	0.426 ± 0.045	43.2 ± 2.8	67.3 ± 3.5	0.138 ± 0.009	61.6 ± 11.8
12.5	0.4	0.866 ± 0.003	9.01 ± 0.41	0.583 ± 0.014	51.1 ± 1.8	81.3 ± 0.7	0.163 ± 0.006	59.2 ± 2.4
25	0.8	0.879 ± 0.016	8.66 ± 0.31	0.533 ± 0.035	49.2 ± 1.4	76.9 ± 1.3	0.157 ± 0.004	51.9 ± 2.9
37.5	1.25	0.863 ± 0.005	8.48 ± 0.09	0.499 ± 0.040	48.1 ± 0.6	78.2 ± 0.3	0.154 ± 0.002	74.4 ± 15.7
50	1.6	0.654 ± 0.014	9.84 ± 0.01	0.413 ± 0.005	55.6 ± 0.1	115 ± 8	0.104 ± 0	34.9 ± 3.3
100	3.33	0.607 ± 0.005	10.1 ± 0.1	0.427 ± 0.005	56.9 ± 0.6	144 ± 0.4	0.106 ±0.001	34.8 ± 3.4
200	6.66	0.599 ± 0.008	7.88 ± 0.88	0.284 ± 0.035	44.5 ± 4.9	109 ± 9	0.083 ± 0.009	33.1 ± 3.5

Table 3.15 Effect of ethanol concentration on photofermentative hydrogen production by *Rb.capsulatus* YO3 (hup^-)

Initial EtOH (mM)	$R_{e/a}$	Maximum Biomass (gdw/L_c)	Cumulative Produced H_2 (mmol)	Maximum Productivity (mmol H_2/Lc/h)	Molar H_2 Yield (% of theoretical maximum)	Product Yield Factor (mmol H_2/gdw)	Light Conversion Efficiency (%)	PHB Content (% of dry cell weight)
0	0	0.626 ± 0.021	15.3 ± 0.1	1.23 ± 0.03	86.6 ± 0.5	171 ± 7	0.365 ± 0.002	2.09 ± 0.05
6.25	0.2	0.547 ± 0.011	14.9 ± 0.1	1.31 ± 0.01	84.4 ± 0.2	191 ± 4	0.356 ± 0.001	4.58 ± 0.15
12.5	0.4	0.622 ± 0.016	14.7 ± 0.4	1.31 ± 0.04	83.2 ± 2.2	165 ± 9	0.351 ± 0.009	7.73 ± 0.54
25	0.8	0.689 ± 0.027	14.2 ± 0.1	1.27 ± 0.05	80.3 ± 0.3	144 ± 7	0.338 ± 0.001	19.9 ± 3.0
37.5	1.25	0.756 ± 0.007	12.9 ± 0.1	1.02 ± 0.04	73.7 ± 0.6	121 ± 2	0.307 ± 0.002	36.6 ± 3.8
50	1.6	0.822 ± 0.021	13.1 ± 0.4	0.980 ± 0.014	74.5 ± 2.5	113 ± 8	0.314 ± 0.011	52.5 ± 3.5
100	3.33	0.854 ± 0.016	11.9 ± 0.4	0.768 ± 0.020	67.6 ± 2.4	99.8 ± 5	0.285 ± 0.010	44.2 ± 0
200	6.66	0.729 ± 0.021	8.9 ± 0.4	0.583 ± 0.014	50.8 ± 1.9	88.1 ± 6	0.214 ± 0.008	48.8 ± 5.1

Cell growth of *Rb. capsulatus* DSM1710 and *Rb.capsulatus* YO3 (hup^-) versus time are plotted for different initial ethanol concentrations (Figures 3.28 and 3.29). The typical cell growth curves were observed in the experiments. Due to the possible inhibitory effect of EtOH on growth of *Rb. capsulatus* DSM1710 (Figure 3.28) and *Rb.capsulatus* YO3 (hup^-) (Figure 3.29), it was expected to have a longer lag phase period especially at 50, 100 and 200 mM EtOH than control PBR. However, it was seen that there was no lag phase period above 50 mM EtOH. On the other hand, Pantazopoulous and Madigan (2000) observed long lag duration when *Rb. capsulatus* strain B10 grew on ethanol and bicarbonate.

The specific growth rates (μ_{max}) of *Rb. capsulatus* DSM1710 cultures showed similar values between 6.25 mM and 100 mM EtOH, the specific growth rates varied between 0.026 h^{-1} and 0.032 h^{-1}. It can be seen in Figure 3.28 at 50 mM EtOH and above this concentration, the characteristics of growth curves changed. However, maximum concentration of bacterial culture and specific growth rate decreased significantly at 200 mM (Tables 3.14 and 3.16). The maxiumum biomass of the *Rb. capsulatus* DSM1710 culture were almost similar between control and 37.5 mM EtOH, which was ~0.85 gdw/L_c; however, at 50, 100 and 200 mM EtOH, a decline to ~0.65 gdw/L_c in maximum biomass was seen (Figure 3.28).

The growth curve of *Rb.capsulatus* YO3 (hup^-) was illustrated in Figure 3.29. Specific growth rates and lag phase period of *Rb.capsulatus* YO3 (hup^-) growth decreased gradually with the increasing EtOH concentration and the least specific growth rate was observed at 200 mM as 0.024 h^{-1}. The specific growth rates of (0-25) mM EtOH and (37.5-200) mM EtOH were almost identical, which are varied between 0.031 and 0.038 h^{-1}; 0.024 and 0.028 h^{-1}, respectively (Table 3.17). Although the lag period got longer with the increasing EtOH, the growth continued slightly with the increasing EtOH concentrations and reached higher cell concentrations than the observed cell growth of *Rb. capsulatus* DSM1710.

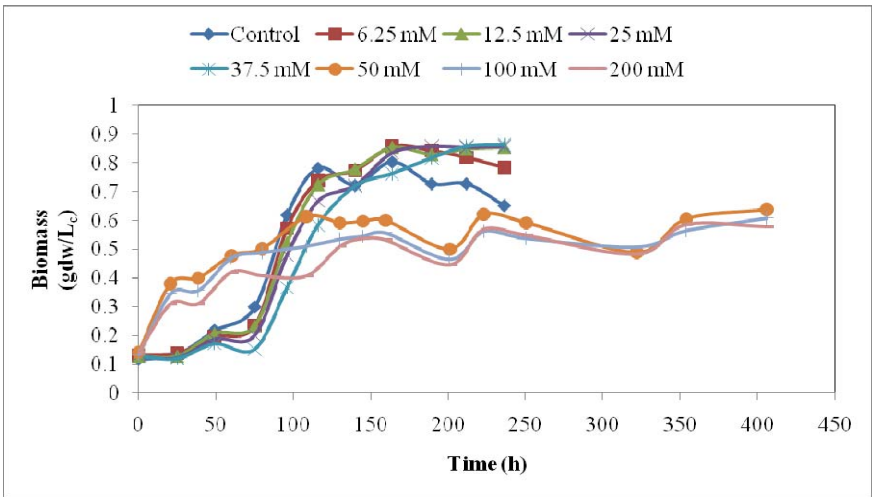

Figure 3.28 Cell growth of *Rb. capsulatus* DSM1710 for different EtOH concentrations

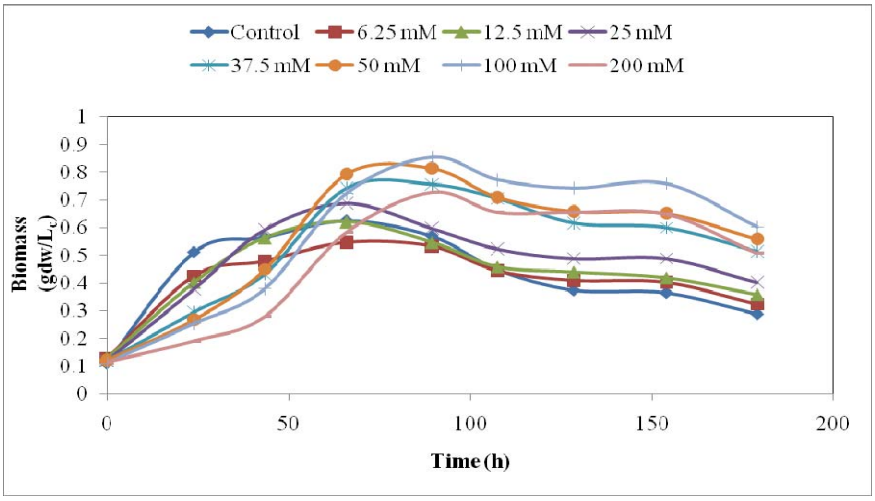

Figure 3.29 Cell growth of *Rb. capsulatus* YO3 (hup$^-$) for different EtOH concentrations

The cell growth of wild type and mutant which are illustrated in Figure 3.28 and 3.29 respectively, were fitted into logistic growth model by Curve Expert 1.4 software. The logistic model curve fits for the different EtOH concentrations varying between 6.25 and 200 mM are shown in Appendix H; the curve for *Rb. capsulatus* DSM1710 at 37.5 mM EtOH and *Rb.capsulatus* YO3 (hup$^-$) at 100 mM EtOH are given in Figure 3.30 and Figure 3.31, respectively, as samples.

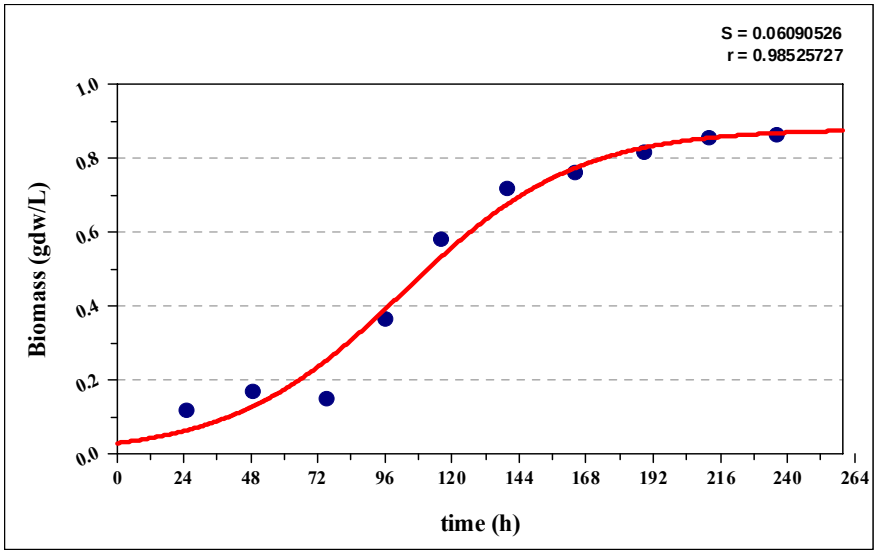

Figure 3.30 The logistic growth model for *Rb. capsulatus* DSM1710 at 37.5 mM EtOH (●: experimental data, ▬: model fit)

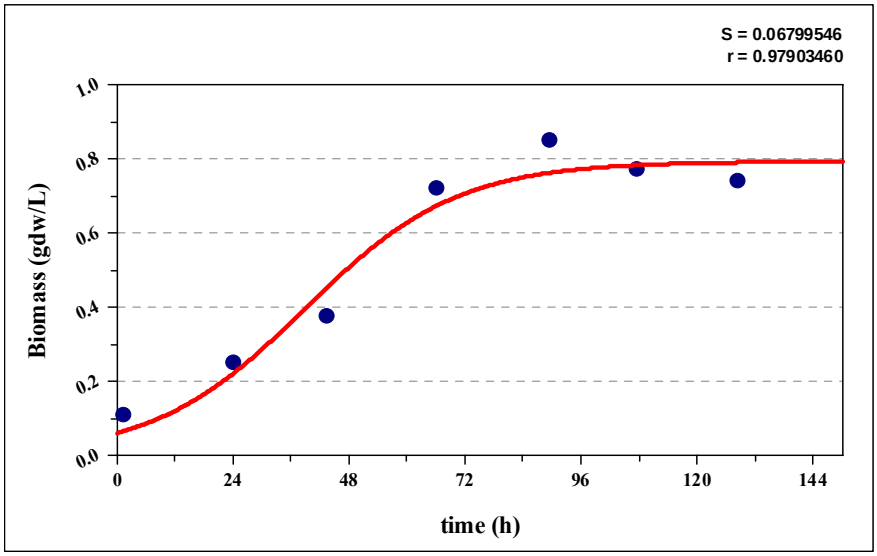

Figure 3.31 The logistic growth model for *Rb.capsulatus* YO3 (hup^-) at 100 mM EtOH (●: experimental data, ▬: model fit)

Table 3.16 Comparison of logistic model constants and experimental for *Rb. capsulatus* DSM1710 at different EtOH concentrations

EtOH (mM)	0 (Control)	6.25	12.5	25	37.5	50	100	200
r	0.971	0.978	0.984	0.986	0.985	0.927	0.95	0.929
$X_{o,e}$	0.117	0.131	0.128	0.129	0.128	0.141	0.133	0.141
$X_{o,m}$	0.029	0.025	0.033	0.035	0.030	0.182	0.168	0.195
$X_{max,e}$	0.803	0.857	0.855	0.857	0.863	0.638	0.608	0.586
$X_{max,m}$	0.775	0.842	0.871	0.882	0.881	0.581	0.539	0.540
μ_{max}	0.019	0.028	0.027	0.029	0.032	0.027	0.026	0.016
k_c	0.045	0.042	0.038	0.034	0.033	0.044	0.044	0.023

Table 3.17 Comparison of logistic model constants and experimental for *Rb.capsulatus* YO3 (hup^-) at different EtOH concentrations

EtOH (mM)	0 (Control)	6.25	12.5	25	37.5	50	100	200
r	0.951	0.918	0.918	0.916	0.951	0.953	0.979	0.977
$X_{o,e}$	0.112	0.128	0.128	0.119	0.119	0.121	0.112	0.114
$X_{o,m}$	0.097	0.108	0.109	0.086	0.080	0.061	0.062	0.047
$X_{max,e}$	0.570	0.550	0.620	0.690	0.760	0.820	0.850	0.730
$X_{max,m}$	0.550	0.470	0.530	0.570	0.670	0.730	0.730	0.690
μ_{max}	0.038	0.031	0.034	0.037	0.027	0.028	0.027	0.024
k_c	0.170	0.140	0.110	0.110	0.070	0.080	0.060	0.060

r: correlation coefficient (extent of fit)

$X_{o,e}$: Experimental initial bacterial concentration, (gdw/L_c)

$X_{o,m}$: Initial bacterial concentration obtained by logistic model, (gdw/L_c)

$X_{max,e}$: Experimental maximum bacterial concentration, (gdw/L_c)

$X_{max,m}$: Maximum bacterial concentration obtained by logistic model, (gdw/L_c)

μ_{max}: Specific growth rate constant obtained by exponential model, (h^{-1})

k_c: Specific growth rate constant obtained by logistic model, (h^{-1})

According to the Tables 3.16 and 3.17, experimental data fitted well to the model (r~1). Initial (X_o) cell concentrations of experimental and model are different between 0-37.5 mM EtOH and the maximum cell concentrations (X_{max}) of experimental and model are close to each other for *Rb. capsulatus* DSM1710 at every EtOH concentration (Table 3.16).

Initial (X_o) cell concentrations of experimental and model are quite different between 50-200 mM EtOH and the maximum cell concentrations (X_{max}) of experimental and model can be said close to each other for *Rb.capsulatus* YO3 (hup^-) at every EtOH concentration (Table 3.17). Sevinç (2010) and Nath et al. (2008) also reported that X_{max} values of experimental and logistic were found to be close to each other. Specific growth rates of *Rb. capsulatus* DSM1710 (k_c) showed unsteady patterns (except the decrease in 200 mM) whereas k_c values of *Rb.capsulatus* YO3 (hup^-) decreased with the increasing EtOH concentration probably indicating the inhibitory effect of EtOH.

In Figure 3.32 and 3.33, the variation of EtOH concentration in the PBR for wild type and mutant strain during the experiment are shown, respectively.

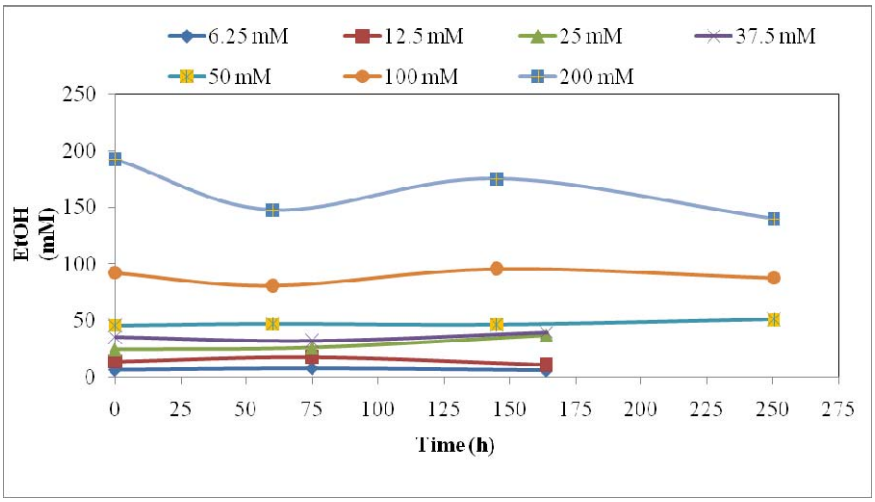

Figure 3.32 Ethanol variation for *Rb.capsulatus* DSM1710

During the experiment, EtOH concentrations remained almost stable in 6.25, 12.5, 25, 37.5 and 50 mM EtOH containing bottles that contained *Rb.capsulatus* DSM1710. However, a slight decrease in EtOH concentration at 100 and 200 mM EtOH containing bottles was noticed (Figure 3.32). Also for the *Rb.capsulatus* YO3 (hup^-), EtOH concentrations stayed almost constant in 6.25, 12.5, 25, 37.5, 50 and 100 mM EtOH containing bottles except 200 mM EtOH containing bottle (Figure 3.33).

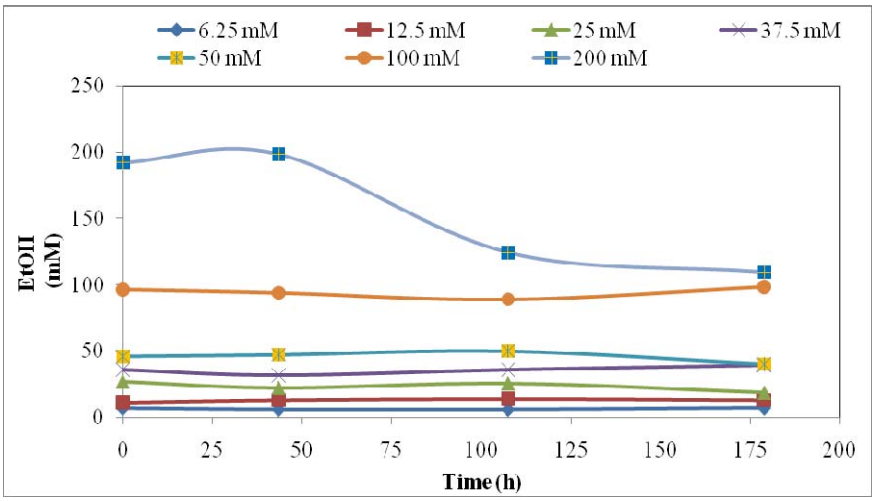

Figure 3.33 Ethanol variation for *Rb.capsulatus* YO3 (hup$^-$)

There was no considerable pH change in both bacteria subjected to different EtOH concentrations (Figures 3.34 and 3.35). pH varied in 6.4 to 7.4 range for *Rb.capsulatus* DSM1710 and in 6.6 to 7.5 range for *Rb. capsulatus* YO3 (hup$^-$). Since it is known that hydrogen is produced in 6.0 to 8.0 pH range (Sasikala et al. 1991), these pH ranges did not generate negative effect on hydrogen production.

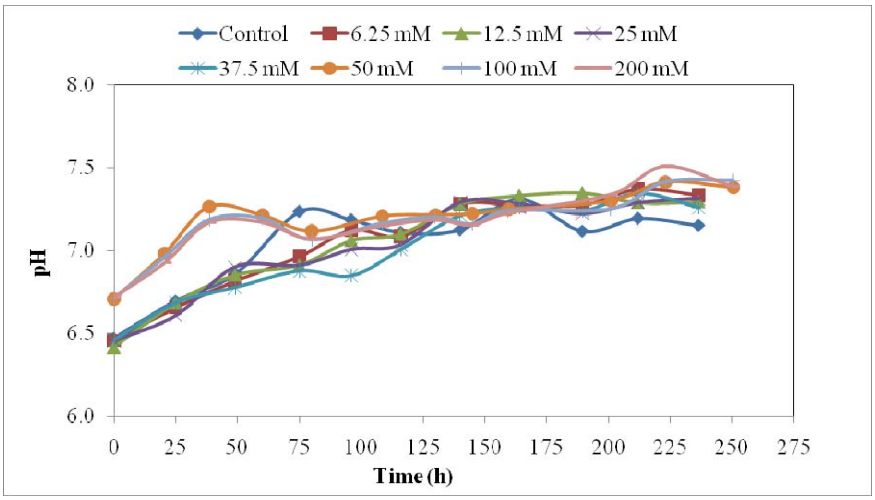

Figure 3.34 Variation of pH with time for different ethanol concentrations using *Rb.capsulatus* DSM1710

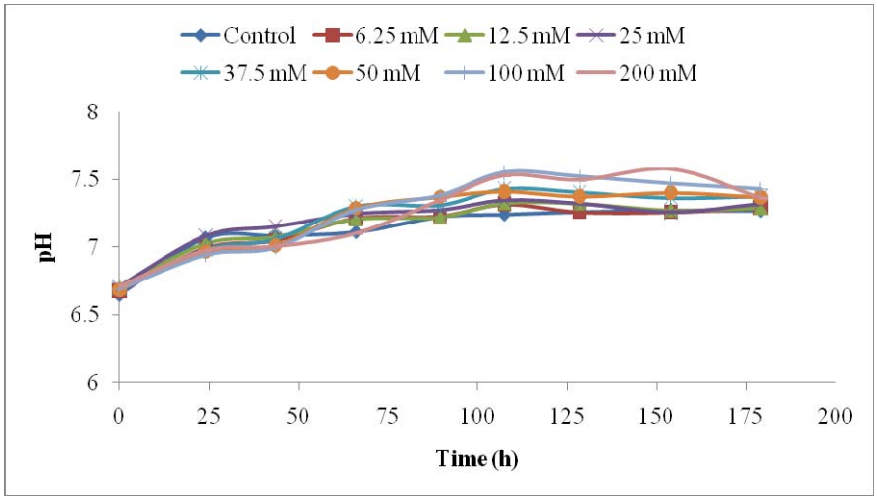

Figure 3.35 Variation of pH with time for different ethanol concentrations for *Rb. capsulatus* YO3 (hup$^-$)

In figure 3.36 and 3.37, the trend of hydrogen production for both bacteria are shown, in which millimoles of hydrogen collected are plotted against time measured in hours.

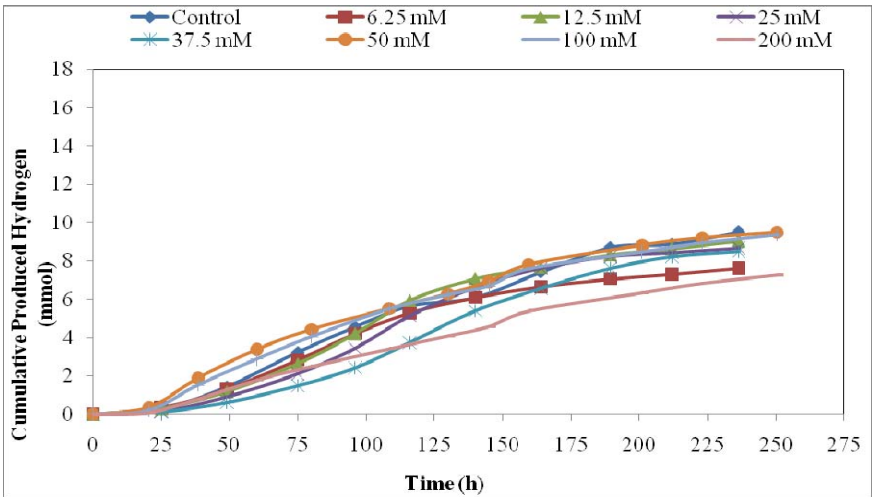

Figure 3.36 Cumulative hydrogen production for different EtOH concentrations for *Rb.capsulatus* DSM1710

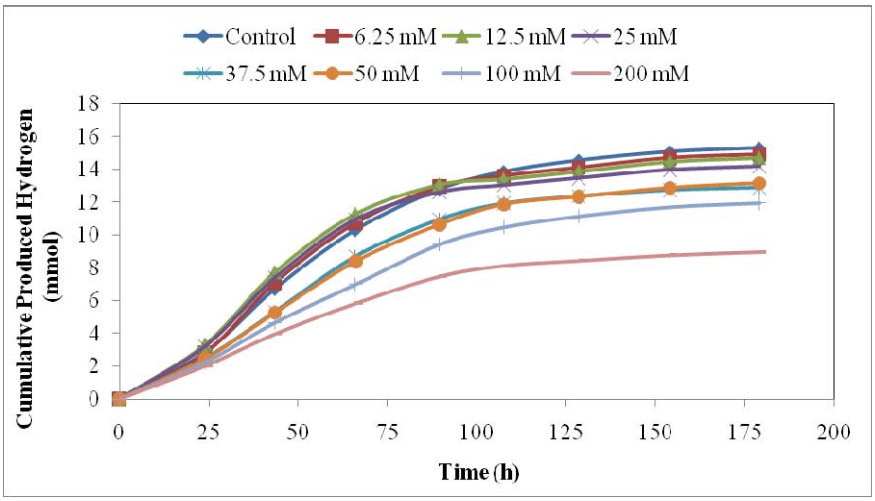

Figure 3.37 Cumulative hydrogen production for different EtOH concentrations using *Rb. capsulatus* YO3 (hup$^-$)

Wild type strain produced nearly same amounts of hydrogen at all EtOH concentrations but in different hydrogen production rates (Figure 3.36 and Table 3.18). The lowest hydrogen production was observed at 200 mM EtOH (7.88 mmol). High amounts of EtOH showed no significant effect on total produced hydrogen amount and productivity for *Rb. capsulatus* DSM1710 (except 200 mM EtOH) and it is interesting due to no consumption of EtOH observed (Figure 3.32), but it may be speculated that EtOH can somehow direct the metabolism of bacteria, up to 100 mM. Therefore, it is difficult to declare a certain correlation between increasing ethanol concentration and hydrogen production for wild type strain. As for mutant strain, the lowest hydrogen production was monitored at 200 mM EtOH (8.96 mmol). Almost same amounts of hydrogen separately in 0 to 25 mM and in 37.5 to 100 mM EtOH range were generated (Figure 3.37 and Table 3.19). There is a significant decrease in hydrogen productivity and cumulative hydrogen production at 200 mM EtOH for both strains.

The hydrogen production experimental data of *Rb.capsulatus* DSM1710 and *Rb.capsulatus* YO3 (hup$^-$) are fitted into the Modified Gompertz and fitted curves at 6.25 mM EtOH are given as samples in Figure 3.38 And 3.39; curves for other ethanol concentrations are given in Appendix I.

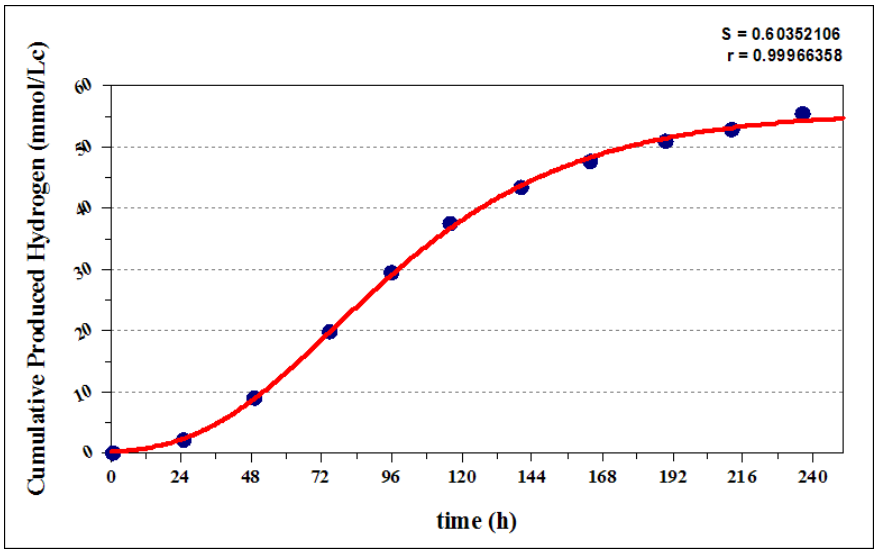

Figure 3.38 The Modified Gompertz Model at 6.25 mM EtOH containing medium for *Rb.capsulatus* DSM1710 (●: experimental data, ▬: model fit)

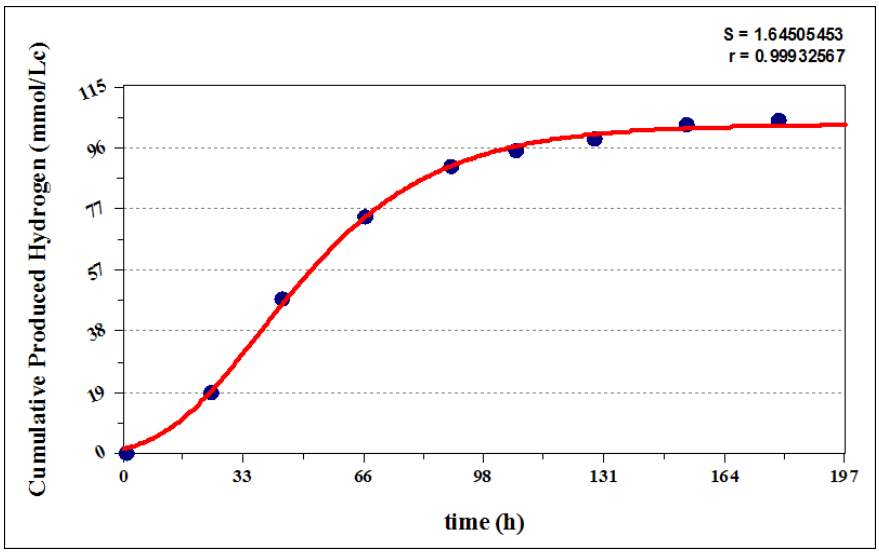

Figure 3.39 The Modified Gompertz Model at 6.25 mM EtOH containing medium for *Rb.capsulatus* YO3 (hup^-) (●: experimental data, ▬: model fit)

Table 3.18 Comparison of the Modified Gompertz Model parameters with the experimental values acquired at different ethanol concentrations for *Rb.capsulatus* DSM1710

EtOH (mM)	**0 (Control)**	**6.25**	**12.5**	**25**	**37.5**	**50**	**100**	**200**
r	0.996	1.000	0.999	0.999	0.999	1.000	1.000	0.998
$H_{max,e}$	65.2	55.4	65.9	63.5	62.9	72.5	74.8	59.2
$H_{max,m}$	71.5	55.9	67.2	66.7	71.3	73.4	75.2	60.9
$R_{max,e}$	0.491	0.426	0.583	0.533	0.499	0.413	0.427	0.284
$R_{max,m}$	0.453	0.453	0.526	0.550	0.471	0.418	0.410	0.302
λ_e	23	28	36	40	54	9	15	18
λ_m	29	31	41	49	58	13	17	28

Table 3.19 Comparison of the Modified Gompertz Model parameters with the experimental values acquired at different ethanol concentrations for *Rb.capsulatus* YO3 (hup^-)

EtOH (mM)	**0 (Control)**	**6.25**	**12.5**	**25**	**37.5**	**50**	**100**	**200**
r	1.000	0.999	0.999	0.999	1.000	1.000	0.999	0.999
$H_{max,e}$	107	104	102	99	90.4	92.6	84.2	63.1
$H_{max,m}$	107	103	100	96	91.1	93.1	85.9	63.2
$R_{max,e}$	1.23	1.31	1.31	1.27	1.02	0.980	0.768	0.583
$R_{max,m}$	1.35	1.45	1.53	1.49	1.16	1.09	0.902	0.741
λ_e	2	8	6	6	8	7	3	1
λ_m	10	11	9	10	11	10	9	7

r: extent of the fit

$H_{max,e}$: experimental maximum cumulative hydrogen (mmol H_2/L_c)

$H_{max,m}$: the maximum cumulative hydrogen obtained by the Modified Gompertz Model (mmol H_2/L_c)

$R_{max,e}$: experimental maximum hydrogen production rate (mmol $H_2/L_c/h$)

$R_{max,m}$: maximum hydrogen production rate obtained by the Modified Gompertz Model (mmol $H_2/L_c/h$)

λ_e : experimental lag time (h)

λ_m : lag time obtained by the Modified Gompertz Model (h)

e : constant (2.718282)

Table 3.18 and 3.19 present a summary of Modified Gompertz and experimental parameters for *Rb.capsulatus* DSM1710 and *Rb.capsulatus* YO3 (hup^-), respectively and the parameters were close to each other as well as the extent of the fit (r~1). However, at some conditions lag time of model was different from lag time of experimental, especially at high concentrations of ethanol, for both strains. This may be caused by a possible shift in metabolism of bacteria forced by high ethanol concentration. In addition, as it stated before, the maximum biomass at these concentration were low compared to other concentrations. In other words, the nutrient balance in the media may direct bacteria to produce hydrogen to maintain its redox poise and not to try to spend energy for biomass.

Molar productivity values for different ethanol concentrations using *Rb.capsulatus* DSM1710 and *Rb.capsulatus* YO3 (hup^-) are given in Figure 3.40. The photofermentative hydrogen production observed in nearly same hydrogen production rates (from 0.413 to 0.583 mmol $H_2/L_c/h$) for *Rb.capsulatus* DSM1710 except 200 mM EtOH condition. Therefore, it can be speculated that up to a certain value (100 mM), hydrogen production rate for *Rb.capsulatus* DSM1710 was not affected by increasing ethanol concentration. However, the product yield factor values increased due to the decrease in biomass concentration with the increasing ethanol. *Rb.capsulatus* YO3 (hup^-) produced higher values of hydrogen along with the higher hydrogen production rates. However, the hydrogen production rates declined gradually with the increasing ethanol concentration (Table 3.15). The lowest hydrogen productivity observed at 200 mM EtOH as 0.583 mmol $H_2/L_c/h$. Laurinavichene et al. (2008) reported that ethanol inhibited hydrogen production by 50% at higher concentrations of EtOH than inhibition of growth.

The molar hydrogen yield varied between 44% and 57% for *Rb.capsulatus* DSM1710 (Table 3.14). The molar hydrogen yield of *Rb.capsulatus* YO3 (hup^-) decreased with the increasing ethanol concentration from 86.6% to 50.8% (Table 3.15).

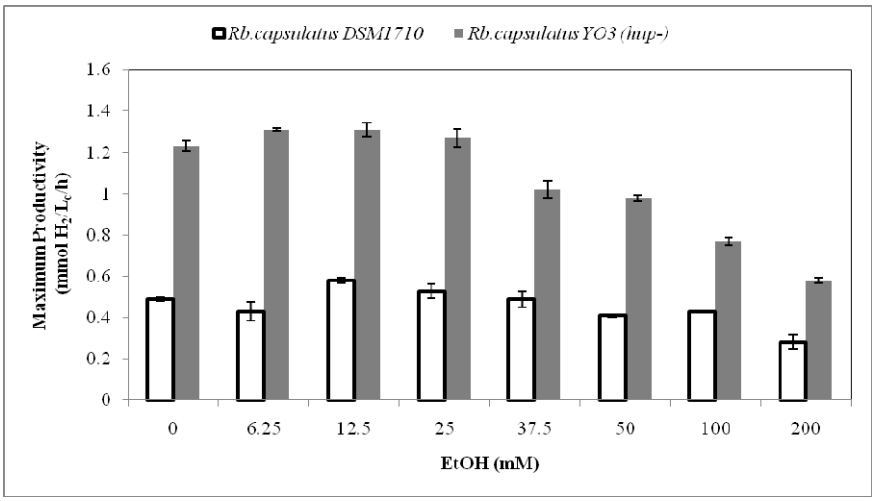

Figure 3.40 Maximum productivity rates for different Ethanol concentrations using *Rb.capsulatus* DSM1710 and *Rb.capsulatus* YO3 (hup^-)

During the experiments, the light intensity (~2500 lux) was constant. Therefore, light conversion efficiencies are also proportional to total produced hydrogen data (Tables 3.14 and 3.15).

Amount of PHB was measured at the end of the experiments. *Rb.capsulatus* YO3 (hup^-) produced less PHB than *Rb.capsulatus* DSM1710. *Rb.capsulatus* DSM1710 produced similar amounts of PHB in the ranges of 6.25-37.5 and 50-200 mM EtOH (Table 3.14). While for *Rb.capsulatus* YO3 (hup^-) the production of PHB increases with the increasing EtOH concentration probably due to the stress effect of increasing EtOH concentration (Table 3.15). It was reported that PHB was enhanced with the stress conditions (Hustede et al., 1993).

In this study, acetate were used as carbon source. The ethanol was not taken into account due to the aim of the study because the main goal was to observe EtOH concentration change and effects on hydrogen production. *Rb.capsulatus* DSM1710 and *Rb.capsulatus* YO3 (hup^-) consumed acetate completely during experiment. Figure 3.41 and 3.42 illustrates the consumption of acetate. Other organic acids, lactic acid, propionic acid and butyric acid produced in negligible amounts in both strains. However, wild type strain produced significant amounts of formic acid at

high concentrations of EtOH (50, 100, 200 mM) during the process (Figure 3.43) while the mutant strain did not produce formic acid. This was presumably occurred due to the effect of ethanol on metabolism of the bacteria. The consumption of acetate in both strains at high ethanol concentrations was slower; therefore, the duration of the acetate consumption endured longer with the increasing ethanol concentration.

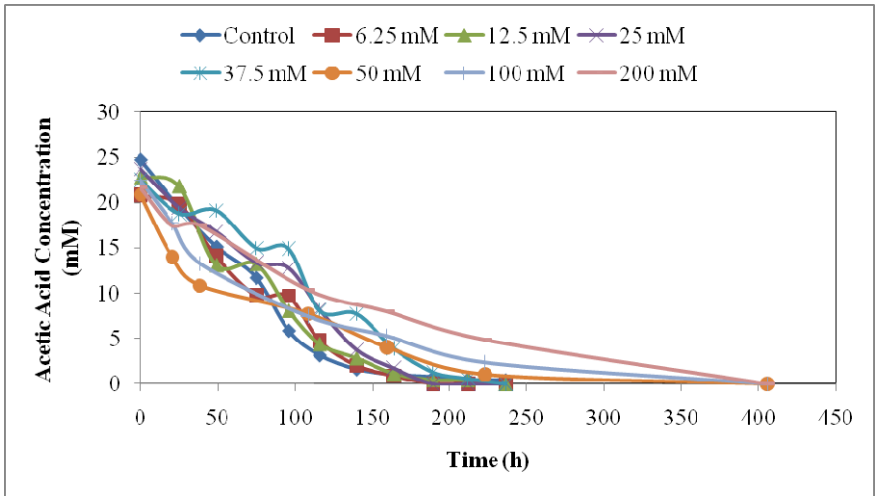

Figure 3.41 Acetic acid consumption for different ethanol concentrations using *Rb.capsulatus* DSM1710

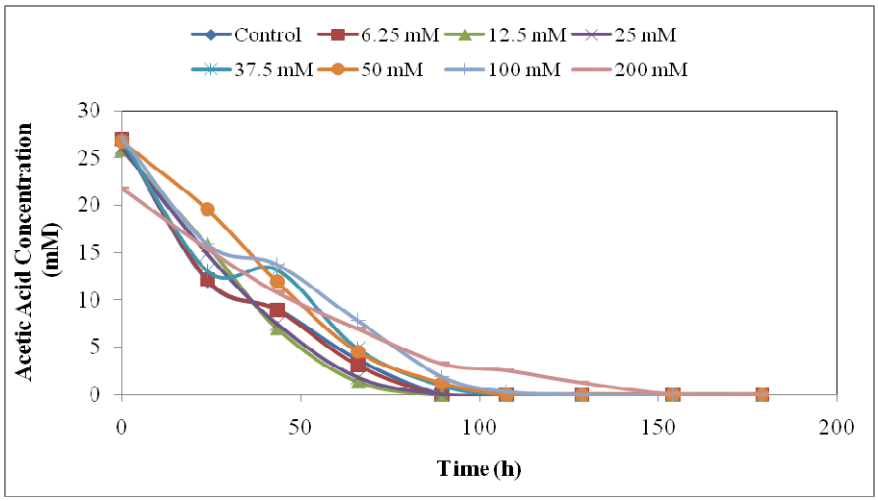

Figure 3.42 Acetic acid consumption for different ethanol concentrations using *Rb.capsulatus* YO3 (hup$^-$)

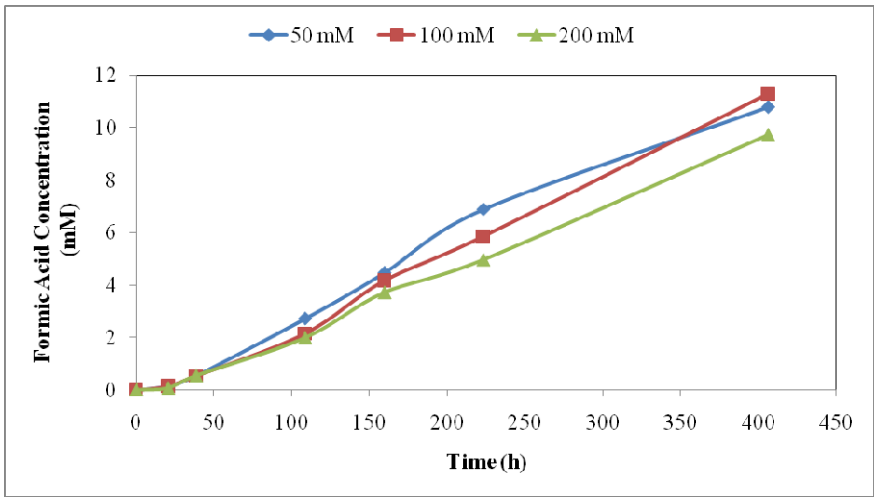

Figure 3.43 Formic acid production for 50, 100 and 200 mM ethanol concentrations using *Rb.capsulatus* DSM1710

Integral method for analysis of data applied to the experimental data of acetic acid consumption. The rate constants (k) and the coefficient of determination values (R^2) of experimental data (Figure 3.41 and 3.42) are tabulated in Table 3.20 and 3.21 for *Rb.capsulatus* DSM1710 and *Rb.capsulatus* YO3 (hup^-), respectively.

Table 3.20 Extent of the fits and rate constants for acetic acid consumption for *Rb.capsulatus* DSM1710 on different EtOH concentrations

EtOH (mM)	Zeroth Order (n=0)		First Order (n=1)		Second Order (n=2)	
	k_0	R^2	k_1	R^2	k_2	R^2
0 (Control)	0.133	0.752	0.018	0.967	0.007	0.725
6.25	0.129	0.970	0.015	0.839	0.004	0.518
12.5	0.127	0.900	0.016	0.875	0.007	0.579
25	0.135	0.985	0.012	0.820	0.002	0.534
37.5	0.107	0.966	0.012	0.775	0.004	0.433
50	0.102	0.712	0.012	0.943	0.027	0.680
100	0.105	0.811	0.009	0.988	0.013	0.855
200	0.083	0.928	0.006	0.993	0.001	0.929

Table 3.21 Extent of the fits and rate constants for acetic acid consumption for *Rb.capsulatus* YO3 (hup$^-$) on different EtOH concentrations

EtOH (mM)	Zeroth Order (n=0)		First Order (n=1)		Second Order (n=2)	
	k_0	R^2	k_1	R^2	k_2	R^2
0 (Control)	0.391	0.871	0.029	0.978	0.003	0.834
6.25	0.398	0.869	0.031	0.969	0.003	0.787
12.5	0.392	0.984	0.038	0.905	0.007	0.653
25	0.393	0.975	0.036	0.931	0.006	0.688
37.5	0.317	0.884	0.031	0.876	0.007	0.565
50	0.308	0.978	0.029	0.902	0.006	0.618
100	0.275	0.934	0.032	0.834	0.014	0.443
200	0.185	0.900	0.020	0.977	0.004	0.728

The acetic acid consumption order varied with the changing EtOH concentrations in the batch experiments using *Rb.capsulatus* DSM1710, control PBR exhibited first order kinetic with the highest R^2 value of 0.978 (Table 3.20). As the EtOH concentration increased the consumption order ranged between zero and first order (6.25-12.5 mM EtOH) and then switched to zero order between 25 and 37.5 mM EtOH. Above 50 mM EtOH, acetic acid consumption kinetic fitted well to first order (Table 3.20). Likewise, in the batch experiments using *Rb.capsulatus* YO3 (hup$^-$), the control and 6.25 mM EtOH containing PBR displayed first order kinetic (Table 3.21). As the EtOH concentration increased, the reaction kinetic ranged between zero and first order and finally at 200 mM EtOH acetic acid consumption kinetic found to be first order (Table 3.21). The shift in the metabolism on acetic acid consumption in both bacterial strains could be attributed to the effect of changing EtOH concentrations. Photo-fermentative bacteria reported to be utilize EtOH as electron donors (Fujii et al., 1987, Imhoff et al., 2005, Garrity et al., 2005, Xie et al., 2010, Pantazopoulous and Madigan 2000); this is likely to affect the metabolism of the photoheterotrophic bacteria such as *Rb.capsulatus* which can use organic acids as electron donors. It can be speculated that electrons from EtOH could have led to the shift in acetic acid consumption kinetic from first order to zero order as the EtOH concentration increased. However, in the presence of high EtOH concentration inhibition of the nitrogenase is likely to have occurred and acetic acid consumption metabolism has shifted to first order kinetics. Inhibiton of nitrogenase (Maeda et al., 1999), changes in activity of nitrogenase (Fujii et al., 1987) and stress responses

(Nepple and Bachofen, 1997) due to EtOH presence in photo-fermentative bacteria were reported in literature. The curve for 37.5 mM EtOH for *Rb.capsulatus* DSM1710 and 200 mM EtOH for *Rb.capsulatus* YO3 (hup^-) is given in Figure 3.44 and 3.45 as an example. The most fitted curves for other ethanol concentrations are given in Appendix J.

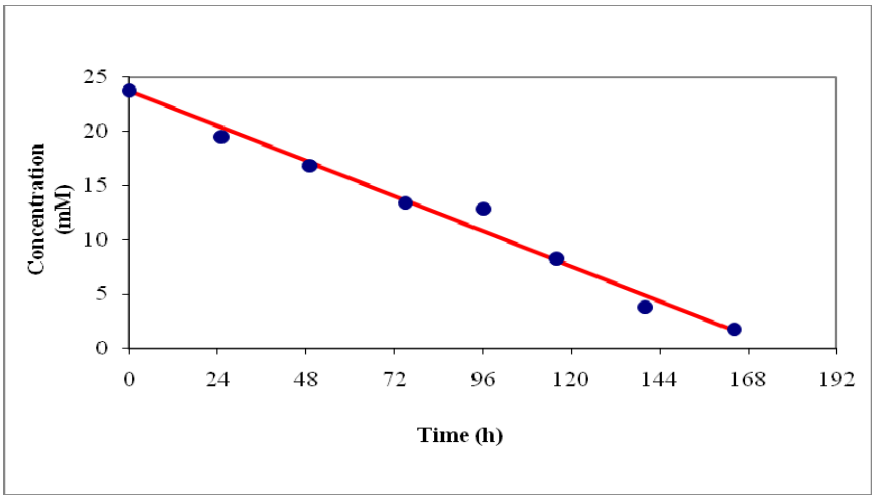

Figure 3.44 Zeroth Order Kinetics for Acetic acid Consumption at 25 mM EtOH containing medium for *Rb.capsulatus* DSM1710 (●: experimental data, ▬: order)

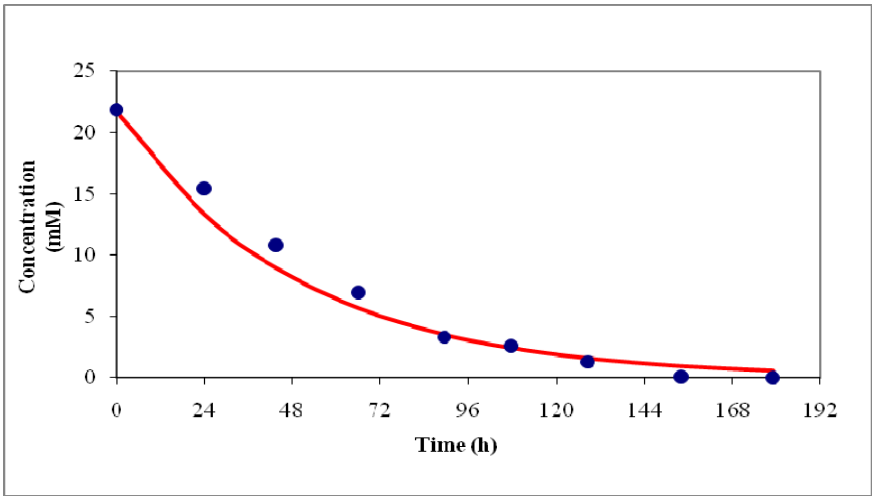

Figure 3.45 First Order Kinetics for Acetic acid Consumption at 200 mM EtOH containing medium for *Rb.capsulatus* YO3 (hup^-) (●: experimental data, ▬: order)

In thesis study, DFESBTJ samples contained ethanol (Tables 2.1 and 3.13) with $R_{e/a}$ ratio of 0.470 and 0.641. According to the results in Table 3.13, found values were comparable with the studies in the literature. For instance, Xie et al. (2010) employed dark and photofermentation from glucose resulting acetate and ethanol as main carbon sources for photofermentation by using co-culture of immobilized *Rhodopseudomonas faecalis* RLD-53 strain and *Ethanoligenens harbinense* B49. They found the hydrogen yield and cumulative hydrogen production increased with $R_{e/a}$ (0-0.8) and then decreased with $R_{e/a}$ (0.8-1.0) and then increased again with $R_{e/a}$ (1.0-1.6). However, the conversion of ethanol was highest between 0.8 and 1.0 $R_{e/a}$ and the utilization of ethanol gradually slow down with the increasing initial ethanol concentration. In an another study, Liu et al. (2009) observed range of 0.6-0.8 $R_{e/a}$ was the most desirable for photofermentation step. Srikanth et al. (2009) observed utilization of ethanol in the effluent of acidogenic and methanogenic processes by using enriched mixed culture. They used synthetic, dairy, and industrial wastewaters for the initial acidogenic and methanogenic processes. However, Tao et al. (2008) could not observe ethanol utilization of ZX-5 PNS bacterial strain when succinate wastewater, or effluents from dark fermentation of wastewater from a fuel ethanol manufacturer or kitchen waste.

CHAPTER 4

CONCLUSIONS

In this study, several subjects were studied and the following conclusions and recomendations can be drawn:

- *Rb. capsulatus* YO3 can grow and produce hydrogen on sugar beet thick juice DFE successfully with a high efficiency in an outdoor panel reactor under natural sunlight; therefore, facilitating the integration of the dark and photo-fermentation for sustainable biohydrogen production. H_2 productivity of 1.12 mmol/L_c/h and molar H_2 yield of 77% of theoretical maximum over consumed substrate were attained over 15 days of operation for panel PBR. It is critical to keep the reactor temperature between 30 to 35 °C during the day. Light intensity is a major factor affecting hydrogen production.

- Panel reactor results showed that dilution of the sugar beet thick juice DFE is necessary to decrease acetate concentration to the required level (circa. 40 mM). However, dilution increases the operating costs, for that reason recycling of wastewater can be done for further analysis.

- During the operation in outdoor conditions bchl *a* content in the cells showed inverse ratio with the global solar radiation and bacteria maintained its bchl a content constant during the night period.

- The NH_4^+ removal results showed that the zeolite was effective in removing NH_4^+ from the DFESBTJ as its concentration decreased by 95% after treatment. In this manner, the inhibitor effect of NH_4^+ on nitrogenase enzyme was prevented by removing NH_4^+ in the effluent for photofermentation.

- The results of hydrogen production experiments using untreated and treated DFESBTJ indicated that the maximum productivities and molar H_2 yields of *Rb.capsulatus* DSM1710 and *Rb.capsulatus* YO3 (hup^-) increased with the decrease in NH_4^+ concentrations of the effluents. The highest maximum productivity (1.62 mmol/L_c/h) and molar H_2 yield (86.4 %) were obtained from treated DFESBTJ samples by *Rb. capsulatus* YO3 (hup^-). Growth and hydrogen production data of all runs were fitted in to Logistic and Modified Gompertz Model, respectively.

- The acetic acid consumption kinetics of untreated and treated DFESBTJ samples for *Rb.capsulatus* DSM1710 and *Rb.capsulatus* YO3 (hup^-) showed varying reaction orders probably due to the complex media that contained different concentrations of anions, cations and organic acids (sourced from the dark fermentation of sugar beet thick juice) which could adversely affect the acetic acid consumption order.

- There was no significant effect of EtOH on H_2 production between the range 6.25 to 100 mM; however, inhibition was observed at 200 mM for both *Rb.capsulatus* DSM1710 and *Rb.capsulatus* YO3 (hup^-). Before using any dark fermentation effluent for photofermentation, $R_{e/a}$ values can signify the possible effect of ethanol which can easily be produced during the dark fermentation. This may prevent the cessation of hydrogen production and PHB production due to the possible negative effect of ethanol on PNS bacteria. Nevertheless, further studies will be neccassary to understand how PNS bacteria use the ethanol in its metabolism.

REFERENCES

Abd El-Hady H.M., Grünwald A., Vlčková K., Zeithammerová J., 2001, "Clinoptilolite in Drinking Water Treatment for Ammonia Removal", *Acta Polytechnica*, 41: 41-5.

Afsar, N., Özgür, E., Gürgan, M., Akköse, S., Yücel, M., Gündüz, U., Eroglu, I., 2011, "Hydrogen productivity of photosynthetic bacteria on dark fermenter effluent of potato steam peels hydrolysate", International Journal of Hydrogen Energy, 36: 432-8.

Akkerman, I., Janssen, M., Rocha, J., Wijffels, R.H., 2002, "Photobiological hydrogen production:photochemical efficiency and bioreactor design", International Journal of Hydrogen Energy, 27: 1195 – 208.

Akköse, S., Gündüz, U., Yücel, M., Eroğlu, I., 2009, "Effects of ammonium ion, acetate and aerobic conditions on hydrogen production and expression levels of nitrogenase genes in *Rhodobacter sphaeroides* O.U.001", International Journal of Hydrogen Energy, 34: 8818-27.

Androga, D.D., 2009, "Biological Hydrogen Production on Acetate in Continues Panel Photobioreactors Using *Rhodobacter capsulatus*", M.Sc.Thesis in Chemical Engineering Department, Middle East Technical University, Ankara, Turkey.

Androga, D.D., Özgür, E., Yücel, M., Gündüz, U., Eroğlu, I., 2011a, "Factors affecting the longterm stability of biomass and hydrogen productivity in outdoor photofermentation", International Journal of Hydrogen Energy, 36: 11368-78.

Androga, D. D., Özgür, E., Eroğlu, İ., Yücel, M., Gündüz, U., 2011b, "Improvement of Integrated Dark & Photo Fermentative Hydrogen Production by Removing Ammonium Ion", In: International Conference on Hydrogen Production ICH2P-11, June 19-22, 2011, Thessaloniki, Greece, Paper No: 140BIO.

Argun, H., Kargi, F., Kapdan, I.K., 2009, "Hydrogen production by combined dark and light fermentation of ground wheat solution", International Journal of Hydrogen Energy, 34: 4305-11.

Argun, H., Kargi, F., 2011, "Bio-hydrogen production by different operational modes of dark and photo-fermentation: An overview", International Journal of Hydrogen Energy, 36: 7443-59.

Asada, Y., Ohsawa, M., Nagai, Y., Ishimi, K., Fukatsu, M., Hideno, A., Wakayama, T., Miyake, J., 2008, "Re-evaluation of hydrogen productivity from acetate by some photosynthetic bacteria", International Journal of Hydrogen Energy, 33: 5147-50.

Avcıoğlu, S.G., 2010, "Scale up of Panel Photobioreactors for Hydrogen Production by PNS Bacteria", MSc. Thesis in Chemical Engineering, Middle East Technical University, Ankara, Turkey.

Avcıoglu, S.G., Özgür, E., Eroglu, I., Yücel, M., Gündüz, U., 2011, "Biohydrogen production in an outdoor panel photobioreactor on dark fermentation effluent of molasses", International Journal of Hydrogen Energy, 36: 11360-68.

Ball, M., Wietschel M., 2009, "The future of hydrogen – opportunities and challenges", International Journal of Hydrogen Energy,34: 615–27.

Bahaallddin D.A., 2010, "Ammonium and lead exchange in clinoptilolite zeolite column", MSc. Thesis in Chemical Engineering Department, Middle East Technical University, Ankara, Turkey.

Basak, N., Das, D., 2007, "The prospect of purple non-sulfur (PNS) photosynthetic bacteria for hydrogen production: the present state of the art", World J. Microbiol. Biotechnol., 23: 31–42.

Bayraktaroğlu, 2006, "Multicomponent Ion Exchange on Clinoptilolite'', MSc. Thesis in Chemical Engineering, Middle East Technical University, Ankara, Turkey.

Biebl, H., Pfennig, N., 1981, "Isolation of Members of the Family *Rhodosprillaceae*.", In: The prokaryotes. Editors: Starr, M.P., Stolp, H., Trüper, H.G., Balows, A., Schlegel, H.G., New York: Springer-Verlag, p.267-73.

Biel, A.J., 1986, "Control of Bacteriochlorophyll Accumulation by Light in *Rhodobacter capsulatus*", Journal of Bacteriology, 168: 655-659.

Boran, E., Özgür, E., Burg, J.V.D., Yücel, M., Gündüz, U., Eroglu, I., 2010, "Biological hydrogen production by *Rhodobacter capsulatus* in solar tubular photo bioreactor", Journal of Cleaner Production, 18: 29-35.

Boran, E., 2011, Process development for continuous photofermentative hydrogen production", MSc. Thesis in Chemical Engineering Department, Middle East Technical University, Ankara, Turkey.

Brentner, L.B., Peccia, J., Zimmerman, J. B., 2010, "Challenges in developing viohydrogen as a sustainable energy source: Implications for a research agenda", Environmental Science and Technology, 44: 2243-54.

Chen, C.Y., Liu, C.H., Lo, Y.C., Chang, J.S., 2011, "Perspectives on cultivation strategies and photobioreactor designs for photo-fermentative hydrogen production", Bioresource Technology, 102: 8484-92.

Claassen, P.A.M., Vrije, T., 2006, "Non-thermal Production of Pure Hydrogen from Biomass: HYVOLUTION", International Journal of Hydrogen Energy, 31: 1416-23.

Clayton, R. K., 1963, "Two Light Reactions of Bacteriochlorophyll in vivo", Proceedings of the National Academy of Sciences, Charles F. Kettering Research Laboratory, Yellow Springs, Ohio., 50: 583-7.

Cohen-Bazire, G., Sistrom W. R., Stanley, R. Y., 1957, "Kinetic Studies of Pigment Synthesis by Non-Purple Sulfur Bacteria", Journal of Cellular and Comparative Physiology, 49: 25-68.

Colella, C., 2005, "Natural zeolites", In: Zeolites and ordered mesoporous materials: Progress and prospects, The 1st FEZA School on Zeolites, Prague, Czech Republic, August 20-21, 2005, Editors: J. Cejka and H. van Bekkum, Elsevier B.V., p.13-40.

Das, D., Veziroglu, T.N., 2001, "Hydrogen production by biological processes: a survey of literature", International Journal of Hydrogen Energy, 26: 13-28.

Dasgupta, C. N., Gilbert, J. J., Lindblad, P., Heidorn, T., Borgvang, S. A., Skjanes, K., Das, D., 2010, "Recent trends on the development of photobiological processes and photobioreactors for the improvement of hydrogen production", International Journal of Hydrogen Energy, 35: 10218-38.

Ditzig, J., Liu, H., Logan, B. E., 2007, "Production of hydrogen from domesticwastewater using a bioelectrochemically assisted microbial reactor (BEAMR)", International Journal of Hydrogen Energy, 32: 2296 – 304.

Dyer, A., 2005, "Ion-exchange properties of zeolites", In: Zeolites and ordered mesoporous materials: Progress and prospects, The 1st FEZA School on Zeolites, Prague, Czech Republic, August 20-21, 2005, Editors: J. Cejka and H. van Bekkum, Elsevier B.V., p.181-204.

Eroglu, I., Kadir, A., Gunduz, U., Yucel, M., Turker, L., 1999, "Substrate consumption rates for hydrogen production by Rhodobacter sphaeroides in a column photobioreactor", Journal of Biotechnology, 70: 103–113.

Eroglu, E., Gündüz, U., Yücel, M., Türker, L., Eroglu, I., 2004, "Photobiological hydrogen production by using olive mill wastewater as a sole substrate source", International Journal of Hydrogen Energy, 29: 163-71.

Eroglu, E., Gündüz, U., Yücel, M., Türker, L., Eroglu, I., 2006, "Biological hydrogen production from olive mill wastewater with two-stage processes", International Journal of Hydrogen Energy, 31: 1527-35.

Eroglu, I., Tabanoglu, A., Gündüz, U., Eroglu, E., Yücel, M., 2008, "Hydrogen production by *Rhodobacter sphaeroides* O.U.001 in a flat plate solar bioreactor", International Journal of Hydrogen Energy, 33: 531-41.

Eroglu, E., Melis, A., 2011, "Photobiological hydrogen production: Recent advances and state of art", Bioresource Technology, 102: 8403-13.

Fang, H.H.P., Zhu, H., Zhang, T., 2006, "Phototrophic hydrogen production from glucose by pure and co-cultures of *Clostridium butyricum* and *Rhodobacter sphaeroides",* International Journal of Hydrogen Energy, 31: 2223 – 30.

Foster, J. W., 1944, "Oxidation of alcohols by non-sulfur photosynthetic bacteria", Journal of Bacteriology, 47: 355-72.

Fujii, T., Nakazawa, A., Sumi, N., Tani, H., Ando, A., Yabuki, M., 1983, "Utilization of Alcohols by Rhodopseudomonas sp. No. 7 Isolated from w-Propanol-Enrichment Cultures", Agricultural and biological chemistry, 47: 2747-53.

Fuji, T., Tarusawa, M., Miyanaga, M., Kıyota, S., Watanabe, T., Yabuki, M., 1987, "Hydrogen Evolution from Alcohols, Malate and Mixed Electron Donors by *Rhodopseudomonas* sp. No.7", Agricultural and biological chemistry, 51 (1), 1-7.

Fujii, T., Sadaie, M., Saijou, M., Nagano, T., Suzuki, T., Ohtani, M., Shinoyama, H., 1998, "Physiological properties of phosphoenolpyruvate carboxylase and phosphoenolpyruvate carboxykinase from *Rhodopseudomonas* sp. No. 7", In: Advances in Chemical Conversions for Mitigating Carbon Dioxide, Studies in Surface Science and Catalysis, Vol. 114. Editors: T. Inui, M. Anpo, K. Izui, S. Yanagida, T. Yamaguchi, Elsevier Science B.V., p.463-6.

Garrity, G. M., Bell, J. A., Lilburn, T., 2005, "Order III. Rhodobacterales ord. nov." In: Bergey's Manual of Systematic Bacteriology, Vol. 2 (The Proteobacteria). Editors: D.J. Brenner, N.R. Krieg, J.T. Staley and G. M., New York: Springer, p. 161.

Gebicki, J., Modigell M., Schumacher M., Van Der Burg J., Roebroeck E., 2010, "Comparison of two reactor concepts for anoxygenic H2 production by *Rhodobacter capsulatus*" Journal of Cleaner Production, 18: S36-S42.

Gest, H., Kamen, M.D., 1949, "Photoproduction of molecular hydrogen by *Rhodospirillum rubrum*", Science, 109: 558-9.

Guwy, A.J., Dinsdale, R.M., Kim, J.R., Massanet-Nicolau, J., Premier, G., 2011, "Fermentative biohydrogen production systems integration", Bioresource Technology, 102: 8534-42.

Hallenbeck, P.C.,Benemann, J.R.,2002, “Biological hydrogen production; fundamentals and limiting processes”, International Journal of Hydrogen Energy, 27:1185-93.

Hallenbeck, P.C., 2009, “ Fermentative hydrogen production: Principles, progress, and prognosis”, International Journal of Hydrogen Energy, 34: 7379-89.

Haselkorn, R., Lapidus, A., Kogan, Y., Vlcek, C., Paces, J., Paces, V., Ulbrich, P., Pecenkova, T., Rebrekov, D., Milgram, A., Mazur, M., Cox, R., Kyrpides, N., Ivanova, N., Kapatral, V., Los, T., Lykidis, A., Mikhailova, N., Reznik, G., Vasieva, O., Fonstein, M., 2001, “The *Rhodobacter capsulatus* genome”, Photosynthesis Research, 70: 43–52.

Hoekema, S., Douma R. D, Janssen M, Tramper J, Wijffels RH., 2006 “Controlling Light-Use by *Rhodobacter capsulatus* Continuous Cultures in a Flat-Panel Photobioreactor” Biotechnology and Bioengineering, 95: 613-626.

Holladay, J.D., Hu, J., King, D.L., Wang, Y., 2009, “An overview of hydrogen production technologies”, Catalysis Today, 139: 244-60.

Hunter, C. N., Tucker, J. D., Niederman, R. A., 2005, “The assembly and organisation of photosynthetic membranes in *Rhodobacter sphaeroides*”, Photochem. Photobiol. Sci., 4: 1023-27.

Hustede, E., Steinbiichel, A., Schlegel, H.G., 1993, “Relationship between the photoproduction of hydrogen and the accumulation of PHB in non-sulphur purple bacteria”, Applied Microbiology and Biotechnology, 39: 87-93.

Imhoff , J. F., Hiraishi, A., Süling , J., 2005, “Anoxygenic Phototrophic Purple Bacteria”, In: Bergey’s Manual of Systematic Bacteriology, Pages 119-132.

Inglezakis, V.J., Hadjiandreou, K.J., Loizidou, M.D., Girgoropoulou, H.P., 2001, “Pretreatment of Natural Clinoptilolite in a Laboratory-Scale Ion Exchange Packed Bed”, Water Research, 35: 2161-66.

Justé, A., Lievens, B., Frans, I., Klingeberg, M., Michiels, C.W., Willems, K.A., 2008, “Present knowledge of the bacterial microflora in the extreme environment of sugar thick juice”, Food Microbiology, 25: 831-6.

Khatipov, E., Miyake, M., Miyake, J., Asada, Y., 1998, “Accumulation of Poly-β-hydroxybutyrate by *Rhodobacter sphaeroides* on various carbon and nitrogen substrates”, FEMS Microbiology Letters, 162: 39-45.

Kapdan, I.K., Kargi, F., 2006, “Bio-hydrogen production from waste materials", Enzyme and Microbial Technology, 38: 569–82.

Karadağ, D., Koç, Y., Turan, M., Armagan, B., 2006, “Removal of ammonium ion from aqueous solution using natural Turkish clinoptilolite”, Journal of Hazardous Materials, B136: 604–9.

Kars, G., Gündüz, U., Rakhely, G., Yücel, M., Eroglu, I., Kovacs, K.L., 2008, "Improved hydrogen production by uptake hydrogenase deficient mutant strain of *Rhodobacter sphaeroides* O.U.001", International Journal of Hydrogen Energy, 33: 3056-60.

Kars G., Gündüz U., 2010, "Towards a super H_2 producer: Improvements in photofermentative biohydrogen production by genetic manipulations", International Journal of Hydrogen Energy, 35: 6646-56.

Keskin, T., Abo-Hashes, M., Hallenbeck, P.C., 2011, "Photofermentative hydrogen production from wastes", Bioresource Technology, 102: 8557-68.

Kim J. S., Ito K., Izaki K., Takahashi H., 1987, "Production of Molecular Hydrogen by a Semi-continuous Outdoor Culture of *Rhodopseudomonas sphaeroides*" Agricultural and Biological Chemistry, 51: 1173-74.

Kim, M.S., Baek, J.S., Lee, J.K., 2006, "Comparison of H_2 accumulation by *Rhodobacter sphaeroides* KD131 and its uptake hydrogenase and PHB synthase deficient mutant", International Journal of Hydrogen Energy, 31: 121-7.

Kim, M. S., Kim, D. H., Son, H. N., Ten, L. N., Lee, J. K., 2011, "Enhancing photo-fermentative hydrogen production by *Rhodobacter sphaeroides* KD131 and its PHB synthase deleted-mutant from acetate and butyrate", International Journal of Hydrogen Energy, 36: 13964-71.

Koku, H., Eroğlu, I., Gunduz, U., Yucel, M., Turker, L., 2002, "Aspects of the Metabolism of Hydrogen Production by *Rhodobacter sphaeroides*‘', International Journal of Hydrogen Energy, **2**:1315-29.

Koku, H., Eroğlu, I., Gündüz, U., Yücel, M., Türker, L., 2003, "Kinetics of biological hydrogen production by the photosynthetic bacterium *Rhodobacter sphaeroides* O.U. 001", International Journal of Hydrogen Energy, 28: 381-388

Laurinavichene, T. V., Tekucheva, D. N., Laurinavichius, K. S., Ghirardi, M. L., Seibert, M., Tsygankov, A. A., 2008, "Towards the integration of dark and photo fermentative waste treatment. 1. Hydrogen photoproduction by purple bacterium *Rhodobacter capsulatus* using potential products of starch fermentation", International Journal of Hydrogen Energy, 33: 7020-6.

Laurinavichene, T.V., Belokopytov, B.F., Laurinavichius, K.S., Tekucheva, D.N., Seibert, M., Tsygankov, A.A., 2010., "Towards the integration of dark- and photo-fermentative waste treatment. 3. Potato as substrate for sequential dark fermentation and light-driven H_2 production", International Journal of Hydrogen Energy, 35: 8536–43.

Leung, S., Barrington, S., Wan, Y., Zhao, X., El-Husseini, B., 2007, "Zeolite (clinoptilolite) as feed additive to reduce manure mineral content", Bioresource Technology, 98: 3309-16.

Liebl, U., Sled, V., Brasseur, G., Ohnishi, T., Daldal, F., 1997, "Conserved Nonliganding Residues of the *Rhodobacter capsulatus* Rieske Iron-Sulfur Protein of the bc1 Complex Are Essential for Protein Structure, Properties of the [2Fe-2S] Cluster, and Communication with the Quinone Pool", Biochemistry, 36: 11675-84.

Liu, B. F., Ren, N. Q., Xing, D. F., Ding, J., Zheng, G. X., Guo, W. Q., Xu, J. F., Xie, G. J., 2009, "Hydrogen production by immobilized *R. faecalis* RLD-53 using soluble metabolites from ethanol fermentation bacteria *E. harbinense* B49", Bioresource Technology, 100: 2719–23.

Madigan, M., Cox, S. S., Stegeman, R. A., 1984, "Nitrogen fixation and nitrogenase activities in members of the family Rhodospirillaceae", Journal of Bacteriology, 157: 73–8.

Maeda, I., Daba, M., Hirose, N., Nagao, H., Idehara, K., Miura, Y., Yagi, K., Mizoguchi, T., 1999, "Repression of nitrogenase by ethanol in nitrogen-deprived cultures of Rhodovulum sulfidophilum", FEMS Microbiology Letters, 171: 121-6.

Manish, S., Banarjee, R., 2008, "Comparison of biohydrogen production processes", International Journal of Hydrogen Energy, 33: 279-86.

Masepohl, B., Hallenbeck, P.C., 2010, "Nitrogen and Molybdenum Control of Nitrogen Fixation in the Phototrophic Bacterium *Rhodobacter capsulatus*", In: Recent Advances in Phototrophic Prokaryotes. Editor: P.C. Hallenbeck, New York: Springer, Vol. 675, pp. 49–70.

Meister, M., Saum, S., Alber, B. E., Fuchs, G., 2005, "L-Malyl-Coenzyme A/β-Methylmalyl-Coenzyme A Lyase Is Involved in Acetate Assimilation of the Isocitrate Lyase-Negative Bacterium *Rhodobacter capsulatus*", Journal of Bacteriology, 187: 1415-25.

Melis, A., 2002, "Green alga hydrogen production: progress, challenges and prospects", International Journal of Hydrogen Energy, 27: 1217-28.

Melis, A. Melnicki M. R., 2006, "Integrated Biological Hydrogen Production", International Journal of Hydrogen Energy, 31: 1563–73.

Mu, Y., Wang, G., Yu, H.-Q., 2006, "Kinetic modeling of batch hydrogen production process by mixed anaerobic cultures", Bioresource Technology, 97, 1302-07.

Mu, Y., Yu, H.Q., Wang, G., 2007, "A kinetic approach to anaerobic hydrogen-producing process", Water Research, 41:1152-60.

Najafpour, G.D., 2007, "Growth Kinetics", In: Biochemical Engineering and Biotechnology. Elsevier, Netherlands, p.81.

Nath, K., Das, D., 2004, "Improvement of fermentative hydrogen production: various Approaches", Applied Microbiology and Biotechnology, 65: 520–9.

Nath, K., Muthukumar, M., Kumar, A., Das, D., 2008, "Kinetics of two-stage fermentation process for the production of hydrogen", International Journal of Hydrogen Energy, 33:1195 – 203.

Nath K., Das D., 2011, "Modeling and optimization of fermentative hydrogen production", Bioresource Technology, 102: 8569-81.

Nepple, B. B., Bachofen, R., 1997, "Induction stress proteins in the phototrophic bacterium *Rhodobacter sphaeroides*", FEMS Microbiology Letters, 153: 173-80.

Nguyen, M. L., Tanner,C. C., 1998, "Ammonium removal from wastewaters using natural New Zealand zeolites", New Zealand Journal of Agricultural Research, 41: 427-446.

Olah, G.A., Goeppert, A., Prakash, G.K.S., "Beyond Oil and Gas: The Methanol Economy", Weinheim: Wiley-VCH 2009. p.143-177.

Özgür, E., Mars, A., Peksel, B., Louwerse, A., Yücel, M., Gündüz, U., Classen, P.A.M., Eroğlu, I., 2010a, "Biohydrogen production from beet molasses by sequential dark and photofermentation", International Journal of Hydrogen Energy, 35: 511-7.

Özgür, E., Afşar, N., Vrije, T., Yücel, M., Gündüz, U., Classen, P.A.M., Eroğlu, I., 2010b, "Potential use of thermophile dark fermentation effluents in photofermentative hydrogen production by *Rhodobacter capsulatus"* Journal of Cleaner Production, 18: S23-S28.

Özgür, E., Uyar, B., Oztürk, Y., Yücel, M., Gündüz, U., Eroglu, I., 2010c, "Biohydrogen Production by *R. capsulatus* on Acetate at Fluctuating Temperatures", Resources, Conservation & Recycling, 54:310–4.

Özgür, E., Uyar, B., Gürgan, M., Yücel, M., 2010d, "Hydrogen Production by Hup$^-$ Mutant and Wild Type Strains of *Rhodobacter capsulatus* on Dark Fermenter Effluent of Sugar Beet Thick Juice in Batch and Continuous Photobioreactors" In: Detlef Stolten, Thomas Grube, Editors, 18th World Hydrogen Energy Conference 2010-WHEC 2010: Parallel Sessions Book 2: Hydrogen Production Technologies-Part 1, Forschungszentrum J¸lich GmbH, Zentralbibliothek, Verlag: WHEC, May 16.-21 2010, Essen; pp.229-33.

Öztürk, Y., Yücel, M., Daldal, F., Mandacı, S., Gündüz, U., Türker, L., Eroglu, I., 2006, "Hydrogen Production by using *Rhodobacter capsulatus* Mutants with Genetically Modified Electron Transfer Chains", International Journal of Hydrogen Energy, 31: 1545-52.

Pantazopoulous, P. E.,Madigan, M. T., 2000, "Primary alcohols and d,-alcohols as growth subctrates for the purple nonsulfur bacterium *Rhodobacter capsulatus*", Canadian Journal of Microbiology, 46: 1166-70.

Pekgöz G., 2010, "Deletion Mutation of GLNB and GLNK Genes in *Rhodobacter capsulatus* to enhance biohydrogen production", MSc. Thesis in Biotechnology Department, Middle East Technical University, Ankara, Turkey.

Pellerin, N.B., and Gest, H., 1983, "Diagnostic Features of the Photosynthetic Bacterium *Rhodopseudomonas sphaeroides*", Current Microbiology, 9: 339-44.

Quayle, J. R., Pfennig, N., 1975, "Utilization of Methanol by Rhodospirillaceae", Archives of Microbiology, 102: 193-8.

Redwood, M.D., Beedle, M.P., Macaskie, L.E., 2009, "Integrating dark and light bio-hydrogen production strategies: towards the hydrogen economy". Reviews in Environmental Science and Biotechnology, 8: 149-85.

Renzo, F.D., Fajula, F., 2005, "Introduction to molecular sieves: trends of evolution of the zeolite community", In: Zeolites and ordered mesoporous materials: Progress and prospects, The 1st FEZA School on Zeolites, Prague, Czech Republic, August 20-21, 2005, Editors: J. Cejka and H. van Bekkum, Elsevier B.V., p.1-12.

Rozendal, R.A., Hamelers, H.V.M., Euverink, G.J.W., Metz, S.J., Buisman, C.J.N., 2006, "Principle and perspectives of hydrogen production through biocatalyzed electrolysisInternational", Journal of Hydrogen Energy, 31: 1632 – 40.

Sasikala, K., Ramana, C.V., Rao, P.R., Kovacs, K.L., 1993, "Anoxygenic phototropic bacteria: Physiology and advances in hydrogen production technology", Advances Applied Microbiology, 38: 211-95.

Senge, M. O., and Smith, K. M., 1995, "Biosynthesis and Structures of the Bacteriochlorophylls", In: Blankenship R. E., Madigan M. T., Bauer C. E., Anoxygenic Photosynthetic Bacteria, Kluwer Academic Publishers, Netherlands.

Sevinç, P., 2010, "Kinetic analyses of the effects of temperature and light intensity on growth, hydrogen production and organic acid utilization by *Rhodobacter capsulatus*", M.sc. thesis in Biotechnology Engineering Department, Middle East Technical University, Ankara, Turkey.

Sharp, R. E., Palmitessa, A., Gibney, B. R., Moser, C. C., Daldal, F., Dutton, P. L., 1998, "Non-inhibiting perturbation of the primary energy conversion site (Qo site) in *Rhodobacter capsulatus* ubihydroquinone:cytochrome c oxidoreductase (cytochrome bc1 complex), FEBS Letters, 431: 423-6.

Srikanth, S., Mohan, S. V., M. Devi, P., Babu, M. L., Sarma, P.N., 2009, "Effluents with soluble metabolites generated from acidogenic and methanogenic processes as substrate for additional hydrogen production through photo-biological process", International Journal of Hydrogen Energy, 34: 1771-9.

Su, H., Cheng, J., Zhou, J., Song, W., Cen, K., 2009, "Improving hydrogen production from cassava starch by combination of dark and photo fermentation", International Journal of Hydrogen Energy, 34: 1780-6.

Tao, Y., He, Y., Wu, Y., Liu, F., Li, X., Zong, W., Zhou, Z., 2008, "Characteristics of a new photosynthetic bacterial strain for hydrogen production and its application in wastewater treatment", International Journal of Hydrogen Energy, 33: 963-73.

Tredici, M.R., 1999, "Bioreactors, photo". In: Encyclopedia of bioprocess technology: fermentation, biocatalysis and bioseparation vol. 1, Editors: Flickinger MC, Drew SW,. New York: Wiley, p.395-419.

Tsygankov, A. A. and Laurinavichene, T. V., 1996, "Influence of the Degree and Mode of Light Limitation on Growth Characteristics of the *Rhodobacter capsulatus* Continuous CuItures", Biotechnology and Bioengineering, 51: 605-12.

Urbaniec, K., Grabarczyk, R., 2009, "Raw materials for fermentative hydrogen production", Journal of Cleaner Production, 17: 959-62.

Uyar, B., Gündüz, U., Yücel, M., Türker, L., Eroglu, I., 2007, "Effect of Light Intensity, Wavelength and Illumination Protocol on Hydrogen Production in Photobioreactors", International Journal of Hydrogen Energy, 32: 4670– 4677.

Uyar, B., 2008, "Hydrogen Production by Microorganisms in Solar Bioreactor", Ph.D. Thesis in Biotechnology Engineering Department, Middle East Technical University, Ankara, Turkey.

Uyar, B., Eroglu, I., Yücel, M., Gündüz ,U., 2009a, "Photofermentative hydrogen production from volatile fatty acids present in dark fermentation effluents", International Journal of Hydrogen Energy, 34: 4517-23.

Uyar, B., Schumacher, M., Gebicki, J., Modigell, M.., 2009b, "Photoproduction of hydrogen by *Rhodobacter capsulatus* from thermophilic effluent", Bioprocess and Biosystems Engineering, 32: 603-6.

Vignais, P.M., Colbeau, A., Willison, J.C., Jouanneau, Y., 1985, "Hydrogenase, Nitrogenase, and Hydrogen Metabolism in Photosynthetic Bacteria", Adv. Microbial Phys., 26: 154-234.

Waligorska, M., Seifert, K., Gorecki, K., Moritz, M., Laniecki, M., 2009, " Kinetic model of hydrogen generation by *Rhodobacter sphaeroides* in the presence of NH_4^+ ions", Journal of Applied Microbiology, 107: 1308-18.

Wang, J., Wan, W., 2009, "Kinetic models for fermentative hydrogen production: A review", International Journal of Hydrogen Energy, 34:3313-3323

Weaver, P. F., Wall, J. D., Gest, H., 1975, "Characterization of Rhodopseudomonas capsulate", Archives of microbiology, 105: 207-16.

Xie,G-J., Feng, L-B., Ren, N-Q., Ding, J., Liu, C., Xing, D-F., Qian, G-W., Ren, H-Y., 2010, "Control strategies for hydrogen production through co-culture of Ethanoligenens harbinense B49 and immobilized Rhodopseudomonas faecalis RLD-53", International Journal of Hydrogen Energy, 35: 1929-35.

Yakunin, A.F., Hallenbeck, P.C., 1998, "Short term regulation of nitrogenase activity by NH_4^+ in *Rhodobacter capsulatus*: multiple in vivo nitrogenase responses to NH_4^+ addition", Journal of Bacteriology, 23: 6392–5.

Yamanaka, K. and Minoshima, R., 1984, "Comparison of TwoDye-linked Alcohol Dehydrogenases of *Rhodopseudomonas acidophila*: Their Substrate Specificity and Behavior toward Oxygen", Agricultural and biological chemistry, 48: 171-9.

Yang, H., Guo, L., Liu, F., 2010, "Enhanced bio-hydrogen production from corncob by a two-step process: dark- and photo-fermentation", Bioresource Technology, 101: 2049−52.

Zuber, H., Cogdell, R. J., 2004, "Structure and Organization of Purple Bacterial Antenna Complexes", In: Anoxygenic Photosynthetic Bacteria. Editors: Robert E. Blankenship, Michael T. Madigan, Carl E. Bauer, Kluwer Academic Publishers, chapter 16: p.315-48.

APPENDIX A

COMPOSITION OF THE MEDIA AND THE SOLUTIONS

Table A.1 Composition of the growth medium (20 mM Acetate/10 mM Glutamate)

Component	Amount
KH_2PO_4 (22 mM)	3 g/L
$MgSO_4.7H_2O$	0.5 g/L
$CaCl_2.2H_2O$	0.05 g/L
Vitamin Solution (1X)	1 ml/L
Trace Element Solution (10X)	0.1 ml/L
Fe-Citrate Solution (50X)	0.5 ml/L
Sodium L Glutamate (10 mM)	1.8 g/L
Acetic acid (20 mM)	1.15 ml/L

Table A.2 Composition of hydrogen production medium (30 mM Acetate/2 mM Glutamate)

Component	Amount
KH_2PO_4 (22 mM)	3 g/L
$MgSO_4.7H_2O$	0.5 g/L
$CaCl_2.2H_2O$	0.05 g/L
Vitamin Solution (1X)	1 ml/L
Trace Element Solution (10X)	0.1 ml/L
Fe-Citrate Solution (50X)	0.5 ml/L
Sodium L Glutamate (2 mM)	0.36 g/L
Acetic acid (30 mM)	1.72 ml/L

Table A.3 The composition of trace element solution (1X)

Component	Amount
HCl (25%v/v)	1ml/L
$ZnCl_2$	70 mg/L
$MnCl_2.4H_2O$	100 mg/L
H_3BO_3	60 mg/L
$CoCl_2.6H_2O$	200 mg/L
$CuCl_2.2H_2O$	20 mg/L
$NiCl_2.6H_2O$	20 mg/L
$NaMoO_4.2H_2O$	40 mg/L

Ferric Citrate Solution:

0.5 g Fe(III)-citrate was dissolved in 100 ml distilled water and sterilized by autoclaving.

APPENDIX B

OPTICAL DENSITY-DRY WEIGHT CALIBRATION CURVE

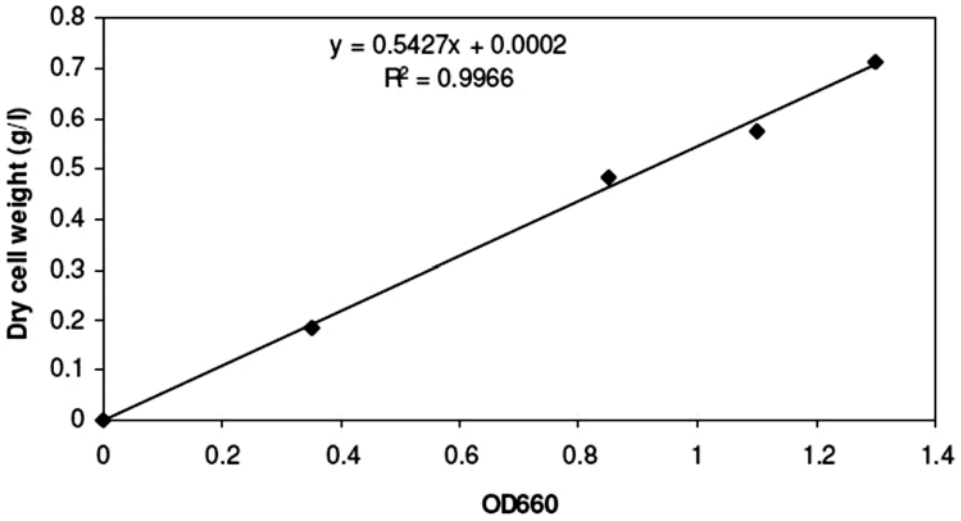

Figure B.1 Calibration curve and the regression trend line for *Rhodobacter capsulatus (*DSM 1710) dry weight versus OD660 (Uyar, 2008)

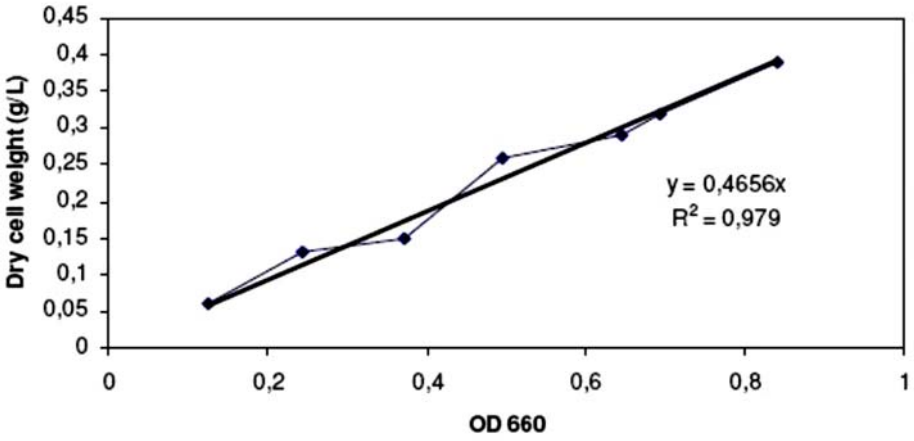

Figure B.2 Calibration curve and the regression trend line for *Rhodobacter capsulatus* YO3 (hup$^-$) dry weight versus OD660 (Öztürk, 2005)

APPENDIX C

SAMPLES OF GAS CHROMATOGRAMS

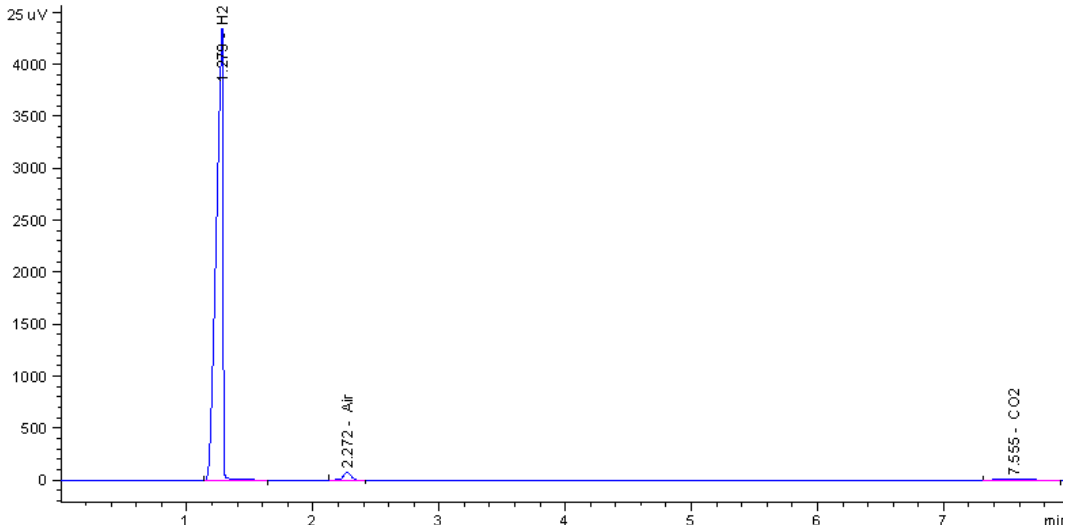

Figure C.1 Sample chromatogram for gas analysis (Boran, 2011). Retention times of hydrogen, air and carbon dioxide are; 1.279, 2.272, 7.555

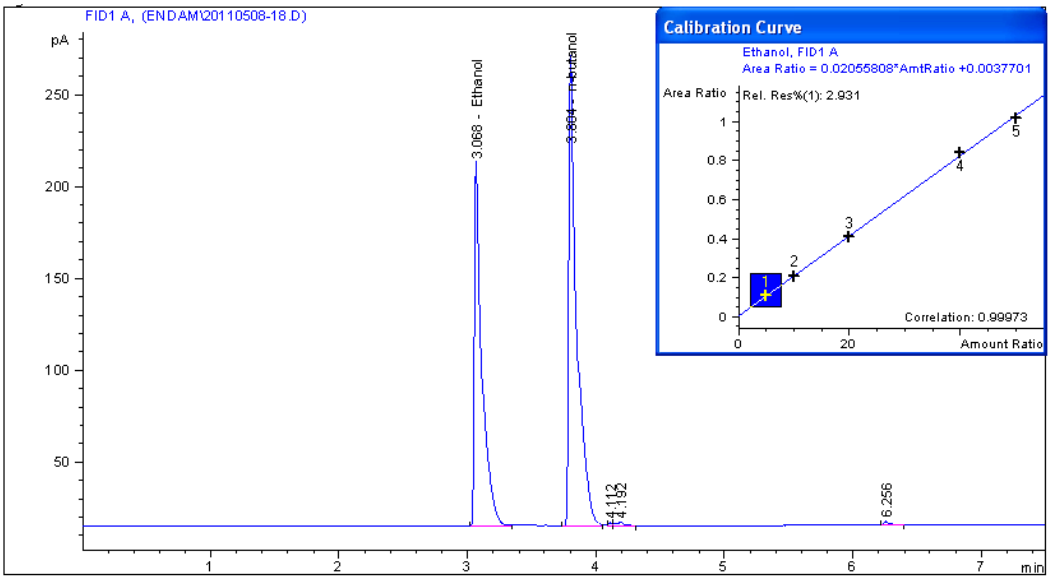

Figure C.2 Sample chromatogram and calibration curve for ethanol analysis. Retention times of ethanol and n-butanol; 3.068 and 3.804 minutes

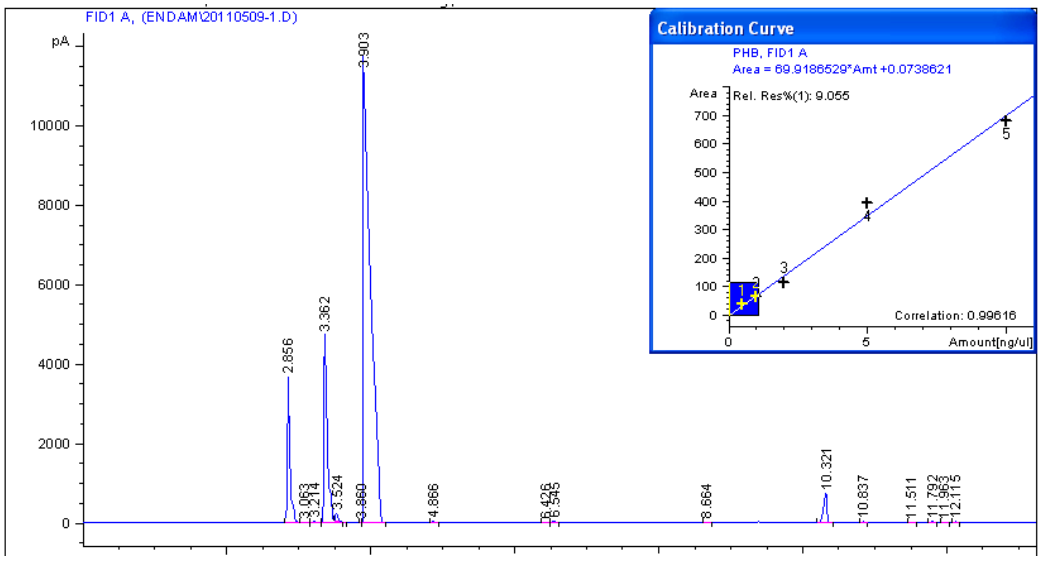

Figure C.3 Sample chromatogram and calibration curve for PHB analysis. Retention times of PHB gives a peak at a retention time of 10.321

APPENDIX D

SAMPLE OF HPLC CHROMATOGRAM

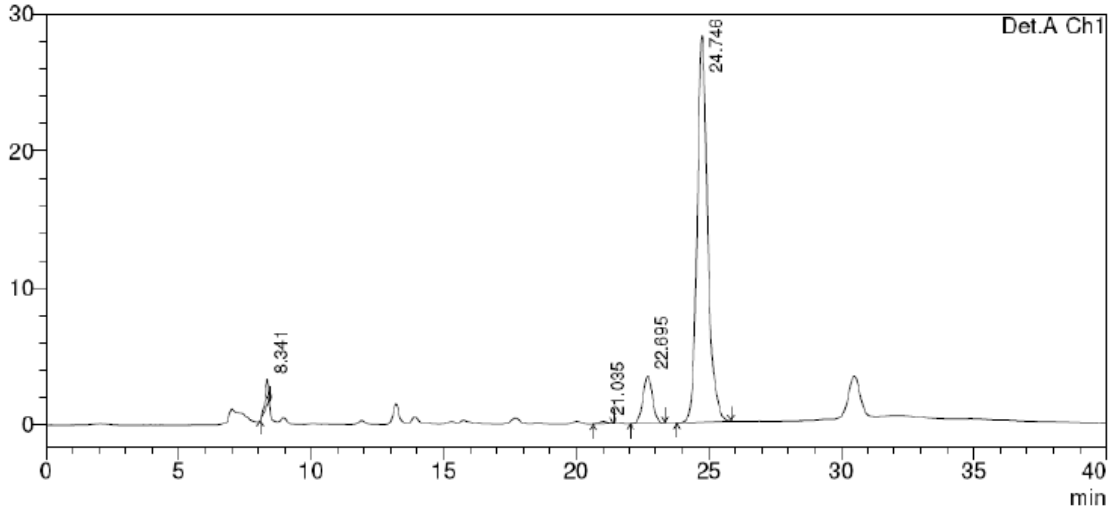

PeakTable

Detector A Ch1 210nm

Peak#	Ret. Time	Area	Height	Area %	Height %
1	8.341	14689	1859	1.654	5.516
2	21.035	3735	182	0.420	0.542
3	22.695	86422	3453	9.730	10.248
4	24.746	783359	28200	88.196	83.694
Total		888205	33695	100.000	100.000

Figure D.1 Sample HPLC analysis chromatogram. Retention times of lactic acid, formic acid and acetic acid; 21.035, 22.695, 24.746 (Sevinç, 2010)

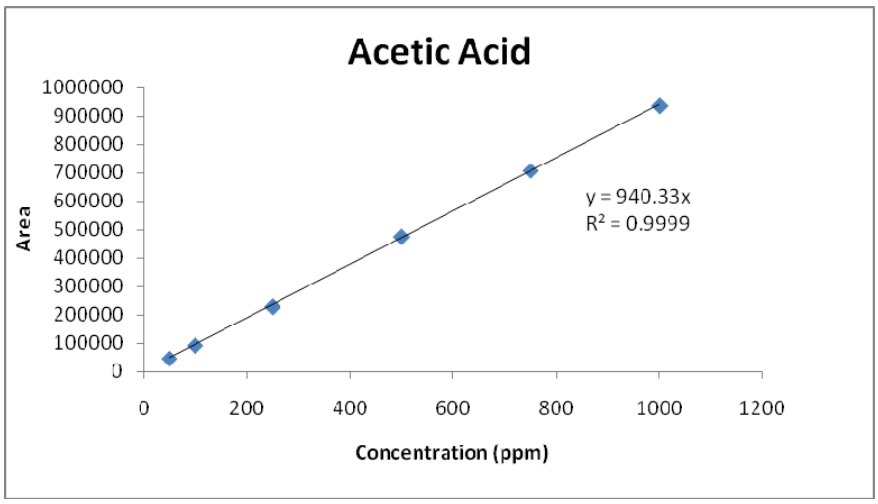

Figure D.2 Sample Acetic Acid Calibration Curve

APPENDIX E

SELECTION of BUFFER for DARK FERMENTATION EFFLUENT of SUGAR BEER THICK JUICE

Buffer selection studies were done, to look for a buffer alternative to KH_2PO_4, that is more environmentally friendly. For this purpose 50 ml photobioreactor and *Rb. capsulatus* DSM1710 were used under illumination at 2500 lux. 5, 10 and 15 mM KH_2PO_4 and 7.5, 10 and 12.5 mM Na_2CO_3 buffer concentrations were tried on DFE of sugar beet thick juice 1 (DFESBTJ1). The results of this run were summarized in Table E.1, the maximum pH, biomass and total produced hydrogen are given with respect to buffers used.

Table E.1 The maximum biomass concentration and pH, and total produced hydrogen with respect to different concentrations of Na2CO3 and KH2PO4 buffer

Concentration of buffer	Maximum pH	Maximum Biomass (gdw/L_c)	Total Produced Hydrogen (ml)
7.5 mM Na_2CO_3	10.122	0.543	5.31
10 mM Na_2CO_3	10.229	0.577	2.13
12.5 mM Na_2CO_3	10.127	0.630	14.76
10 mM KH_2PO_4	8.963	0.910	14.23
15 mM KH_2PO_4	8.384	0.784	23.16
20 mM KH_2PO_4	8.104	0.839	20.61

According to Figure E.1 and Table E.1, Na_2CO_3 buffer tried were not adequate to keep the pH in this desired range. And the average biomass and total produced hydrogen amounts are very low due to the high pH. However, it was observed that KH_2PO_4 is a better buffer than Na_2CO_3 and the best concentration is 20 mM.

APPENDIX F

CALCULATIONS FOR EVALUATION OF THE ANALYSIS

F.1 Calculation of Dry Cell Weight

In order to calculate bacterial cell concentration (gdw/L_c), OD660 measurement value multiplied by the slope of the standard calibration curve for *Rb. capsulatus* DSM1710 (m=0.5427) and *Rb. capsulatus* YO3 (hup^-) (m=0.4656). The formula is given below;

$$\text{Biomass (gdw/L}_c\text{)}=\text{OD}_{660} \text{ x m} \quad \text{(F.1)}$$

$$0.5427 \text{ gdw/L}_c = 1 \text{ x gdw/L}_c \quad \text{(F.2)}$$

F.2 Calculation of Specific Growth Rate

In order to interpret the bacterial growth for the experiments, the specific growth rates were calculated. Under ideal conditions for growth, when batch fermentation is carried out, growth increases exponentially with to respect time. Thus, the overall rate of biomass formation is proportional to the biomass itself. This leads to an autocatalytic reaction, which is described by a first order rate expression as:

$$\frac{dx}{dt} = \mu.X \quad \text{(F.3)}$$

Hereby, X is the bacterial concentration, t is the time and μ is the specific growth rate with the dimension of 1/time. This equation expresses the growth rate in exponential phase. Integrating and reordering the equation gives:

$$\mu = \frac{\ln\left(X_2/X_1\right)}{\left(t_2 - t_1\right)} \tag{F.4}$$

$$\mu = \frac{\ln(0.656/0.149)}{(37.5\text{-}0)\ \text{h}} = 0.039\ \text{h}^{-1} \tag{F.5}$$

F.3 Calculation of Bacteriochlorophyll a Content and Cellular Bacteriochlorophyll a Content

Bacteriochlorophyll *a* concentration is calculated by the formula (F.6), and cellular bacteriochlorophyll *a* concentration is calculated by dividing bacteriochlorophyll *a* concentration with bacterial cell concentration (gdw/L_c) (F.7).

$$\text{Bchl } a \text{ concentration} = [OD_{770}/(\varepsilon \times L)] \times MW_{\text{bchl } a} \tag{F.6}$$

$$\text{Cellular Bchl } a \text{ concentration} = \text{Bchl } a \text{ concentration/Biomass (gdw/}L_c\text{)} \tag{F.7}$$

Where OD_{770} is absorbance at 770 nm, ε is the extinction coefficient (75), L is the length of the liquid in the cuvette (1 cm) and $MW_{\text{bchl } a}$ is the molecular weight of bacteriochlorophyll *a* (911.5 mg/mmol).

$$2.42\ mg_{\text{bchl } a}/L_c = [0.202/(75\ mM^{-1}\ cm^{-1} \times 1\ cm)] \times 911.5\ mg/mmol \tag{F.8}$$

$$2.28\ mg_{\text{bchl } a}/gdw = (2.42\ mg_{\text{bchl } a}/L_c)/(1.06\ gdw/L_c) \tag{F.9}$$

F.4 Calculation of Molar Productivity

Molar Productivity defined as:

$$\frac{\text{millimoles of hydrogen produced}}{\text{Volume of culture (L) x t (hour)}} \qquad \text{(F.10)}$$

For the outdoor panel PBR experiment, molar productivity was calculated as moles of hydrogen produced per liter of culture per illuminated hours, considering the local temperature and pressure changes. The total local temperature and pressure data were taken from the National Meteorology Institute in Ankara. First, produced hydrogen is converted to moles of hydrogen (F.11, F.12).

$$P \times V = n \times R \times T \qquad \text{(F.11)}$$

Where P is the barometric pressure of hydrogen in the hydrogen collection column at the recording time, V is the produced hydrogen in liters, R is the gas constant and T is the temperature of the hydrogen at recording time.

$$910.2 \times 10^3 \text{ bar} \times 0.777 \text{ L} = 28.6 \text{ mmol} \times 83.144 \frac{\text{bar.L}}{\text{mmol.K}} \times 297.4 \text{ K} \qquad \text{(F.12)}$$

For the small scale batch experiments (bottles), maximum productivity was calculated from the slope of the cumulative hydrogen production versus time graph ($mmol/L_c/h$).

F.5 Calculation of Molar Yield

The molar hydrogen yield defined was calculated as the percent of the ratio of mole of hydrogen produced per mole of the theoretical hydrogen that can be formed from fed/consumed substrate (F.13, F.14).

$$\frac{\text{Actual millimoles of hydrogen produced}}{\text{theoretical millimoles of hydrogen produced}} \text{x}100 \qquad \text{(F.13)}$$

The stoichiometric equations for hydrogen production from acetate and lactate are given in Reactions 1.9 and 1.10.

$$32.7\% = \frac{8.68 \text{ mmol hydrogen}}{26.55 \text{ mmol hydrogen}} \text{x}100 \qquad \text{(F.14)}$$

F.6 Product Yield Factor

Product yield factor defined as:

$$\frac{\text{cumulative millimoles of hydrogen produced}}{\text{maximum dry cell weight (g)}} \qquad \text{(F.15)}$$

Product yield factor, defined as the ratio of cumulative hydrogen produced in millimoles to the maximum dry cell weight in grams.

$$65 = 10.1 \text{ mmol } H_2/0.155 \text{ g} \qquad \text{(F.16)}$$

F.7 Calculation of Light Conversion Efficiency

For the small scale indoor experiments light conversion efficiency was calculated. 150 mL bottles were used during the experiments and the irradiated area of these bottles were 0.011 m^2. The light intensity adjusted to 2500 lux.

Light conversion efficiency, η is defined as the ratio of the total energy value (heat of combustion) of the hydrogen that has been produced to the total energy input to the photobioreactor by light radiation and it is calculated by:

$$\eta(\%) = \frac{33.6 \times \rho_{H_2} \times V_{H_2}}{I \times A \times t} \times 100 \quad \text{(F.17)}$$

where V_{H2} is the volume (L) of produced H_2, ρ_{H2} is the density (g/L) of the produced hydrogen gas, I is the light intensity (W/m^2), A is the irradiated area (m^2) and t is the duration of hydrogen production from the end of the lag phase, λ, to the end of the run.

$0.143\% = [(33.6 \times 0.089\ g/L \times 0.241\ L)/(142.8\ W/m^2 \times 0.011 m^2 \times 319.5\ h)] \times 100$ (F.18)

F.8 Procedure for Organic Acid Consumption Kinetics

The general procedure of the integral method of analysis is to define a rate equation on to experimental data by integrating and comparing the concentration of a reactant or product versus time. If the fit is unsatisfactory, another rate equation is guessed and tested. It can be expressed as:

$$-\frac{dC}{dt} = k.C^n \quad \text{(F.19)}$$

where k is the rate constant and n is the order. C(t) is the function of time and integration of this equation regarding to order (n) of the equation gives:

- Zeroth order: $C-C_o = -k(t-t_o)$ (F.20)
- First order: $\ln\frac{C}{C_o} = -k(t-t_o)$ (F.21)
- Second order: $\frac{1}{C} - \frac{1}{C_o} = k(t-t_o)$ (F.22)

C(t) is calculated for each order by using the experimental data

APPENDIX G

SAMPLE PICTURE OF CLINOPTILOLITE ZEOLITE

(1) **(2)**

Figure G.1 Clinoptilolite Zeolite: (1) Larger particle Size (>1 mm), (2) Smaller Particle Size (0.25-0.50 mm) (Bahaallddin, 2010)

APPENDIX H

LOGISTIC MODEL

H.1-H.4 Curves fitted to the logistic model together with the experimental data for treated/untreated DFESBTJ for *Rb.capsulatus* DSM1710

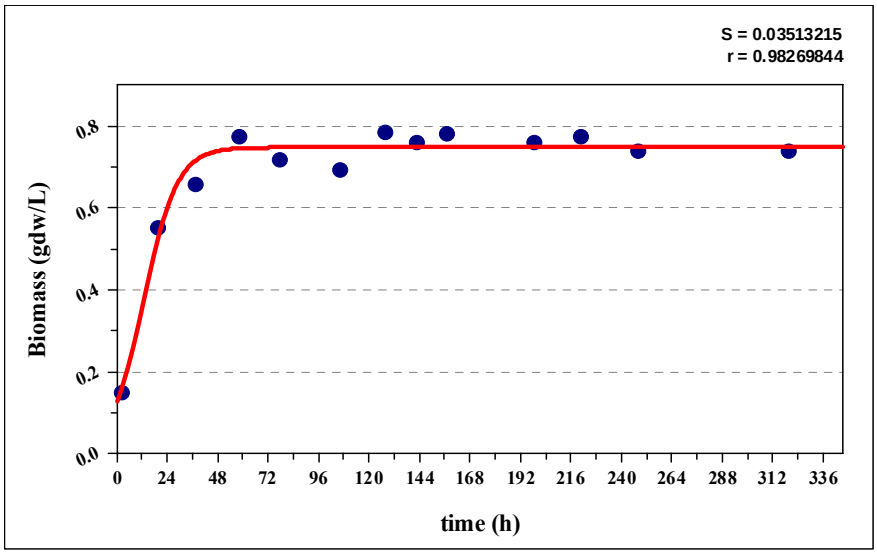

Figure H.1 The logistic growth model on treated DFESBTJ2 for *Rb.capsulatus* DSM1710 (●: experimental data, ▬: model fit)

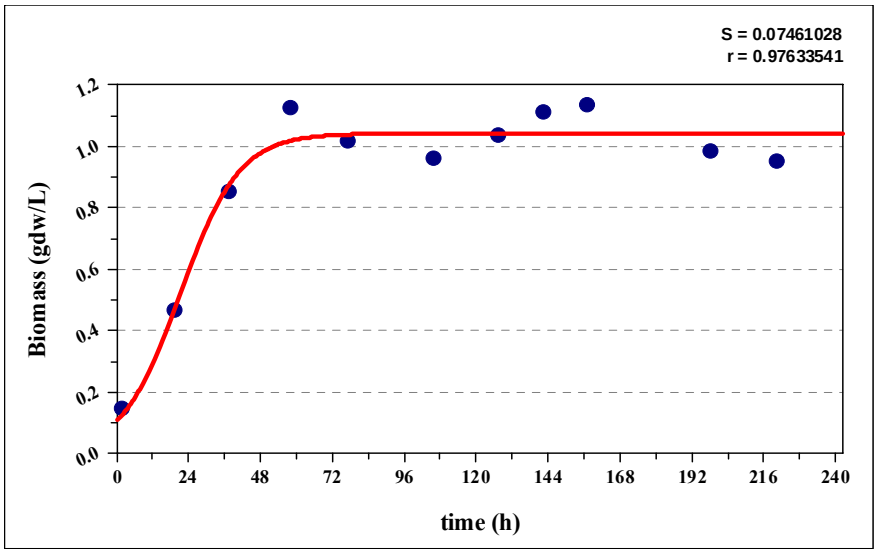

Figure H.2 The logistic growth model on untreated DFESBTJ2 for *Rb.capsulatus* DSM1710 (●: experimental data, ▬: model fit)

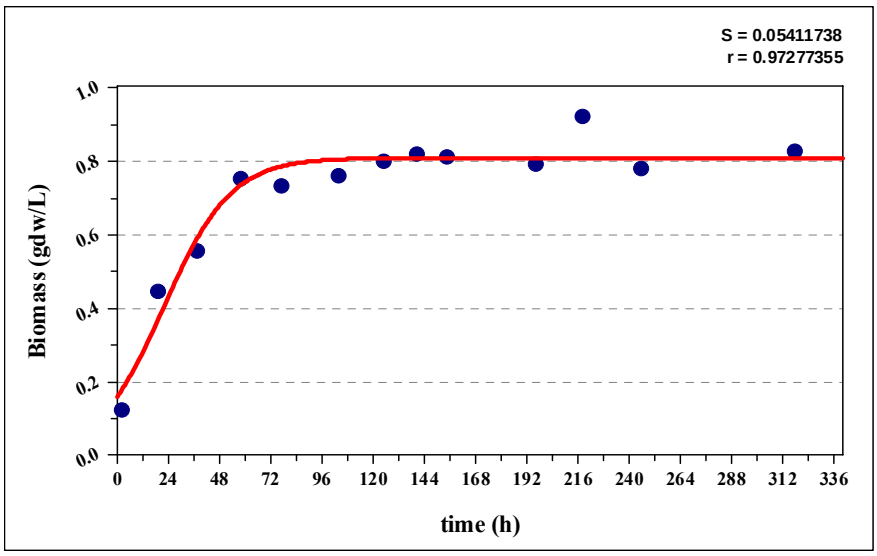

Figure H.3 The logistic growth model on treated DFESBTJ3 for *Rb.capsulatus* DSM1710 (●: experimental data, ▬: model fit)

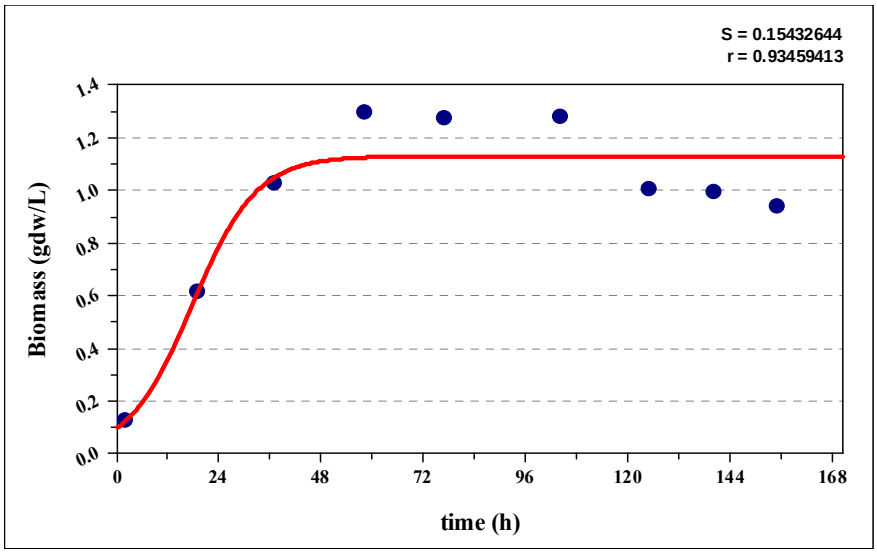

Figure H.4 The logistic growth model on untreated DFESBTJ3 for *Rb.capsulatus* DSM1710 (●: experimental data, ▬: model fit)

H.5-H.8 Curves fitted to the logistic model together with the experimental data for treted/untreated DFESBTJ DFE for *Rb.capsulatus* YO3 (hup$^-$)

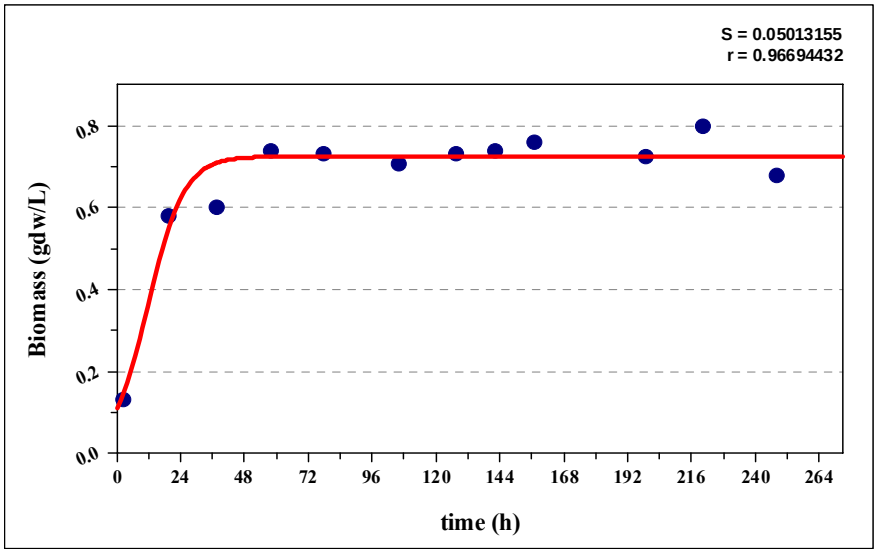

Figure H.5 The logistic growth model on treated DFESBTJ2 for *Rb.capsulatus* YO3 (hup$^-$) (●: experimental data, ▬: model fit)

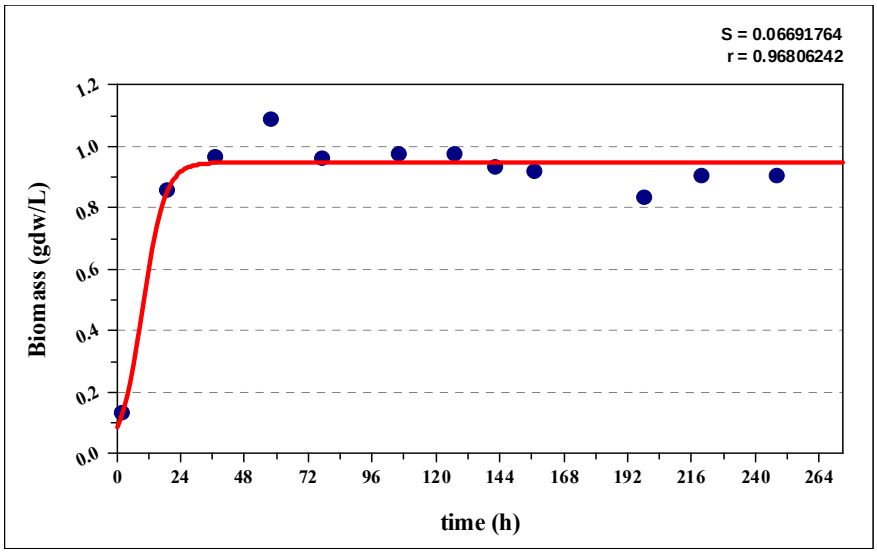

Figure H.6 The logistic growth model on untreated DFESBTJ2 for *Rb.capsulatus* YO3 (hup$^-$) (●: experimental data, ▬: model fit)

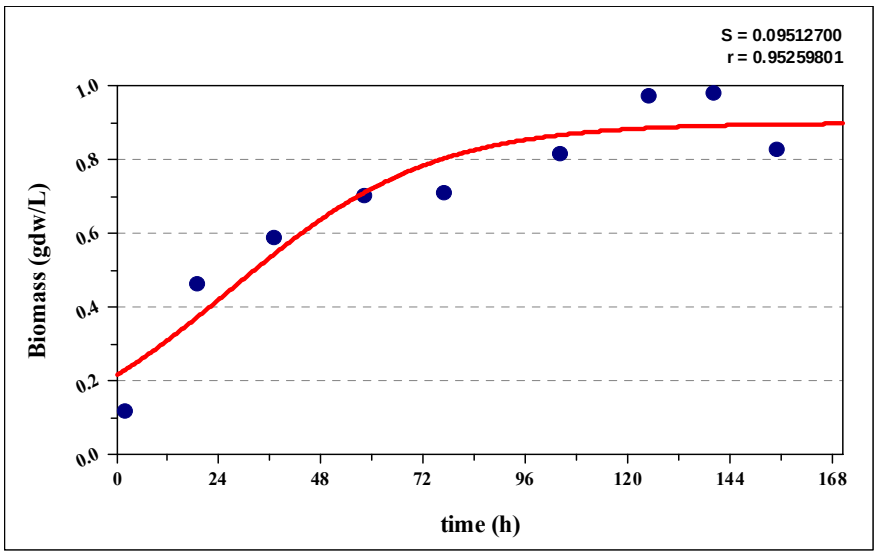

Figure H.7 The logistic growth model on treated DFESBTJ3 for *Rb.capsulatus* YO3 (hup$^-$) (●: experimental data, ▬: model fit)

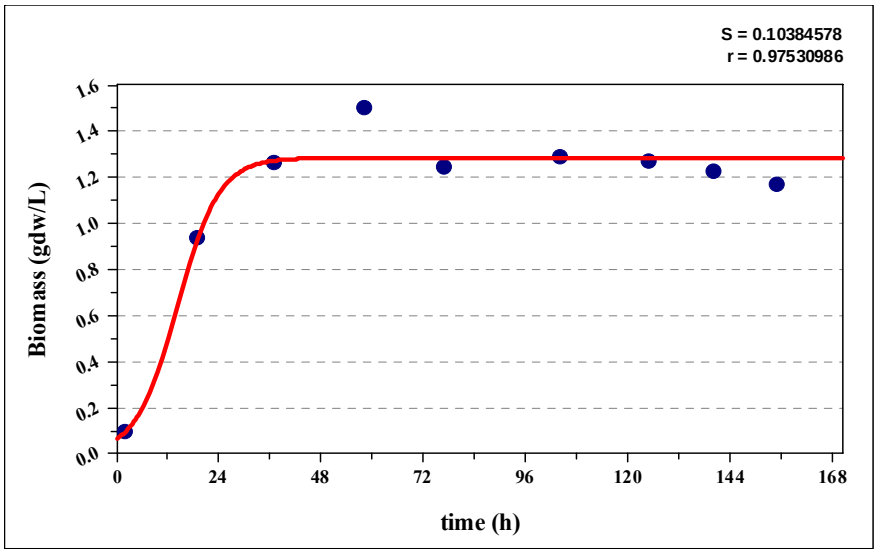

Figure H.8 The logistic growth model on untreated DFESBTJ3 for *Rb.capsulatus* YO3 (hup$^-$) (●: experimental data, ▬: model fit)

H.9-H.16 Curves fitted to the logistic model together with the experimental data for different EtOH concentrations for *Rhodobacter capsulatus* DSM1710

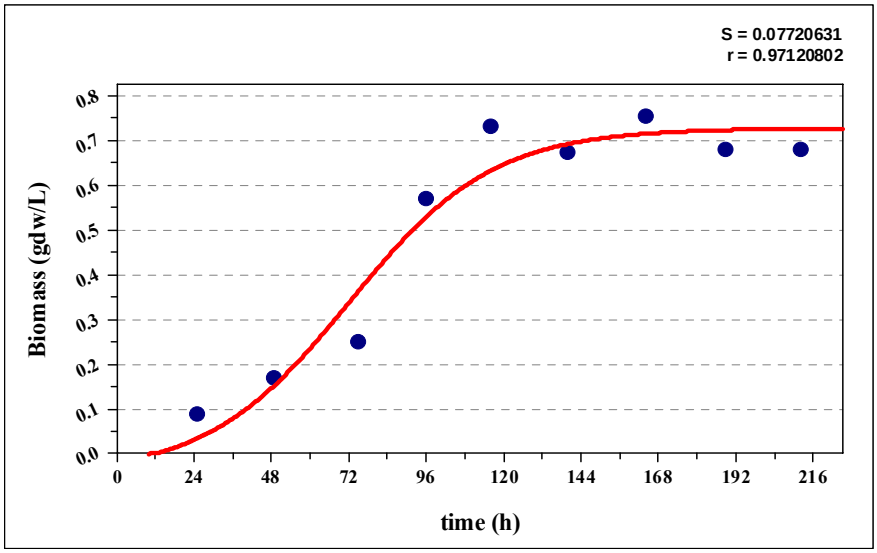

Figure H.9 The logistic growth model at control medium for *Rb. capsulatus* DSM1710 (●: experimental data, ▬: model fit)

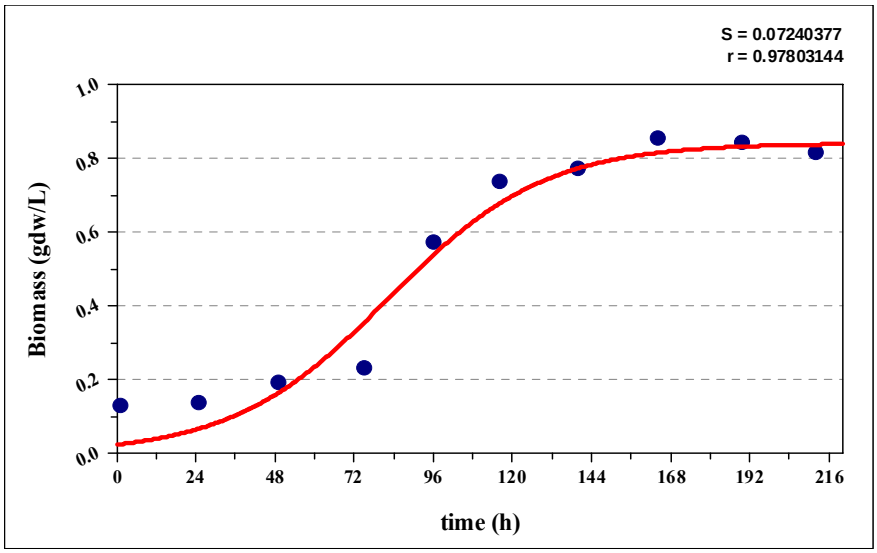

Figure H.10 The logistic growth model at 6.25 mM EtOH containing medium for *Rb. capsulatus* DSM1710 (●: experimental data, ▬: model fit)

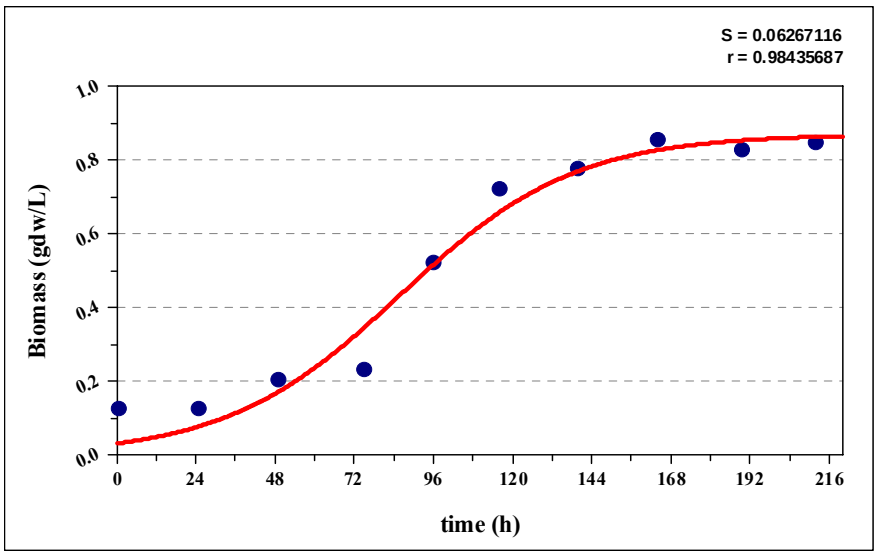

Figure H.11 The logistic growth model at 12.5 mM EtOH containing medium for *Rb. capsulatus* DSM1710 (●: experimental data, ▬: model fit)

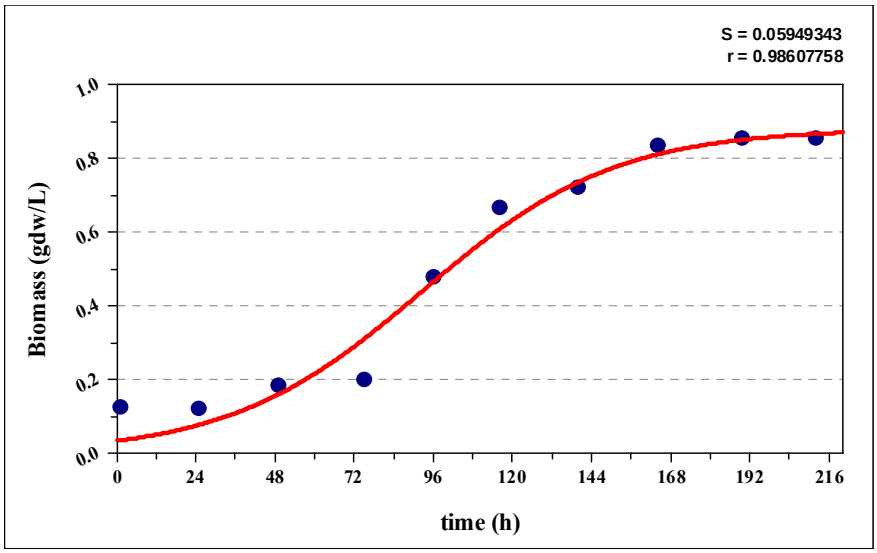

Figure H.12 The logistic growth model at 25 mM EtOH containing medium for *Rb. capsulatus* DSM1710 (●: experimental data, ▬: model fit)

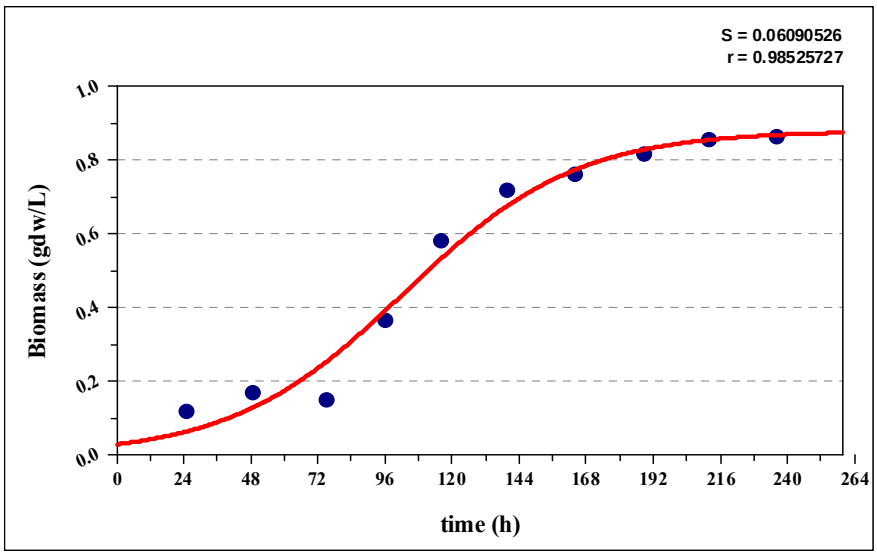

Figure H.13 The logistic growth model at 37.5 mM EtOH containing medium for *Rb. capsulatus* DSM1710 (●: experimental data, ▬: model fit)

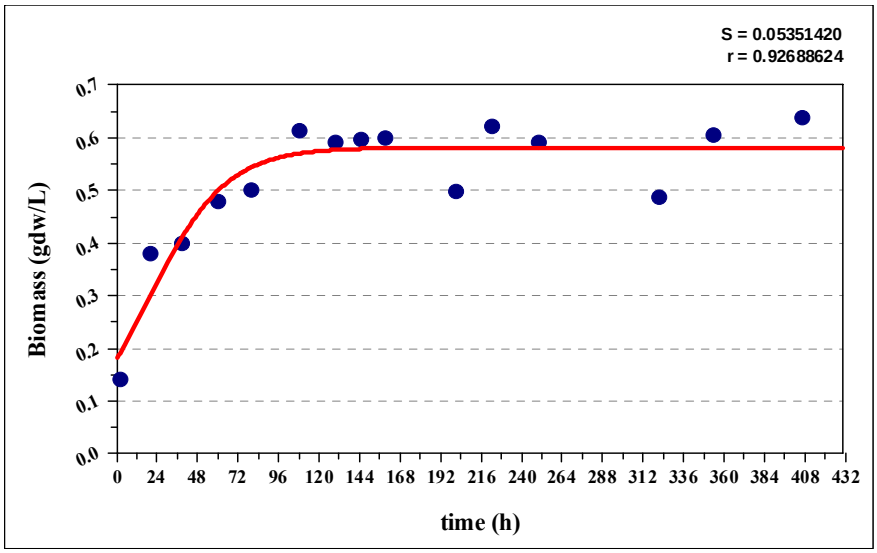

Figure H.14 The logistic growth model at 50 mM EtOH containing medium for *Rb. capsulatus* DSM1710 (●: experimental data, ▬: model fit)

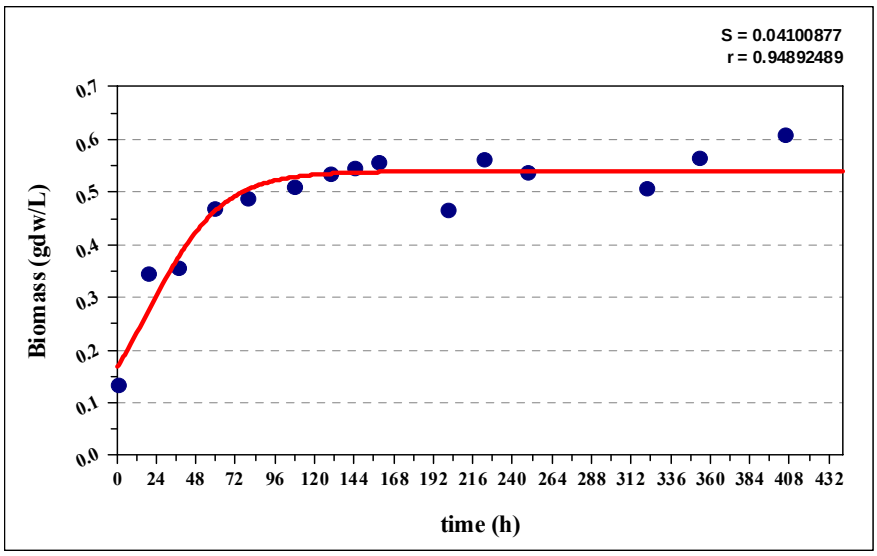

Figure H.15 The logistic growth model at 100 mM EtOH containing medium for *Rb. capsulatus* DSM1710 (●: experimental data, ▬: model fit)

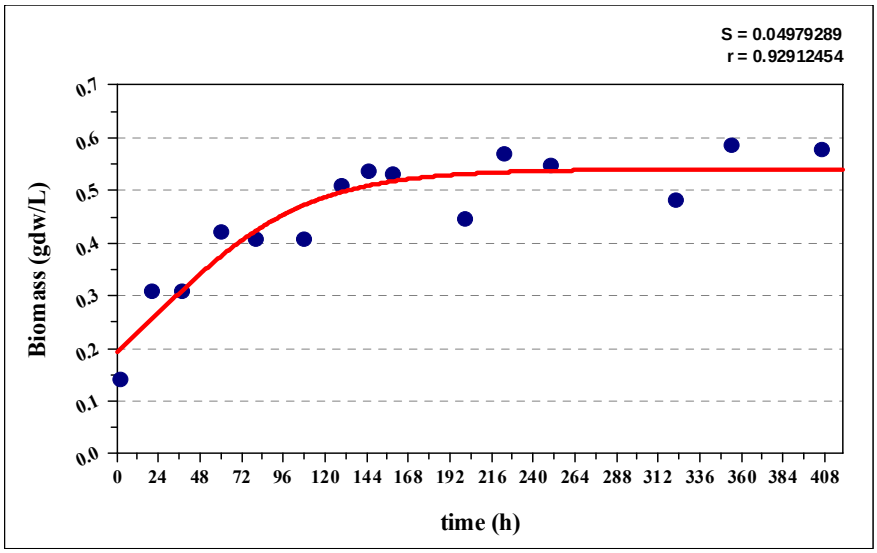

Figure H.16 The logistic growth model at 200 mM EtOH containing medium for *Rb. capsulatus* DSM1710 (●: experimental data, ▬: model fit)

H.17-H.24 Curves fitted to the logistic model together with the experimental data for different EtOH concentrations for *Rb.capsulatus* YO3 (hup$^-$)

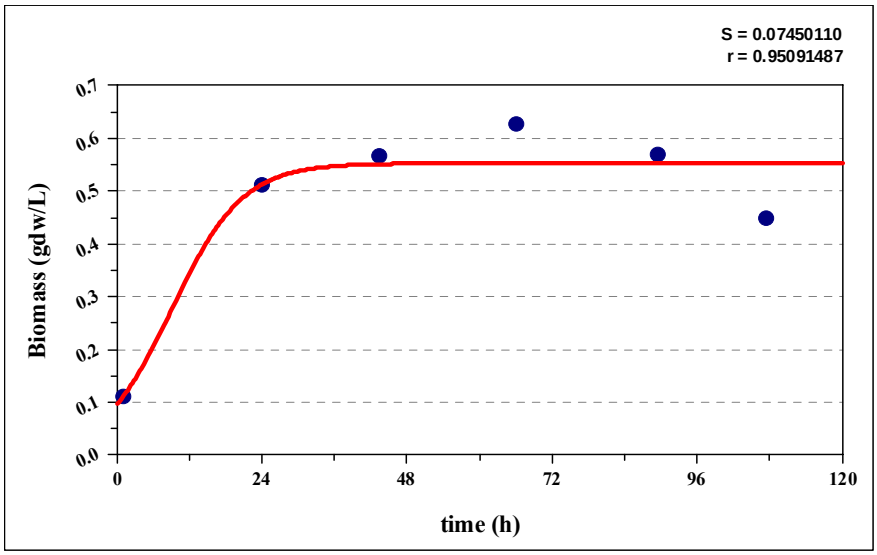

Figure H.17 The logistic growth model at control medium for *Rb.capsulatus* YO3 (hup$^-$) (●: experimental data, ▬: model fit)

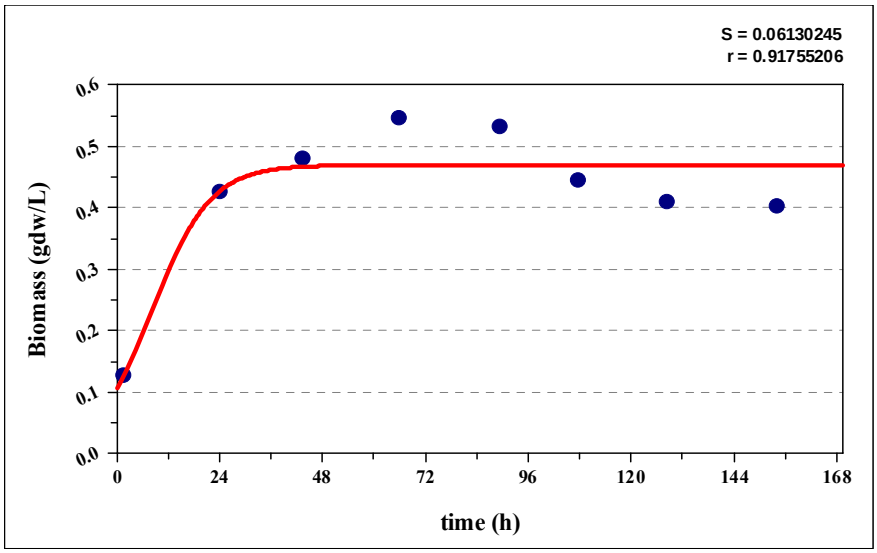

Figure H.18 The logistic growth model at 6.25 mM EtOH containing medium for *Rb.capsulatus* YO3 (hup$^-$) (●: experimental data, ▬: model fit)

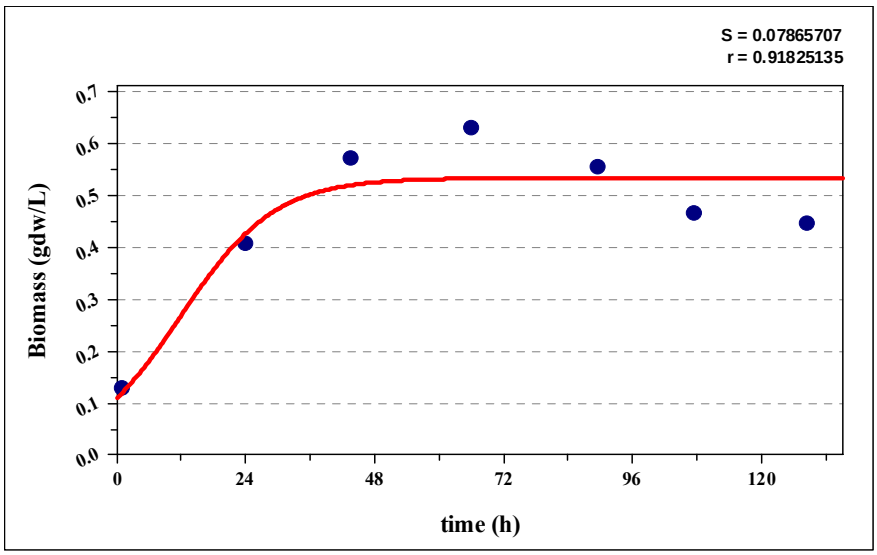

Figure H.19 The logistic growth model at 12.5 mM EtOH containing medium for *Rb.capsulatus* YO3 (hup$^-$) (●: experimental data, ▬: model fit)

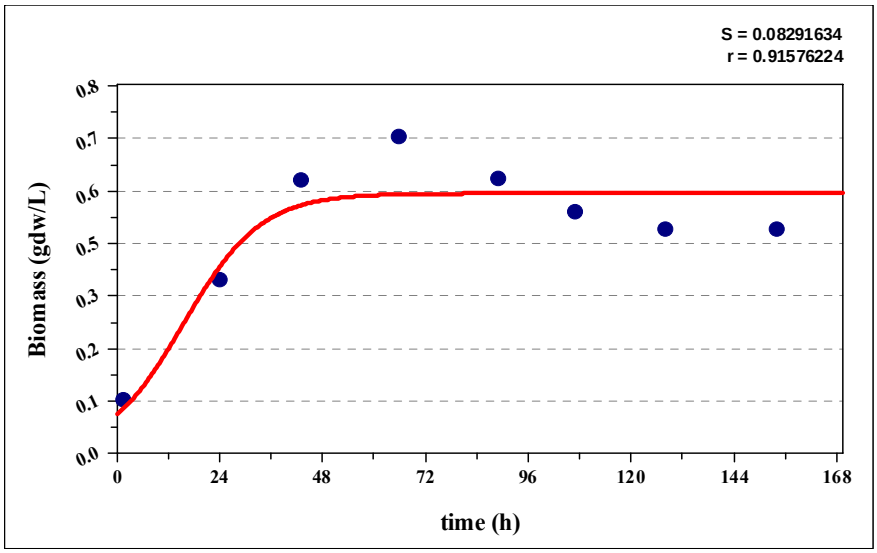

Figure H.20 The logistic growth model at 25 mM EtOH containing medium for *Rb.capsulatus* YO3 (hup$^-$) (●: experimental data, ▬: model fit)

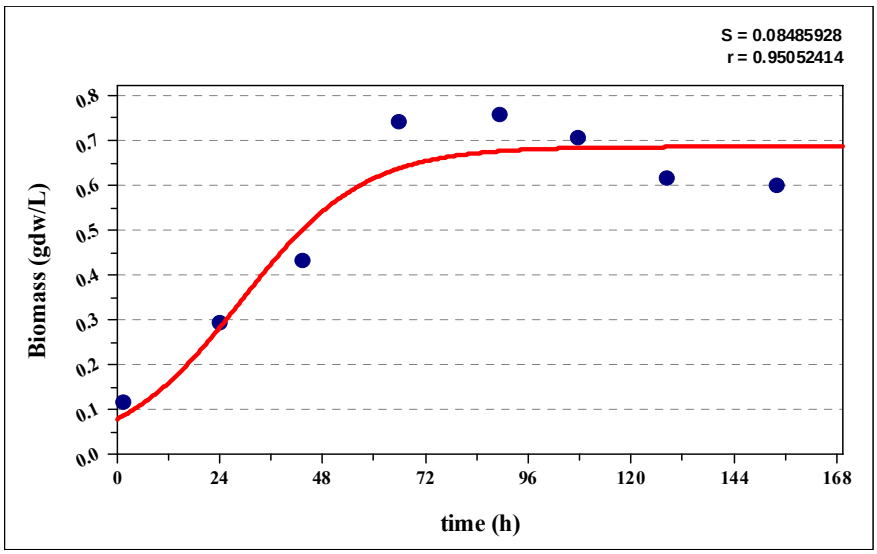

Figure H.21 The logistic growth model at 37.5 mM EtOH containing medium for *Rb.capsulatus* YO3 (hup$^-$) (●: experimental data, ▬: model fit)

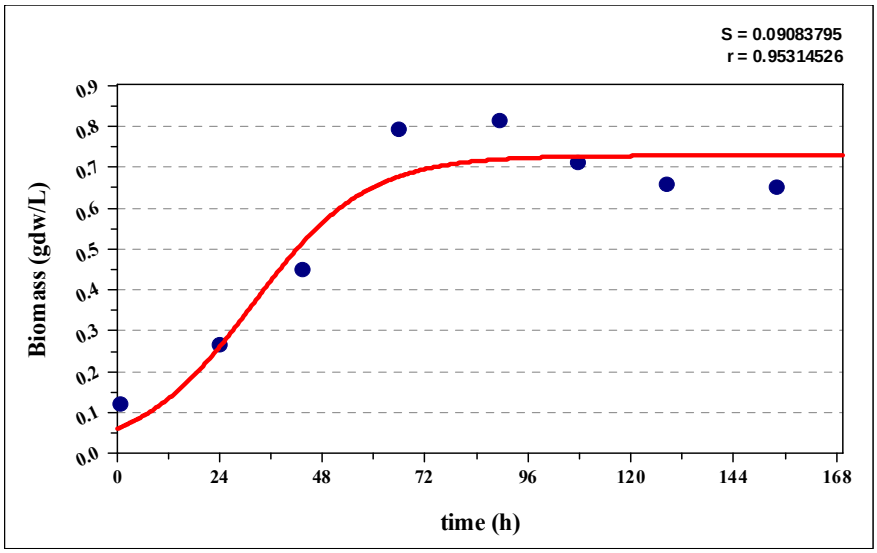

Figure H.22 The logistic growth model at 50 mM EtOH containing medium for *Rb.capsulatus* YO3 (hup$^-$) (●: experimental data, ▬: model fit)

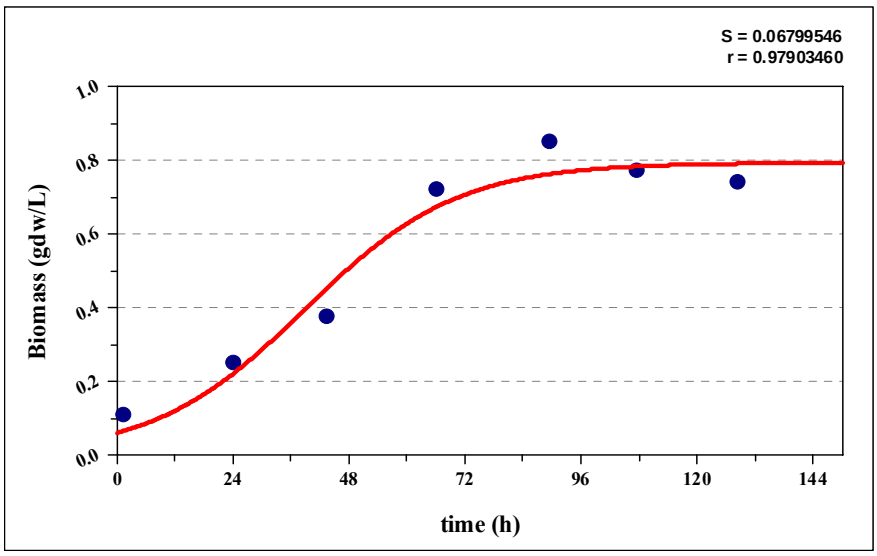

Figure H.23 The logistic growth model at 100 mM EtOH containing medium for *Rb.capsulatus* YO3 (hup$^-$) (●: experimental data, ▬: model fit)

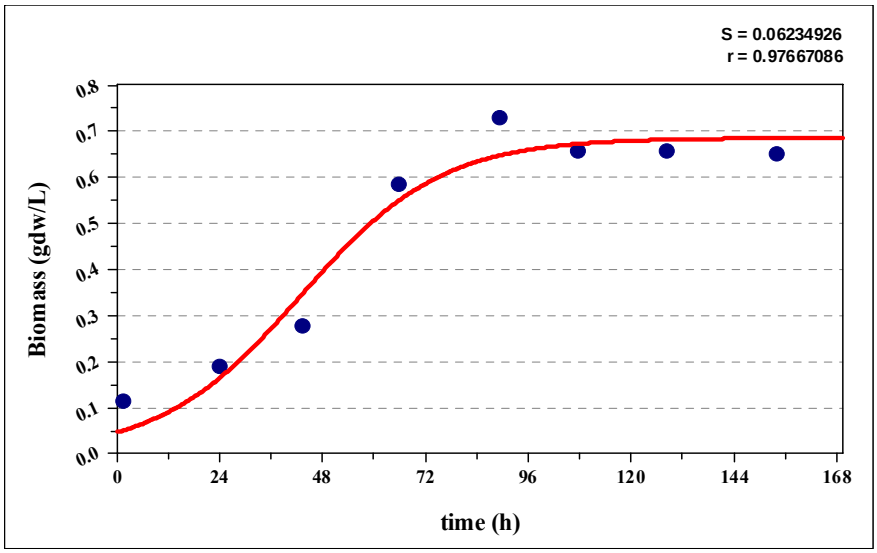

Figure H.24 The logistic growth model at 200 mM EtOH containing medium for *Rb.capsulatus* YO3 (hup$^-$) (●: experimental data, ▬: model fit)

APPENDIX I

MODIFIED GOMPERTZ MODEL

I1-I4. Curves fitted to the Modified Gompertz Model together with the experimental data for treated/untreated DFESBTJ for *Rb.capsulatus* DSM1710

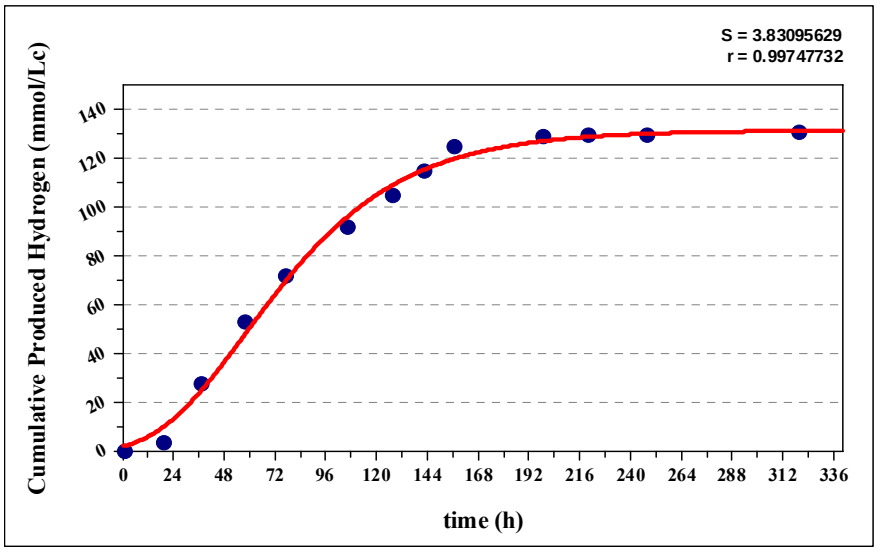

Figure I.1 The Modified Gompertz Model on treated DFESBTJ2 *Rb.capsulatus* DSM1710 (●: experimental data, ▬: model fit)

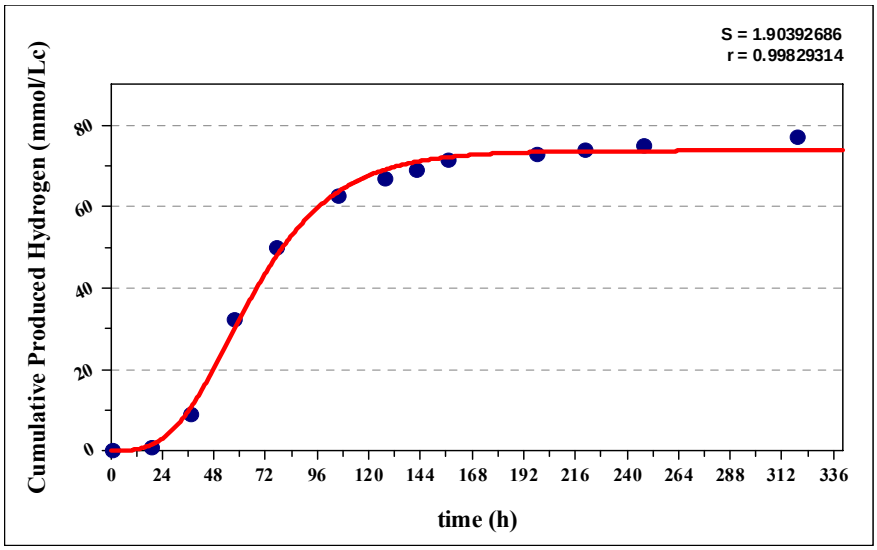

Figure I.2 The Modified Gompertz Model on untreated DFESBTJ2 *Rb.capsulatus* DSM1710 (●: experimental data, ▬: model fit)

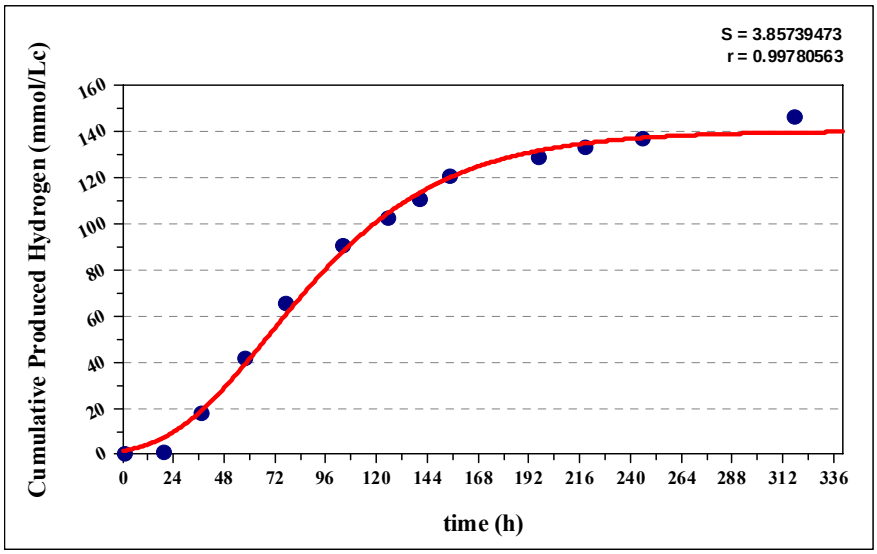

Figure I.3 The Modified Gompertz Model on treated DFESBTJ3 *Rb.capsulatus* DSM1710 (●: experimental data, ▬: model fit)

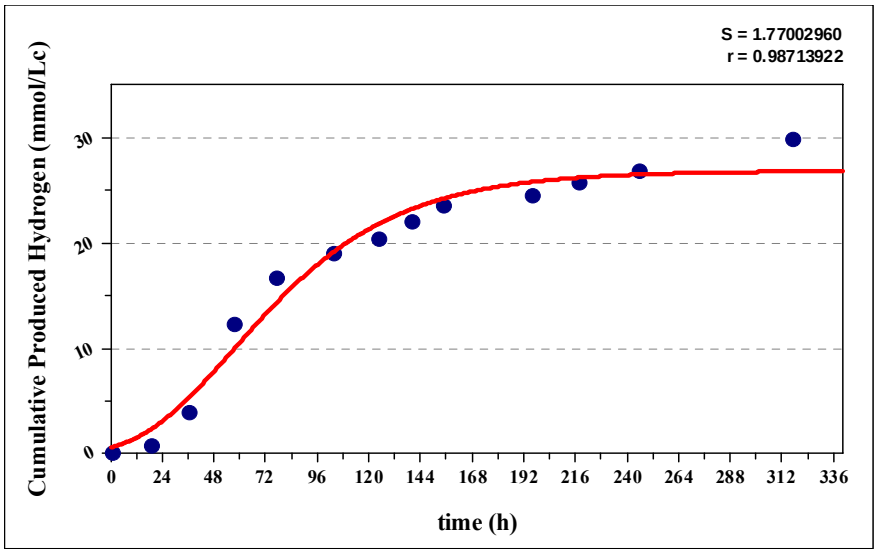

Figure I.4 The Modified Gompertz Model on untreated DFESBTJ3 *Rb.capsulatus* DSM1710 (●: experimental data, ▬: model fit)

I5-I8. Curves fitted to the Modified Gompertz Model together with the experimental data for treated/untreated DFESBTJ for *Rb.capsulatus* YO3 (hup$^-$)

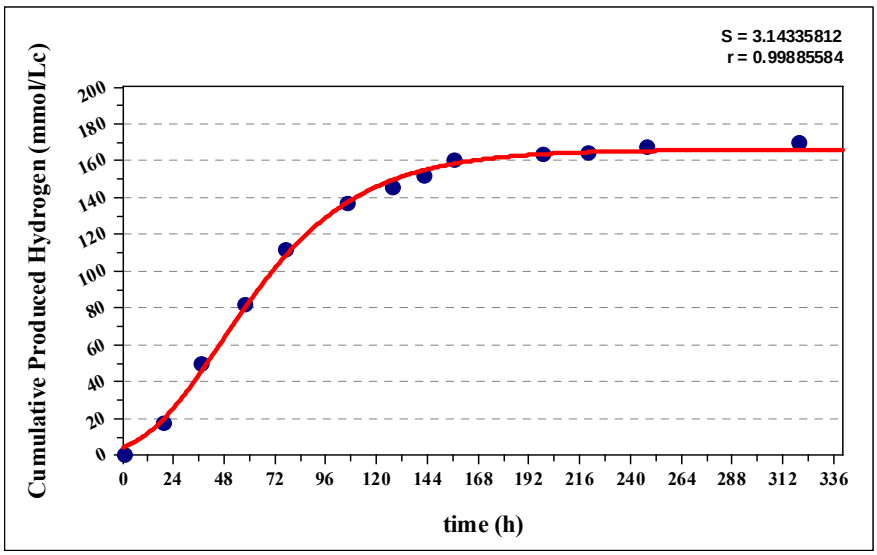

Figure I.5 The Modified Gompertz Model on treated DFESBTJ2 *Rb.capsulatus* YO3 (hup$^-$) (●: experimental data, ▬: model fit)

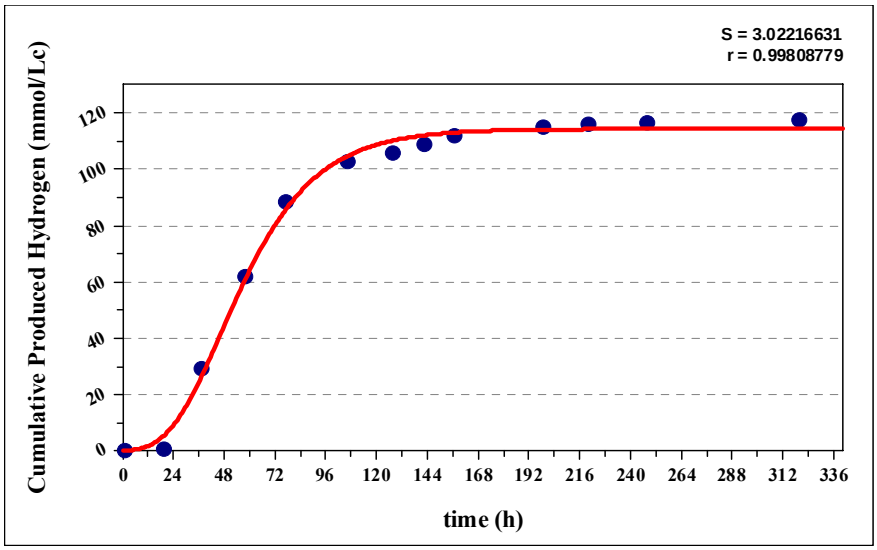

Figure I.6 The Modified Gompertz Model on untreated DFESBTJ2 *Rb.capsulatus* YO3 (hup$^-$) (●: experimental data, ▬: model fit)

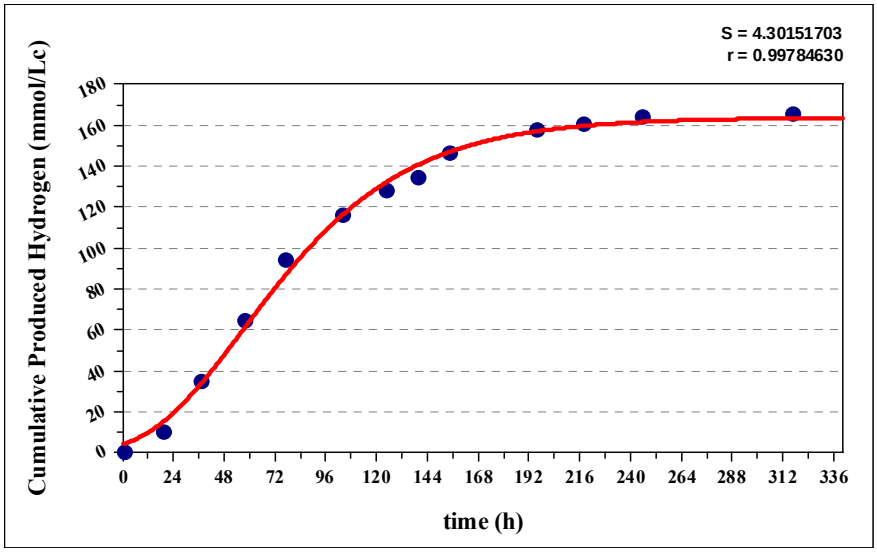

Figure I.7 The Modified Gompertz Model on treated DFESBTJ3 *Rb.capsulatus* YO3 (hup$^-$) (●: experimental data, ▬: model fit)

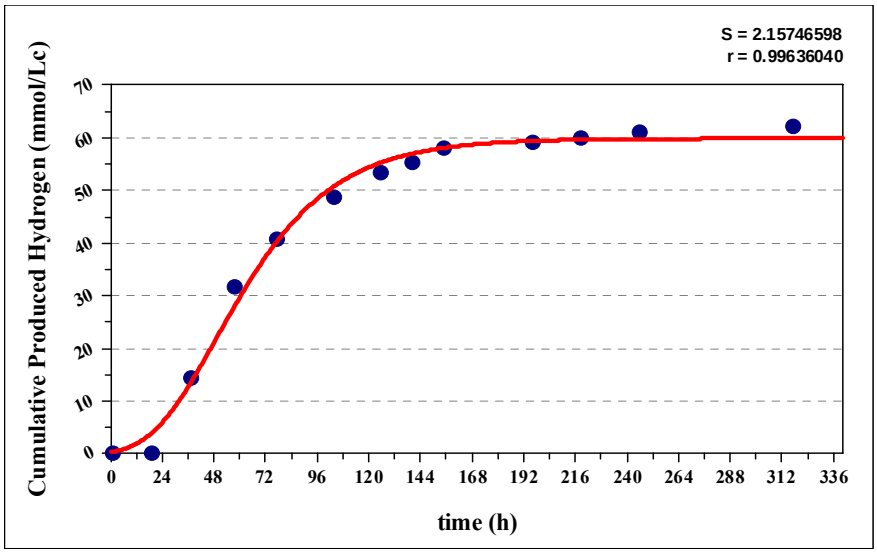

Figure I.8 The Modified Gompertz Model on untreated DFESBTJ3 *Rb.capsulatus* YO3 (hup$^-$) (●: experimental data, ▬: model fit)

I9-I16. Curves fitted to the Modified Gompertz Model together with the experimental data for different EtOH Concentrations for wild type *Rb.capsulatus* DSM1710

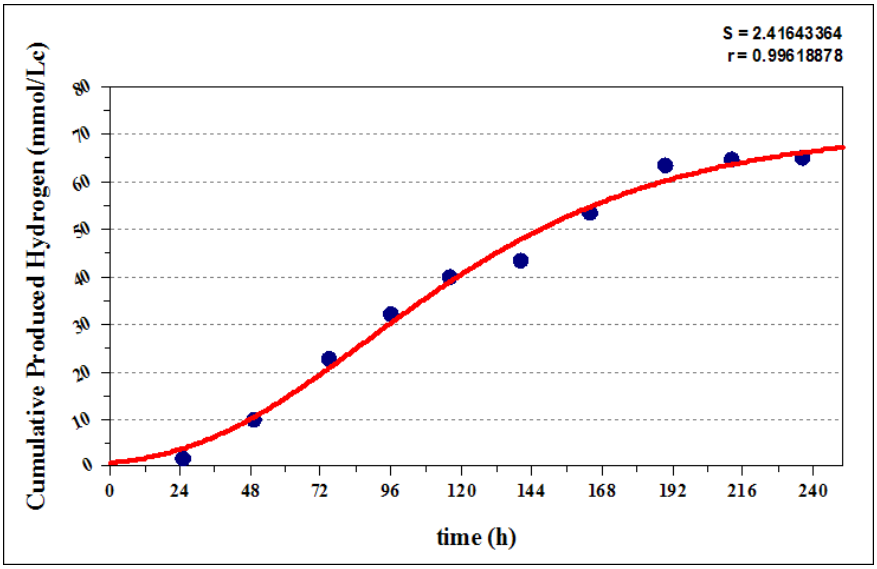

Figure I.9 The Modified Gompertz Model at control medium for *Rb.capsulatus* DSM1710 (●: experimental data, ▬: model fit)

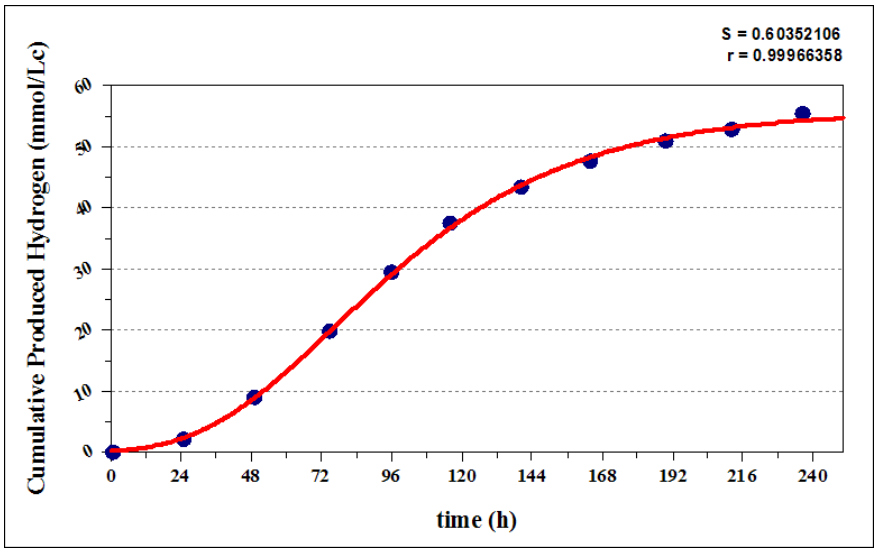

Figure I.10 The Modified Gompertz Model at 6.25 mM EtOH containing medium for *Rb.capsulatus* DSM1710 (●: experimental data, ▬: model fit)

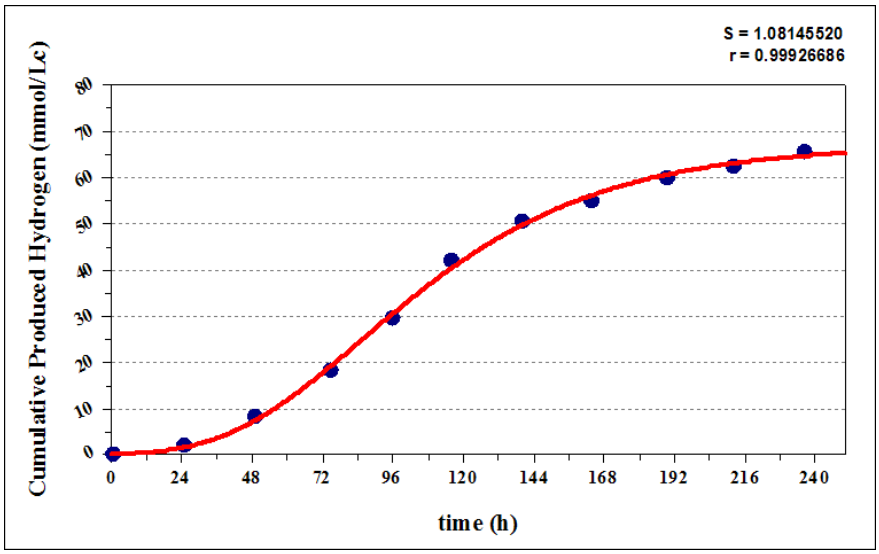

Figure I.11 The Modified Gompertz Model at 12.5 mM EtOH containing medium for *Rb.capsulatus* DSM1710 (●: experimental data, ▬: model fit)

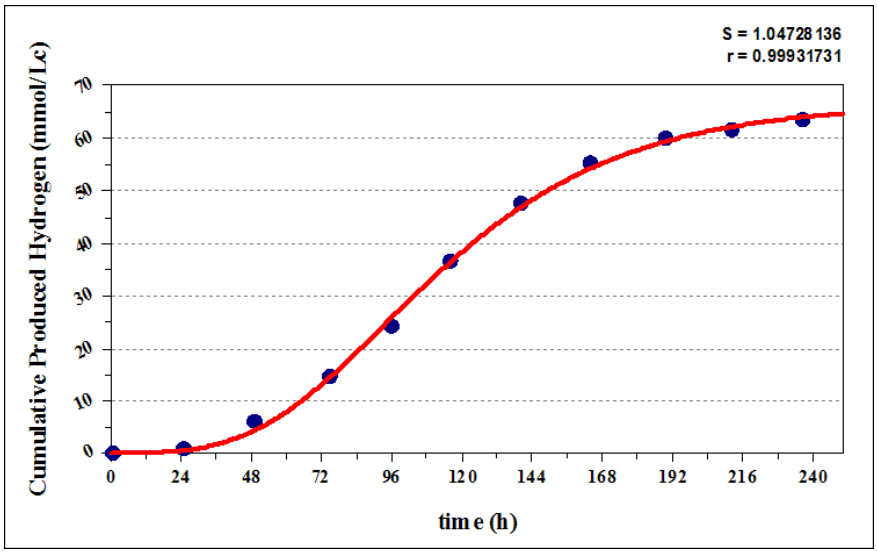

Figure I.12 The Modified Gompertz Model at 25 mM EtOH containing medium for *Rb.capsulatus* DSM1710 (●: experimental data, ▬: model fit)

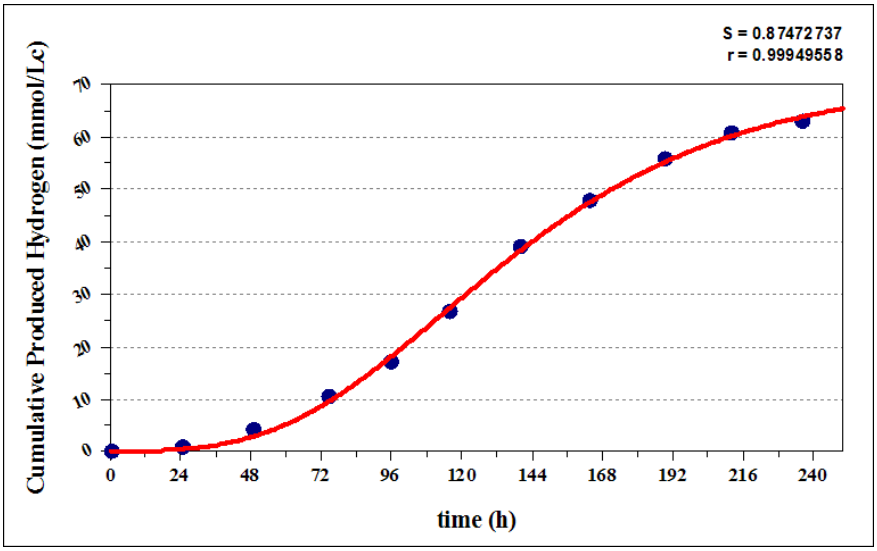

Figure I.13 The Modified Gompertz Model at 37.5 mM EtOH containing medium for *Rb.capsulatus* DSM1710 (●: experimental data, ▬: model fit)

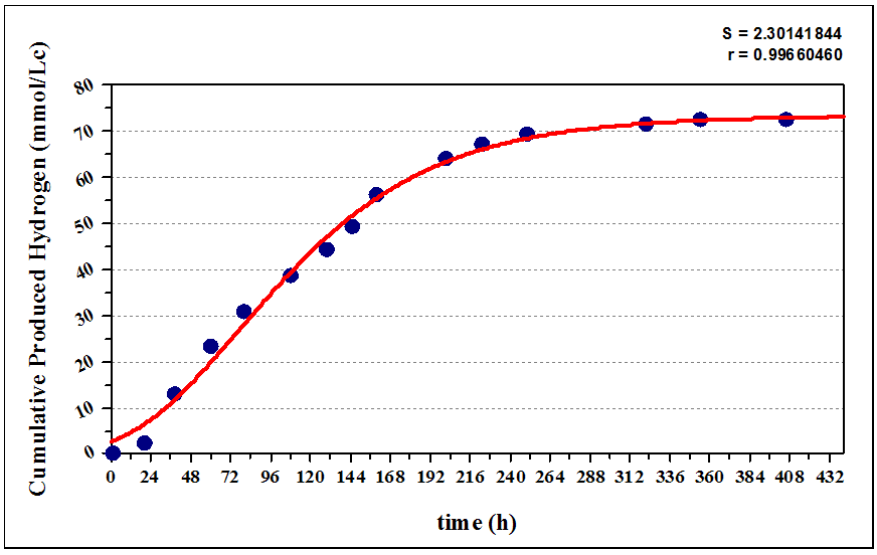

Figure I.14 The Modified Gompertz Model at 50 mM EtOH containing medium for *Rb.capsulatus* DSM1710 (●: experimental data, ▬: model fit)

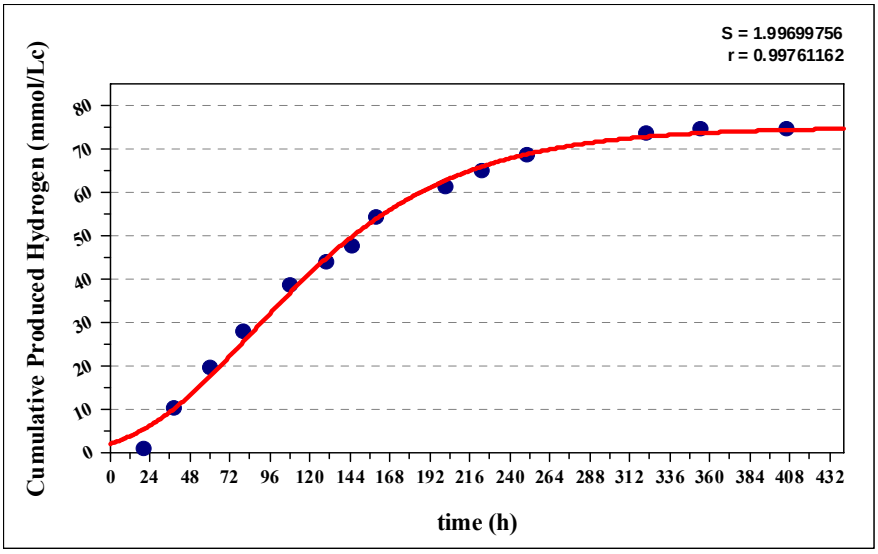

Figure I.15 The Modified Gompertz Model at 100 mM EtOH containing medium for *Rb.capsulatus* DSM1710 (●: experimental data, ▬: model fit)

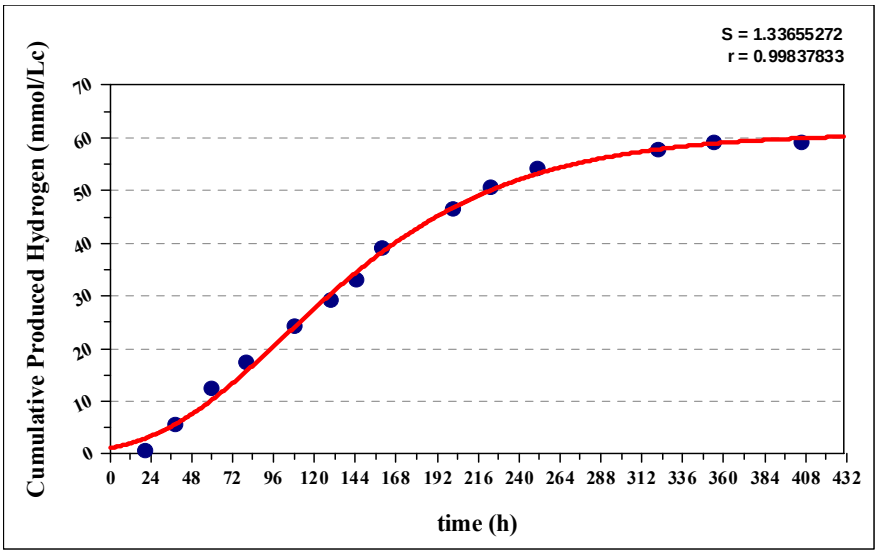

Figure I.16 The Modified Gompertz Model at 200 mM EtOH containing medium for *Rb.capsulatus* DSM1710 (●: experimental data, ▬: model fit)

I17-I24. Curves fitted to the Modified Gompertz Model together with the experimental data for different EtOH Concentrations for *Rb.capsulatus* YO3 (hup$^-$)

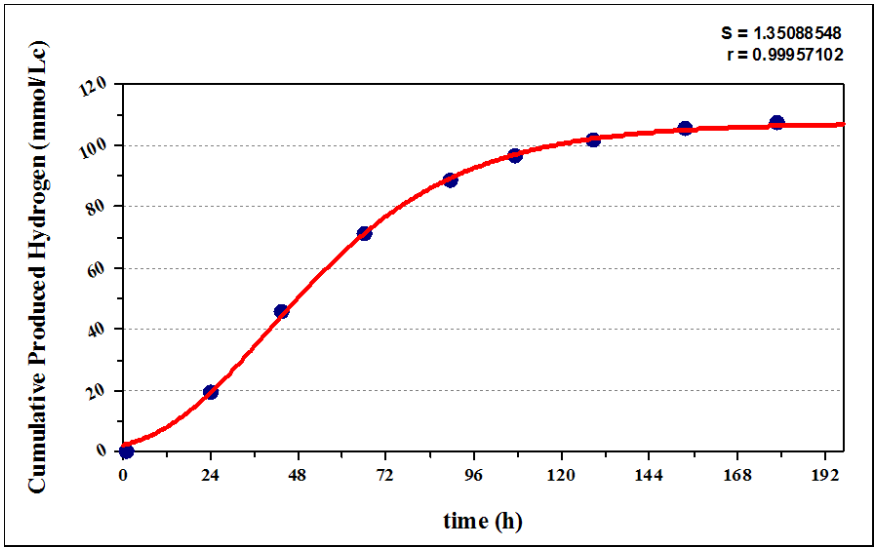

Figure I.17 The Modified Gompertz Model at control medium for *Rb.capsulatus* YO3 (hup$^-$) (●: experimental data, ▬: model fit)

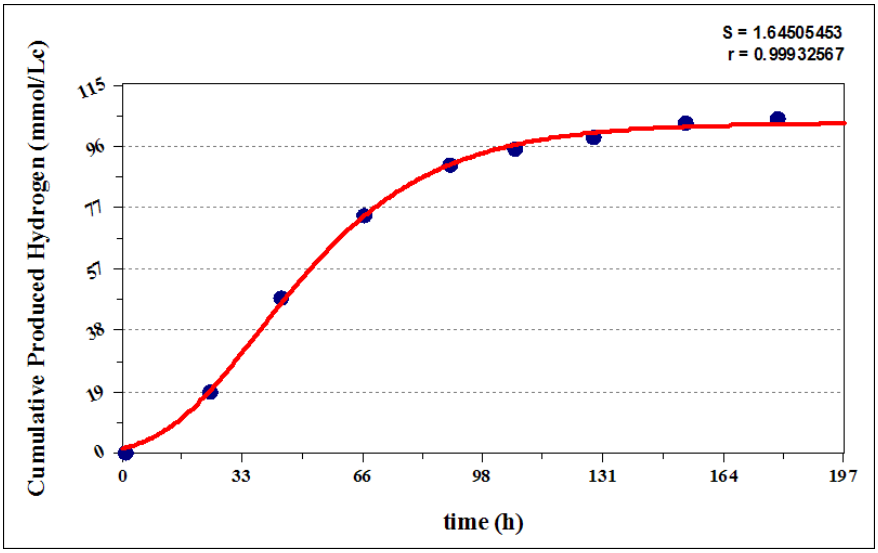

Figure I.18 The Modified Gompertz Model at 6.25 mM EtOH containing medium for *Rb.capsulatus* YO3 (hup$^-$) (●: experimental data, ▬: model fit)

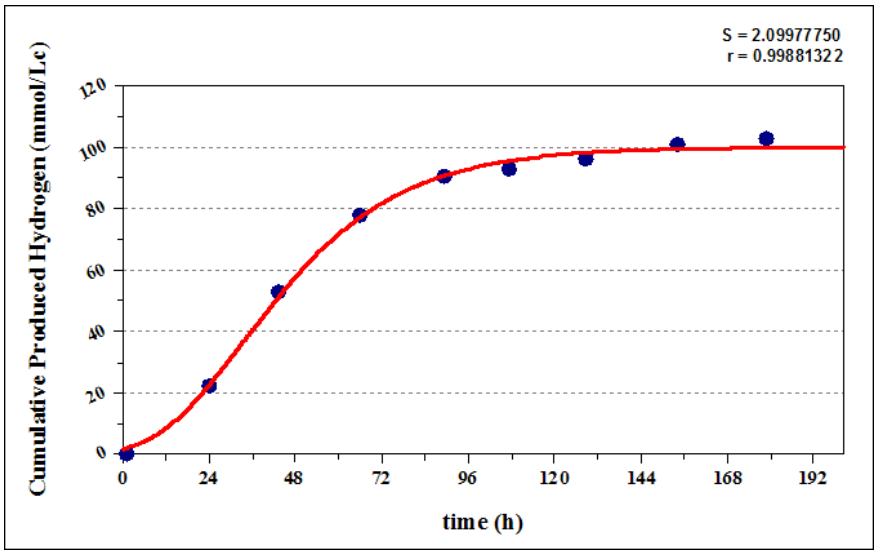

Figure I.19 The Modified Gompertz Model at 12.5 mM EtOH containing medium for *Rb.capsulatus* YO3 (hup$^-$) (●: experimental data, ▬: model fit)

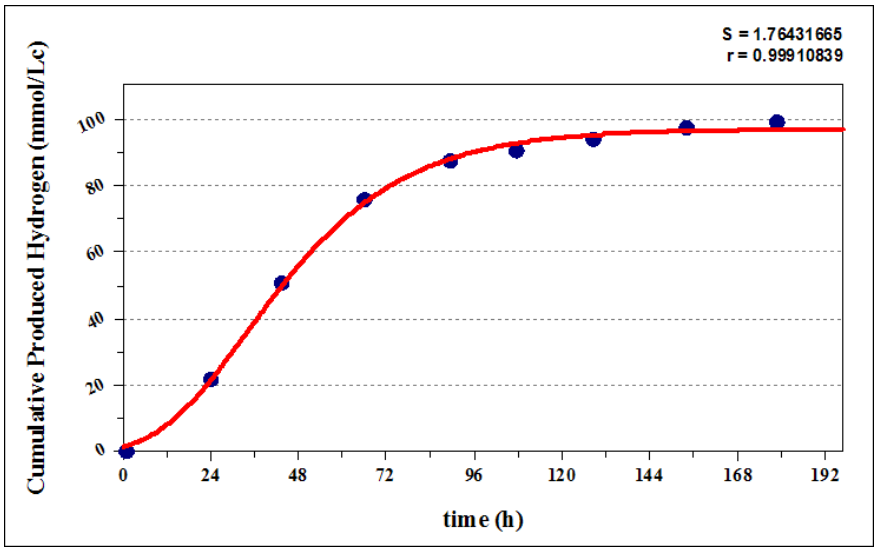

Figure I.20 The Modified Gompertz Model at 25 mM EtOH containing medium for *Rb.capsulatus* YO3 (hup$^-$) (●: experimental data, ▬: model fit)

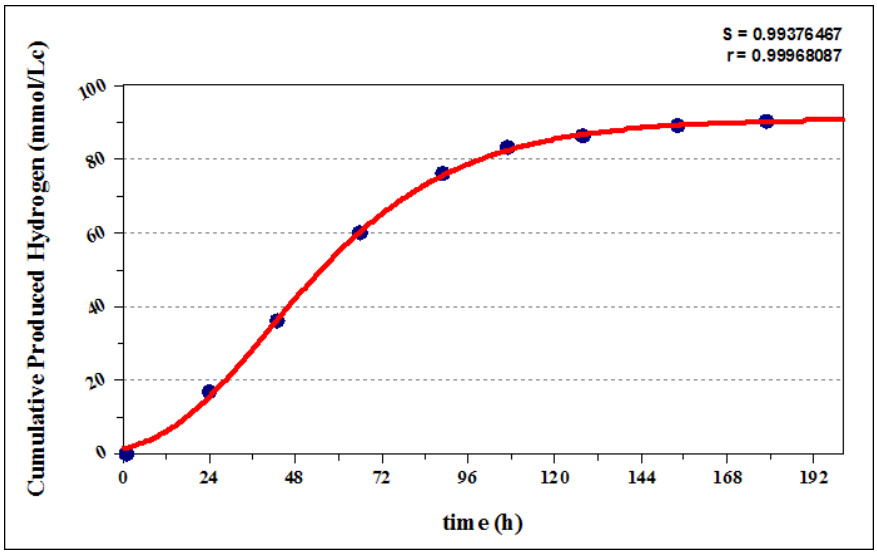

Figure I.21 The Modified Gompertz Model at 37.5 mM EtOH containing medium for *Rb.capsulatus* YO3 (hup$^-$) (●: experimental data, ▬: model fit)

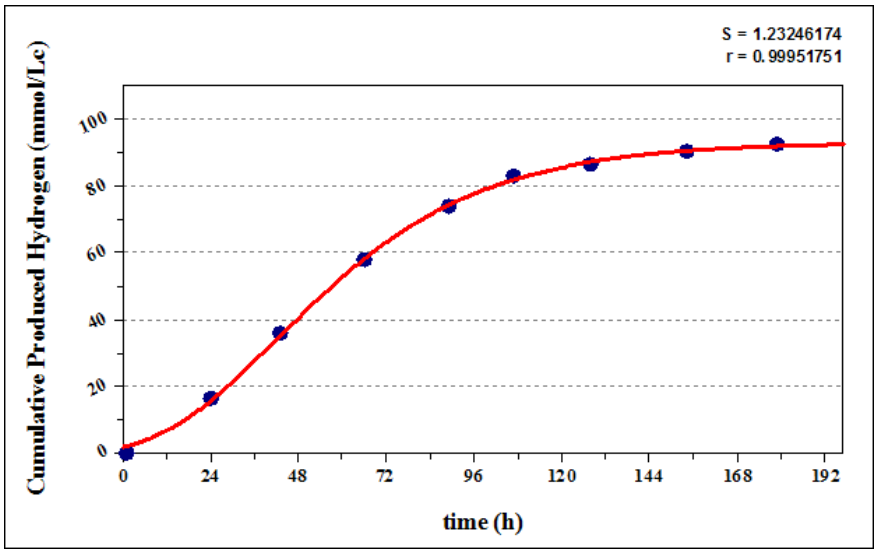

Figure I.22 The Modified Gompertz Model at 50 mM EtOH containing medium for *Rb.capsulatus* YO3 (hup$^-$) (●: experimental data, ▬: model fit)

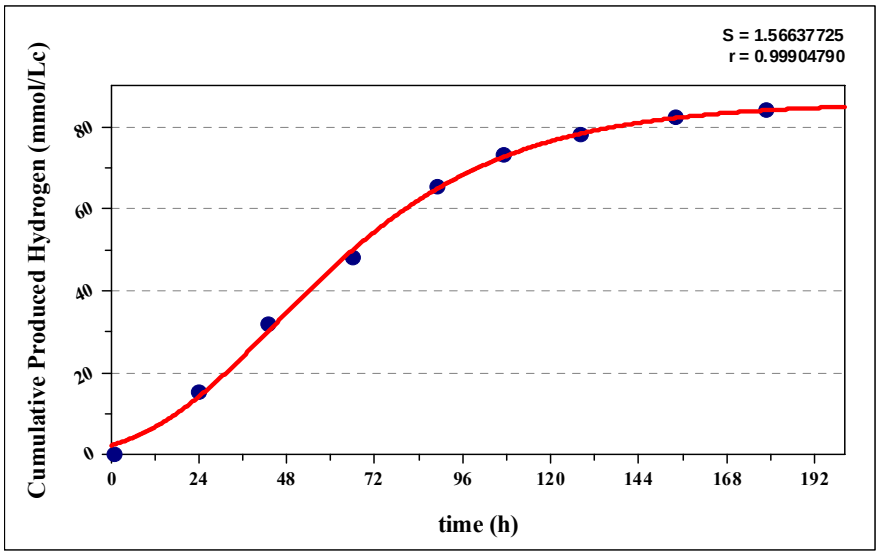

Figure I.23 The Modified Gompertz Model at 100 mM EtOH containing medium for *Rb.capsulatus* YO3 (hup$^-$) (●: experimental data, ▬: model fit)

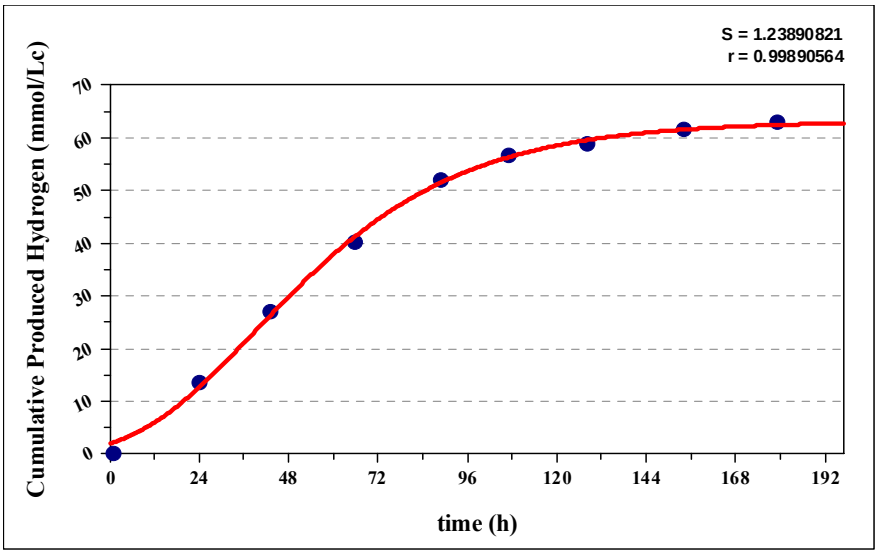

Figure I.24 The Modified Gompertz Model at 200 mM EtOH containing medium for *Rb.capsulatus* YO3 (hup$^-$) (●: experimental data, ▬: model fit)

APPENDIX J

ACETIC ACID CONSUMPTION KINETICS

J1-J4. Acetic Acid Consumption Kinetics *Rhodobacter capsulatus* DSM1710 together with the experimental data for untreated/treated DFESBTJ

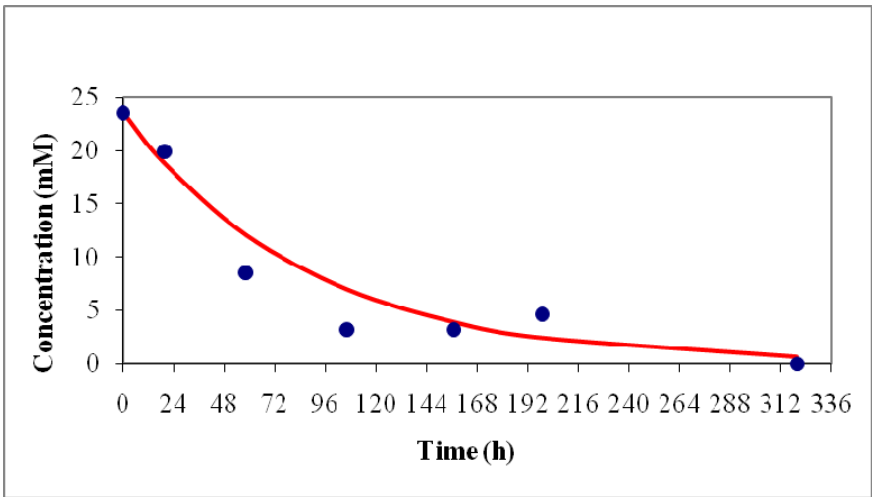

Figure J.1 First order kinetics for acetic acid consumption for *Rb.capsulatus* DSM1710 on untreated DFESBTJ2 (●: experimental data, ▬: order)

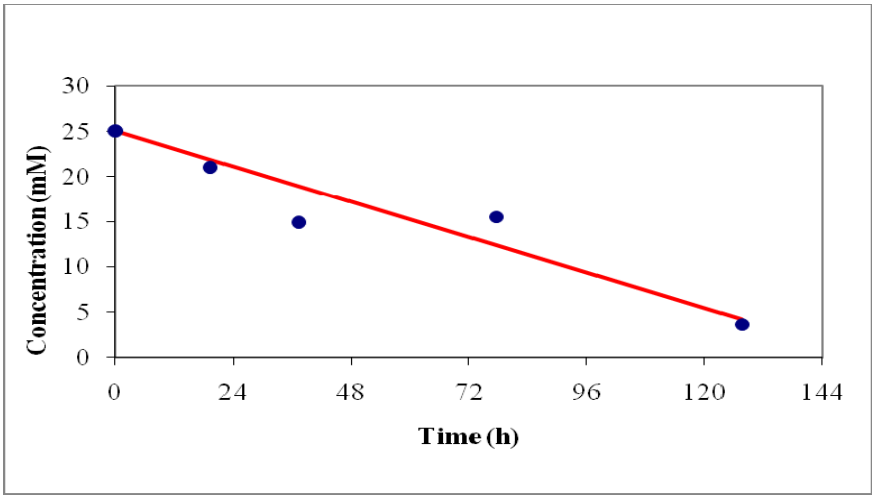

Figure J.2 Zeroth order kinetics for acetic acid consumption for *Rb.capsulatus* DSM1710 on treated DFESBTJ2 (●: experimental data, ▬: order)

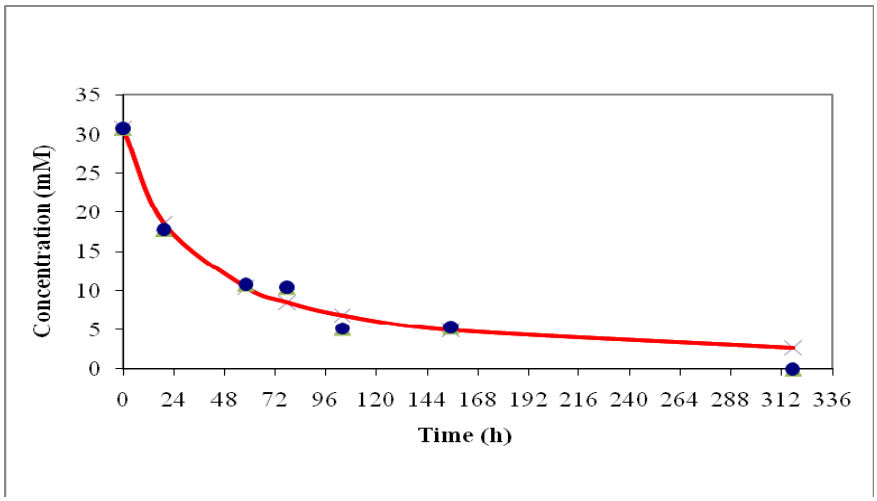

Figure J.3 Second order kinetics for acetic acid consumption for *Rb.capsulatus* DSM1710 on untreated DFESBTJ3 (●: experimental data, ▬: order)

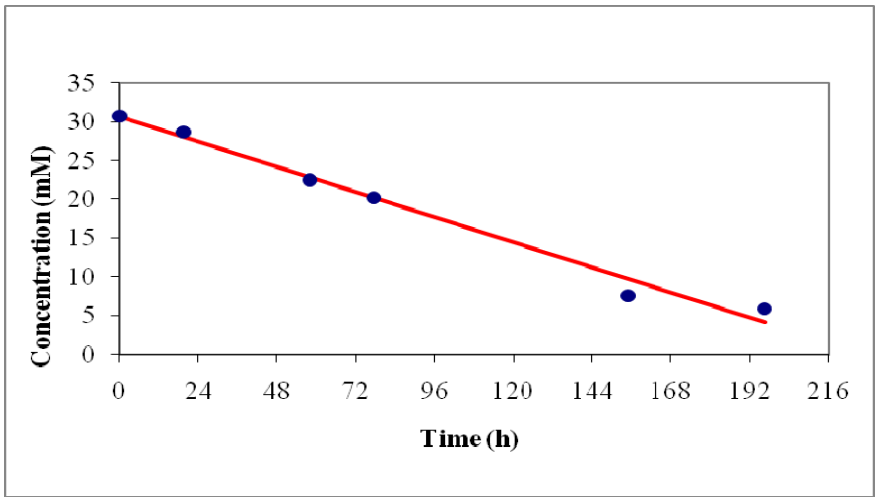

Figure J.4 Zeroth order kinetics for acetic acid consumption for *Rb.capsulatus* DSM1710 on treated DFESBTJ3 (●: experimental data, ▬: order)

J5-J8. Acetic Acid Consumption Kinetics *Rhodobacter capsulatus* YO3 (hup$^-$) together with the experimental data for untreated/treated DFESBTJ

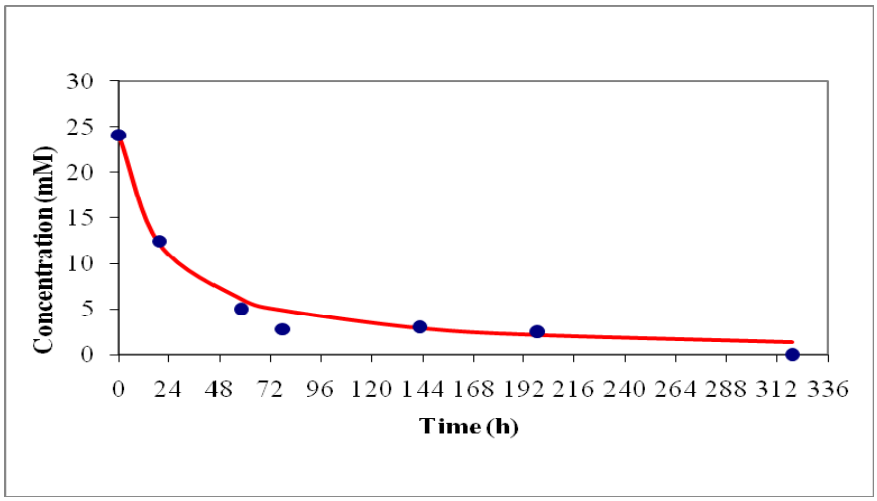

Figure J.5 Second order kinetics for acetic acid consumption for *Rb.capsulatus* YO3 (hup$^-$) on untreated DFESBTJ2 (●: experimental data, ▬: order)

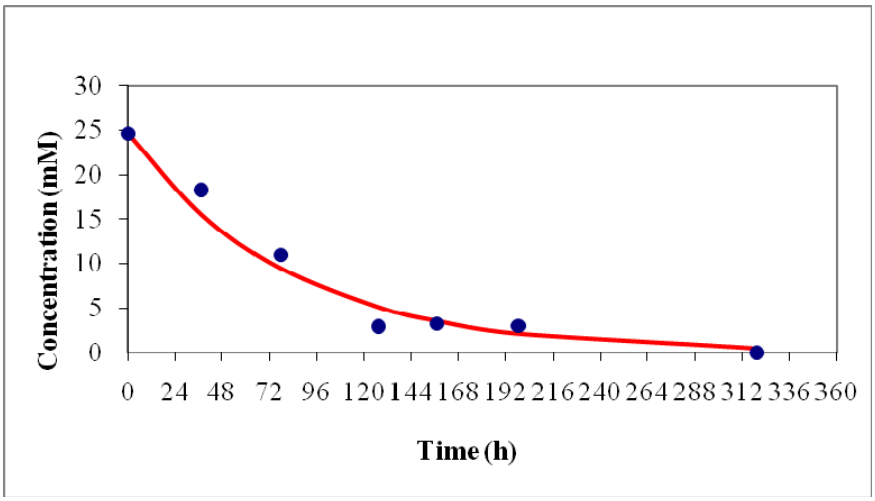

Figure J.6 First order kinetics for acetic acid consumption for *Rb.capsulatus* YO3 (hup$^-$) on treated DFESBTJ2 (●: experimental data, ▬: order)

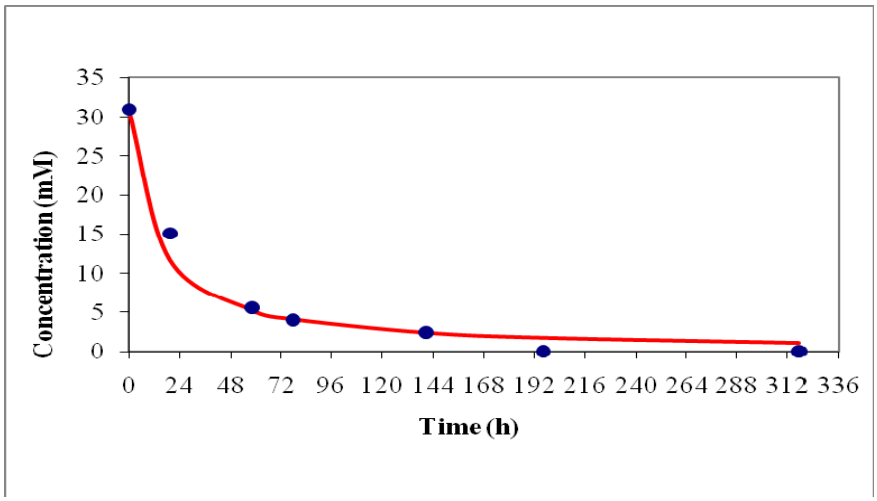

Figure J.7 Second order kinetics for acetic acid consumption for *Rb.capsulatus* YO3 (hup$^-$) on untreated DFESBTJ3 (●: experimental data, ▬: order)

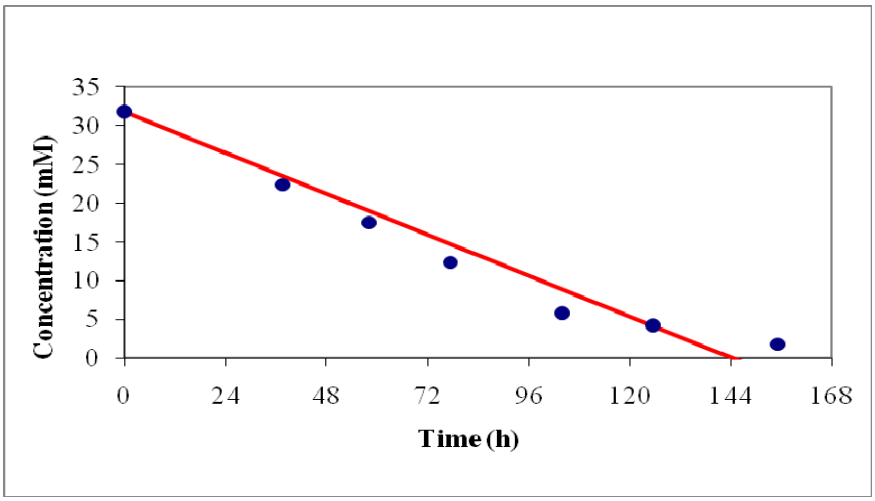

Figure J.8 Zeroth order kinetics for acetic acid consumption for Rb.capsulatus YO3 (hup$^-$) on treated DFESBTJ3 (●: experimental data, ▬: order)

J.9-J.16 Acetic Acid Consumption Kinetics *Rhodobacter capsulatus* DSM1710 together with the experimental data for defined medium containing different ethanol concentrations

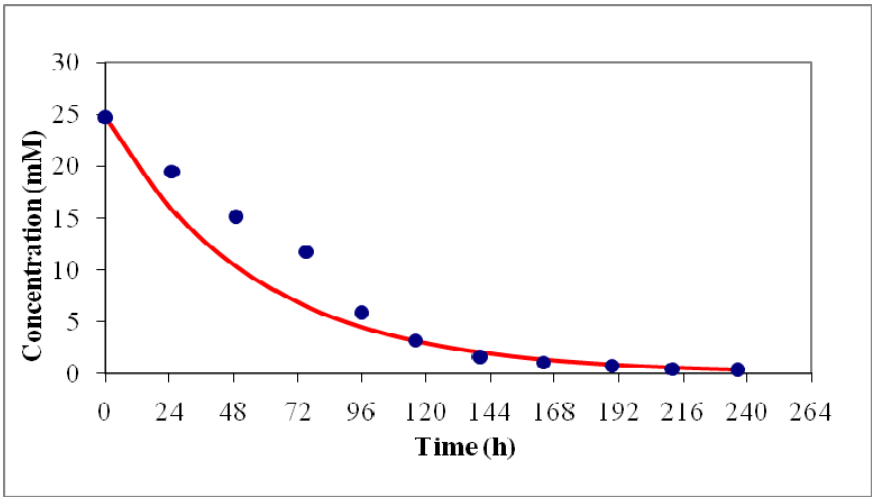

Figure J.9 First Order Kinetics for Acetic acid Consumption at control medium for *Rb.capsulatus* DSM1710 (●: experimental data, ▬: order)

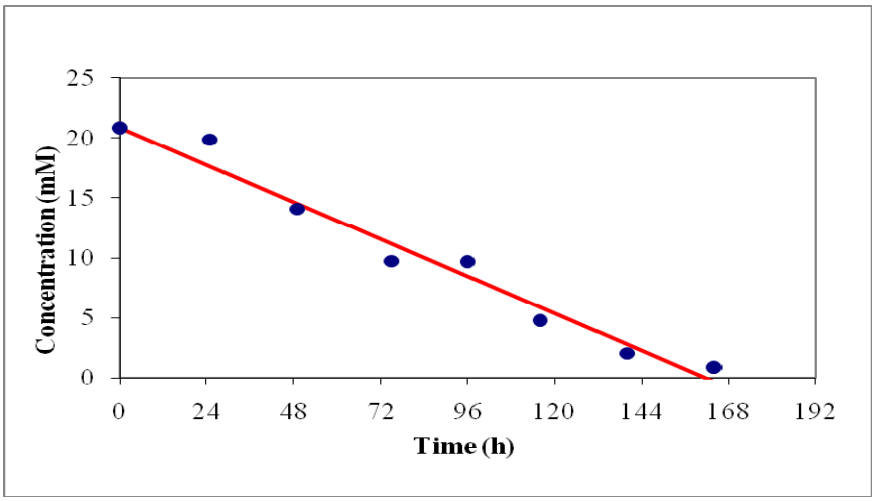

Figure J.10 Zeroth Order Kinetics for Acetic acid Consumption at 6.25 mM EtOH containing medium for *Rb.capsulatus* DSM1710 (●: experimental data, ▬: order)

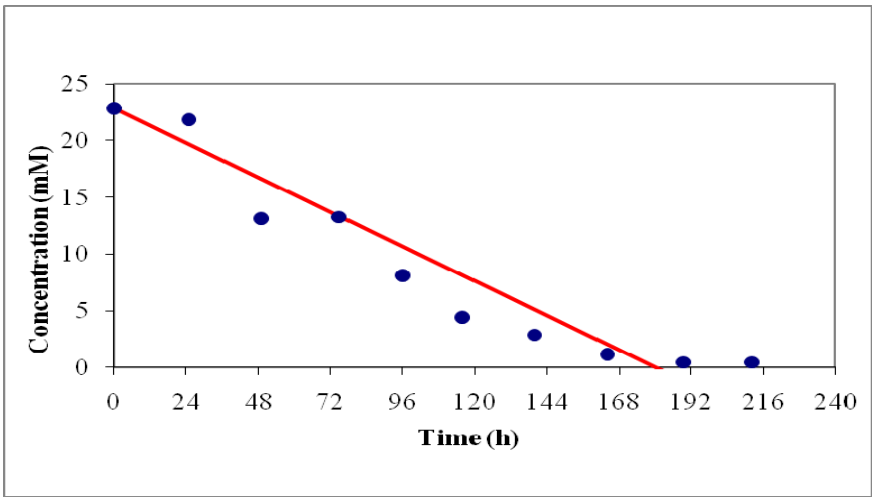

Figure J.11 Zeroth Order Kinetics for Acetic acid Consumption at 12.5 mM EtOH containing medium for *Rb.capsulatus* DSM1710 (●: experimental data, ▬: order)

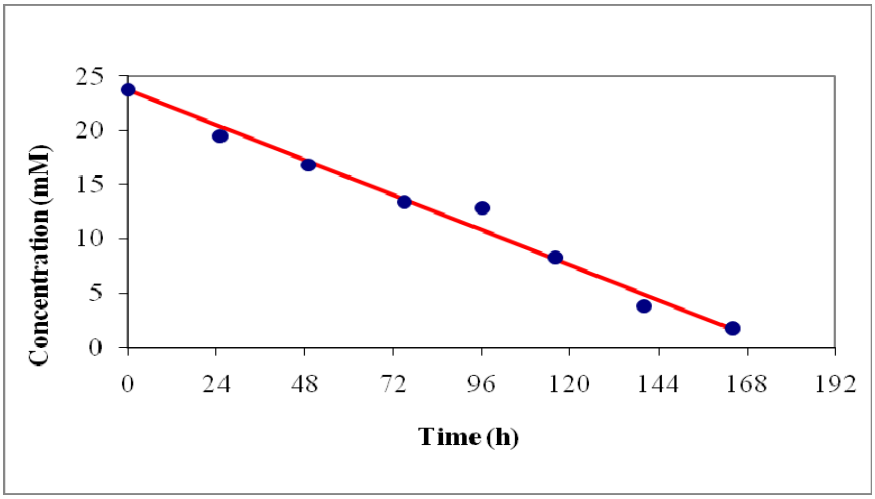

Figure J.12 Zeroth Order Kinetics for Acetic acid Consumption at 25 mM EtOH containing medium for *Rb.capsulatus* DSM1710 (●: experimental data, ▬: order)

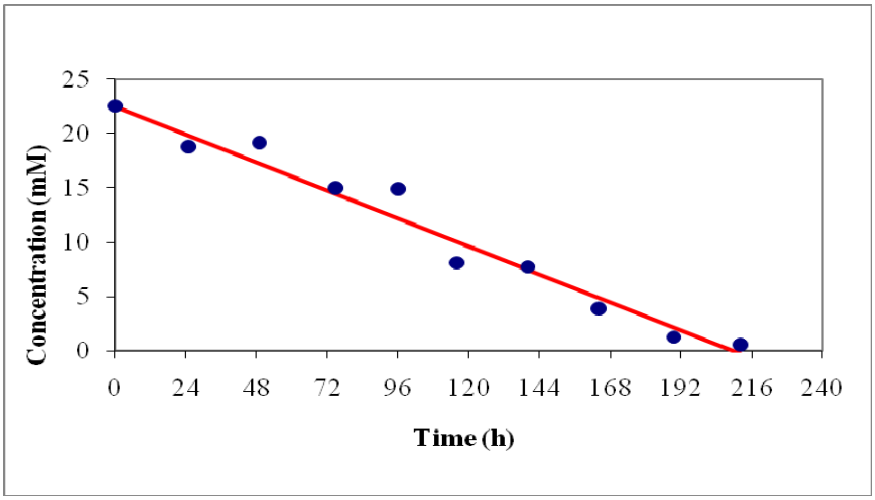

Figure J.13 Zeroth Order Kinetics for Acetic acid Consumption at 37.5 mM EtOH containing medium for *Rb.capsulatus* DSM1710 (●: experimental data, ▬: order)

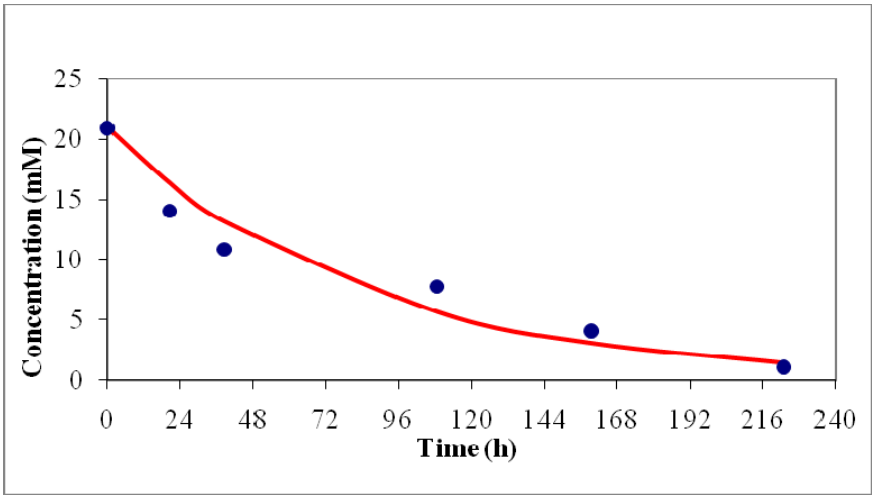

Figure J.14 First Order Kinetics for Acetic acid Consumption at 50 mM EtOH containing medium for *Rb.capsulatus* DSM1710 (●: experimental data, ▬: order)

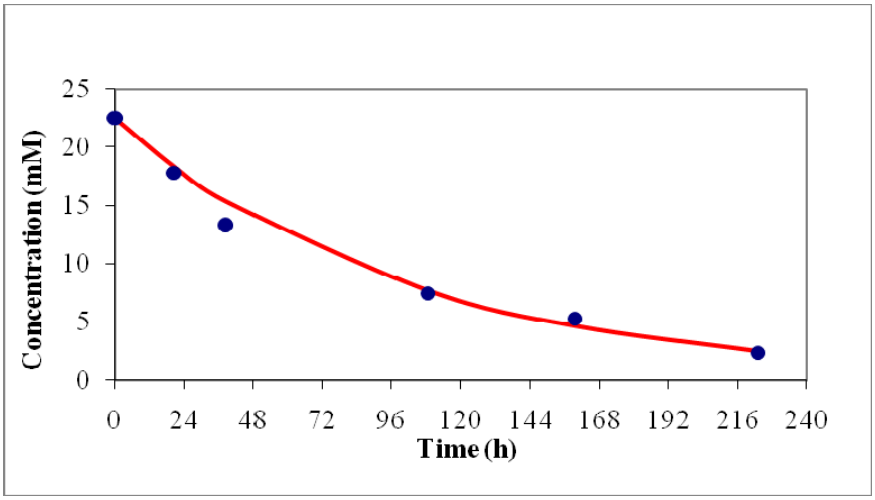

Figure J.15 First Order Kinetics for Acetic acid Consumption at 100 mM EtOH containing medium for *Rb.capsulatus* DSM1710 (●: experimental data, ▬: order)

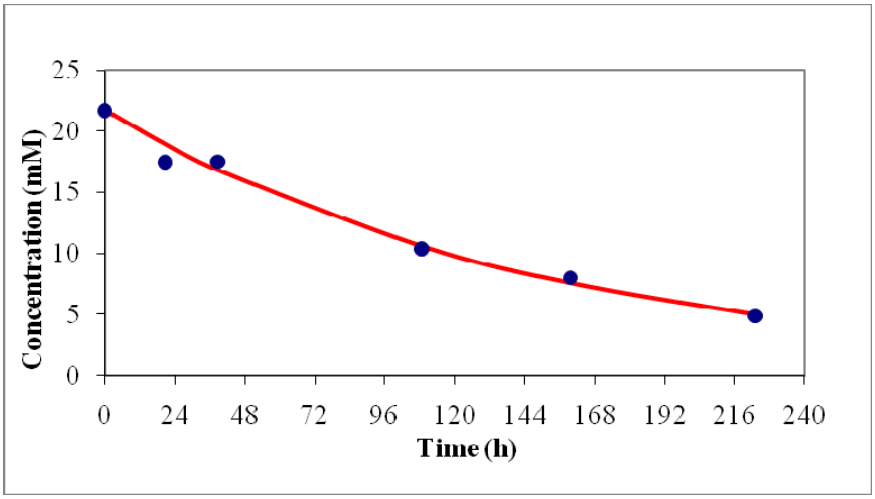

Figure J.16 First Order Kinetics for Acetic acid Consumption at 200 mM EtOH containing medium for *Rb.capsulatus* DSM1710 (●: experimental data, ▬: order)

J17-J24. Acetic Acid Consumption Kinetics of *Rb.capsulatus* YO3 (hup$^-$) together with the experimental data for defined medium containing different ethanol concentrations

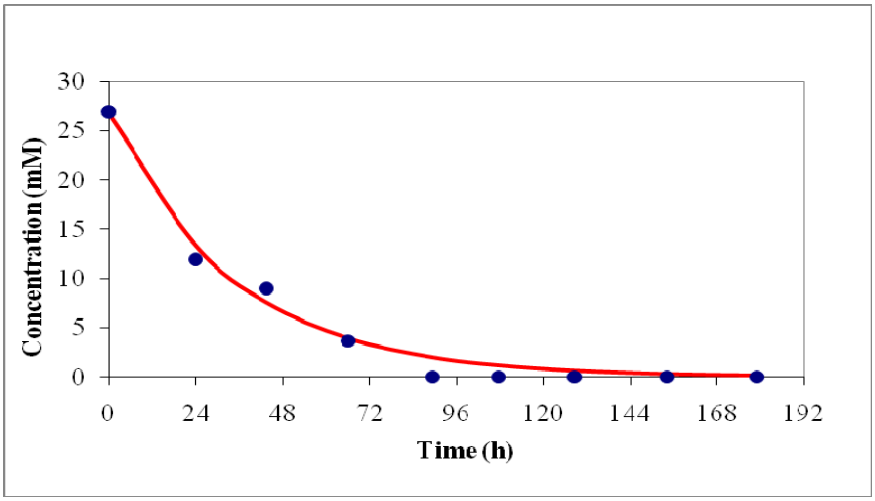

Figure J.17 First Order Kinetics for Acetic acid Consumption at control medium for *Rb.capsulatus* YO3 (hup$^-$) (●: experimental data, ▬: order)

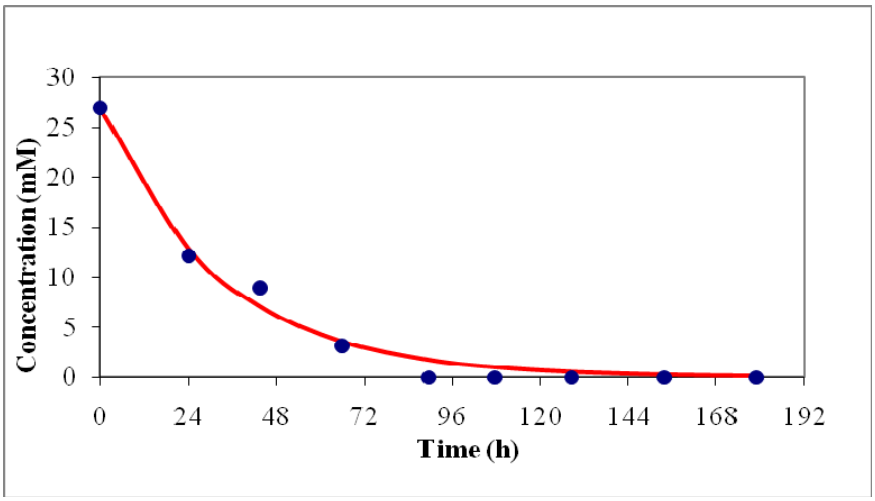

Figure J.18 First Order Kinetics for Acetic acid Consumption at 6.25 mM EtOH containing medium for *Rb.capsulatus* YO3 (hup$^-$) (●: experimental data, ▬: order)

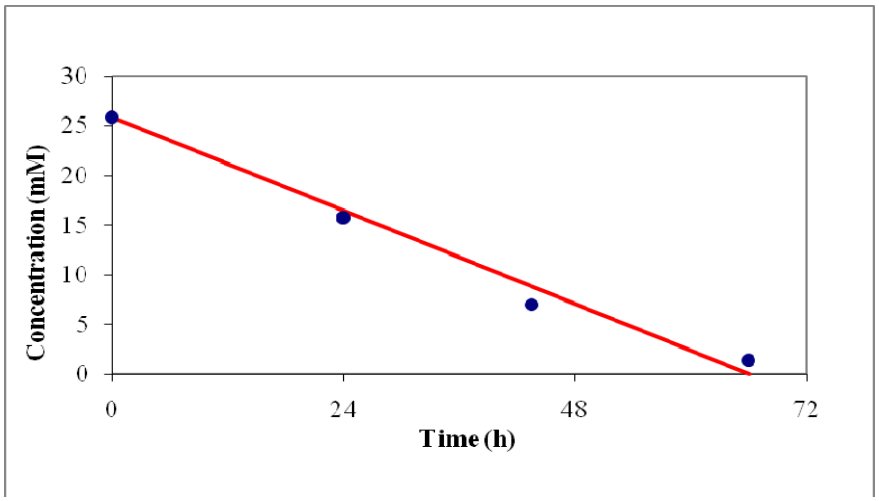

Figure J.19 Zeroth Order Kinetics for Acetic acid Consumption at 12.5 mM EtOH containing medium for *Rb.capsulatus* YO3 (hup$^-$) (●: experimental data, ▬: order)

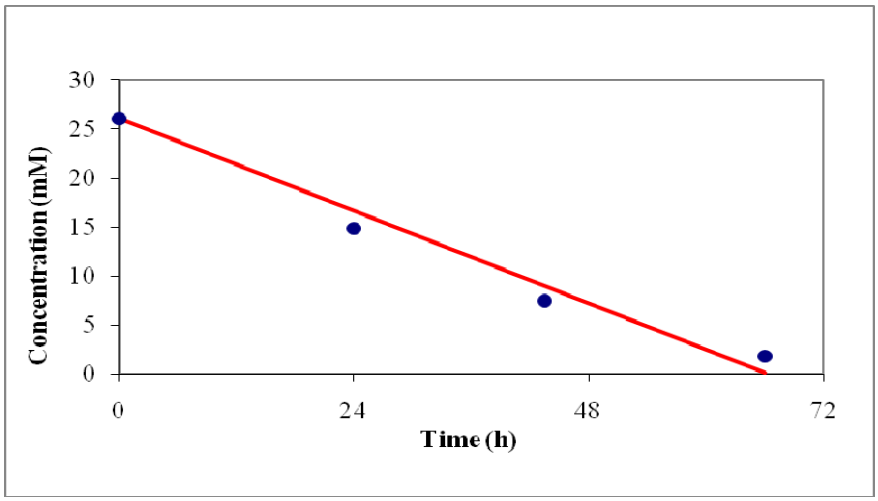

Figure J.20 Zeroth Order Kinetics for Acetic acid Consumption at 25 mM EtOH containing medium for *Rb.capsulatus* YO3 (hup$^-$) (●: experimental data, ▬: order)

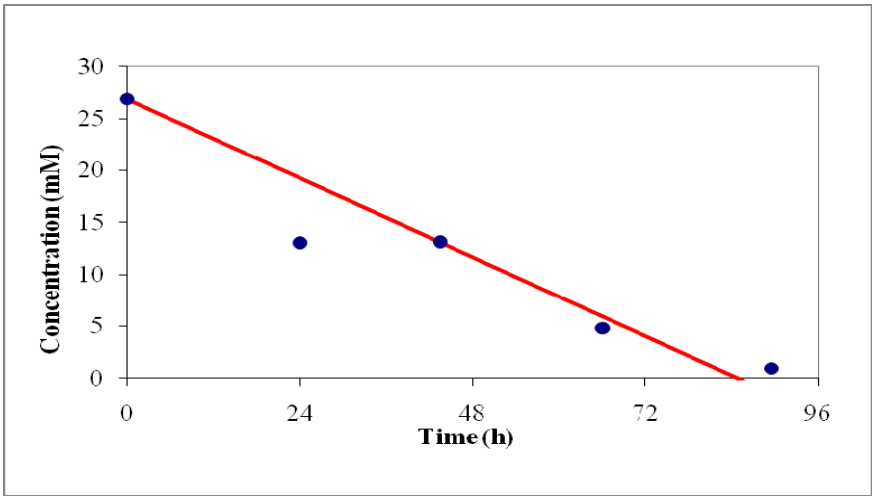

Figure J.21 Zeroth Order Kinetics for Acetic acid Consumption at 37.5 mM EtOH containing medium for *Rb.capsulatus* YO3 (hup$^-$) (●: experimental data, ▬: order)

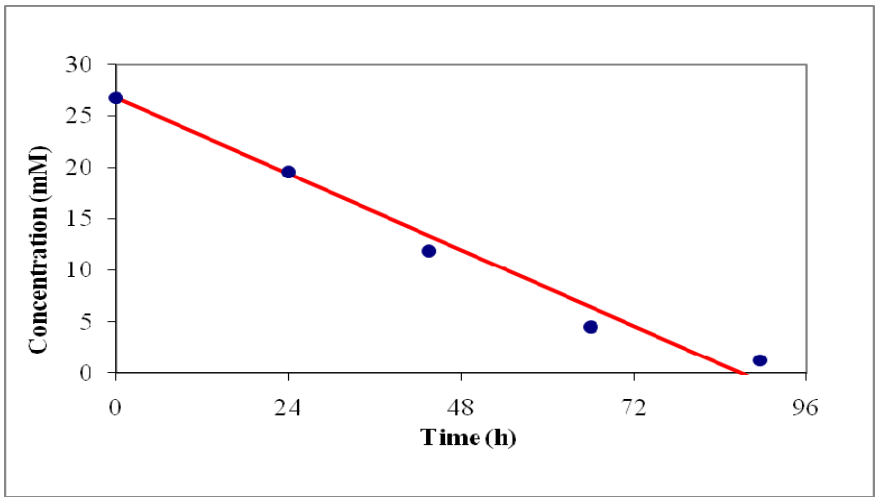

Figure J.22 Zeroth Order Kinetics for Acetic acid Consumption at 50 mM EtOH containing medium for *Rb.capsulatus* YO3 (hup$^-$) (●: experimental data, ▬: order)

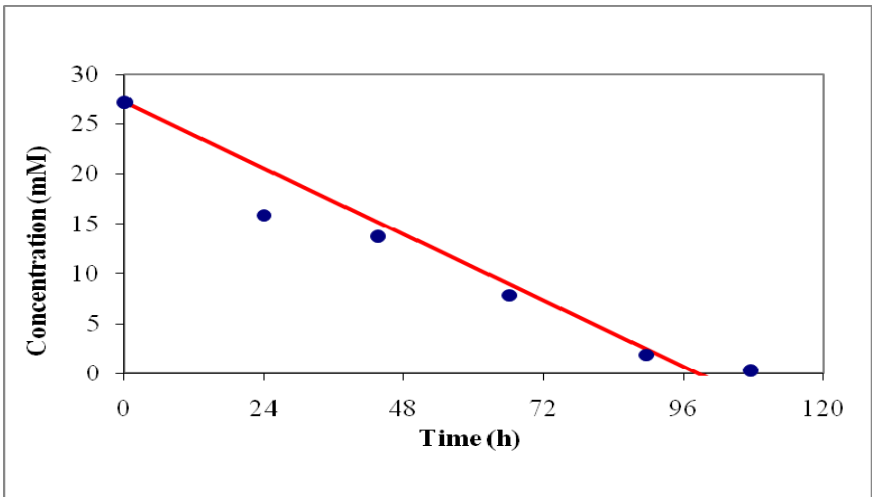

Figure J.23 Zeroth Order Kinetics for Acetic acid Consumption at 100 mM EtOH containing medium for *Rb.capsulatus* YO3 (hup$^-$) (●: experimental data, ▬: order)

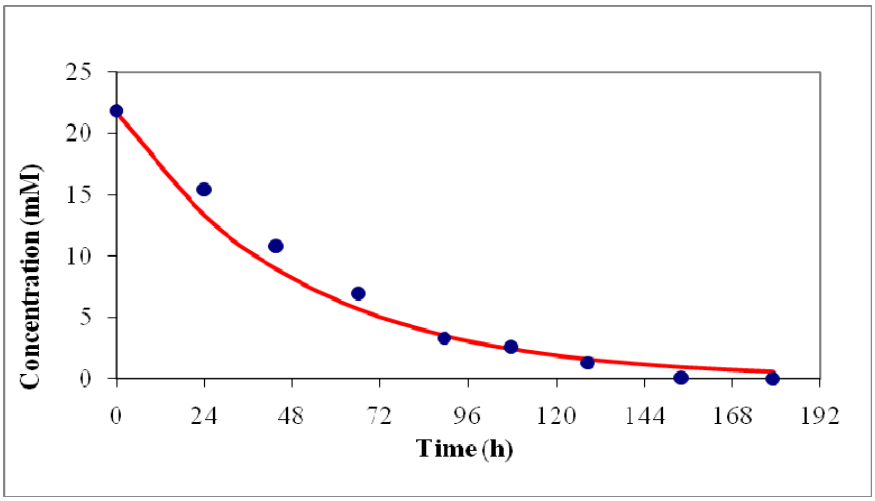

Figure J.24 First Order Kinetics for Acetic acid Consumption at 200 mM EtOH containing medium for *Rb.capsulatus* YO3 (hup$^-$) (●: experimental data, ▬: order)

APPENDIX K

EXPERIMENTAL DATA

K.1-L.3 Experimental data for panel PBR

Table K.1 Cumulative H2 production pH, OD values of outdoor fed-batch PBR by *Rb. capsulatus* YO3 (hup^-) on DFESGTJ

Time (day)	OD	gdw/L_c	pH	Cum. H_2 (L)
0.0	0.411	0.191	6.48	0
0.5	0.400	0.186	6.14	0
1.1	0.495	0.230	6.62	0
2.1	0.535	0.249	6.59	0
3.1	0.761	0.354	6.81	0
4.1	1.86	0.867	7.54	0.778
5.1	2.02	0.939	7.59	2.05
6.1	1.89	0.884	7.43	4.03
7.1	1.76	0.818	7.09	6.36
8.1	1.81	0.841	7.15	8.84
9.1	1.77	0.827	6.94	9.89
10.1	1.77	0.818	7.13	11.2
11.1	1.85	0.860	7.38	12.5
12.1	1.96	0.912	7.45	13.4
13.2	2.15	0.999	7.51	13.7
14.1	2.31	1.07	7.51	13.9
15.0	2.24	1.04	7.33	13.9

Table K.2 Organic acid and PHB values of outdoor fed-batch PBR by *Rb. capsulatus* YO3 (hup^-) on DFESGTJ

Acetic Acid (mM)	Formic Acid (mM)	Lactic Acid (mM)	Propionic Acid (mM)	Butyric Acid (mM)	PHB (%)
34.4	0.9	0	0	0	10.4
30.4	1.70	0	0	0	NA
17.9	1.10	0	0	0	NA

Table K.2 (Continued)

19.5	1.70	0	0	0	NA
17.4	2.01	0	0	0	NA
20.1	3.61	0	0	0	NA
11.8	3.22	0	1.13	0	NA
4.2	4.11	0	0	0	NA
2.5	3.65	0	0	0	NA
0	2.63	0	0	0	NA
0.8	4.22	0	0	0	4.73
0	4.95	0	0	0	NA
1.6	5.33	0	0.611	0	2.01
0	5.71	0	0.651	0	NA
0	17.5	0	0.331	0	NA
4.5	11.4	0	0	0	1.01
5.6	8.91	0	0	0	NA

Table K.3 48 hours cellular bacteriochlorophyll a levels of *Rb.capsulatus* YO3 (hup^-) in DFESBTJ

Time	Cellular bacteriochlorophyll *a* content (mgbchl/gdw)
9:00 AM	2.28
11:00 AM	4.62
1:00 PM	2.92
3:00 PM	3.34
5:00 PM	7.02
7:00 PM	7.70
9:00 PM	7.01
11:00 PM	7.93
1:00 AM	8.09
3:00 AM	6.13
5:00 AM	5.68
7:00 AM	7.36
9:00 AM	1.69
11:00 AM	6.07
1:00 PM	6.17
3:00 PM	6.18
5:00 PM	6.66
7:00 PM	7.39
9:00 PM	6.72
11:00 PM	7.51
1:00 AM	6.91
3:00 AM	7.25
5:00 AM	6.56
7:00 AM	6.32
9:00 AM	4.18

K.4-K.8 Experimental data for ammonium removal from DFESBTJ2

Table K.4 Temperature, pH, NH4+ and color values for 2 g zeolite treatment

Time	T (^{0}C)	pH	NH_4^+ (mM)	% NH_4^+ Removed	Color
0	23.8	5.98	8.91	0	130
15	24.1	6.00	3.06	66	260
30	24	6.08	3.11	65	140
45	23.8	6.07	2.22	75	170
60	24.8	6.11	1.67	81	190
75	24.5	5.97	1.11	82	310
90	24.3	6.02	1.61	82	190
105	23.8	6.04	2.83	81	240
120	23.8	5.98	1.78	80	300

Table K.5 Temperature, pH, NH4+ and color values for 4 g zeolite treatment

Time	T (^{0}C)	pH	NH_4^+ (mM)	% NH_4^+ Removed	Color
0	23.8	5.98	8.91	0	130
15	24.1	6.01	2.61	71	140
30	24	6.09	2.50	72	160
45	23.8	6.03	1.33	85	220
60	24.8	6.04	1.00	89	260
75	24.5	6.03	0.67	93	260
90	24.3	6.03	1.33	92	350
105	23.8	6.04	0.780	91	280
120	23.8	5.95	0.731	92	560

Table K.6 Temperature, pH, NH4+ and color values for 6 g zeolite treatment

Time	T (^{0}C)	pH	NH_4^+ (mM)	% NH_4^+ Removed	Color
0	23.8	5.98	8.91	0	130
15	24.1	6.05	2.22	75	320
30	24	6.09	1.33	85	310
45	23.8	6.09	1.22	86	240
60	24.8	6.04	0.78	91	380
75	24.5	6.01	0.615	93	360
90	24.3	6.04	0.612	93	390
105	23.8	6.04	0.611	93	430
120	23.8	5.96	0.491	95	510

Table K.7 Temperature, pH, NH4+ and color values for 8 g zeolite treatment

Time	T (^{0}C)	pH	NH_4^+ (mM)	% NH_4^+ Removed	Color
0	23.8	5.98	8.91	0	130
30	24	6.08	0.721	92	560
60	24.8	6.05	0.332	96	570
90	24.3	6.05	0.223	98	380
120	23.8	5.98	0.035	100	530

Table K.8 Temperature, pH, NH4+ and color values for 10 g zeolite treatment

Time	T (^{0}C)	pH	NH_4^+ (mM)	% NH_4^+ Removed	Color
0	23.8	5.98	8.91	0	130
30	24	6.12	0.801	90	430
60	24.8	6.06	0.502	94	470
90	24.3	6.08	0.162	98	410
120	23.8	6.00	0	100	730

K.9-K.12 Experimental data for ammonium removal from DFESBTJ3

Table K.9 Temperature, pH, NH4+ and color values for 5 g zeolite treatment

Time	T (^{0}C)	pH	NH_4^+ (mM)	% NH_4^+ Removed	Color
0	23.8	6.03	23.6	0	500
30	26	6.01	6.44	73	520
60	25.9	6.03	4.83	80	600
90	25.6	6.03	5.38	77	410
120	25.8	6.03	4.88	79	520
150	25.4	6.04	4.50	81	580
180	25.3	6.01	4.16	82	620

Table K.10 Temperature, pH, NH4+ and color values for 10 g zeolite treatment

Time	T (^{0}C)	pH	NH_4^+ (mM)	% NH_4^+ Removed	Color
0	23.8	6.03	23.6	0	500
30	26	6.11	6.83	71	560
60	25.9	6.02	4.56	81	540
90	25.6	6.03	3.50	85	740
120	25.8	6.04	1.94	86	700
150	25.4	6.03	3.06	87	630
180	25.3	6.07	2.50	89	680

Table K.11 Temperature, pH, NH_4^+ and color values for 15 g zeolite treatment

Time	T (^{0}C)	pH	NH_4^+ (mM)	% NH_4^+ Removed	Color
0	23.8	6.03	23.6	0	500
30	26	6.04	3.61	85	850
60	25.9	6.03	2.61	89	740
90	25.6	6.13	1.72	93	800
120	25.8	6.09	1.33	94	720
150	25.4	6.05	1.72	93	710
180	25.3	6.07	1.06	96	760

Table K.12 Temperature, pH, NH4+ and color values for 20 g zeolite treatment

Time	T (^{0}C)	pH	NH_4^+ (mM)	% NH_4^+ Removed	Color
0	23.8	6.03	23.6	0	500
30	26	6.03	3.67	84	780
60	25.9	6.05	1.39	94	650
90	25.6	6.04	1.83	92	940
120	25.8	6.04	1.11	95	680
150	25.4	6.04	1.33	94	880
180	25.3	6.05	1.06	96	810

K.13-K.29 Experimental data for *Rhodobacter capsulatus* DSM1710 and *Rhodobacter capsulatus* YO3 (hup$^-$) on DFESBTJ2 and DFESBTJ3

Table K.13 OD, cell dry weight, pH and cumulative hydrogen produced values for treated DFESBTJ2 of *Rhodobacter capsulatus* DSM1710 (Mean of 2 runs)

Time (h)	OD	gdw/Lc	pH	Cum. H_2 (ml)	Cum. H_2 (mmol)
0	0.275	0.149	6.72	0	0
19.5	1.01	0.550	7.20	13.1	0.585
37.5	1.21	0.656	7.05	92.1	4.09
58	1.43	0.776	7.03	173	7.70
77.5	1.32	0.719	6.81	232	10.3
106	1.28	0.694	7.08	293	13.03
127.5	1.44	0.784	6.97	332	14.78
142.5	1.40	0.762	7.02	362	16.1
157	1.44	0.781	7.42	391	17.4
198.5	1.40	0.759	7.35	403	17.9
220.5	1.42	0.773	7.60	404	17.9
248	1.36	0.740	7.41	405	18.1
319.5	1.36	0.738	7.38	407	18.1

Table K.14 Organic Acid concentrations for treated DFESBTJ2 of *Rhodobacter capsulatus* DSM1710 (Mean of 2 runs)

Time (hour)	Acetic Acid (mM)	Formic Acid (mM)	Lactic Acid (mM)	Propionic Acid (mM)	Butyric Acid (mM)
0	25.1	0	10.8	0	0
19.5	21.1	4.17	7.86	0	0
37.5	14.9	9.20	4.87	0	0.06
77.5	15.5	13.6	2.97	0	0.13
127.5	3.6	16.4	0	0	0
157	0	19.4	0	0	0
220.5	0	17.7	0	0	0
319.5	0	16.6	0	0	0

Table K.15 OD, cell dry weight, pH and cumulative hydrogen produced values for untreated DFESBTJ2 of *Rhodobacter capsulatus* DSM1710 (Mean of 2 runs)

Time (h)	OD	gdw/Lc	Ph	Cum. H_2 (ml)	Cum. H_2 (mmol)
0	0.275	0.149	6.43	0	0
19.5	0.865	0.469	6.89	2.73	0.121
37.5	1.57	0.854	7.39	29.7	1.32

Table K.15 (Continued)

58	2.07	1.12	7.35	104	4.65
77.5	1.87	1.01	7.06	159	7.11
106	1.77	0.963	7.27	199	8.86
127.5	1.91	1.03	7.15	211	9.43
142.5	2.05	1.11	7.33	218	9.71
157	2.09	1.13	7.48	225	10.0
198.5	1.82	0.987	7.66	229	10.1
220.5	1.75	0.952	7.72	231	10.3
248	1.47	0.797	7.33	235	10.4
319.5	1.36	0.738	6.45	241	10.7

Table K.16 Organic Acid concentrations for untreated DFESBTJ2 of *Rhodobacter capsulatus* DSM1710 (Mean of 2 runs)

Time (hour)	Acetic Acid (mM)	Formic Acid (mM)	Lactic Acid (mM)	Propionic Acid (mM)	Butyric Acid (mM)
0	23.5	0	10.2	0	0
19.5	19.8	4.11	7.95	0	0
58	8.53	11.4	0	0	0
106	3.20	9.18	0	0	0
157	3.19	11.6	0	0	0
198.5	4.62	9.05	0	0	0
319.5	0	5.13	0	0	1.02

Table K.17 OD, cell dry weight, pH and cumulative hydrogen produced values for treated DFESBTJ2 of *Rhodobacter capsulatus* YO3 (hup^-) (Mean of 2 runs)

Time (h)	OD	gdw/Lc	Ph	Cum. H_2 (ml)	Cum. H_2 (mmol)
0	0.285	0.132	6.78	0	0
19.5	1.24	0.579	6.94	58.7	2.61
37.5	1.29	0.600	6.70	163	7.28
58	1.58	0.737	7.13	265	11.8
77.5	1.57	0.733	6.91	359	16.0
106	1.52	0.707	7.28	437	19.4
127.5	1.57	0.733	7.53	462	20.5
142.5	1.59	0.740	7.37	482	21.4
157	1.63	0.761	7.49	507	22.5
198.5	1.56	0.726	7.64	515	22.9
220.5	1.72	0.800	7.85	518	23.1
248	1.46	0.679	7.69	526.	23.4
319.5	1.19	0.554	7.17	533	23.7

Table K.18 Organic Acid concentrations for treated DFESBTJ2 of *Rhodobacter capsulatus* YO3 (hup^-) (Mean of 2 runs)

Time (hour)	Acetic Acid (mM)	Formic Acid (mM)	Lactic Acid (mM)	Propionic Acid (mM)	Butyric Acid (mM)
0	24.6	0	10.5	0	0
37.5	18.3	9.15	5.26	0	0
77.5	10.9	15.1	1.16	0	0
127.5	2.93	14.0	0	0	0
157	3.24	19.6	0	0	0
198.5	3.00	12.3	0	0	0
319.5	0	15.6	0.05	0.59	0.18

Table K.19 OD, cell dry weight, pH and cumulative hydrogen produced values for untreated DFESBTJ2 of *Rhodobacter capsulatus* YO3 (hup^-) (Mean of 2 runs)

Time (h)	OD	gdw/Lc	Ph	Cum. H_2 (ml)	Cum. H_2 (mmol)
0	0.29	0.135	6.44	0	0
19.5	1.84	0.859	7.45	1.81	0.080
37.5	2.08	0.968	7.09	95.8	4.26
58	2.34	1.08	7.44	199	8.89
77.5	2.07	0.963	7.13	283	12.5
106	2.1	0.977	7.19	327	14.5
127.5	2.1	0.977	7.26	337	15.1
142.5	2.01	0.933	7.30	345	15.3
157	1.98	0.921	7.33	355	15.8
198.5	1.79	0.833	7.45	363	16.1
220.5	1.94	0.905	7.84	366	16.3
248	1.94	0.905	7.72	368	16.3
319.5	1.61	0.751	7.27	370	16.5

Table K.20 Organic Acid concentrations for untreated DFESBTJ2 of *Rhodobacter capsulatus* YO3 (hup^-) (Mean of 2 runs)

Time (hour)	Acetic Acid (mM)	Formic Acid (mM)	Lactic Acid (mM)	Propionic Acid (mM)	Butyric Acid (mM)
0	24.1	0.62	10.1	0	0
19.5	12.4	3.09	6.33	0	0
58	5.03	9.44	0	0	0
77.5	2.80	8.06	0	0	0
142.5	3.05	11.7	0	0	0

Table K.20 (Continued)

198.5	2.54	10.0	0	0	0
319.5	0.00	8.42	0	0.171	0.742

Table K.21 OD, cell dry weight, pH and cumulative hydrogen produced values for treated DFESBTJ3 of *Rhodobacter capsulatus* DSM1710 (Mean of 2 runs)

Time (h)	OD	gdw/Lc	Ph	Cum. H_2 (ml)	Cum. H_2 (mmol)
0	0.225	0.122	6.54	0	0
19.5	0.82	0.445	6.68	4.11	0.183
37.5	1.02	0.556	6.81	58.1	2.58
58	1.39	0.754	6.94	135	6.03
77.5	1.35	0.732	6.81	209	9.33
106	1.40	0.762	6.89	286	12.7
127.5	1.47	0.800	6.92	322	14.3
142.5	1.51	0.819	6.94	347	15.4
157	1.49	0.811	7.02	377	16.7
198.5	1.46	0.792	6.98	400	17.8
220.5	1.7	0.922	7.08	412	18.3
248	1.44	0.781	7.08	422	18.7
319.5	1.52	0.827	6.83	448	19.9

Table K.22 Organic Acid concentrations for treated DFESBTJ3 of *Rhodobacter capsulatus* DSM1710 (Mean of 2 runs)

Time (hour)	Acetic Acid (mM)	Formic Acid (mM)	Lactic Acid (mM)	Propionic Acid (mM)	Butyric Acid (mM)
0	30.7	0.57	8.87	0	0.00
19.5	28.6	0.55	7.95	0	0.21
58	22.4	7.15	3.58	0	0.31
77.5	20.1	12.6	2.36	0	0.13
155	7.55	12.3	0	0	0.00
196.5	5.88	12.0	0	0	0.24
317.5	0.00	16.9	0	0	0.28

Table K.23 OD, cell dry weight, pH and cumulative hydrogen produced values for untreated DFESBTJ3 of *Rhodobacter capsulatus* DSM1710 (Mean of 2 runs)

Time (h)	OD	gdw/Lc	Ph	Cum. H_2 (ml)	Cum. H_2 (mmol)
0	0.24	0.130	6.51	0	0
19.5	1.14	0.618	6.73	2.28	0.101
37.5	1.89	1.02	7.18	12.6	0.563
58	2.39	1.29	7.27	39.7	1.76
77.5	2.35	1.27	7.18	53.2	2.37
106	2.36	1.28	7.28	60.6	2.70
127.5	1.85	1.01	7.17	64.9	2.81
142.5	1.84	0.998	7.19	69.8	3.11
157	1.73	0.938	7.29	74.1	3.29
198.5	1.25	0.681	7.22	76.8	3.41
220.5	1.3	0.740	7.30	80.2	3.57
248	1.31	0.710	7.34	83.3	3.71
319.5	1.23	0.667	7.07	91.4	4.06

Table K.24 Organic Acid concentrations for untreated DFESBTJ3 of *Rhodobacter capsulatus* DSM1710 (Mean of 2 runs)

Time (hour)	Acetic Acid (mM)	Formic Acid (mM)	Lactic Acid (mM)	Propionic Acid (mM)	Butyric Acid (mM)
0	30.7	0.41	8.87	0	0
19.5	17.7	0.78	4.63	0	0.21
58	10.8	6.42	0	0	0
77.5	10.3	11.7	0	0	0
104	5.16	6.98	0	0	0
155	5.30	2.76	0	0	0
317.5	0.00	2.06	0	0	1.73

Table K.25 OD, cell dry weight, pH and cumulative hydrogen produced values for treated DFESBTJ3 of *Rhodobacter capsulatus* YO3 (hup^-) (Mean of 2 runs)

Time (h)	OD	gdw/Lc	Ph	Cum. H_2 (ml)	Cum. H_2 (mmol)
0	0.26	0.121	6.53	0	0
19.5	1	0.465	6.73	34.5	1.53
37.5	1.26	0.588	6.80	113	5.04
58	1.51	0.703	7.04	209	9.31
77.5	1.52	0.710	7.01	303	13.4
106	1.75	0.817	7.12	371	16.5
127.5	2.09	0.975	7.16	407	18.1
142.5	2.11	0.982	7.20	425	18.9
157	1.78	0.828	7.27	461	20.5

Table K.25 (Continued)

198.5	1.58	0.735	7.35	493	21.9
220.5	1.55	0.721	7.48	501	22.3
248	1.48	0.691	7.37	510.	22.7
319.5	1.17	0.547	6.94	515	22.9

Table K.26 Organic Acid concentrations for treated DFESBTJ3 of *Rhodobacter capsulatus* YO3 (hup^-) (Mean of 2 runs)

Time (hour)	Acetic Acid (mM)	Formic Acid (mM)	Lactic Acid (mM)	Propionic Acid (mM)	Butyric Acid (mM)
0	31.8	0.63	9.18	0	0
37.5	22.4	8.92	3.86	0	0.341
58	17.5	11.6	1.75	0	0.372
77.5	12.4	10.4	1.61	0	0
104	5.87	6.84	0	0	0
125.5	4.28	10.7	0	0	0
155	1.79	9.18	0	0	0
317.5	0.00	9.84	0	0	0.311

Table K.27 OD, cell dry weight, pH and cumulative hydrogen produced values for untreated DFESBTJ3 of *Rhodobacter capsulatus* YO3 (hup^-) (Mean of 2 runs)

Time (h)	OD	gdw/Lc	Ph	Cum. H_2 (ml)	Cum. H_2 (mmol)
0	0.21	0.097	6.50	0	0
19.5	2.01	0.938	6.96	0	0
37.5	2.72	1.26	7.27	46.9	2.09
58	3.22	1.50	7.42	102	4.54
77.5	2.68	1.24	7.21	131	5.83
106	2.77	1.28	7.21	155	6.91
127.5	2.73	1.27	7.17	169	7.56
142.5	2.63	1.22	7.20	175	7.80
157	2.52	1.17	7.13	183	8.16
198.5	1.83	0.852	6.94	186	8.30
220.5	1.93	0.900	6.89	189	8.41
248	1.88	0.877	6.87	191	8.52
319.5	1.4	0.651	6.75	195	8.68

Table K.28 Organic Acid concentrations for untreated DFESBTJ3 of *Rhodobacter capsulatus* YO3 (hup$^-$) (Mean of 2 runs)

Time (hour)	Acetic Acid (mM)	Formic Acid (mM)	Lactic Acid (mM)	Propionic Acid (mM)	Butyric Acid (mM)
0	30.9	0.70	9.16	0	0
19.5	15.0	0.23	4.45	0	0.321
58	5.61	10.4	0	0	0
77.5	3.98	7.85	0	0	0
140.5	2.41	12.8	0	0	0
196.5	0.00	5.11	0	0	0.611
317.5	0.00	4.47	0	0	1.13

Table K.29 PHB values for *Rhodobacter capsulatus* DSM1710 and *Rhodobacter capsulatus* YO3 (hup$^-$) on DFESBTJ2 and DFESBTJ3 (Mean of 2 runs)

	PHB (%) Treated DFESGTJ2	PHB (%) Untreated DFESGTJ2	PHB (%) Treated DFESGTJ3	PHB (%) Untreated DFESGTJ3
***Rb. capsulatus* DSM1710**	25.5	4.7	13.5	1.9
***Rb. capsulatus* YO3 (hup$^-$)**	10.8	2.6	2.1	0.4

K.30-K.45 Experimental data *for Rhodobacter capsulatus* DSM1710 on defined medium in different ethanol concentrations

Table K.30 OD, cell dry weight, pH and cumulative hydrogen produced values for control of *Rhodobacter capsulatus* DSM1710 (Mean of 2 runs)

Time (h)	OD	gdw/Lc	pH	Cum. H_2 (ml)	Cum. H_2 (mmol)
0	0.215	0.116	6.61	0	0
25	0.25	0.135	6.68	6.08	0.270
49	0.4	0.217	7.17	32.2	1.43
75	0.55	0.298	7.13	72.9	3.24
96	1.14	0.618	7.43	102	4.57
116	1.44	0.781	7.37	127	5.65
140	1.33	0.721	7.36	137	6.10
164	1.48	0.803	7.49	166	7.42
189.5	1.34	0.727	7.25	195	8.72
212	1.34	0.727	7.32	199	8.88
236.5	1.2	0.651	7.39	214	9.52

Table K.31 Organic Acid concentrations for control of *Rhodobacter capsulatus* DSM1710 (Mean of 2 runs)

Time (hour)	Acetic Acid (mM)	Formic Acid (mM)	Lactic Acid (mM)	Propionic Acid (mM)	Butyric Acid (mM)
0	24.7	0	0	0	0
25	19.5	0	0.071	0	0
49	15.1	0	0	0.041	0
75	11.7	0	0	0	0
96	5.90	0	0	0	0
116	3.18	0	0	0.052	0
140	1.64	0	0	0	0
164	1.05	0	0	0	0
189.5	0.78	0	0	0	0
212	0.47	0	0	0	0
236.5	0.42	0	0	0	0

Table K.32 OD, cell dry weight, pH and cumulative hydrogen produced values for 6.25 mM ethanol of *Rhodobacter capsulatus* DSM1710 (Mean of 2 runs)

Time (h)	OD	gdw/Lc	pH	Cum. H_2 (ml)	Cum. H_2 (mmol)
0	0.242	0.131	6.45	0	0
25	0.255	0.138	6.65	7.66	0.341
49	0.36	0.195	6.81	29.3	1.31
75	0.43	0.233	6.93	63.7	2.83
96	1.05	0.572	7.12	94.4	4.20
116	1.36	0.738	7.08	118	5.29
140	1.42	0.773	7.27	136	6.09
164	1.58	0.857	7.26	149	6.65
189.5	1.55	0.843	7.27	158	7.05
212	1.51	0.819	7.36	164	7.30
236.5	1.44	0.784	7.33	171	7.62

Table K.33 Organic Acid concentrations for 6.25 mM ethanol of *Rhodobacter capsulatus* DSM1710 (Mean of 2 runs)

Time (hour)	Acetic Acid (mM)	Formic Acid (mM)	Lactic Acid (mM)	Propionic Acid (mM)	Butyric Acid (mM)
0	20.8	0	0	0	0
25	19.8	0	0.021	0.101	0
49	14.1	0	0.032	0.102	0
75	9.73	0	0.031	0.081	0

Table K.33 (Continued)

96	9.69	0	0.071	0	0
116	4.78	0	0	0	0
140	2.01	0	0	0.061	0
164	0.87	0	0	0	0
189.5	0.00	0	0	0.011	0
212	0.00	0	0	0	0
236.5	0.00	0	0	0	0

Table K.34 OD, cell dry weight, pH and cumulative hydrogen produced values for 12.5 mM ethanol of *Rhodobacter capsulatus* DSM1710 (Mean of 2 runs)

Time (h)	OD	gdw/Lc	pH	Cum. H_2 (ml)	Cum. H_2 (mmol)
0	0.235	0.127	6.41	0	0
25	0.235	0.127	6.68	6.76	0.301
49	0.38	0.206	6.85	26.6	1.18
75	0.43	0.233	6.91	59.2	2.63
96	0.965	0.523	7.06	94.4	4.20
116	1.33	0.724	7.09	133	5.93
140	1.43	0.778	7.27	158	7.06
164	1.57	0.854	7.33	172	7.66
189.5	1.53	0.830	7.34	186	8.30
212	1.56	0.849	7.28	193	8.62
236.5	1.57	0.854	7.29	202	9.02

Table K.35 Organic Acid concentrations for 12.5 mM ethanol of *Rhodobacter capsulatus* DSM1710 (Mean of 2 runs)

Time (hour)	Acetic Acid (mM)	Formic Acid (mM)	Lactic Acid (mM)	Propionic Acid (mM)	Butyric Acid (mM)
0	22.8	0	0	0	0
25	21.8	0	0.021	0.111	0
49	13.1	0	0.031	0.081	0
75	13.2	0	0.071	0.081	0
96	8.10	0	0.063	0.083	0
116	4.41	0	0	0	0
140	2.86	0	0	0.092	0
164	1.16	0	0	0	0
189.5	0.44	0	0	0	0
212	0.43	0	0	0	0
236.5	0.00	0	0	0	0

Table K.36 OD, cell dry weight, pH and cumulative hydrogen produced values for 25 mM ethanol of *Rhodobacter capsulatus* DSM1710 (Mean of 2 runs)

Time (h)	OD	gdw/Lc	pH	Cum. H_2 (ml)	Cum. H_2 (mmol)
0	0.238	0.129	6.45	0	0
25	0.225	0.122	6.60	3.15	0.140
49	0.345	0.187	6.89	20.2	0.902
75	0.37	0.200	6.90	47.4	2.10
96	0.885	0.480	7.00	77.2	3.43
116	1.23	0.667	7.03	115	5.12
140	1.33	0.721	7.28	148	6.61
164	1.54	0.835	7.27	171	7.62
189.5	1.58	0.857	7.22	184	8.22
212	1.57	0.854	7.28	189	8.42
236.5	1.58	0.857	7.31	194	8.66

Table K.37 Organic Acid concentrations for 25 mM ethanol of *Rhodobacter capsulatus* DSM1710 (Mean of 2 runs)

Time (hour)	Acetic Acid (mM)	Formic Acid (mM)	Lactic Acid (mM)	Propionic Acid (mM)	Butyric Acid (mM)
0	23.7	0	0	0	0
25	19.4	0	0.021	0.111	0
49	16.8	0	0.061	0.092	0
75	13.4	0	0.063	0.083	0
96	12.8	0	0.084	0.093	0
116	8.24	0	0.083	0	0
140	3.81	0	0	0.043	0
164	1.75	0	0	0	0
189.5	0	0	0	0	0
212	0	0	0	0	0
236.5	0	0	0	0	0

Table K.38 OD, cell dry weight, pH and cumulative hydrogen produced values for 37.5 mM ethanol of *Rhodobacter capsulatus* DSM1710 (Mean of 2 runs)

Time (h)	OD	gdw/Lc	pH	Cum. H_2 (ml)	Cum. H_2 (mmol)
0	0.236	0.128	6.45	0	0
25	0.22	0.119	6.68	2.92	0.130
49	0.315	0.170	6.77	13.7	0.611
75	0.287	0.151	6.87	33.5	1.49
96	0.675	0.366	6.84	54.3	2.41

Table K.38 (Continued)

116	1.07	0.583	7.00	84.1	3.74
140	1.32	0.719	7.20	121.2	5.39
164	1.40	0.762	7.25	147	6.56
189.5	1.50	0.816	7.23	171	7.60
212	1.58	0.857	7.34	184	8.21
236.5	1.59	0.862	7.25	190	8.49

Table K.39 Organic Acid concentrations for 37.5 mM ethanol of *Rhodobacter capsulatus* DSM1710 (Mean of 2 runs)

Time (hour)	Acetic Acid (mM)	Formic Acid (mM)	Lactic Acid (mM)	Propionic Acid (mM)	Butyric Acid (mM)
0	22.5	0	0	0	0
25	18.7	0	0.021	0.11	0
49	19.1	0	0.042	0.097	0
75	15.0	0	0.063	0.075	0
96	14.9	0	0.092	0.102	0
116	8.10	0	0	0	0
140	7.75	0	0	0.071	0
164	3.92	0	0	0.094	0
189.5	1.29	0	0	0	0
212	0.58	0	0	0	0
236.5	0.00	0	0	0	0

Table K.40 OD, cell dry weight, pH and cumulative hydrogen produced values for 50 mM ethanol of *Rhodobacter capsulatus* DSM1710 (Mean of 2 runs)

Time (h)	OD	gdw/Lc	pH	Cum. H_2 (ml)	Cum. H_2 (mmol)
0	0.260	0.141	6.70	0	0
20.5	0.706	0.379	6.98	8.13	0.362
38.5	0.735	0.398	7.26	42.5	1.89
60	0.884	0.477	7.21	75.9	3.38
80	0.925	0.501	7.11	99.4	4.42
108.5	1.13	0.613	7.20	123	5.51
130	1.09	0.591	7.21	141	6.27
145	1.1	0.596	7.22	155	6.92
159.5	1.10	0.599	7.24	175	7.80
201	0.92	0.499	7.29	197	8.80
223	1.14	0.621	7.41	206	9.20
250.5	1.09	0.591	7.38	213	9.48
322	0.9	0.488	7.33	218	9.73
354	1.11	0.605	7.28	221	9.84
406	1.17	0.637	7.31	221	9.84

Table K.41 Organic Acid concentrations for 50 mM ethanol of *Rhodobacter capsulatus* DSM1710 (Mean of 2 runs)

Time (hour)	Acetic Acid (mM)	Formic Acid (mM)	Lactic Acid (mM)	Propionic Acid (mM)	Butyric Acid (mM)
0	20.9	0	0	0	0
20.5	14.0	0.16	0.071	0	0
38.5	10.8	0.54	0.111	0	0
108.5	7.75	2.72	0	0	0
159.5	4.07	4.46	0	0	0
223	1.06	6.89	0.453	0	0
406	1.18	10.7	0	0	0

Table K.42 OD, cell dry weight, pH and cumulative hydrogen produced values for 100 mM ethanol of *Rhodobacter capsulatus* DSM1710 (Mean of 2 runs)

Time (h)	OD	gdw/L_c	pH	Cum. H_2 (ml)	Cum. H_2 (mmol)
0	0.245	0.132	6.70	0	0
20.5	0.635	0.344	6.95	4.15	0.184
38.5	0.655	0.355	7.18	33.9	1.50
60	0.865	0.469	7.19	64.3	2.86
80	0.9	0.488	7.06	90.7	4.03
108.5	0.94	0.510	7.16	123	5.48
130	0.985	0.534	7.20	139	6.22
145	1.00	0.545	7.15	150	6.68
159.5	1.02	0.556	7.23	170	7.57
201	0.855	0.464	7.24	190	8.45
223	1.03	0.561	7.41	200	8.92
250.5	0.99	0.537	7.42	210	9.35
322	0.935	0.507	7.34	223	9.96
354	1.04	0.564	7.30	226	10.0
406	1.12	0.607	7.27	226	10.1

Table K.43 Organic Acid concentrations for 100 mM ethanol of *Rhodobacter capsulatus* DSM1710 (Mean of 2 runs)

Time (hour)	Acetic Acid (mM)	Formic Acid (mM)	Lactic Acid (mM)	Propionic Acid (mM)	Butyric Acid (mM)
0	22.4	0	0	0	0
20.5	17.7	0.153	0.091	0	0
38.5	13.3	0.543	0.081	0	0
108.5	7.45	2.15	0.261	0	0

Table K.43 (Continued)

159.5	5.29	4.17	0	0	0
223	2.37	5.86	0.741	0	0
406	0.00	11.3	0	0	0

Table K.44 OD, cell dry weight, pH and cumulative hydrogen produced values for 200 mM ethanol of *Rhodobacter capsulatus* DSM1710 (Mean of 2 runs)

Time (h)	OD	gdw/Lc	pH	Cum. H_2 (ml)	Cum. H_2 (mmol)
0	0.26	0.141	6.71	0	0
20.5	0.57	0.309	6.92	2.07	0.092
38.5	0.57	0.309	7.16	18.0	0.801
60	0.775	0.420	7.16	40.1	1.78
80	0.75	0.407	7.06	56.0	2.49
108.5	0.75	0.407	7.14	76.8	3.41
130	0.94	0.510	7.18	92.0	4.09
145	0.99	0.537	7.15	103	4.59
159.5	0.98	0.531	7.22	121	5.39
201	0.82	0.445	7.33	142	6.35
223	1.05	0.569	7.50	153	6.84
250.5	1.01	0.548	7.38	163	7.28
322	0.89	0.483	7.35	173	7.71
354	1.08	0.586	7.33	177.	7.88
406	1.06	0.577	7.31	177	7.88

Table K.45 Organic Acid concentrations for 200 mM ethanol of *Rhodobacter capsulatus* DSM1710 (Mean of 2 runs)

Time (hour)	Acetic Acid (mM)	Formic Acid (mM)	Lactic Acid (mM)	Propionic Acid (mM)	Butyric Acid (mM)
0	21.6	0	0	0	0
20.5	17.4	0.073	0.103	0	0
38.5	17.5	0.535	0.085	0	0
108.5	10.3	1.98	0.204	0	0
159.5	7.99	3.71	0	0	0
223	4.87	4.96	0	0	0
406	0	9.72	0	0	0

K.46-K.62 Experimental data for *Rhodobacter capsulatus* YO3 (hup$^-$) on defined medium in different ethanol concentrations

Table K.46 OD, cell dry weight, pH and cumulative hydrogen produced values for control of *Rhodobacter capsulatus* YO3 (hup$^-$) (Mean of 2 runs)

Time (h)	OD	gdw/Lc	pH	Cum. H_2 (ml)	Cum. H_2 (mmol)
0	0.24	0.111	6.65	0	0
24	1.1	0.512	7.06	64.2	2.86
43.5	1.21	0.565	7.08	151	6.72
66	1.34	0.626	7.11	231	10.3
89.5	1.22	0.570	7.22	286	12.7
107.5	0.965	0.449	7.24	311	13.8
128.5	0.805	0.374	7.26	326	14.5
154	0.785	0.365	7.27	338	15.0
179	0.623	0.288	7.26	343	15.2

Table K.47 Organic Acid concentrations for control of *Rhodobacter capsulatus* YO3 (hup$^-$) (Mean of 2 runs)

Time (hour)	Acetic Acid (mM)	Formic Acid (mM)	Lactic Acid (mM)	Propionic Acid (mM)	Butyric Acid (mM)
0	26.8	0	0	0	0
24	11.9	0	0	0.082	0
43.5	9	0	0	0.072	0
66	3.66	0	0	0.053	0
89.5	0	0	0	0.064	0
107.5	0	0	0	0	0
128.5	0	0	0	0	0
154	0	0	0	0	0
179	0	0	0	0.101	0

Table K.48 OD, cell dry weight, pH and cumulative hydrogen produced values for 6.25 mM ethanol of *Rhodobacter capsulatus* YO3 (hup$^-$) (Mean of 2 runs)

Time (h)	OD	gdw/Lc	pH	Cum. H_2 (ml)	Cum. H_2 (mmol)
0	0.275	0.128	6.67	0	0
24	0.915	0.426	6.99	63.0	2.80
43.5	1.03	0.479	7.05	159	7.10
66	1.17	0.547	7.21	240	10.7
89.5	1.14	0.533	7.23	290	12.9

Table K.48 (Continued)

107.5	0.955	0.444	7.31	305	13.5
128.5	0.88	0.409	7.26	316	14.1
154	0.865	0.402	7.26	330	14.6
179	0.695	0.323	7.29	334	14.8

Table K.49 Organic Acid concentrations for 6.25 mM ethanol of *Rhodobacter capsulatus* YO3 (hup^-) (Mean of 2 runs)

Time (hour)	Acetic Acid (mM)	Formic Acid (mM)	Lactic Acid (mM)	Propionic Acid (mM)	Butyric Acid (mM)
0	26.9	0	0	0	0
24	12.1	0	0	0.091	0
43.5	8.93	0	0	0.083	0
66	3.13	0	0	0.055	0
89.5	0	0	0	0.043	0
107.5	0	0	0	0	0
128.5	0	0	0	0	0
154	0	0	0	0	0
179	0	0	0	0.081	0

Table K.50 OD, cell dry weight, pH and cumulative hydrogen produced values for 12.5 mM ethanol of *Rhodobacter capsulatus* YO3 (hup^-) (Mean of 2 runs)

Time (h)	OD	gdw/Lc	pH	Cum. H_2 (ml)	Cum. H_2 (mmol)
0	0.275	0.128	6.70	0	0
24	0.865	0.402	7.02	74.7	3.32
43.5	1.21	0.563	7.07	173	7.72
66	1.33	0.621	7.20	253	11.2
89.5	1.17	0.547	7.22	293	13.0
107.5	0.985	0.458	7.32	300	13.3
128.5	0.945	0.439	7.32	311	13.8
154	0.9	0.419	7.27	324	14.4
179	0.77	0.358	7.29	329	14.6

Table K.51 Organic Acid concentrations for 12.5 mM ethanol of *Rhodobacter capsulatus* YO3 (hup^-) (Mean of 2 runs)

Time (hour)	Acetic Acid (mM)	Formic Acid (mM)	Lactic Acid (mM)	Propionic Acid (mM)	Butyric Acid (mM)
0	25.8	0	0	0	0
24	15.7	0	0	0.092	0

Table K.51 (Continued)

43.5	7.01	0	0	0.073	0
66	1.38	0	0.022	0.054	0
89.5	0	0	0.043	0	0
107.5	0	0	0	0	0
128.5	0	0	0	0	0
154	0	0	0	0.065	0
179	0	0	0	0.073	0

Table K.52 OD, cell dry weight, pH and cumulative hydrogen produced values for 25 mM ethanol of *Rhodobacter capsulatus* YO3 (hup^-) (Mean of 2 runs)

Time (h)	OD	gdw/Lc	pH	Cum. H_2 (ml)	Cum. H_2 (mmol)
0	0.255	0.118	6.70	0	0
24	0.815	0.379	7.08	72.3	3.21
43.5	1.27	0.593	7.15	166.3	7.40
66	1.48	0.689	7.24	245	10.9
89.5	1.28	0.598	7.27	282	12.5
107.5	1.12	0.523	7.34	292	13.0
128.5	1.05	0.488	7.32	302	13.4
154	1.05	0.488	7.25	313	13.9
179	0.865	0.402	7.32	318	14.1

Table K.53 Organic Acid concentrations for 25 mM ethanol of *Rhodobacter capsulatus* YO3 (hup^-) (Mean of 2 runs)

Time (hour)	Acetic Acid (mM)	Formic Acid (mM)	Lactic Acid (mM)	Propionic Acid (mM)	Butyric Acid (mM)
0	26.0	0	0	0	0
24	14.8	0	0	0.091	0
43.5	7.46	0	0	0.074	0
66	1.81	0	0.054	0.056	0
89.5	0.011	0	0.092	0.052	0
107.5	0	0	0.033	0	0
128.5	0	0	0	0	0
154	0	0	0	0.101	0
179	0	0	0	0.044	0

Table K.54 OD, cell dry weight, pH and cumulative hydrogen produced values for 37.5 mM ethanol of *Rhodobacter capsulatus* YO3 (hup$^-$) (Mean of 2 runs)

Time (h)	OD	gdw/Lc	pH	Cum. H_2 (ml)	Cum. H_2 (mmol)
0	0.255	0.118	6.69	0	0
24	0.635	0.295	6.98	56.2	2.50
43.5	0.93	0.433	7.06	119	5.32
66	1.59	0.742	7.30	195	8.69
89.5	1.62	0.756	7.31	245	10.9
107.5	1.51	0.705	7.43	267	11.9
128.5	1.32	0.616	7.40	277	12.3
154	1.29	0.600	7.36	286	12.7
179	1.10	0.514	7.3	289	12.8

Table K.55 Organic Acid concentrations for 37.5 mM ethanol of *Rhodobacter capsulatus* YO3 (hup$^-$) (Mean of 2 runs)

Time (hour)	Acetic Acid (mM)	Formic Acid (mM)	Lactic Acid (mM)	Propionic Acid (mM)	Butyric Acid (mM)
0	26.8	0	0	0.00	0
24	13.0	0	0	0.074	0
43.5	13.1	0	0	0.084	0
66	4.84	0	0.022	0.056	0
89.5	0.953	0	0.095	0.063	0
107.5	0	0	0.036	0	0
128.5	0	0	0	0	0
154	0	0	0	0.084	0
179	0	0	0	0	0

Table K.56 OD, cell dry weight, pH and cumulative hydrogen produced values for 50 mM ethanol of *Rhodobacter capsulatus* YO3 (hup$^-$) (Mean of 2 runs)

Time (h)	OD	gdw/Lc	pH	Cum. H_2 (ml)	Cum. H_2 (mmol)
0	0.26	0.121	6.68	0	0
24	0.575	0.267	6.96	55.3	2.46
43.5	0.965	0.449	7.01	118	5.25
66	1.70	0.793	7.28	188	8.37
89.5	1.75	0.814	7.37	238	10.6
107.5	1.52	0.710	7.41	266	11.8
128.5	1.41	0.658	7.37	276	12.3
154	1.4	0.651	7.40	288	12.8
179	1.2	0.558	7.37	295	13.1

Table K.57 Organic Acid concentrations for 50 mM ethanol of *Rhodobacter capsulatus* YO3 (hup^-) (Mean of 2 runs)

Time (hour)	Acetic Acid (mM)	Formic Acid (mM)	Lactic Acid (mM)	Propionic Acid (mM)	Butyric Acid (mM)
0	26.7	0	0	0.005	0
24	19.5	0	0	0.083	0
43.5	11.9	0	0	0.063	0
66	4.50	0	0	0.053	0
89.5	1.21	0	0	0.065	0
107.5	0	0	0.051	0	0
128.5	0	0	0	0	0
154	0	0	0	0	0
179	0	0	0	0	0

Table K.58 OD, cell dry weight, pH and cumulative hydrogen produced values for 100 mM ethanol of *Rhodobacter capsulatus* YO3 (hup^-) (Mean of 2 runs)

Time (h)	OD	gdw/Lc	pH	Cum. H_2 (ml)	Cum. H_2 (mmol)
0	0.24	0.111	6.69	0	0
24	0.545	0.253	6.94	50.4	2.24
43.5	0.815	0.379	6.99	104	4.65
66	1.55	0.724	7.27	156	6.98
89.5	1.83	0.854	7.38	211	9.41
107.5	1.66	0.772	7.55	235	10.4
128.5	1.59	0.742	7.52	250	11.1
154	1.63	0.758	7.46	262	11.6
179	1.29	0.602	7.42	268	11.9

Table K.59 Organic Acid concentrations for 100 mM ethanol of *Rhodobacter capsulatus* YO3 (hup^-) (Mean of 2 runs)

Time (hour)	Acetic Acid (mM)	Formic Acid (mM)	Lactic Acid (mM)	Propionic Acid (mM)	Butyric Acid (mM)
0	27.1	0	0	0	0
24	15.9	0	0	0.085	0
43.5	13.7	0	0	0.065	0
66	7.83	0	0	0.083	0
89.5	1.91	0	0	0	0
107.5	0.34	0	0.013	0	0
128.5	0.00	0	0	0	0
154	0	0	0	0	0
179	0	0	0	0	0

Table K.60 OD, cell dry weight, pH and cumulative hydrogen produced values for 200 mM ethanol of *Rhodobacter capsulatus* YO3 (hup$^-$) (Mean of 2 runs)

Time (h)	OD	gdw/Lc	pH	Cum. H_2 (ml)	Cum. H_2 (mmol)
0	0.245	0.114	6.71	0	0
24	0.41	0.190	6.97	45.4	2.02
43.5	0.6	0.279	7.00	89.1	3.96
66	1.25	0.584	7.10	131	5.83
89.5	1.56	0.728	7.34	167	7.47
107.5	1.41	0.656	7.53	182	8.12
128.5	1.41	0.656	7.49	189	8.43
154	1.39	0.649	7.57	197	8.77
179	1.09	0.507	7.36	201	8.96

Table K.61 Organic Acid concentrations for 200 mM ethanol of *Rhodobacter capsulatus* YO3 (hup$^-$) (Mean of 2 runs)

Time (hour)	Acetic Acid (mM)	Formic Acid (mM)	Lactic Acid (mM)	Propionic Acid (mM)	Butyric Acid (mM)
0	21.8	0	0	0	0
24	15.4	0	0	0.084	0
43.5	10.8	0	0	0.052	0
66	6.97	0	0	0.056	0
89.5	3.29	0	0.023	0.042	0
107.5	2.58	0	0	0	0
128.5	1.30	0	0.012	0.064	0
154	0.08	0	0	0.084	0
179	0	0	0	0	0

Table K.62 PHB values for *Rhodobacter capsulatus* DSM1710 and *Rhodobacter capsulatus* YO3 (hup$^-$) in different concentrations of ethanol (Mean of 2 runs)

EtOH (mM)	*Rb. capsulatus* DSM1710 PHB (%)	*Rb. capsulatus* YO3 (hup$^-$) PHB (%)
0	41.2	2.1
6.25	61.6	4.6
12.5	59.2	7.7
25	52.0	19.9
37.5	74.4	36.6
50	34.9	52.5
100	34.8	44.2
200	33.1	48.8